UNIVERSITY OF CALIFORNIA,
IRVINE

Isoforms, Clocks, and Acetylcholine: Regulation of Cocaine's Effects by Dopamine D2 Receptors

DISSERTATION

submitted in partial satisfaction of the requirements
for the degree of

DOCTOR OF PHILOSOPHY

in Biomedical Sciences

by

Robert Gary Lewis

Dissertation Committee:
Chancellor's Professor Emiliana Borrelli, Chair
Associate Professor Christie Fowler
Distinguished Professor Bert Semler
Professor Yongsheng Shi
Professor Marcelo Wood

2022

DEDICATION

To

My parents and siblings.
Mom, Dad, David, and Jen – thank you for making this possible.

TABLE OF CONTENTS

LIST OF FIGURES

LIST OF TABLES

ACKNOWLEDGEMENTS

I would first like to express the deepest appreciation to my committee chair, Emiliana Borrelli. Emiliana gave me my first opportunity to do research when I was a second-year undergraduate; her lab is where I really found my passion for science and is where realized that I wanted to pursue a PhD. I was rejected from every PhD program that I applied to. The disappointment I felt made me question if I would ever be good enough to get in and almost made me abandon my hopes of being a researcher altogether. Emiliana saw my potential though, and she believed in my ability to become a great scientist when it felt like no one else did. She took me in as her student, and it is entirely possible that I would not be writing a dissertation at all if not for her. I am truly grateful for the opportunity she gave me and for her mentorship over the course of my training.

I write this dissertation in memory of Paolo Sassone-Corsi. I am thankful for his perspectives on life and science. It was truly a special opportunity to learn from him. Working with Emiliana and Paolo on several projects was a rare collaboration that gave me an opportunity to learn from incredible scientists. Memories of laughs we shared at conferences, Center for Epigenetics and Metabolism events, and manuscript preparation meetings are ones I will never forget.

I am thankful for the all the past and present members of the Borrelli Lab. A special thank you to Daniela Radl and Karen Brami-Cherrier, my first in-lab mentors. I cannot thank you both enough for taking me under your wings and for your patience while teaching me. Martina, Ludovico, Marcello, Daniela, Ermanno, and Lauren, thank you for your help, advice, and for all the cherished memories. The patience and kindness you showed me during my training will always be remembered. I'm grateful to our lab technicians – Jihua and Jonathan for helping things run smoothly. Additionally, I would like to thank my students Catherine, Daniel, Michela, Tiffany, Leyna, Jerry and Stepheny. I appreciate all your help over the years and for teaching me as much as I hope that I taught you.

I am grateful to the other members of my committee: Christie Fowler, Bert Semler, Yongsheng Shi, and Marcelo Wood. I appreciate all of your insightful questions and discussions which allowed me to greatly improve my projects and become a better scientist. Each member of my committee went above and beyond to support me and my work. I am indebted to all of you for your help which undoubtably allowed me to prosper during my training. A special thank you to Christie, who opened her laboratory up to me and allowed me to work with- and learn from- her and her team.

Thank you to my family for their support over during my studies. My parents, Bob and Candi, who always encouraged me to pursue my passions, emphasized the importance of education, and instilled the mental fortitude in me to accomplish this goal. Thank you to my sister, Jen, for her encouragement when things were going well and advice when things were hard. A huge thank you to my brother, David, who has been by my side from day one and was the person I could talk to about anything going on in my life. I am grateful to my uncle Jim Bohm who supported me immensely during my graduate studies and undoubtably made this phase of my life

easier. My family's support allowed me to focus on doing the best science I could, and this would not have been possible without them.

I also want to thank my friends for being there for all the successes, failures, laughs, and tears. A special thank you to my colleague and one of my closest friends, Marlene, who gave me (and continues to give me) advice that I credit a lot of my graduate school success to. Thank you to Tiffany for making the tough days in the lab fun and the good days even better. I am also grateful to Maggie for her unwavering support and for all the long runs that helped me complete the mental marathon of graduate school. Thank you to Ian, who encouraged my path into research since my undergraduate days. Your help and support of made this possible and I am eternally grateful to all of you.

I would like to acknowledge the funding that supported my studies which included a University of California, Irvine School of Medicine Dean's Fellowship, the Dr. Lorna Carlin Scholar Award, a University of California, Irvine Graduate Dean's Dissertation Fellowship, and a National Institute on Drug Abuse T32 Predoctoral Training Grant (DA050558-01/02). Funding is incredibly competitive - I was truly fortunate to have the support of UC Irvine, Dr. Carlin, and the NIH. Thank you all!

Content from Chapter 2 came from Radl D, Chiacchiaretta M, Lewis RG, et al (2018) Differential regulation of striatal motor behavior and related cellular responses by dopamine D2L and D2S isoforms. PNAS 115:198–203.

We wish to acknowledge all members of the Borrelli's laboratory for interest, help and discussions; in particular we thank Maria Ramos, Claudia De Mei, Hyuna Lee and Tam Phan. M.C. is supported by AIRC – Associazione per la Ricerca sul Cancro. This work was funded by NIDA DA033554 and INSERM.

Content from Chapter 3 came from Brami-Cherrier K, Lewis RG, Cervantes M, et al (2020) Cocaine-mediated circadian reprogramming in the striatum through dopamine D2R and PPARγ activation. Nature Communications 11:4448.

We thank all the members of the Sassone-Corsi and Borrelli laboratories for scientific discussion and technical assistance. We also thank Siwei Chen for computational assistance. We greatly appreciate Melanie Oakes, Christophe Magnan, Seung-Ah Chung and Valentina Ciobanu at the UCI Genomics High-Throughput Facility. RGL was supported by the University of California, Irvine School of Medicine Dean's Fellowship, and the Dr. Lorna Carlin Scholar Award. MC was supported by predoctoral fellowships from the National Institutes of Health (NIH) (GM117942) and the American Heart Association (17PRE33410952). PT by Human Frontier Science Program LT 000576/2013. This work was supported by grants from NIH (DA 035600 to EB and PSC) and by the French Institut National de la Santé et de la Recherche Médicale (INSERM).

Content from Chapter 4 came from Cervantes M, Lewis RG, Della-Fazia MA, et al (2022) Dopamine D2 receptor signaling in the brain modulates circadian liver metabolomic profiles. Proceedings of the National Academy of Sciences 119:e2117113119.

We thank all the members of the E.B. and P.S.-C. laboratories for scientific discussion. We appreciate K. Brami-Cherrier and D. Radl for their initial interest in this work. M.C. was supported by predoctoral fellowships from the NIH (F31GM117942) and the American Heart Association (17PRE33410952). R.G.L. was supported by a University of California, Irvine School of Medicine Dean's Fellowship, the Dr. Lorna Carlin Scholar Award, a University of California, Irvine Graduate Dean's Dissertation Fellowship, and a National Institute on Drug Abuse T32 Predoctoral Training Grant (DA050558-02). M.A.D.-F. was a recipient of FP7 Marie Curie Actions grant agreement COFUND N.267232 Project I-MOVE n.13001106001802512447. This work was supported by grants from the NIH (DA035600 to E.B. and P.S.-C.) and by the French Institut National de la Sante et de la Recherche Medicale (INSERM).

Content from Chapter 4 came from Cervantes M, Lewis RG, Della-Fazia MA, et al (2022) Dopamine D2 receptor signaling in the brain modulates circadian liver metabolomic profiles. Proceedings of the National Academy of Sciences 119:e2117113119.

Lewis RG, et al (2020) Dopaminergic Control of Striatal Cholinergic Interneurons Underlies Cocaine-Induced Psychostimulation. Cell Reports 31

We thank Dr. Melanie Oaks and Seung-Ah Chung of the University of California, Irvine Genomics High Throughput facility for RNA sequencing support. We also would like to thank Drs. M. Seldin and P. Sassone-Corsi and members of the lab for discussion and critical reading of the manuscript. R.G.L was supported by the University of California, Irvine, School of Medicine Dean's Fellowship and the Dr. Lorna Carlin Scholar Award. This work was supported by funds from the Institut de la Santé et de la Recherche Medicale (INSERM).

VITA

ROBERT G. LEWIS

Education

Ph.D.	University of California – Irvine, School of Medicine Biomedical Sciences – Genetics, Epigenetics, and Genomics Concentration Irvine, CA	2022
B.S.	University of California – Irvine Genetics Irvine, CA	2017

Honors and Awards

Harris Moyed Outstanding Graduate Student in Microbiology and Molecular Genetics 2022
University of California – Irvine, School of Medicine

Annual Outstanding Graduate Student Research Award 2022
University of California – Irvine, School of Medicine

Annual Outstanding Graduate Student Research Award (Runner-Up) 2021
University of California – Irvine, School of Medicine

Substance Use and Use Disorders T32 Predoctoral Training Grant (Renewal) 2021
National Institute on Drug Abuse, Grant No. DA050558-02

Substance Use and Use Disorders T32 Predoctoral Training Grant 2020
National Institute on Drug Abuse, Grant No. DA050558-01

Graduate Dean's Dissertation Fellowship 2020
University of California – Irvine

Dr. Lorna Carlin Scholar Award 2020
University of California – Irvine, School of Medicine

School of Medicine Dean's Fellowship 2019
University of California – Irvine, School of Medicine

Excellence in Research in the Biological Sciences 2017
University of California – Irvine

Excellence in Research in the Biological Sciences 2016
University of California – Irvine

Professional Experience

Graduate Student Researcher

2017-Present

University of California – Irvine, School of Medicine
Advisor: Emiliana Borrelli, PhD
Field: Neuroscience | Molecular Genetics

Undergraduate Student Researcher. 2014-2017
University of California – Irvine, School of Medicine
Advisor: Emiliana Borrelli, PhD
Field: Neuroscience | Molecular Genetics

Publications

Cervantes M*, **Lewis RG***, Della-Fazia MA, Borrelli E, Sassone-Corsi P. Dopamine D2 receptor signaling in the brain modulates circadian liver metabolomic profiles. ***Proc Natl Acad Sci.*** 2022.

Lewis RG, Florio E, Punzo D, Borrelli E. The Brain's Reward System in Health and Disease. ***Adv Exp Med Biol***. 2021.

Lewis RG & Borrelli E. A mechanism of cocaine addiction susceptibility through dopamine D2 receptor-mediated regulation of nucleus accumbens cholinergic interneurons. ***Biol Psychiatry.*** 2020.

Brami-Cherrier K*, **Lewis RG***, Cervantes M*, Liu Y, Tognini P, Baldi P, Sassone-Corsi P, Borrelli E. Cocaine-mediated circadian reprogramming in the striatum through dopamine D2R and PPARγ activation. ***Nat Commun***. 2020.

Lewis RG, Serra M, Radl D, Gori M, Tran C, Michalak SE, Vanderwal CD, Borrelli E. Dopaminergic control of striatal cholinergic interneurons underlies cocaine-induced psychostimulation. ***Cell Rep.*** 2020.

Radl D*, Chiacchiaretta M*, **Lewis RG***, Brami-Cherrier K, Arcuri L, Borrelli E. Differential regulation of striatal motor behavior and related cellular responses by dopamine D2L and D2S isoforms. ***Proc Natl Acad Sci USA.*** 2018.

Kharkwal G, Radl D, **Lewis RG**, Borrelli E. Dopamine D2 receptors in striatal output neurons enable the psychomotor effects of cocaine. ***Proc Natl Acad Sci USA***. 2016.

In Preparation

Serra M*, Florio E*, **Lewis RG**, Kramer E, Freidberg M, Wood M, Borrelli E. D2R signaling in indirect pathway medium spiny neurons regulates the intensity of L-DOPA induced dyskinesia. ***In Preparation.***

*Equal Contribution

Teaching Experience

University of California – Irvine — Jun 2019 to Aug 2019
Teaching Assistant, Department of Developmental and Cell Biology
Biological Sciences 97: Genetics
Instructor: Lee Bardwell, PhD

University of California – Irvine — Sept 2018 to Dec 2018
Teaching Assistant, Department of Developmental and Cell Biology
Biological Sciences 97: Genetics
Instructors: Rahul Warrior, PhD & Lee Bardwell, PhD

University of California – Irvine. — Aug 2018 to Sept 2018
Teaching Assistant, Department of Developmental and Cell Biology
Biological Sciences 97: Genetics
Instructor: Rahul Warrior, PhD

Mentoring Experience

Hsui-An (Jerry) Cheng[#], B.S. Biological Sciences 2023 — 2021-present
Undergraduate Student at UC Irvine

Stepheny Wu[#], B.S. Biological Sciences 2023 — 2021-present
Undergraduate Student at UC Irvine

Leyna Vu[##], B.S. Pharmaceutical Sciences 2022 — 2020-present
Undergraduate Student at UC Irvine

Thu (Tiffany) Dihn Nha Pham[##], B.S. Neurobiology & Behavior 2021 — 2018-2021
Junior Research Specialist at UC Irvine

Michela Gori[##], B.S. Biomedical Engineering 2020 — 2017-2020
Consumables Engineer at COMBiNATi
Co-Author *Cell Reports*

Daniel Reyes[#], B.S. Biological Sciences 2019 2018-2019
Nursing Student High Desert Medical College

Catherine Tran[#], B.S. Biological Sciences/Education 2019 2017-2019
High School Science Teacher at Los Angeles Unified School District
Co-Author *Cell Reports*

Xochitl Luna, High School Intern (Summer) 2017
Undergraduate Student at MIT

#Undergraduate Research Opportunity Program Grant Recipient

Presentations

Seminars

Cracking the epigenetic code of addiction: a critical role for the striatal dopamine—acetylcholine balance. Jan 2022. UC Irvine School of Medicine Dept of Microbiology and Molecular Genetics Seminar Series

Epigenetic links to addiction: the critical role of the striatal dopamine/acetylcholine balance. Jan 2022. Division of Genetic and Genomic Medicine Case Conference. UC Irvine School of Medicine

Medium spiny neuron D2 receptor signaling modulates liver metabolomic profiles after cocaine administration
May 2021. UC Irvine/UCLA T32 Joint Retreat Data Blitz Talk

Mechanisms of addiction to cocaine and morphine: The essential role of the dopamine-acetylcholine balance. Feb 2021. UC Irvine School of Medicine Dept of Microbiology and Molecular Genetics Seminar Series

Dopaminergic control of striatal cholinergic interneurons underlies cocaine-induced psychostimulation.
Jan 2020. UC Irvine School of Medicine Dept of Microbiology and Molecular Genetics Seminar Series

Posters

Dopaminergic control of striatal cholinergic interneurons underlies cocaine-induced psychostimulation. **Lewis RG**, Serra M, Radl D, Gori M, Tran C, Michalak SE, Vanderwal CD, Borrelli E. UCI School of Medicine Graduate Studies Day Poster Presentation. Oct 2020.

Dopaminergic control of striatal cholinergic interneurons underlies cocaine-induced psychostimulation. **Lewis RG**, Serra M, Radl D, Gori M, Tran C, Michalak SE, Vanderwal CD, Borrelli E. UCI School of Medicine Graduate Studies Day Poster Presentation. Oct 2020.

D2R-mediated control of cholinergic interneurons underlies cocaine-induced psychostimulation. **Lewis RG**, Serra M, Radl D, Gori M, Tran C, Michalak SE, Vanderwal CD, Borrelli E. Interdepartmental Neuroscience Recruitment Poster Presentation. Oct 2019.

D2R-mediated control of cholinergic interneurons underlies cocaine-induced psychostimulation. **Lewis RG**, Serra M, Radl D, Gori M, Tran C, Michalak SE, Vanderwal CD, Borrelli E. University of California, Irvine, School of Medicine Grad Day Poster Presentation: Oct 2019.

Dopamine D2 receptor isoforms in the psychomotor response to cocaine. **Lewis RG** & Borrelli E. Interdepartmental Neuroscience Recruitment Poster Presentation. Feb 2018.

Dopamine D2 receptor isoforms in the psychomotor response to cocaine. **Lewis RG** & Borrelli E. Cellular and Molecular Biosciences Recruitment Poster Presentation. Feb 2018.

Critical role of striatal D2R signaling in the psychomotor effects of cocaine. Radl D, Kharkwal G, **Lewis RG**, Borrelli E. Society for Neuroscience Annual Meeting. Nov 2016.

Professional Training & Conferences

- **Division of Genetic and Genomic Medicine Weekly Case Conference**
  UC Irvine – Medical Center, Dec 2019 – Present
- **Microbiology and Molecular Genetics Weekly Seminar Series**
  UC Irvine, Sept 2017 – Present
- **Columbia – Mount Sinai Brain Symposium**
  Virtual, May 2021
- **Society of Biological Psychiatry Annual Meeting**
  SoBP Virtual, April 2021
- **American College of Medical Genetics and Genomics Annual Symposium**
  ACMG Virtual, April 2021
- **Southern California Rare Disorders Symposium**
  UC Irvine Virtual, April 2021
- **Rare Disease Day**
  National Institutes of Health Virtual, March 2021
- **Diagnostic Utility of RNA-Seq in Neurodevelopmental Disorders**
  ACMG Virtual, Oct 2020
- **Epigenetics Day**
  UC Irvine, Dec 2019
- **Center for Addiction Neuroscience Symposium**

UC Irvine, Oct 2019

- **Genomic and Precision Medicine Short Course**
  Coursera, Dec 2018
- **New Disease Gene Discoveries - Genetic and Functional Evidence**
  ACMG Genomics Case Conference, Oct 2018
- **International Symposium on Epigenetic Control and Cellular Plasticity**
  UC Irvine, Oct 2018
- **Center for Addiction Neuroscience Symposium**
  UC Irvine, June 2018
- **Epigenetics Day**
  UC Irvine, Dec 2017
- **Center for Addiction Neuroscience Symposium**
  UC Irvine, July 2017
- **International Symposium on Epigenetic Control and Cellular Plasticity**
  UC Irvine, October 2016
- **Center for Addiction Neuroscience Symposium**
  UC Irvine, June 2016

Professional Affiliations

American College of Medical Genetics and Genomics	2017-Present
American Association for the Advancement of Science	2017-Present

Professional Service

Therapeutics Committee Student Volunteer
April 2021-present
American College of Medical Genetics (ACMG)

ClinGen Curator
April 2021-present
Baseline, Basic Evidence Curator: Limb Girdle Muscular Dystrophy Variant Curation
Evaluate evidence supporting or refuting a claim that variation
in genes associated with LGMD cause disease.

Invited Speaker
Oct 2020
UC Irvine - School of Biological Sciences
Made a 7-minute video about my experiences as an undergraduate student
in the School of Biological Sciences for first-year biology majors interested
in research and graduate school.

Orientation Breakout Room Leader
Sept 2020
UC Irvine - School of Medicine
Facilitated breakout room discussions to introduce new graduate students to current graduate students and provided information about studies at the School of Medicine.

Alumni Panelist
Sept 2018
UC Irvine - School of Biological Sciences
Invited to speak about my experiences as an undergraduate student in the School of Biological Sciences to first-year biology majors interested in research and different careers in the life sciences.

Community Service

Invited Career Day Speaker
Oct 2020
Redlands Unified School District
Made a video describing what research scientists at a university do for 7th and 8th grade mild/moderate special education students.

Science Fair Judge
Feb 2019
Irvine Unified School District
Evaluated and provided feedback on 5th and 6th grade science projects.

Keynote Speaker Outreach Program for Santa Ana High School
April 2018
Pre-Health Undergraduate Student Organization
Invited to speak about my experiences with college admissions and the transition from high school to college as a first-generation college student.

Ask a Scientist Night Advisor
Sept 2017
Irvine Unified School District
Provided guidance and feedback on 5th and 6th grade science projects.

Skills

Molecular Biology & Biochemistry: immunofluorescence (IF), in-vitro transcription, fluorescent in-situ hybridization (FISH), nucleic acid extraction, protein purification, PCR, qPCR, immunoprecipitation (IP), chromatin immunoprecipitation (ChIP), Western blot, molecular cloning, enzyme activity and kinetics profiling.

Behavioral Testing: novel home cage, open field, rotarod, stereotypy assessment, conditioned place preference, intravenous self-administration, catalepsy test, levodopa-induced dyskinesia scoring, novel object recognition.

Surgery: self-administration intravenous catheter insertion, intracranial stereotaxic surgery, cardiac perfusion.

Computational: R, RNA-sequencing, differential expression analysis, ImageJ, Leica Application Suite X, GraphPad Prism, Photoshop, MacOS, Windows OS, Linux/Unix.

Language: English (Native Language), American Sign Language (Elementary Level)

ABSTRACT OF THE DISSERTATION

Isoforms, Clocks, and Acetylcholine: Regulation of Cocaine's Effects
by Dopamine D2 Receptors
by
Robert Gary Lewis
Doctor of Philosophy in Biomedical Sciences
University of California, Irvine, 2022
Professor Emiliana Borrelli, Chair

Cocaine is a highly addictive stimulant which immensely raises dopamine levels in brain areas controlling motor and reward functions. Dopamine signaling is controlled by the five dopamine receptors (D1-D5) which are part of the G-protein coupled receptor superfamily. The dopamine D2 receptor (D2R) plays a key role regulating cocaine's effects. However, its study has been difficult due to its ubiquitous expression throughout the brain using pharmacological tools alone. Moreover, the presence of two D2R isoforms has further complicated the study of this receptor. Using a combination of pharmacological and genetic approaches, we investigated the isoform- and cell- specific roles of D2R in mediating the effects and consequences of cocaine in mouse models. Here, we show that while both isoforms of D2R are sufficient in the control of basal behaviors, under dopaminergic challenge the long D2R isoform (D2L) contributes largely to post-synaptic heteroreceptor functions while the short D2R isoform (D2S) has a predominant pre-synaptic autoreceptor function (Radl et al. 2018). Furthermore, we show that D2R signaling in indirect pathway medium spiny neurons (iMSNs) has a major control of the circadian transcriptome and metabolome in the nucleus accumbens through control of PPARγ activation (Brami-Cherrier et al. 2020). Relatedly, we show that D2R signaling in iMSNs contributes to the synchrony of the liver metabolic clock (Cervantes et al. 2022). Lastly, by regulating the balance of dopamine and acetylcholine in the striatum, D2R signaling in cholinergic interneurons (ChIs), underlies cocaine's psychostimulating and rewarding effects (Lewis et al. 2020).

INTRODUCTION

The Dopamine System

Dopaminergic projections to the striatum are critical for the control of psychostimulating and rewarding properties of cocaine. Dorsal and ventral regions of this key integrating center have collaborative roles in mediating cocaine's effects. The ventral striatum, including the nucleus accumbens (NAcc), is critically involved in incentive-based learning in addition to reward processing and evaluation (Marche et al. 2017). Meanwhile, the dorsal striatum is critically involved in action selection and initiation components of decision making and mediates feedback properties such as valiance and magnitude in addition to controlling habitual behavior (Balleine et al. 2007; Burton et al. 2015; Lipton et al. 2019).

Medium spiny neurons (MSNs) represent 90-95% of striatal neurons (Kemp and Powell 1971; Graveland and DiFiglia 1985) and are the striatum's sole output neurons. MSNs outputs generate two pathways: the direct pathway formed by dopamine D1 receptor (D1R) expressing medium spiny neurons (dMSNs) and the indirect pathway by dopamine D2 receptor (D2R) expressing medium spiny neurons (iMSNs). Coordinated dopamine signaling to dMSNs and iMSNs within the striatum is critical for integrating and responding to rewarding stimuli.

The other 5-10% of striatal neurons are interneurons, which serve as intrastriatal regulators of MSNs activity (Oorschot 2013). The majority of interneurons are inhibitory GABAergic interneurons which modulate reward through their signaling to MSNs and expression of a variety of modulatory peptides (Gittis et al. 2010). 1-2% of striatal neurons are formed by the tonically active cholinergic interneurons (ChIs) which, despite their low abundance, critically regulate MSNs (Kharkwal et al. 2016a; Lewis et al. 2020). Indeed, activation of ChIs has been linked to

the salience of events (Gittis and Kreitzer 2012). Thus, inter- and intra- striatal connections modulate striatal circuits and play a critical role in reward processing.

Although our understanding of the specific actions of drugs on the reward system has grown, it has simultaneously illuminated the complexity of mechanisms driving the transition from recreational use to a use disorder. A general feature of drugs of abuse is the elevation of dopamine levels in the brain which underlies their rewarding effects. With continued use in vulnerable individuals, substance use disorders can develop (Swendsen and Moal 2011).

Cocaine is a psychostimulant whose primary mechanism of action is to block the dopamine transporter, thereby preventing reuptake of this neuromodulator into presynaptic terminals from dopaminergic afferents. As a result, areas that are innervated by dopaminergic neurons, such as the striatum, become overstimulated. At the cellular level, cocaine alters neuronal plasticity, leading to alterations of gene expression and the consequent modification of neuronal circuits which underlies the characteristic behaviors of addiction.

Dopamine D2 Receptors

Dopamine is synthesized using tyrosine hydroxylase to convert tyrosine to L-DOPA which is then converted into dopamine by DOPA decarboxylase (Meiser et al. 2013). When dopamine neurons fire, dopamine is released into the synaptic cleft where it can then act on its associated receptors. The five dopamine receptors are G protein coupled receptors which are subtyped based on their linkage to stimulatory or inhibitory G_α subunits. Dopamine D1-Like receptors include D1R and D5R while dopamine D2-like receptors include D2R, D3R, and D4R. Activation of D1-like receptors leads to adenylyl activity which increases cAMP and downstream signaling cascades

(Beaulieu et al. 2015). Conversely, D2-like receptor activation decreases cAMP and downstream signaling cascades by inhibiting adenylyl cyclase(Beaulieu et al. 2015).

D2R is a highly abundant dopamine receptor localized throughout the brain and is found at pre- and post- synaptic sites (Anzalone et al. 2012). Presynaptic D2R serves as an autoreceptor controlling the synthesis of dopamine through its control of tyrosine hydroxylase phosphorylation, the active state of this enzyme. When dopamine levels in the synaptic cleft are high, presynaptic D2R signaling decreases dopamine synthesis, allowing reduced dopamine release and increased reuptake of dopamine through the dopamine transporter. In contrast, postsynaptic D2R serves as a heteroreceptor which controls the release of heterogeneous neurotransmitters including GABA, glutamate, and acetylcholine (Anzalone et al. 2012; Kharkwal et al. 2016a, b; Lewis et al. 2020; Puighermanal et al. 2020). D2R is thought to have key role in compulsive behavior and addiction as people with substance use disorders and obesity show lower binding availability in the striatum (Volkow et al. 1997, 2011). Indeed, pharmacological blockade or genetic deletion of D2R shows differential responses to cocaine which will be highlighted in this work.

Drd2, the gene encoding D2R, generates two molecularly distinct isoforms known as D2L (long) and D2S (short). D2L differs from D2S by an additional 29 amino acids located in the third intracellular loop of the receptor. The region is critical as it interacts with signal transduction proteins. Thus, it was suggested and confirmed that D2L and D2S interact and regulate different proteins and signal transduction pathways. Both isoforms are expressed in all cell types in a ratio favoring the D2L isoform (Montmayeur et al. 1991). However, the pre- or post-synaptic localization of the D2R isoforms has been thought to determine which version of this receptor has predominant function in regulating cellular activity.

Dopaminergic control of Circadian Clocks

Rhythmic control of an organism's behavior is a critical part of adapting and anticipating environmental changes in light, temperature, and resources. Though time keeping mechanisms are more complex and developed in mammals, diurnal control is conserved throughout nature (Edgar et al. 2012). In mammals, the suprachiasmatic nucleus (SCN) organizes behavior and its correlated cellular activity through hormone and neurotransmitter release, in a 24-hour cycle based on daily light and dark phases (Dunlap 1999).

Dopamine levels rise in the active phase and fall in the resting phase of the day (Smith et al. 1992; Hood et al. 2010; Ferris et al. 2014), as does its precursor and metabolites (Paulson and Robinson 1996; Castañeda et al. 2004). Rhythmic expression of clock genes including *Clock*, *Rev-ERBα, Per, Npas2* and *Bmal1* are involved in dopamine metabolism (McClung et al. 2005; Chung et al. 2014). Indeed, *Clock* and *Rev-ERBα* negatively regulate the expression of tyrosine hydroxylase. Levels of TH increase during the active phase, which is opposite to that of *Clock* and *Rev-ERBα;* loss of either circadian gene results in disrupted rhythmic TH expression (McClung et al. 2005; Chung et al. 2014).

Dopamine's influence on the SCN was inferred by expression of both D1R and D5R on its neurons (Weiner et al. 1990; Rivkees and Lachowicz 1997; Doyle et al. 2002). In neonatal hamsters, light pulses mirror the effects of D1R agonists suggesting that the maternal levels of DA correspond to the active phase in the fetal SCN (Viswanathan and Davis 1997). Dopamine has been reported to play a critical role in entraining fetal development through the SCN and that after this period, the SCN's responsiveness to dopamine declines (Weaver and Reppert 1995; Mendoza and Challet 2014). Nevertheless, D1R activation in the SCN shifts the phase of circadian rhythms

and a direct connection between the ventral tegmental area (VTA) and the SCN has been described (Grippo and Güler 2019). Furthermore, D2R seems to be required for the light-induced suppression of locomotor activity (masking), whereas other visual or nonvisual photic responses seem to be D2R independent (Doi et al. 2006). Thus, the daily fluctuation in VTA dopamine neuron activity has a substantial role in SCN entrainment and other circadian activities.

Cholinergic Interneurons

Striatal cholinergic interneurons (ChIs) represent 1-2% of striatal neurons but have a significant role in regulating striatal output (Oorschot 2013). The influence of ChI activity on the overall regulation of striatal circuitries has been difficult to assess due to their low abundance. Dopamine inhibits ChIs' activity through D2R with consequent lowering of striatal ACh levels (Pisani et al. 2000; Oldenburg and Ding 2011; Kharkwal et al. 2016a). By lowering ACh levels D2R indirectly controls MSNs activity through activation of muscarinic M4 and M1 receptors located on dMSNs and iMSNs, respectively (Shen et al. 2007; Jeon et al. 2010; Threlfell et al. 2010; Mamaligas and Ford 2016; Moehle et al. 2017). At the same time, ACh acts on nicotinic and muscarinic receptors found on striatal dopaminergic inputs as well as on cortical inputs. Previous studies examining mice with a deletion of D2R in ChIs (ChI-D2RKO mice) found that while motor behavior in basal conditions was unaffected, these mice were resistant to haloperidol induced catalepsy (Kharkwal et al. 2016a) due to dysregulated acetylcholine release. Thus, dopamine mediated control of ChIs activity and the balance of DA/ACh in the striatum is pivotal in regulating striatal circuits and has implications in responding to the motor and rewarding effects of drugs of abuse, like cocaine.

Chapter 2: Differential regulation of striatal motor behavior and related cellular responses by dopamine D2L and D2S isoforms

Abstract

The dopamine D2 receptor (D2R) is a major component of the dopamine system. D2R-mediated signaling in dopamine neurons is involved in the presynaptic regulation of dopamine levels. Postsynaptically, i.e., in striatal neurons, D2R signaling controls complex functions such as motor activity through regulation of cell firing and heterologous neurotransmitter release. The presence of two isoforms, D2L and D2S, which are generated by a mechanism of alternative splicing of the *Drd2* gene, raises the question of whether both isoforms may equally control pre- and post-synaptic events. Here, we addressed this question by comparing behavioral and cellular responses of mice with the selective ablation of either D2L or D2S isoform. We establish that the presence of either D2L or D2S can support postsynaptic functions related to the control of motor activity in basal conditions. On the contrary, absence of D2S but not D2L prevents the inhibition of tyrosine hydroxylase (TH) phosphorylation and thereby of dopamine synthesis, supporting a major presynaptic role for D2S. Interestingly, boosting dopamine signaling in the striatum by acute cocaine administration reveals that absence of D2L, but not of D2S, strongly impairs the motor and cellular response to the drug, in a manner similar to the ablation of both isoforms. These results suggest that when the dopamine system is challenged, D2L signaling is required for the control of striatal circuits regulating motor activity. Thus, our findings show that D2L and D2S share similar functions in basal conditions but not in response to stimulation of the dopamine system.

Significance Statement

Dopamine signaling modulates important physiological functions such as reward and motor activity through activation of five different receptors. Dopamine D2 receptors (D2R) are critical in the control of motor behavior. D2Rs are composed of long (D2L) and a short (D2S) isoforms, expressed both in dopamine neurons as well as in cells receiving dopaminergic afferents. Such diversity questions their individual contribution to pre-and post-synaptic events. Using isoform-specific knockout mice, we report that while either isoform can mediate the control of basal behaviors, upon pharmacological stimulation of the dopaminergic system, isoform specific functions are observed at the behavioral and cellular levels. Therapeutic strategies targeting specific D2R isoforms may present treatment for ailments caused by the activation or blockade of both isoforms.

Introduction

The dopamine (DA) D2 receptor (D2R) is a key element of the dopaminergic system. D2Rs have critical presynaptic autoreceptor functions in dopaminergic neurons that enable a finely tuned control of DA synthesis and release (Rouge-Pont et al. 2002; Schmitz et al. 2002; Bello et al. 2011; Anzalone et al. 2012). Postsynaptically, D2Rs control the signaling and firing properties of neurons receiving DA afferents and, acting as heteroreceptors, regulate the release of heterogeneous neurotransmitters (DeBoer and Abercrombie 1996; Centonze et al. 2002, 2003; Rice et al. 2011).

D2Rs are composed by two almost identical isoforms, D2L (long) and D2S (short), generated by alternative splicing of the *Drd2* gene. The search for cells expressing only one of the isoforms failed, and indeed at the mRNA level, the two isoforms are both present in each location expressing D2R (Montmayeur et al. 1991). D2L differs from D2S by the insertion of 29 amino acids in the third intracellular loop of the putative conformation of seven transmembrane domain G-protein coupled receptors family. This region is the site of the receptor's interaction with signal transduction proteins; thus, suggesting that D2L and D2S might interact and regulate different proteins and signaling pathways. In agreement with this hypothesis, we found that in the pituitary D2L-mediated signaling inhibits the AKT pathway, while D2S is instead required for the activation of the ERK pathway (Iaccarino et al. 2002; Radl et al. 2013). In addition, studies performed in cell culture suggested that D2L and D2S might be segregated in different neuronal compartments and therefore differentially respond to DA stimulation(Tirotta et al. 2008).

In the striatum, in vivo studies performed using mice lacking D2L (D2L-/-) (Usiello et al. 2000), showed that this isoform is required for the cataleptic effect of haloperidol, the prototype of typical antipsychotics, as well as for the inhibition of the AKT pathway (Beaulieu et al. 2007).

These findings together with an intact control of DA synthesis and release in D2L-/- mice, led us to propose that in vivo D2S might have a preponderant presynaptic role in DA neurons, while D2L might have postsynaptic functions (De Mei et al. 2009). However, using viral-mediated re-expression of D2L or D2S in dopaminergic neurons of D2R-/- mice, it was proposed that D2S could not operate as the exclusive autoreceptor since it was insufficient to account for drug-induced plasticity in these neurons (Gantz et al. 2015).

Thus, the question of whether endogenous D2S has equal or different functions than D2L in vivo is yet to be directly explored. Using mice with the selective deletion of individual D2R isoforms, we have been able to study the behavioral and cellular characteristics of D2L-/- with that of D2S -/- mice as compared to WT littermates. We characterized the impact of loss of either D2 isoforms on motor behavior under basal conditions and in response to pharmacological challenge with D2 agonists and antagonists. Interestingly, in striking contrast with the strong impairment of motor activity observed in the absence of D2R signaling either in the constitutive (Baik et al. 1995) or striatal medium spiny neurons (MSNs)-specific knockout (Anzalone et al. 2012), each of the D2 isoform mutants does not differ from WT littermates under basal conditions. These results indicate that the presence of either D2L or D2S is sufficient to guarantee the control of striatal neurons and normal behavior. This observation suggests also that the two isoforms can compensate for each other in MSNs and possibly other D2R expressing neurons. However, upon pharmacological stimulation either by D2 specific ligands or by cocaine, we observed different responses between isoform specific mutants and a strong degree of specialization in the response of each isoform to pre- and post-synaptic functions.

Therapeutics targeting a selective isoform might constitute an effective strategy to treat D2L- or D2S-specific alterations and alleviate side effects due to activation/blockade of both isoforms.

Results

Absence of D2S does not affect D2L expression and number of sites in the striatum.

D2S-/- mice were generated by removal of the exon 6 and flanking introns and replacement of this region with a fragment of the D2L cDNA (Radl et al. 2013). To assess whether the absence of D2S would affect D2L expression in the striatum, we performed RT-PCR analyses of striatal mRNAs. Analyses of PCR products show the presence of bands corresponding to both D2R isoforms in WT striata, while the selective expression of either only D2L (245 base pairs (bp) band) or of only D2S (158 bp) was observed in samples from D2S-/- and D2L-/- striata, respectively (Fig. 1A). Quantification by qRT-PCR of the overall expression levels of the *Drd2* gene in the striatum of WT, D2S-/- and D2L-/- mice showed similar levels of D2R mRNA expression in all genotypes (Fig. 1B). To get information at the protein level, we analyzed the pharmacological characteristics of the D2 binding sites in D2S-/- striatal extracts using ^{3}H-spiperone; also at this level D2S-/- did not differ from their WT littermates (Fig. 1C). These results indicate that in D2S-/- mice there is a complete transition from the expression of the two isoforms into a single one, in this case D2L, maintaining however intact the total number of D2 binding sites as in WT striata (Fig. 1C), as also previously reported in D2L-/- mice (Usiello et al. 2000).

The basal motor activity of D2S-/- does not differ from that of D2L-/- or of WT littermates

In the striatum, D2Rs are expressed by the medium spiny neurons that form the indirect pathway (iMSNs) (Delle Donne et al. 1997). We have shown that D2R-mediated signaling in iMSNs is essential in the control of motor behavior, as demonstrated by analyses performed using conditional iMSN-D2RKO mice (Anzalone et al. 2012) that perfectly recapitulate the motor phenotype of the constitutive D2R-/- mutants (Baik et al. 1995). In agreement with the importance of D2R signaling in iMSNs for motor activity, D2R ablation either in dopaminergic neurons (DA-D2RKO mice) (Anzalone et al. 2012) or in striatal cholinergic interneurons (ChI-D2RKO mice) (Kharkwal et al. 2016a) does not affect the basal locomotor activity. Importantly, absence of D2L in D2L-/- mice did not result into motor abnormalities in basal conditions (Usiello et al. 2000; Wang et al. 2000). To assess whether D2S is principally involved in the control of motor behavior, we analyzed and compared the forward locomotion of D2S-/- mice in a novel home cage (NHC) to that of D2L-/- mice and WT littermates. Interestingly, these analyses show that absence of D2S in mice does not affect basal locomotor activity; indeed, D2S-/- mice behaved similarly to WT and D2L-/- mice ($F_{(2,\ 25)}$=1.583; p=0.2253) (Fig. 2A). The analysis of stereotypies (rearing and grooming) in the three groups also suggests that the removal of either D2L or D2S does not affect these behaviors (Fig. 2B) (grooming: $F_{(2,\ 26)}$=0.78 p=0.46; rearing: $F_{(2,\ 28)}$=0.018 p=0.98). In addition, forward locomotion either during the light/dark cycle (Fig. 2C) (time x genotype: $F_{(2,\ 22)}$=0.22, p=0.8) or in the open field (Fig. 2D) ($F_{(2,\ 27)}$=1.102, p=0.34) does not differ between WT and D2S-/- or D2L-/- mice.

These results show that D2S-/- mice perform as WT littermates indicating that, in contrast to D2R-/- or iMSN-D2RKO mice, the presence of either D2L or D2S is sufficient to maintain a normal control of motor activity.

Absence of D2S affects D2 autoreceptor-mediated functions

Next, we analyzed the presynaptic versus postsynaptic functions of the D2 isoforms in response to pharmacological stimulations. The administration of low doses of quinpirole (a specific D2R agonist) activates D2 autoreceptors in DA neurons reducing DA release and consequently motor activity (Usiello et al. 2000). Thus, we performed a dose-response analysis of quinpirole and analyzed the effects on forward locomotion comparing D2S-/-, D2L-/- and their WT littermates. Mice of the three genotypes were administered (i.p.) quinpirole at 0.02, 0.04, 0.08 and 0.2 mg/kg (Fig. 3A). Interestingly, the results of these experiments revealed a statistically significant difference in the effects elicited by quinpirole in D2S-/- as compared to WT and D2L-/- mice (Fig. 3A) (genotype x treatment: $F_{(8, 136)}=2.508$ $p<0.01$; genotype: $F_{(2, 136)}=10.81$ $p<0.0001$; treatment: $F_{(4, 136)}= 64.35$ $p<0.0001$). The most relevant difference was observed at the lowest dose (0.02 mg/kg) tested. At this dose quinpirole was ineffective in decreasing motor activity in D2S-/- mice while it did in the other genotypes. The different responses of D2S-/- mice as compared to WT and D2L-/- mice at low concentration of quinpirole support previous conclusions of a specific role of D2S as presynaptic receptor in DA neurons (Usiello et al. 2000).

To further assess this point, we tested the level of phosphorylation of tyrosine hydroxylase (TH) in D2 mutants and their WT siblings (Fig. 3B). TH is the rate-limiting enzyme in DA synthesis; its activity is regulated by activation of the cAMP/PKA pathway through phosphorylation of the serine 40 (Ser40) (Lindgren et al. 2001). Activation of D2Rs inhibits the cAMP pathway and reduces Ser40 phosphorylation (Anzalone et al. 2012). Thus, Ser40 TH phosphorylation (p-TH) was analyzed in D2S-/-, D2L-/- and WT littermates at the lowest and highest dose of quinpirole used (0.02 and 0.2 mg/kg) in behavioral studies. Mice of the three

genotypes were administered either quinpirole or saline and euthanized 30 min later. Striatal tissue punches were obtained from the dorsal striatum (DS). While efficiently decreasing TH phosphorylation in WT and D2L-/- mice, our analyses showed that quinpirole at both doses were unable to elicit a decrease in TH phosphorylation in D2S-/- mice (Fig. 3B) (DS, genotype x treatment: $F_{(4, 28)}$=2.589; p=0.0584). Similar results were obtained analyzing tissue punches from the ventral striatum (VS) (Fig. S1) (genotype x treatment: $F_{(4, 29)}$=3.603; p=0.0167).

These results indicate that the presynaptic effect of D2R on DA synthesis in dopaminergic neurons is mostly exerted by D2S. Postsynaptic effects might explain the similar motor response of D2S-/- mice to the other genotypes at higher quinpirole concentrations (Fig. 3A).

The D2R-mediated postsynaptic signaling in striatal neurons primarily requires D2L

Administration of haloperidol, a D2R antagonist, reduces mouse locomotor activity in a dose-dependent manner and leads to catalepsy or inability to perform voluntary movements. We tested haloperidol effects on both parameters by analyzing motor activity in a NHC for 1 hr and subsequently the mice performance in the bar test. The results of these tests showed that while motor activity was similarly impaired by haloperidol in all genotypes (treatment: $F_{(2, 91)}$=92.71, p<0.0001; genotype: $F_{(2, 91)}$=1.057, p=0.3517) (Fig. 3C), catalepsy was only observed in WT and D2S-/- mice, but not in D2L-/- mice (genotype x treatment: $F_{(4, 84)}$=14.45, p<0.0001), as previously reported (Usiello et al. 2000) (Fig. 3D). Thus, absence of D2S does not affect the response to haloperidol, further confirming the significant postsynaptic role of D2L in striatal neurons.

Heterosynaptic role of D2L in cocaine-evoked motor activity

We and others have recently reported a critical role of iMSNs in the psychomotor response to cocaine (Dobbs et al. 2016; Kharkwal et al. 2016b). Indeed, absence of D2R in iMSNs abolishes the cocaine-dependent induction of both motor activity and the immediate early gene (c-*fos*) expression in the MSNs of the direct pathway expressing D1R (dMSNs). Thus, stimulation of D2R enables dMSNs mediated responses to cocaine. D2R in striatal neurons has a heterosynaptic role that governs the release of heterogeneous neurotransmitters such as GABA from iMSNs (Centonze et al. 2004). Previous experiments showed that the cocaine phenotype of iMSN-D2RKO mice could be reversed by intrastriatal injections of bicuculline, a $GABA_A$ receptor antagonist, suggesting a heterosynaptic role of D2R in iMSNs.

To gain further insight into the respective role of the D2R isoforms as heteroreceptors, we investigated the impact of absence of D2S or D2L signaling on cocaine-mediated behavioral and cellular responses. Upon habituation to a NHC, WT, D2S-/- and D2L-/- mice were administered either saline or cocaine (10 mg/kg and 20 mg/kg) and their locomotion recorded for the following hour. Interestingly, while WT and D2S-/- mice showed a similar significant motor response to cocaine, D2L-/- mice did not (genotype x treatment: $F_{(4, 78)}=2.93$, $p=0.02$; treatment: $F_{(2, 78)}=32.62$, $p<0.0001$; genotype: $F_{(2, 78)}=7.99$, $p<0.001$) (Fig. 4A) These results show that absence of D2L strongly impairs the response to cocaine, indicating a preponderant role of D2L in enabling the dMSNs-mediated motor response to the drug.

Analyses of cocaine (20 mg/kg)-mediated c-*fos* induction in WT, D2S-/- and D2L-/- mice showed the expected c-*fos* expression in dMSNs in WT and D2S-/- mice, but not in D2L-/- mice (genotype x treatment: $F_{(2, 14)}=8.99$, $p=0.003$) (Fig 4B), suggesting a critical role of the D2L isoform as heterosynaptic receptors in iMSNs.

Bicuculline reestablishes the motor and cellular response to cocaine of D2L-/- mice

Intrastriatal injection of bicuculline, a $GABA_A$ receptor antagonist, is able to restore cocaine mediated c-*fos* induction in iMSN-D2RKO mice to WT levels. Accordingly, we tested whether a similar effect would also be obtained in the striatum of bicuculline injected D2L-/- mice. For this purpose, cannulas were implanted in the DS of D2L-/- and WT littermates, followed one week later by the administration of either saline or bicuculline (0.01μg/0.3μl/side). Cocaine was given systemically 5 min after bicuculline or saline administration. Brains were collected 1 hr after cocaine and c-*fos* induction quantified by immunofluorescence analyses. Bicuculline alone did not induce c-*fos* expression in either genotype (Fig. 5A). Importantly, when administered before cocaine, bicuculline fully restored c-*fos* induction in the dMSNs of D2L-/- mice to WT levels (Fig. 5B), as compared to D2L-/- only treated with cocaine (genotype x treatment: $F_{(3, 21)} = 7.894$; $p=0.001$) (Fig. 5B). These results support a heterosynaptic role of D2L in the control of cocaine-mediated effects.

Discussion

The presence of two almost identical receptors for D2R, D2L and D2S, which differ only in the presence of an additional small stretch of 29 amino acids in D2L, has generated interest in unraveling the biological significance of such diversity in vivo. Studies performed in cultured cells have shown that both isoforms have similar affinity for dopamine and canonical signaling pathways (De Mei et al. 2009). To analyze the role and properties of the D2 isoforms in vivo, we have generated D2L and D2S isoform-specific mutants, either by removing exon 6 (D2L-/- mice;(Usiello et al. 2000)) or by replacing the genomic sequence containing exon 5, 6 and 7 with the cDNA of the corresponding region of D2L (D2S-/- mice; (Radl et al. 2013)). D2L-/- and D2S-/- mice express a similar number of D2 receptors binding sites as WT mice, although formed by only one isoform instead than two. Studies performed in the pituitary gland of D2L-/- and D2S-/- mice, showed that D2L and D2S signaling differentially affects the ERK and AKT pathways (Radl et al. 2013). These results suggest that in vivo D2L and D2S might play different roles in the striatum, where D2Rs are largely expressed by iMSNs (Delle Donne et al. 1997) and cholinergic interneurons (Kharkwal et al. 2016a). Absence of striatal D2R affects motor outputs (Anzalone et al. 2012; Dobbs et al. 2016; Kharkwal et al. 2016b), though we found that the presence either D2L or D2S is sufficient to insure a normal basal motor activity. This experimental evidence indicates that D2L and D2S share common basal signaling essential to various critical functions, however the presence of compensatory mechanisms in each of the isoform-specific knockout animals cannot be excluded.

Nevertheless, compensatory mechanisms seem less likely as the response of the two mutants is different when either receptor is challenged by D2 specific drugs. Indeed, when D2L-/- and D2S-/- mice are challenged with D2 specific agonists or antagonists, we observed some

relevant differences. Administration of quinpirole, a D2-specific agonist, at low doses induces a decrease of motor activity. This effect depends on activation of presynaptic dopamine autoreceptors and the consequent reduction of DA release and activation of postsynaptic receptors. Interestingly, the lowest dose of quinpirole in D2S-/- mice was totally ineffective in reducing motor activity as compared to the effect in WT and D2L-/- mice. These results suggest that autoreceptors functions are compromised by absence of D2S. In support of this conclusion, we observed that the D2-mediated inhibition of TH phosphorylation on Ser40 is prevented by absence of D2S in quinpirole treated D2S-/-, but not in WT or D2L-/- mice. Interestingly, TH phosphorylation in D2S-/- mice was not inhibited even at quinpirole concentrations that induced a reduction of motor activity in mice of all genotypes by acting on postsynaptic receptors. These results strongly support the view that D2S has major presynaptic functions as compared to D2L.
In contrast, absence of D2S does not interfere with haloperidol-induced catalepsy. Indeed, by difference with D2L-/- mice (Fig. 3D) (Usiello et al. 2000), D2S-/- and WT mice showed a dose-dependent cataleptic response to haloperidol.

The different responses of D2L-/- and D2S-/- mice to quinpirole or haloperidol raise the questions of whether differences arise from the higher affinity for either D2L or D2S of these drugs or from unique isoform-mediated signaling in specific cell-types upon pharmacological challenge. Although we cannot exclude slight pharmacological differences of either D2S or D2L for D2 ligands, as previously observed using cell lines (Castro and Strange 1993), we are more in favor the second hypothesis. Indeed, despite the slight difference on motor behavior between D2S and D2L mutants at low quinpirole concentration, a clear D2S-mediated cell-specific effect on the inhibition of TH phosphorylation is observed at any dose tested. Haloperidol, while similarly

affecting horizontal locomotion, is not able to induce catalepsy in D2L-/- mice, suggesting similar affinity for both isoforms.

Interestingly, we have recently shown that absence of D2R-mediated control of cholinergic interneurons abolishes haloperidol-induced catalepsy through a mechanism involving acetylcholine stimulation of iMSNs (Kharkwal et al. 2016a). Thus suggesting that the haloperidol effect is due to the absence of D2L signaling, which either plays a critical role in the regulation of acetylcholine in cholinergic interneurons or in the control of iMSNs responses or in both. Future studies should be aimed at generating mouse lines with a striatal cell-specific deletion of D2L to assess these possibilities.

Importantly, the response to acute cocaine challenges of D2S-/- and D2L-/- mice with respect to WT animals was also different. Indeed, while D2S-/- mice showed a dose-dependent increase of motor activity in response to cocaine (paralleling WT mice), D2L-/- mice did not. Interestingly, also c-*fos* induction by cocaine was absent in D2L-/- as compared to D2S-/- and WT littermates. The blunted response to cocaine of D2L-/- mice is reminiscent of that of D2RKO and iMSN-D2RKO mice (Welter et al. 2007; Kharkwal et al. 2016b) and suggests that absence of D2L in iMSNs might be responsible for it. This suggestion is supported by the rescue of the motor and cellular responses to cocaine induced by the intracellular injection of bicuculline, as previously shown in D2RKO and iMSN-D2RKO mice (Kharkwal et al. 2016b). In conclusion, our findings assign to D2L a critical role in the response to drugs of abuse (possibly mediated by absence of D2L signaling in iMSNs). Therefore, the analysis of D2 isoform-specific knockout mice (see scheme in Fig. 5C) shows a clear impact of D2S as presynaptic autoreceptor on dopaminergic neurons. Conversely, D2L appears to possess postsynaptic functions responsible for the regulation of striatal acetylcholine and activity of iMSNs.

Materials and Methods

Mice: The D2S-/- mouse line was generated by a knock-in strategy aimed at preventing alternative splicing of exon 6, through replacement of the *Drd2* genomic region containing part of exon 5, exon 6 and part of exon 7 with the corresponding cDNA of D2L; thus, allowing the synthesis of only D2L in vivo (27). The D2L-/- mouse line was generated by the replacement of exon 6 with a neomycin cassette, thus generating mice expressing only D2S (13). 8-12 week old D2L-/- (13), D2S-/- (11) and WT littermates were used. Mice were maintained in standard conditions (12 hr light/dark cycle) with food and water *ad libitum*. For genotyping D2S-/-, D2L-/- and WT littermates, genomic DNA was extracted from tail biopsies and analyzed by PCR, as previously described (11). All protocols were approved by the Institutional Animal Care and Use Committee in accordance with the NIH guidelines.

Drugs: Quinpirole (Sigma), cocaine hydrochloride (Sigma) and bicuculline methiodide (Fluka) were dissolved in saline (0.9% NaCl). Haloperidol (Sigma) was dissolved in a drop of glacial acetic acid; pH was adjusted to 6 and the solution brought to volume with saline (13).

RNA extraction and PCR: Total RNA was extracted from the striatum using TRIzol (Invitrogen). 1µg of total RNA was retro-transcribed using the iScript cDNA Synthesis kit (Bio-Rad). qRT-PCR were performed on striatal cDNAs to quantify D2R expression using the iQ SYBR Green Supermix (BIO-RAD) and the CFX96 Real-Time System (Bio-Rad). GAPDH was used as internal control. The following primers were used: D2R forward (5'-AGTGGCCCCACTGCCCCAAT-3') and reverse (5'-TCCAGATAGACGACCCAGGGC-3'); GAPDH forward (5'-

AGGTCGGTGTGAACGGATTTG-3') and reverse (5'-TGTAGACCATGTAGTTGAGGTCA-3'). qRT-PCR were run for 40 cycles, 10 seconds at 95°C followed by 30 sec at 60°C.

We also performed RT-PCR followed by analyses of the PCR products on 2% agarose gel (Fig.1A). PCR buffer contained 4 mM $MgCl_2$, 0.2 mM of each dNTP 2 µl Taq DNA polymerase (1U/□l) and 0.8 µM of the following primers: D2R forward (exon 5), 5'-CCTTCATCGTCACCCTGCTGG-3' and reverse (exon 7), 5'-CTCCATTTCCAGCTCCTGAG-3'. Cycles were: 94°C for 3 min, and 40 cycles of 40 sec at 94°C, 40 sec at 57°C and 1 min at 72 °C, with a final extension period of 10 min at 72 °C.

Binding analyses: Striatal membranes and ligand binding analyses for D2S-/- and WT mice were performed as previously described (13, 17). 20 µg of membrane extracts per sample were used in binding assays using ^{3}H-Spiperone (84.8 Ci/mmol, Perkin Elmer) at concentrations ranging from 0.01 to 0.6 nM; non-specific binding was determined in the presence of 1.3 µM (±) butaclamol. Binding assays were performed in triplicates and repeated three times. Results were analyzed with GraphPad Prism 6.

Behavioral analyses: To analyze motor behavior, mice were handled (5 min/day) for 2 days and basal locomotor activity in the new home cage (NHC, 20 x 30 cm transparent plastic box, 1 hr) or open field (white square box, 30 × 30 cm; 70 lux, 30 min) was recorded using a video-tracking system (Viewpoint, Lyon France). Rearing and grooming were measured in NHC and scored for 60 sec every 10 min for 1 hr period. Activity during 24 hr was measured in an actimetric rack (individual cages 10 x 20 cm, Viewpoint, Lyon France). The effect of quinpirole (0.02 to 0.2 mg/kg, i.p.) and haloperidol (0.1 to 0.25 mg/kg, i.p.) on locomotor activity was measured for 30

min or 1 hr respectively in the NHC. Cocaine effect was tested for 1 hr, after 2 hr habituation to the NHC.

Bar test: The bar test was performed as previously described (2), 1 hr after haloperidol administration. The time spent immobile (cutoff 120 sec.) was measured during 3 consecutive trials (13, 28). The average of the three trials was used for the statistical analyses.

Western Blot analyses: Mice were sacrificed 30 min after saline or quinpirole (0.02 and 0.2 mg/kg) administration and processed as previously described (2). Protein content was determined using the BCA kit (Thermo). 30 µg of extracts were loaded onto 10% SDS-PAGE and transferred to nitrocellulose membranes (Biorad). Antibodies directed against phosphorylated TH-Ser40 (1/1000 Millipore) followed by the appropriate secondary antibodies were used. Bands were revealed using the ECL Plus reagent (Millipore). Actin was used as control of loaded quantities (anti-actin antibody 1/5000; Millipore). Quantifications were done using ImageJ (version 1.42q) software. The value of the pTH/actin ratio obtained in WT saline treated mice was arbitrarily set to 1.

Immunofluorescence: Mice were anesthetized with Euthasol and transcardially perfused with 4% PFA. 30 µm vibratome coronal striatal sections were used for immunofluorescence experiments to detect c-fos induction by cocaine. Tissue sections were washed 3 times in PBS, permeabilized for 15 min in PBS with 0.5% Triton X-100, incubated in PBS with 5% horse serum (HS) for 1 hr at room temperature followed by incubations using c-fos antibody (1/2000, Santa Cruz) in PBS 1% HS over night at 4°C. Sections were rinsed 3 times in PBS for 10 min. Secondary antibodies were incubated for 1 hr in PBS 1% HS. c-fos positive neurons were quantified in the DS in 387.5 x

387.5 µm regions of interest from 3-4 mice/treatment/genotype.

Statistical Analyses: All values are mean ± SEM. Statistical analyses were made using GraphPad Prism 6 (La Jolla California USA). Data were analyzed by Two-way ANOVA followed by Bonferroni's post-hoc or Student's t-test, as appropriate; $p<0.05$ was considered statistically significant.

Figure Legends

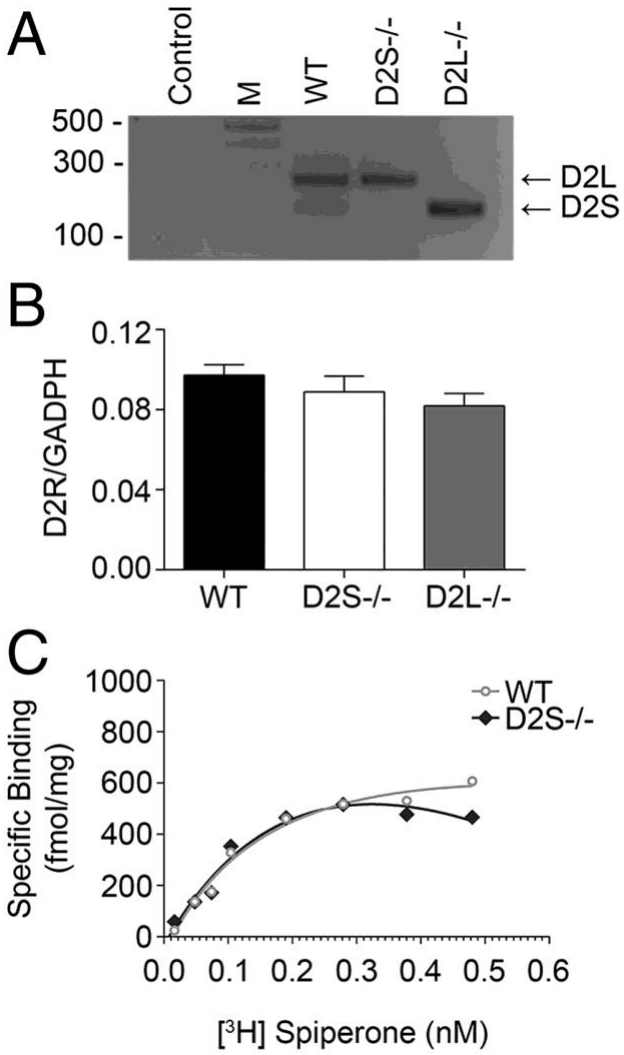

Figure 1. Characterization of D2S-/- mice. A) RT-PCR analyses of D2R expression in striatal mRNAs from WT, D2S−/− and D2L−/− mice. The upper band (245 bp) corresponds to D2L whereas the lower (158 bp) to D2S, as indicated by arrows. **B)** qRT-PCR based quantifications of D2R expression in striatal extracts of WT, D2S−/−, and D2L−/− mice, using primers common to both isoforms (exon 2), using GAPDH as control. Bars are mean ± SEM of D2R/GAPDH ratios (n=4/genotype). **C)** Saturation isotherm analyses for binding of the D2R antagonist [^{3}H]-Spiperone to striatal membranes from WT (●) (Bmax = 720 ± 85 fmol/mg protein; Kd = 30 ± 2 pM) and D2S-/- mice (◆) (Bmax = 600 ± 67 fmol/mg protein; Kd = 28 ± 1 pM)(n=3/genotype).

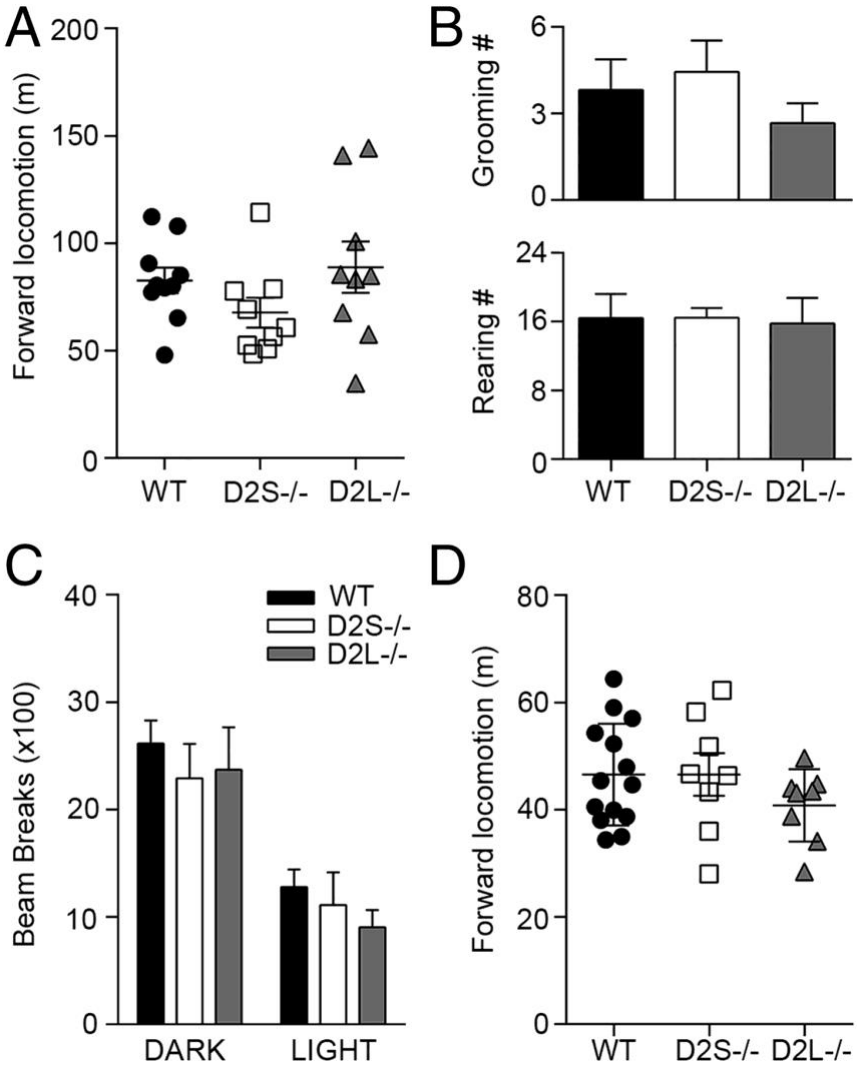

Figure 2. Basal motor activity is unaffected by deletion of either D2L or D2S. A) Scatter plot representation of WT, D2S-/- and D2L-/- motor activity during 1 hr in NHC (n=9-10/genotype) ($F_{(2, 25)}$=1.583; p=0.2253). **B)** Quantification of grooming or rearing activity during 1 hr in NHC (n=9-13/genotype) ($F_{(2, 26)}$=0.78 p=0.46; and $F_{(2, 28)}$=0.018 p=0.98 for grooming and rearing, respectively). **C)** Motor activity in actimetric cages during the dark/light cycle (n=6-14/genotype) ($F_{(2, 22)}$=0.22, p=0.8). D) Scatter plot representation of motor activity in the open field of WT, D2L-/- and D2S-/- mice during 30 min (n=8-13/genotype) ($F_{(2, 27)}$=1.102, p=0.34). Values are mean ± SEM.

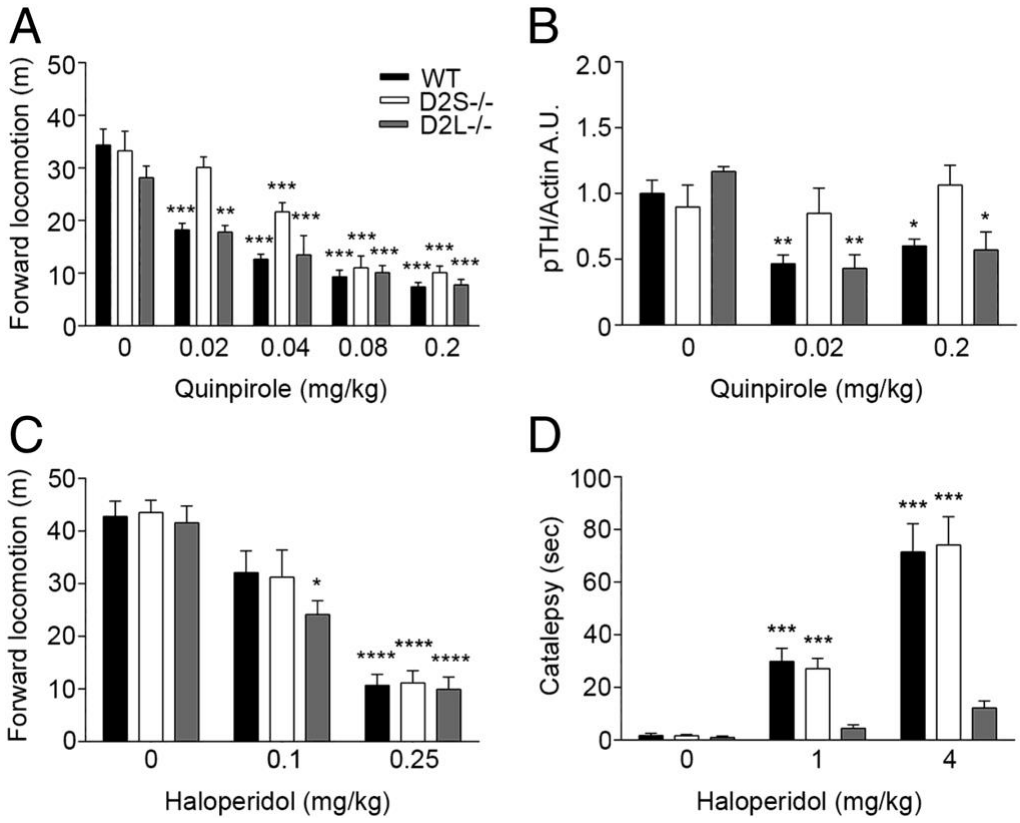

Figure 3. Locomotor activity induced by quinpirole and haloperidol. A) Quinpirole effect on locomotor activity in WT, D2S-/- and D2L-/- mice (genotype: $F_{(2, 136)}$=10.81 p<0.0001) **p<0.01, ***p<0.001 vs saline treated mice. **B)** Quantifications of western blot analyses of TH phosphorylation on Ser40 in protein extracts from the DS of WT, D2S-/- and D2L-/- mice injected with saline or 0.02 and 0.2 mg/kg of quinpirole. Two-way ANOVA, genotype x treatment: $F_{(4, 28)}$ = 2.589; p=0.0584, n=3-5 samples/treatment/genotype. *p<0.05, **p<0.01, vs saline treated mice. **C)** Motor activity recorded for 1 hr in NHC of WT, D2S-/- and D2L-/- mice injected with either saline or haloperidol (0.1, 0.25 mg/kg). Two-way ANOVA, treatment: $F_{(2, 91)}$=92.71, p<0.0001; genotype: $F_{(2, 91)}$= 1.057, p=0.3517, n=7-16. *p<0.05, ****p<0.0001 vs saline treated mice. **D)** Quantification of the cataleptic behavior upon saline or haloperidol (1 and 4 mg/kg) treatment in WT, D2S-/- and D2L-/- mice. Two-way ANOVA, genotype x treatment: $F_{(4, 84)}$=14.45, p<0.0001, n=7-15. ***p<0.001 vs saline treated mice.

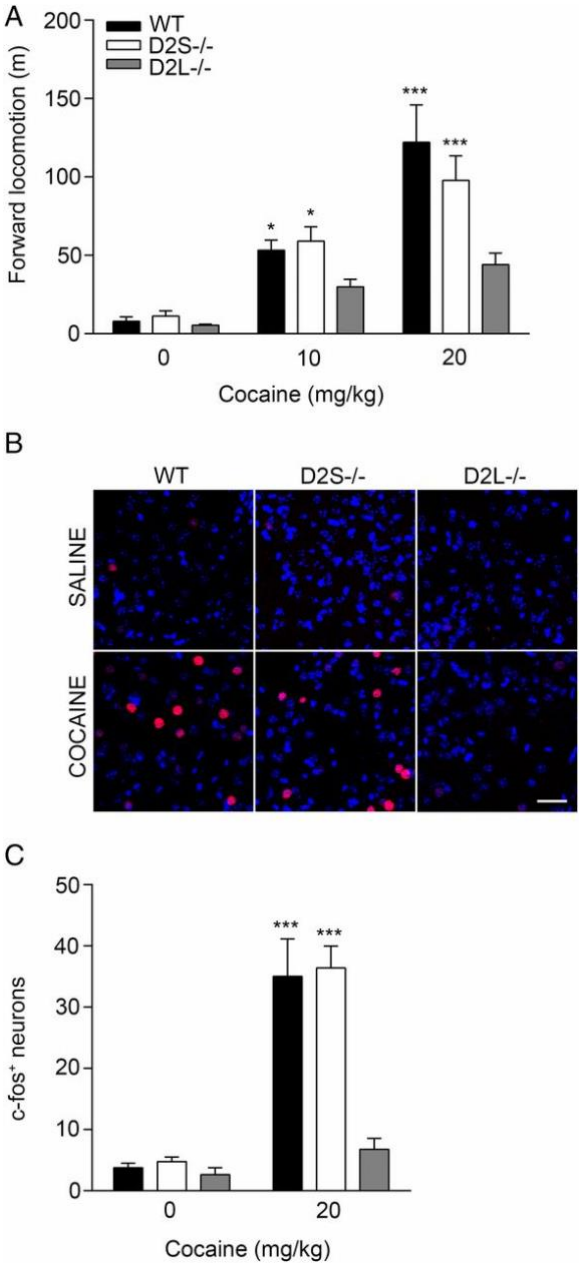

Figure 4. Different motor and cellular responses to cocaine in D2 isoform mutants. A) Motor activity in NHC of WT, D2S-/- and D2L-/- mice administered either saline or cocaine (10 and 20 mg/kg) recorded for 1 hr. Two-way ANOVA, genotype x treatment: $F_{(4, 78)}$=2.93, p=0.02, n=7-14 mice/treatment/genotype.*p<0.05, ***p<0.001 vs saline treated mice. **B)** Representative images of immunofluorescence analyses using anti c-*fos* antibodies (red) and Draq7 labelled nuclei (blue) in the DS of WT, D2S-/- and D2L-/- mice following saline or cocaine treatment (20mg/kg), as indicated. Scale bar: 30 µm. **C)** Quantifications of the number of c-*fos* positive neurons in same experiments. Values are mean±SEM of c-*fos*$^+$ neurons/region of interest (385.7 x 385.7 µm). Two-way ANOVA, genotype: $F_{(2, 14)}$=11.30, p=0.0012 genotype x treatment: $F_{(2, 14)}$=8.99, p=0.003, n=3-4 mice/treatment/genotype). ***p<0.001 vs saline treated mice.

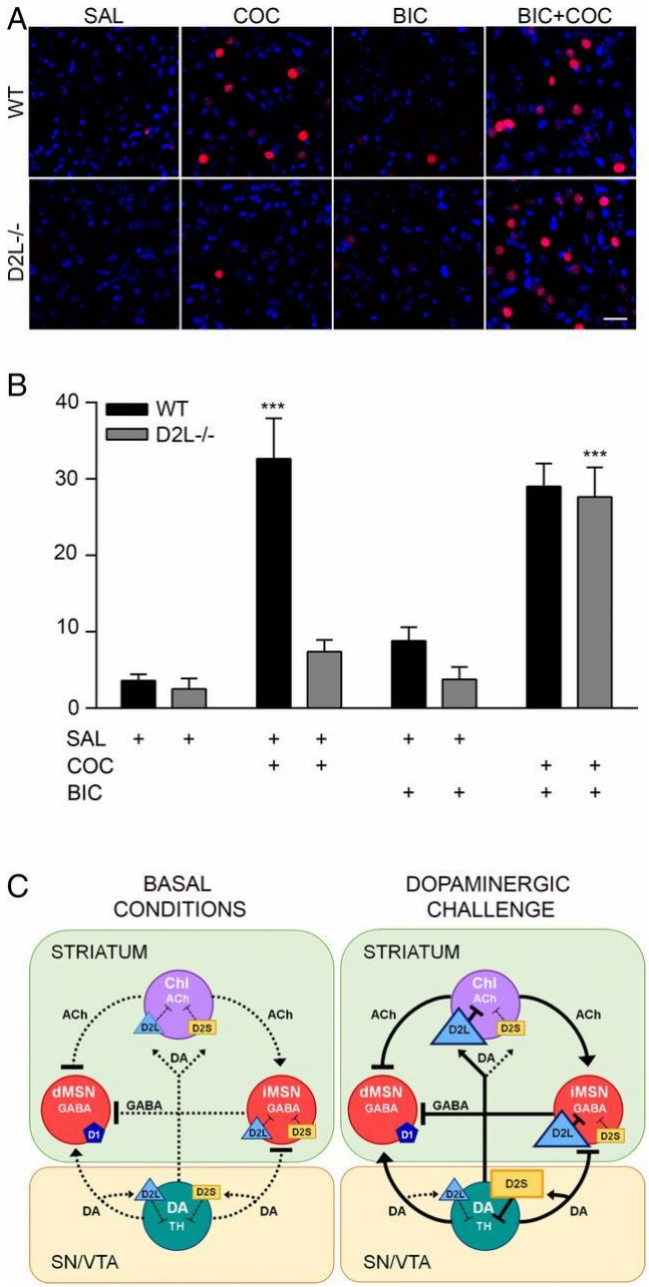

Figure 5. Bicuculline treatment restores cocaine-mediated c-fos induction in D2L-/- mice. A) Representative images of immunofluorescent analyses using c-*fos* antibodies (red) and Draq7 (blue) labeled nuclei on striatal sections from WT and D2L-/- mice following saline (SAL) or cocaine (COC) (20 mg/kg, i.p.) or bicuculline (BIC i.c.) or bicuculline plus cocaine (BIC+COC) treatments as indicated. Scale bar: 30 µm. **B)** Quantifications of the number of c-*fos* $^{+}$ cells/region of interest of the experiments shown in A. Values are mean ±SEM. Two-way ANOVA, genotype: $F_{(1,\ 21)}$=11.48, p=0.0028; genotype x treatment: $F_{(3,\ 21)}$ = 7.894; p=0.001, n=3 mice/treatment/genotype). ***p<0.001vs WT or D2L -/- saline treated mice. **C)** Schematic representation of the findings obtained by the analysis of D2L-/- and D2S-/- mice. Collectively, our data suggest that under basal conditions, signaling from either D2R isoforms is sufficient to control D2-mediated functions (i.e. presynaptic control of DA synthesis and postsynaptic ACh and

GABA release) as shown by the normal motor behavior (Left panel: Basal Conditions). However, upon dopaminergic challenge, while D2S signaling in DA neurons is critical for the inhibition of TH phosphorylation and DA synthesis, D2L signaling appears required for the inhibition of iMSNs collaterals to dMSNs, which is critically involved in the psychomotor response to cocaine (22, 23) as well as c-fos induction (22)(Right panel: Dopaminergic Challenge). The preferential presynaptic and postsynaptic involvement of D2S and D2L, respectively, upon challenge is indicated by the enlargement of the rectangle (D2S) or triangle (D2L). The dashed lines represent the basal striatal tone of neurotransmitters while the solid line the striatal tone upon dopaminergic stimulation.

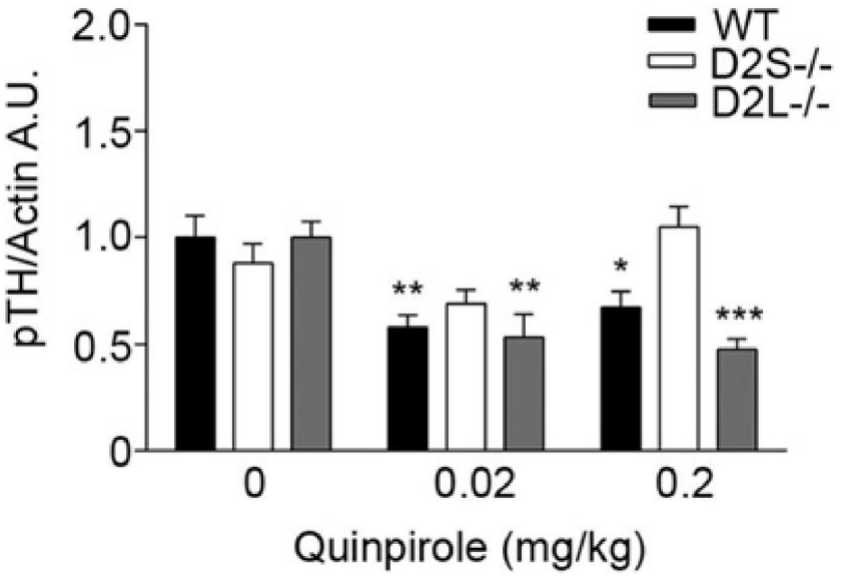

Figure S1. TH phosphorylation levels upon quinpirole challenge. Quantifications of western blot analyses of TH phosphorylation on Ser40 in protein extracts from the ventral striatum (VS) of WT, D2S-/- and D2L-/- mice injected with saline, 0.02 and 0.2 mg/kg of quinpirole. Two-way ANOVA, genotype x treatment: $F_{(4, 29)}=3.603$; $p=0.0167$, n=3-5 samples/treatment/genotype. *$p<0.05$, **$p<0.01$, vs saline treated mice.

Chapter 3: Cocaine-mediated circadian reprogramming in the striatum through dopamine D2R and PPARγ activation

Abstract

Substance abuse disorders are linked to alteration of circadian rhythms, although the molecular and neuronal pathways implicated have not been fully elucidated. Addictive drugs, such as cocaine, induce a rapid increase of dopamine levels in the brain. Here we show that acute administration of cocaine triggers reprogramming in circadian gene expression in the striatum, an area involved in psychomotor and rewarding effects of drugs. This process involves the activation of peroxisome protein activator receptor gamma (PPARγ), a nuclear receptor involved in inflammatory responses. PPARγ reprogramming is altered in mice with cell-specific ablation of the dopamine D2 receptor (D2R) in the striatal medium spiny neurons (MSNs) (iMSN-D2RKO). Administration of a specific PPARγ agonist in iMSN-D2RKO mice elicits substantial rescue of cocaine-dependent control of circadian genes. These findings have potential implications for development of strategies to treat substance abuse disorders.

Introduction

A variety of fundamental biological processes, ranging from the sleep-wake cycle and metabolism, to immune responses and behavior, is regulated by the circadian clock (Green et al. 2008; Scheiermann et al. 2013). In mammals, the central clock is located in the suprachiasmatic nucleus (SCN) within the hypothalamus that is entrained by light as an external *zeitgeber* (time-giver) (Welsh et al. 2010). As master regulator of organismal circadian rhythms, the SCN is thought to orchestrate the phase of oscillation of extra-SCN clocks (Albrecht 2012). Peripheral clocks are present in virtually all organs and cells within the body and recent findings have revealed that clocks communicate in order to achieve systemic homeostasis (Bass and Lazar 2016; Dyar et al. 2018). Diverse environmental cues, such as feeding behavior, also act as robust *zeitgebers* for peripheral clocks in metabolic tissues through mechanisms that appear SCN-independent (Asher and Sassone-Corsi 2015; Panda 2016). From a molecular standpoint, the circadian clock drives oscillations in expression of a large number of genes through transcriptional-translational feedback loops composed of cycling activators and inhibitors (Partch et al. 2014).

Drugs of abuse have been shown to induce severe perturbation of circadian rhythms (Iijima et al. 2002; Mohawk et al. 2012; Gallardo et al. 2014), such as disruption of the sleep/wake cycle, eating habits, blood pressure, hormone secretion and body temperature (Hasler et al. 2012; Logan et al. 2014). Importantly, desynchronization of circadian rhythms has been linked to the switch from recreational consumption to addictive behavior (Korpi et al. 2015). Cocaine, as well as other psychoactive drugs, affects the function of brain circuits such as the basal ganglia by increasing neurotransmitter release to the medium spiny neurons (MSNs), which are the principle striatal neurons and the striatum's only output neurons. This is the case for cocaine-mediated activation of dopamine (DA) signaling in MSNs that leads to long-term adaptations of cellular programs and behavioral responses (Di Chiara and Bassareo 2007; Girault 2012). Importantly, there are

indications that DA signaling impacts central and peripheral circadian rhythms (McClung et al. 2005; Logan et al. 2019). In the striatum, DA levels oscillate in a circadian manner (Castañeda et al. 2004; Ferris et al. 2014) and are involved in the regulation of the neuronal circadian clock gene expression (Imbesi et al. 2009; Hood et al. 2010). To date, however, characterization of the molecular mechanisms by which drugs of abuse alter circadian rhythms in a tissue-specific manner remains incomplete.

Under physiological conditions, the endogenous clocks coordinate transcriptional and metabolic cycles in distinct organs (Asher and Sassone-Corsi 2015; Panda 2016). The capacity of peripheral clocks to be highly flexible through transcriptional and metabolic reprogramming is highlighted by experiments involving nutritional challenges such as fasting, high fat diet, ketogenic diet or caloric restriction (Ribas-Latre and Eckel-Mahan 2016; Brown 2016; Challet 2019). It is unclear whether neuronal clocks are capable of similar reprogramming. We hypothesized that the short and long-term adaptation of neuronal circuits in response to cocaine would involve changes in circadian rhythmicity within the ventral striatum and in particular the Nucleus Accumbens (NAcc).

Our recent findings show that D2R-mediated signaling in MSNs critically modulates striatal responses to cocaine (Kharkwal et al. 2016b; Radl et al. 2018). These results indicate that D2R signaling plays a critical role in the mechanisms by which drugs of abuse affect striatal physiological responses. Thus, we explored how the circadian program of striatal neurons is influenced by acute administration of cocaine in WT mice and in mutants with D2R ablation exclusively in D2R-expressing MSNs (iMSN-D2RKO mice)(Anzalone et al. 2012; Kharkwal et al. 2016b). Our results show that cocaine induces a drastic reprogramming of the diurnal transcriptome in the NAcc. There is a remarkable difference in the number, type and cycling

profiles of cocaine-driven oscillatory genes in iMSN-D2RKO mice. Using combined metabolomic and transcriptomic approaches, we show that D2R in iMSNs contributes to cocaine-induced activation of peroxisome protein activator receptor gamma (PPARγ) a nuclear receptor implicated in inflammatory responses (Kliewer et al. 1994; Khan et al. 2019). PPARγ drives a significant fraction of *de novo* cocaine-induced transcriptional response, which is impaired in the absence of D2R signaling in iMSNs. Pharmacological activation of PPARγ by pioglitazone[32] in iMSN-D2RKO mice leads to restoration of the cocaine-induced profile of circadian gene expression. Our findings unveil a D2R signaling- PPARγ connection in circadian regulation linked to cocaine-mediated rewiring in striatal neurons.

Results

Response of Core Clock Genes to Cocaine in both WT and iMSN-D2RKO Mice

We previously reported that iMSN-D2RKO mice display reduced motor activity in basal conditions (Anzalone et al. 2012) and absence of cocaine-induced hyperlocomotion (Kharkwal et al. 2016b). We sought to study the effects of cocaine in WT and iMSN-D2RKO mice by analyzing circadian motor activity along the daily cycle, four days before and four days after acute cocaine administration (Fig. 1a and 1b). Circadian motor activity was quantified as infrared beam breaks per minute at each circadian time in mice housed in home cages. Interestingly, acute cocaine does not affect the diurnal pattern of locomotor activity either in WT or iMSN-D2RKO mice, indicating that D2R deletion in iMSNs does not alter the physiology and function of the SCN central clock (Fig. 1c). Nevertheless, circadian motor activity of iMSN-D2RKO mice was decreased with respect to WT mice in the active phase before ($p<0.0001$) and after ($p=0.0004$) cocaine administration (Fig. 1d and 1e), consistent with results obtained in non-circadian behavioral

settings (Anzalone et al. 2012; Dobbs et al. 2016; Kharkwal et al. 2016b). To determine the effect of cocaine challenge on the striatal expression of clock genes, WT and iMSN-D2RKO mice received an intraperitoneal (i.p.) injection of either cocaine (Coc 20 mg kg^{-1}) or saline (Sal), shortly after the beginning of the resting phase (zeitgeber time, ZT3). Animals from both groups were sacrificed every 4 hours (n=5 or 6/time point) and tissue punches from the NAcc collected at six time points to cover the full circadian cycle (Fig. 1f). To investigate the direct effect of cocaine in the NAcc of WT and iMSN-D2RKO mice on the core-clock machinery, we analyzed the expression of *Bmal1, Cry1, Dbp* and *Per1* in saline and cocaine-treated mice (Fig. 1g). We observed a significant effect of time for all tested core-clock genes ($p \leq 0.0005$), indicating that expression of all genes follows the typical circadian cycle in both genotypes. There was no substantial alteration in the expression profiles of these clock genes upon cocaine treatment (*Bmal1*: p=0.7389; *Cry1*: p=0.7529; *Per1*: p=0.6765), as well as a clock output gene, as exemplified by *Dbp* expression profile (p=0.1495) (see Supplementary Table 1). A slight but nevertheless significant difference was found in *Per1* expression level between WT and iMSND2RKO mice (p=0.0022). Thus, acute cocaine treatment, whether in the presence or absence of D2R in iMSNs, does not alter the rhythmic expression of this group of circadian genes.

Reprogramming of the Striatal Circadian Transcriptome by Cocaine

Cocaine intake induces an increase of DA accumulation in the synaptic cleft through blockade of the DA transporter prolonging activation of postsynaptic neurons (Nestler 2005; Beuming et al. 2008). The dopaminergic mesolimbic pathway connecting the ventral tegmental area to the NAcc and cortex is critically involved in the effects of drugs of abuse (Lüscher and Malenka 2011).

To analyze the acute cocaine-dependent genome-wide rhythmicity, RNAs were extracted from NAcc punches from brains harvested every four hours throughout a full circadian cycle (Fig. 1f) and processed for RNA-seq analyses. Rhythmic transcripts were identified using the non-parametric test JTK_CYCLE (Hughes et al. 2010), an algorithm that includes Bonferroni-adjusted multiple comparisons and incorporates a window of 20-28 hours for the determination of diurnal periodicity. Out of a combined 2314 cycling transcripts identified, 1157 (50%) were rhythmic only in the saline condition. An additional 294 (~13%) were cycling in both saline- and cocaine-treated mice and, notably, 863 (~37%) *de novo* oscillating transcripts were identified upon cocaine challenge (Fig. 2a). The phases of oscillation of genes diurnal in both conditions were similar (Fig. 2b and 2c). The newly cocaine-induced oscillating transcripts display a peak at around ZT7, which is absent in saline condition. Moreover, 13% of the common oscillating genes showed a decrease in amplitude, while 35% displayed an increase upon cocaine treatment with respect to saline conditions (Fig. 2d). Thus, the circadian program of cycling genes in the NAcc is profoundly modified upon acute cocaine administration.

Pathway analyses were performed using Database for Annotation, Visualization and Integrated Discovery (DAVID) (Fig. 2e) and Reactome (Supplementary Fig. 1a-c). Both approaches identified analogous pathways in the common rhythmic transcripts between saline- and cocaine-treated NAcc. Gene Ontology (GO) annotation revealed clusters in the protein folding and rhythmic process pathways in both treatments. The saline-only specific circadian transcripts were enriched in RNA splicing, cell projection, and protein monoubiquitination pathways. Conversely, the cocaine-only specific transcripts were highly enriched in the transmembrane transport, ER to Golgi vesicle mediated transport and cell projection pathways (see Fig. 2e and

Supplementary Fig. 1a and 1b). These results highlight the effect of a single, acute cocaine challenge on circadian function in the NAcc.

Cocaine-Driven Circadian Reprogramming is dependent on D2 Receptors

Both D1R- and D2R-mediated signaling play a fundamental role in the psychomotor and rewarding properties of cocaine (Vallone et al. 2000). Importantly, mice carrying selective ablation of D2R in the iMSNs display impaired cellular and motor response to acute cocaine administration (Kharkwal et al. 2016b). To determine the role of D2R-mediated signaling in the regulation of circadian gene oscillation in the NAcc, iMSN-D2RKO mice were treated with saline or cocaine (as shown in Fig. 1f), as previously described for their WT counterparts. RNA-seq analyses along the circadian cycle showed a substantial difference in the number of oscillatory genes as compared to WT mice in the saline condition (Fig. 3a). Indeed, we observed a drastic decrease in the number of genes oscillating in iMSN-D2RKO mice (359 transcripts) as compared to the same condition in WT mice (1399 transcripts); 53 oscillating genes were common to both genotypes (Fig. 3a). The phase of the overlapping genes was similar in both genotypes (Supplementary Fig. 2a and 2b) with a higher percentage of genes with greater amplitude in iMSN-D2RKO mice (Supplementary Fig. 2c). Moreover, transcripts exclusively diurnal in iMSN-D2RKO had phase distributions at approximately ZT4 and ZT16 (Fig. 3b and 3c). Genes oscillating only in iMSN-D2RKO mice clustered in GO annotations including transmembrane transport and steroid metabolic process (Fig. 3d and Supplementary Fig. 2d and 2e). It is relevant that annotation analyses of genes oscillating in both WT and iMSN-D2RKO mice include classic terms required for normal neuronal function (Supplementary Fig. 2f and 2g).

Acute cocaine treatment revealed a unique circadian signature in the NAcc of iMSN-D2RKO mice. Notably, a total of 1131 cycling genes were found in the cocaine-treated WT. Of these, 25 were common to iMSN-D2RKO mice. An additional 171 genes were rhythmic in iMSN-D2RKO mice only (Fig. 3e). Phase distribution analyses also revealed unique features of cocaine-induced reprogramming of circadian gene expression in WT and iMSN-D2RKO mice. Notably, a unique phase distribution peak observed at ~ZT18 in WT mice was almost completely absent in iMSN-D2RKO mice (Fig. 3f and 3g). On the other hand, genes oscillating in both conditions display a peak at ZT6-ZT8 (Supplementary Fig. 3a and 3b) and maintain similar amplitudes (Supplementary Fig. 3c). GO term analyses revealed unique pathways enriched in WT vs iMSN-D2RKO mice (Fig. 3h and Supplementary Fig. 3d and 3e), such as protein folding, transport, cell projection in WT, and transcription, negative regulation of apoptotic process, positive regulation of cytosolic Ca^{2+} concentration in iMSN-D2RKO. Moreover, GO annotation analyses showed a common enrichment of genes that belong to the circadian regulation of gene expression in both genotypes (Supplementary Fig. 3f and 3g). Taken together our results demonstrate that D2R signaling in iMSNs is critical for basal and cocaine-driven circadian oscillations in the NAcc.

Cocaine-induced Circadian Response of PPARγ Target Genes

To explore the molecular mechanisms by which cocaine induces *de novo* oscillations of striatal genes, we used MotifMap (Daily et al. 2011) to identify transcription factor binding motifs selectively represented in rhythmic genes under saline conditions and after cocaine challenge. A profound reorganization in transcription factor pathway usage was observed upon cocaine challenge, with a significant enrichment of genes containing PPARγ binding sites for genes oscillating in WT mice (Fig. 4a). Indeed, 372 out of 863 cocaine-induced newly oscillating genes

are PPARγ targets (Fig. 2a and 4b-c). Importantly, cocaine-induced enrichment of PPARγ binding sites is not observed in the iMSN-D2RKO cocaine-treated mice. Thus, ablation of D2R from iMSNs significantly reduces the cocaine-induced PPARγ oscillatory program observed in WT mice (Fig. 4b). Among the cocaine-induced PPARγ target genes, none were common oscillators in both genotypes. The significant fraction of *de novo* cycling PPARγ target genes induced by the first exposure to cocaine in WT mice, prompted us to further explore the involvement of this nuclear factor. Phase oscillation analyses of PPARγ cycling targets revealed a specific phase distribution in cocaine treated WT mice at ZT6-ZT8 and ZT18 (Fig. 4d). GO biological process analyses of the PPARγ-target genes in WT cocaine-treated mice revealed transport, translation initiation, positive regulation of apoptotic process, and transcription as key annotations (Fig. 4e and Supplementary Fig. 4a). Taken together, our data underscore the involvement of PPARγ signaling pathway in cocaine-induced transcriptional reprogramming of the NAcc clock. This unique cocaine-induced transcriptional feature is absent in mice with ablation of D2R from iMSNs.

D2R-driven PPARγ Nuclear Enrichment upon Cocaine

PPARγ localizes in the cytoplasm and upon activation translocates to the nucleus to activate transcription of specific genes (Mangelsdorf et al. 1995). We performed immunofluorescence analyses using a nuclear-specific PPARγ antibody to quantify the induction of nuclear PPARγ staining in the NAcc of WT and iMSN-D2RKO mice upon cocaine treatment. For this purpose, mice of both genotypes were administered either saline or cocaine (20 mg kg^{-1}) at ZT3 and sacrificed at ZT7. A diffuse nuclear PPARγ staining was observed in NAcc neurons in saline conditions in both genotypes (Fig. 5a). After cocaine we observed a significant increase in nuclear PPARγ staining in WT NAcc neurons, which was absent in iMSN-D2RKO mice. Quantification

of PPARγ nuclear intensity per cell, as well as of the number of cells with nuclear PPARγ staining, shows a statistically significant increase of nuclear PPARγ localization upon cocaine in WT as compared to iMSN-D2RKO NAcc neurons (Fig. 5b, p=0.0030; Fig. 5c, p=0.0124). To establish the identity of the MSNs showing the heightened intensity of PPARγ nuclear staining, we performed *in-situ* hybridization coupled to immunohistochemistry using probes specific for the two subtypes of MSNs. This allowed for the unambiguous identification of D2R-expressing iMSNs from D1R-expressing dMSNs. Double *in-situ* hybridization/immunohistochemistry analyses were performed using riboprobes for *enkephalin* (Enk) (Baik et al. 1995), an iMSNs specific marker or the dopamine D1 receptor (*D1R)*, a dMSN specific marker, together with the specific PPARγ antibody. These experiments demonstrated that the cocaine-driven increase in PPARγ nuclear staining occurs in iMSNs (p=0.0030) and not in dMSNs (p=0.9991) (Fig. 5d and 5e). Importantly, the increase of PPARγ in iMSNs nuclei after cocaine was not observed in the NAcc of iMSN-D2RKO mice (p=0.8693) (Fig. 5d and 5e). These results point to a cocaine-mediated D2R-dependent activation of PPARγ.

Lack of PPARγ Activation and Function in iMSN-D2RKO mice

To ascertain whether the metabolic consequences of acute cocaine treatment may be linked to PPARγ activation, we performed mass-spectrometry (MS) metabolomics analyses from isolated NAcc at ZT7 after either saline or cocaine (20 mg kg^{-1}; i.p.) administration at ZT3. We identified a significant effect of cocaine on lipid metabolism (Fig. 6a). Among 180 metabolites analyzed, 145 were lipids including: phospholipids, acylcarnitines and sphingolipids. In WT, but not in iMSN-D2RKO mice, phosphatidylcholine levels were significantly decreased after cocaine treatment while most lysophosphatidylcholines increased. D2R activation is involved in the

conversion of phosphatidylcholine into lysophosphatidylcholine and arachidonic acid (AA) (Kanterman et al. 1991; Neve et al. 2004), the latter being a precursor of prostaglandins (Kuehl and Egan 1980; Piomelli et al. 1991). Importantly, prostaglandins are well-characterized PPARγ natural ligands (Nosjean and Boutin 2002). Interestingly, AA release in the striatum is regulated by D1R and D2R in an opposite manner (Piomelli et al. 1991; Schinelli et al. 1994); D1R signaling inhibits while D2R signaling increases AA release. Based on these findings, we reasoned that the efficient turnover of phosphatidylcholine levels in response to cocaine would be dampened in mice with D2R ablation in iMSNs. We thereby analyzed the levels of the PGJ2-type prostaglandin (15-deoxy-$\Delta^{12,14}$-PGJ2) (Scheer et al. 2013), a prostaglandin that specifically binds and activates PPARγ (Forman et al. 1995), in the NAcc of WT and iMSN-D2RKO mice. Indeed, we observed that in response to cocaine, there is a significantly lower level of 15-deoxy-$\Delta^{12,14}$-PGJ2 in the NAcc of iMSN-D2RKO mice as compared to saline treated mice ($p=0.0153$) (Fig. 6b). In contrast, WT mice show no significant change in 15-deoxy-$\Delta^{12,14}$-PGJ2 levels after cocaine treatment, a response that mirrors results obtained in human cocaine users (Samikkannu et al. 2014). These findings point to D2R signaling as a key player in the cocaine-driven prostaglandin production involved in PPARγ activation.

We next assessed the downstream effects of PPARγ activation by analyzing the expression of specific genes from the list of PPARγ circadian putative targets (Fig. 4c). Among these genes, *Adora2a* (Adenosine A2a Receptor), *Kcnd1* (Potassium Voltage-Gated Channel Subfamily D Member 1), and *Gabrδ* (Gamma-Aminobutyric Acid Type A Receptor Delta Subunit) are not oscillatory under normal conditions in WT mice (Fig. 6c). However, upon cocaine treatment, their expression displayed *de novo* oscillatory profiles. In contrast, in cocaine treated iMSN-D2RKO mice, these genes were not cyclically expressed, their circadian expression parallels that of saline-

control mice (Fig. 6c). Next, we analyzed the molecular mechanism of control at the promoter level by chromatin immunoprecipitation assays (ChIP) using NAcc nuclear extracts from both WT and iMSN-D2RKO cocaine-treated mice harvested at ZT7. Using PPARγ nuclear-specific antibodies, we show that PPARγ chromatin recruitment to *Adora2a* and *Kcnd1* promoters was significantly reduced in iMSN-D2RKO animals as compared to WT (Fig. 6d) (*Adora2a:* p=0.0361 and *Kcnd1*: p=0.0252). An analogous trend was observed for the *Gabrδ* promoter (p=0.1549). These results support a scenario in which PPARγ activation by cocaine leads to the *de novo* program of D2R signaling-dependent circadian genes in the NAcc.

Rescue of PPARγ Function using the Specific Agonist Pioglitazone

To validate the critical role played by PPARγ in D2R signaling-dependent circadian reprogramming upon cocaine, WT and iMSN-D2RKO mice were subjected to oral gavage with pioglitazone, a specific PPARγ activator (Swanson et al. 2011) that crosses the blood brain barrier (Kiyota et al. 1997). Pioglitazone or vehicle, were administered at ZT1, 2 hours before the acute cocaine injection (Fig. 7a). Expression of the *Adora2a*, *Kcnd1* and *Gabrδ* genes was analyzed at ZT7 and at ZT19 (Fig. 7b). Pioglitazone treatment before cocaine reestablished the induction of *Adora2a* (p=0.0388), *Kcnd1* (p<0.0001), and *Gabrδ* (p=0.0019) gene expression in iMSN-D2RKO mice at ZT7, which nicely paralleled WT expression levels (Fig. 7b). Thus, PPARγ activation operates as a direct link between cocaine, D2R-signaling (Kanterman et al. 1991; Neve et al. 2004) and downstream gene expression (Fig. 7c). These results identify PPARγ as a critical factor that intervenes in the transcriptional reprogramming of the striatal clock upon acute cocaine treatment.

Discussion

Drugs of abuse, such as cocaine, are known to alter human physiology and circadian rhythms (Hasler et al. 2012). While relevant information about the molecular mechanisms by which cocaine affects short or long-term neuronal plasticity has been accumulated (Lüscher and Bellone 2008), little is known about how it interplays with the circadian system. Deciphering how cocaine alters circadian regulation may provide critical knowledge to design strategies aimed at mitigating the daily dysfunctions of drug addicts. Previous studies have addressed this question through the analysis of chronically treated WT mice (Ozburn et al. 2017) or mutant mice for specific clock genes (Abarca et al. 2002; Iijima et al. 2002; McClung et al. 2005; Brager et al. 2013). In this study, we first sought to decipher how a single acute cocaine treatment affects genome-wide circadian oscillations within the NAcc, and secondly to dissect the D2R-mediated signaling pathways in striatal neurons. For this purpose, we exploited mouse models in which genetic ablation of D2R is targeted uniquely to striatal iMSNs. We demonstrate that cocaine generates a profound reprogramming of circadian gene expression and identified PPARγ as one critical player that elicits the acute effects of cocaine through D2R-mediated signaling.

D2R is essential for the psychomotor and rewarding effects of psychoactive drugs such as cocaine(Caine et al. 2002; Welter et al. 2007; Kharkwal et al. 2016b). Indeed, constitutive D2R knockout mice self-administer higher amounts of cocaine as compared to WT littermates (Caine et al. 2002). Importantly, lower striatal D2R levels have been observed in cocaine abusers as well as in rodent models (Volkow et al. 1997; Nader et al. 2006; Czoty et al. 2010). Thus, ablation of D2R from the main striatal population, as achieved in iMSN-D2RKO mice, represents an ideal model to study the mechanisms by which cocaine affects striatal signaling and circuitry. Previous studies revealed the importance of D2R for intrastriatal connections (i.e. collaterals between iMSN

and dMSN) necessary for the psychomotor effects of cocaine (Anzalone et al. 2012; Dobbs et al. 2016; Kharkwal et al. 2016b; Lewis et al. 2020).

Our findings place D2R in a central position in the modulation of circadian rhythmicity in the striatum. Indeed, D2R ablation in iMSNs leads to a significant reduction in the number of oscillating genes in the NAcc. Our data reinforce emerging evidence suggesting that cocaine-mediated increase of dopamine is involved in maintaining circadian rhythms in brain areas including the retina, olfactory bulb, striatum, midbrain and hypothalamus (Korshunov et al. 2017). Remarkably, cocaine administration is significantly less effective on circadian reprogramming in the absence of D2R.

Previous reports have indicated that D2R-mediated signaling modulates *Clock* and *Per2* gene expression (Imbesi et al. 2009; Hood et al. 2010). Our results show that D2R also modulates *Per1* expression (Supplementary Table 1). Cocaine treatment does not lead to major alterations in the circadian oscillation of the core clock genes *Bmal1, Cry1* and *Dbp* in striatal neurons. On the other hand, we observe induction of newly oscillatory genes. This is remarkable when considering the extensive changes in circadian gene expression observed between WT and iMSN-D2RKO mice. Altogether these observations point to a D2R signaling-driven cocaine-induced reprogramming of the NAcc. Our study allows the identification of PPARγ as a key mediator of cocaine-induced rhythmic transcriptional reprogramming.

While originally characterized for its role in adipogenesis and glucose metabolism, PPARγ has been recently linked to neurological disorders such as neurodegeneration and neuro-inflammation (Jiang et al. 2008; Chaturvedi and Beal 2008). Importantly, we have demonstrated that D2R ablation prevents cocaine-driven PPARγ activation and the consequent *de novo* oscillation of PPARγ target genes. Dependence on D2R can be circumvented by the administration

of the specific PPARγ agonist pioglitazone. Our results support recent findings suggesting the involvement of PPARγ in cocaine use disorder. Indeed, pioglitazone treatment during abstinence has a positive effect on cocaine addiction by reducing cocaine self-administration(Miller et al. 2018). GO analyses of the cocaine treated WT and iMSN-D2RKO NAcc transcriptomes shows that the most significant annotation in iMSN-D2RKO is transcription factors which is absent in WT mice. This notion supports a modulatory role of D2R signaling in NAcc-dependent molecular responses to cocaine. Thus, while dMSNs have been critically involved in cocaine-mediated responses(Kelz et al. 1999; Zhang et al. 2006; Bateup et al. 2008; Hikida et al. 2010; Cates et al. 2019; Parekh et al. 2019), the modulatory role of D2R signaling needs to be further highlighted. Along these lines, it is tempting to speculate that alteration of cocaine-induced circadian reprogramming in absence of D2R might also occur in cocaine abusers where the levels of D2R are dampened(Volkow et al. 1997). Notably, the full D2R knockout mice show heightened intake of cocaine as measured in cocaine self-administration studies (Caine et al. 2002). Since the iMSN-D2RKO mice show multiple features of the full D2R knockout mice, it is tempting to speculate that they might also self-administer higher amounts of cocaine. Future studies will address this question.

Our findings reveal the fundamental role of D2R in circadian physiology of the brain's reward system. D2R signaling plays a crucial role in the reprogramming of diurnal transcription driven by acute cocaine in the NAcc. Unsuspected to date, D2R-mediated signaling triggers a regulatory circuit that leads to PPARγ activation. This response underlies the cyclic activation of a large number of *de novo* oscillatory genes. These results exemplify the complexity underlying the effects of cocaine in the brain by adding a member of the nuclear receptor family to the molecular circuitry previously implicated in the response to cocaine (Lobo and Nestler 2011;

Everitt and Robbins 2013; Yager et al. 2015; Chandra and Lobo 2017; Walker et al. 2018). Finally, the identification of the PPARγ pathway as a mediator of D2R signaling represents an important promising target for the clinical treatment of drug addiction.

Methods

Animals

iMSN-D2RKO mice were generated by mating $D2R^{flox/flox}$ mice with $D2R^{flox/flox/D1R\text{-}CRE+/-}$ mice[29]. In $D2R^{flox/flox/D1R\text{-}CRE+/-}$ mice, the DA D1R promoter drives the CRE recombinase. The ability of this CRE to eliminate D2R in iMSNs (Anzalone et al. 2012) resides in the common expression of D1R and D2R in embryonic MSN precursors (Aizman et al. 2000). Absence of D2R from iMSNs was previously shown by binding analyses on striatal extracts using a D2R-specific 3H-labeled ligand, as well as by double *in-situ* hybridization experiments using GAT1 as marker of MSNs and D2R exon 2 specific probes (Anzalone et al. 2012). Mice were maintained on a standard 12h light/ 12h dark cycle; food and water were available *ad libitum* in ~25ºC and 40-60% humidity. Animals' care and use was in accordance with guidelines of the Institutional Animal Care and Use Committee at the University of California, Irvine. Genotype identification was performed by Southern blot and PCR analyses of DNA extracted from tails biopsies.

Drugs

Before pharmacological treatments, mice were handled for at least 3 days for 5 min. On the day of the test, mice were habituated to the novel home cage for 2 hours and then administered either cocaine or saline. Cocaine (Sigma Cat. #C5776) was dissolved in saline (NaCl 0.9%) and injected intraperitoneally (i.p.) at the dose of 20 mg kg^{-1}. Pioglitazone (Cayman Chemical Cat. # 71745)

was dissolved in DMSO to have a stock solution of 10 mg mL^{-1}. Pioglitazone solution was diluted 1:1 in PBS and administered 2 hours prior to either cocaine or saline injection by oral gavage at a dose of 60 mg kg^{-1}.

Locomotor activity analysis

Activity was measured on individually housed mice n=4-5/group for 11 days using Actimetrics optical beam motion detection (Philips Respironics). Data was collected using Minimitter Vital View v5.0 data acquisition software and analyzed through Matlab R2013a v9.7.0.1296695 software and Clocklab software v2.72.

Quantitative RT–PCR

Striatum samples were homogenized in TRIzol lysis reagent (Thermo Fisher) following manufacturer's instructions. Total RNA was reverse-transcribed using iScript Reverse Transcription Supermix (Biorad Cat. N. 1708840). Gene expression was analyzed by Real-Time PCR (BIO-RAD Real-Time System; BIO-RAD CFX Manager Software v3.1) using SsoAdvanced Universal SYBR Green Supermix (Biorad Cat. N. 172-5270). The sequences of the primers used for RT-PCR are Kcnd1 Forward: 5'-TCCGTTTGGCAAAGAGTGGT-3', Kcnd1 Reverse: 5'-AGCTCGTCTGTGAACTCGTG-3'; Gabrd Forward: 5'-GGCGCCAGGGCAATGAAT-3', Gabrd Reverse: 5'-GTCAATGCTGGCCACCTCTA-3'; Adora2a Forward: 5'-TTCATCGCCTGCTTTGTCCT-3', Adora2a Reverse: 5'-AATGATGCCCTTCGCCTTCA-3'; Bmal1 Forward: 5'-GCAGTGCCACTGACTACCAAGA-3', Bmal1 Reverse: 5'-TCCTGGACATTGCATTGCAT-3'; Per1 Forward: 5'-ACCAGCGTGTCATGATGACATA-3', Per1 Reverse: 5'-GTGCACAGCACCCAGTTCCC-3'; Dbp Forward: 5'-

AATGACCTTTGAACCTGATCCCGCT-3', Dbp Reverse: 5'-GCTCCAGTACTTCTCATCCTTCTGT-3'; Cry1 Forward: 5'-CAGACTCACTCACTCAAGCAAGG-3', Cry1 Reverse 5'-TCAGTTACTGCTCTGCCGCTGGAC-3'.

RNA-seq analysis

RNA library preparation and sequencing were performed at the UCI Genomics High-throughput Facility, University of California, Irvine. Briefly, total RNA was monitored for quality control using the Agilent Bioanalyzer Nano RNA chip and Nanodrop absorbance ratios for 260/280 nm and 260/230 nm. Library construction was performed according to the Illumina TruSeq® Stranded mRNA Sample Preparation Guide. The input quantity for total RNA was 700 ng and mRNA was enriched using oligo dT magnetic beads. The enriched mRNA was chemically fragmented for 3 minutes. First strand synthesis used random primers and reverse transcriptase to make cDNA. After second strand synthesis the ds cDNA was cleaned using AMPure XP beads and the cDNA was end repaired and then the 3' ends were adenylated. Illumina barcoded adapters were ligated on the ends and the adapter ligated fragments were enriched by nine cycles of PCR. The resulting libraries were validated by qPCR and sized by Agilent Bioanalyzer DNA high sensitivity chip. The concentrations for the libraries were normalized and then multiplexed together. The multiplexed libraries were sequenced on four lanes using single end 100 cycles chemistry on the HiSeq 2500. The version of HiSeq control software was HCS 2.2.58 with real time analysis software, RTA v1.18.64. Sequence alignment was performed using TopHat v2.1.1 while assembly and expression estimation was done using Cufflinks v0.12.1(Trapnell et al. 2013). Reads were mapped to the mouse genome mm10 and expression values were estimated as FPKM. DETAILS:

FASTQ files were obtained from the sequencing facility and processed through the standard Tuxedo protocol[79]. Reads were then aligned to the UCSC mm10 mouse reference genome using TopHat and Bowtie2 v2.3.4. Assembled transcripts were obtained via Cufflinks with the mm10 reference annotation file. Genome assembly was obtained using Cuffmerge and expression levels (summarized to genes) were calculated using Cuffquant and then normalized via Cuffnorm to FPKM values. For each condition, 24 hr time series data from six time points with three replicates each were collected. In total, expression levels of 24138 unique genes were considered for further analysis. Data was further split to pairwise time series format for comparative analysis (e.g. WT Saline vs WT Cocaine treatment, KO Saline vs KO Cocaine treatment etc).

Bioinformatics and Pathway Analysis

Bioinformatics analysis was performed on RNA-seq data using JTK_CYCLE(Hughes et al. 2010) v3.1 and pipelines for CircadiOmics (circadiomics.ics.uci.edu) (Patel et al. 2012). Pathway analysis was performed using DAVID (Huang et al. 2009) and Reactome (Fabregat et al. 2017; Sidiropoulos et al. 2017) software. Details: Statistical and bioinformatics analyses were performed based on pairwise comparisons, where the effect of cocaine treatment was analyzed while controlling the genotype or the difference between genotypes (WT or KO) were compared while controlling the treatment. Dixon's test was performed on replicates of transcriptomic data to reduce outlier effects, filtering out up to 1 outlier replicate from each time point. For transcriptomic data, genes with consistently low expression values (FPKM < 1) were filtered out from further analysis to reduce noise. Time series data was then used to determine circadian behavior of genes using JTK_CYCLE, including the p-value for whether the time series is considered circadian, its periodicity (between 20-28 hrs), amplitude and phase. A gene is considered circadian if its

JTK_CYCLE p-value passed the cutoff of 0.01. Heatmaps of circadian transcripts were generated using the R package gplots v3.0.3, where the values on each row were normalized and rows were sorted by the JTK_CYCLE phase. The Database for Annotation, Visualization and Integrated Discovery (DAVID) pathway and Reactome analysis tools were used to identify enriched KEGG pathways for circadian genes in each condition. Pathways were ranked by the number of genes found annotated with the pathway information or with the negative natural log of p-values for enrichment, which behave similarly to z-scores where larger values indicate higher confidence. Putative TFBS information from MotifMap (Daily et al. 2011) were used to determine the enriched TFs in each condition. Fisher's test was conducted comparing the relative abundance of binding sites in the promoter regions (-10000 bps to +2000 bps of transcription start site) of circadian genes in each condition, as opposed to the genomic background (defined as all 24138 genes from the RNA-seq data with FPKM > 0 at any time point). In addition, a filtering parameter of BBLS>1, FDR<0.25 was used to obtain high quality binding sites while TFs with motifs that are too short or degenerate (more than 50000 binding sites under the filtering criteria) were removed as they tend to be unreliable. TFs were ranked by the negative log of their Fisher p-values. Enrichment results from different pairwise comparisons were also compared in a meta-analysis to identify condition-specific TFs, in particular PPARγ which was found to be exclusively enriched in WT-Cocaine condition. PPARγ targeted genes were filtered using a combination of MotifMap data and ChIP-Seq data from GSE64458 (Soccio et al. 2015). Binding sites were searched within a smaller promoter region of -3000 bps to +1000 bps of the TSS while filtering parameters for MotifMap were kept the same as mentioned above. Other visualization and statistical analyses were performed in R or in python using pandas and scikit-learn.

Metabolomics analysis

Metabolomic analyses were performed using p180 from the Biocrates facility (Innsbruck, Austria). Metabolite levels were measured at ZT7 after an intraperitoneal injection of saline or cocaine at a dose of 20 mg kg^{-1} at ZT3, 5 replicates each. Statistical and bioinformatics analyses were performed based on pairwise comparisons, where the effect of cocaine treatment was analyzed while controlling the genotype or the difference between genotypes (WT or KO) were compared while controlling the treatment. Dixon's test was performed to reduce outlier effects, filtering out up to 1 outlier replicate from each condition. Heatmaps for the metabolite profiles were generated using the RStudio software. Row z-scores are displayed and were calculated using the 'heatmap.2' function of the gplots package.

Immunohistochemistry and Fluorescent In situ Hybridization Analysis

Single immunostaining was performed on vibratome sections as described previously (Brami-Cherrier et al. 2005) using anti- PPARγ antibody (1:1000; Novus Biotechnologies Cat. #NB120-19481). Nuclei staining was obtained using Draq7 (Biostatus, Cat# DR70250). For quantifications, frames of 375x375 µm/image (n=4) were analyzed. ROIs were drawn around individual cells using LASX software v3.7.0 (Leica); mean gray values/cell were obtained and background subtracted. Double immunohistochemistry/in situ hybridization staining were obtained using striatal sections which were hybridized with digoxigenin (DIG)-Enkephalin or (DIG)-D1R riboprobes (RNA labeling mix; Roche, Cat# 11277073910) (Anzalone et al. 2012). After incubating the probe for overnight (ON) at 60°C, sections were washed with PBS (Phosphate Buffered Saline) 3 times (5min), permeabilized with Triton 0.3% in PBS (15 min), blocked with normal horse serum 5% for 1h and incubated ON with rabbit PPARγ antibody (1:1000) at 4°C. On

day 3, after 3 washes in PBS, sections were incubated for 1h with an anti-rabbit Alexa488 (1:600, Life technologies) followed by an incubation for 1h with anti–DIG-AP (1:5000, Roche) antibody. To amplify the signal, the HNPP (2-hydroxy-3-naphtoic acid-2'-phenylanilide phosphate) fluorescent Detection Set (Roche) was used. Quantifications were performed on confocal images (SP5, Leica) of coronal striatal slices (3 slices/animal and 3 brains/genotype/condition) using LASX v3.7.0. The number of MSNs showing the induction of PPARγ was quantified in frames of 246x246 µm/image (n=3); iMSNs were defined as the number of PPARγ $^{+}$ and Enkephalin^{+} cells while dMSNs as PPARγ $^{+}$ and D1R+ colocalizing cells.

Chromatin immunoprecipitation

Chromatin immunoprecipitation (ChIP) procedure was performed (Murakami et al. 2016). Punches of striatum from frozen brains of two mice were pooled. Tissue was minced and double crosslinked with DSG for 20 min and 1% formaldehyde for 10 min followed by adding glycine (0.125 M final concentration) at room temperature for 10 min. After homogenizing tissue pellets in PBS, 1 ml of lysis buffer was added. Samples were sonicated (20 cycles, every cycle: 30 sec ON / 30 sec OFF, power high) to generate 200-500 base pairs fragments and centrifuged at 14000g at 4^{o}C. Supernatants were diluted in a dilution buffer (1.1% Triton X100, 1.2 mM EDTA, 16.7 mM Tris-HCl, 167 mM NaCl). The diluted chromatin was incubated with 2 mg of anti- PPARγ antibody (Abcam Cat. # ab41928), overnight at 4^{o}C. To monitor the specificity of ChIP assays, samples were also immunoprecipitated with a specific-antibody isotype matched control immunoglobulin (IgG). 10ul of Dynabeads Protein G (Invitrogen, Cat. # 10003D) were added to the supernatant and incubated for 2 hrs at 4^{o}C. Beads were recovered, washed in low salt buffer, high salt buffer, LiCl buffer, followed by washing in TE for three times. Elution buffer (300 mM

NaCl, 0.5% SDS, 10 mM Tris-HCl, 5mM EDTA) was added to the washed beads, treated with RNase at 37°C for 2 hrs and Proteinase K at 65°C overnight. Equal amount of Phenol-Chloroform-Isoamyl alcohol was added to the samples and the aqueous phase was recovered. DNA was precipitated by adding 100% Ethanol, NaOAc and glycogen and kept at -20°C overnight. Samples were centrifuged at 14000g for 30 min at 4°C and washed with 70% ethanol followed by centrifugation at 14000g for 30 min at 4°C. Quantitative PCRs were performed using SsoAdvanced Universal SYBR Green Supermix (Biorad Cat. N. 172-5270), according to the manufacturer's protocol. Primers used for ChIP analysis by RT-PCR: Kcnd1 Forward: 5'-CTCACGAGGCTAGGCAGTTC -3', Kcnd1 Reverse: 5'-CCTTGATCGGGTGACTTGTT -3'; Gabrd Forward: 5'- CTGTTCACCTGCAATCAGGA-3', Gabrd Reverse: 5'-GGTCTGCCCTTGAGAAATGA -3'; Adora2a Forward: 5'- AAAGATGTGGGGGAGGAGTC -3', Adora2a Reverse: 5'- TTGCCCTTTATCGGAGCTAA -3'.

Prostaglandins PGJ2 Analysis

15-deoxy-$\Delta^{12,14}$-PGJ2 Elisa KIT (Enzo Life Sciences Cat. # ADI-900-023) was used to determine striatal Prostaglandin J2 concentration. ELISA tests were performed following manufacturer's instructions. Samples were prepared as follows: striatal punches of the NAcc were minced in Phosphate buffer and the solution was then acidified by addition of HCl (2M) to pH 3.5. Samples were centrifuged and the supernatant was passed through a C18 column (Pierce) and eluted with 20µl of ethyl acetate. After evaporation (O/N, RT), samples were reconstituted in 250µl of Assay Buffer and used for the Elisa assay.

Additional Statistical analyses

For all non-circadian statistics, data were analyzed either by Student's t-test, or by two- or three-way ANOVA (GraphPad Prism8.3.0), followed by Tukey's or Bonferroni's post hoc analyses, as appropriate. Statistical significance was assigned with p-value < 0.05. For circadian analysis, JTK_Cycle was used with a p-value < 0.01 cutoff.

Data Availability

The GEO accession number for the RNA-seq data set reported in this paper is GSE142657 (https://www.ncbi.nlm.nih.gov/geo/query/acc.cgi?acc=GSE142657). RNA-seq data was used for Figure 2, Figure 3, and Figure 4, and Supplementary Figures 1-4. UCSC mm10 mouse reference genome was used for alignment. All the transcriptomic data associated with this work is publicly available on the resource circadiomics.ics.uci.edu. PPARγ ChIP-seq data used for Figure 4 was downloaded from GEO, accession number GSE64458 (https://www.ncbi.nlm.nih.gov/geo/query/acc.cgi?acc=GSE64458) (Soccio et al. 2015).

Figure Legends

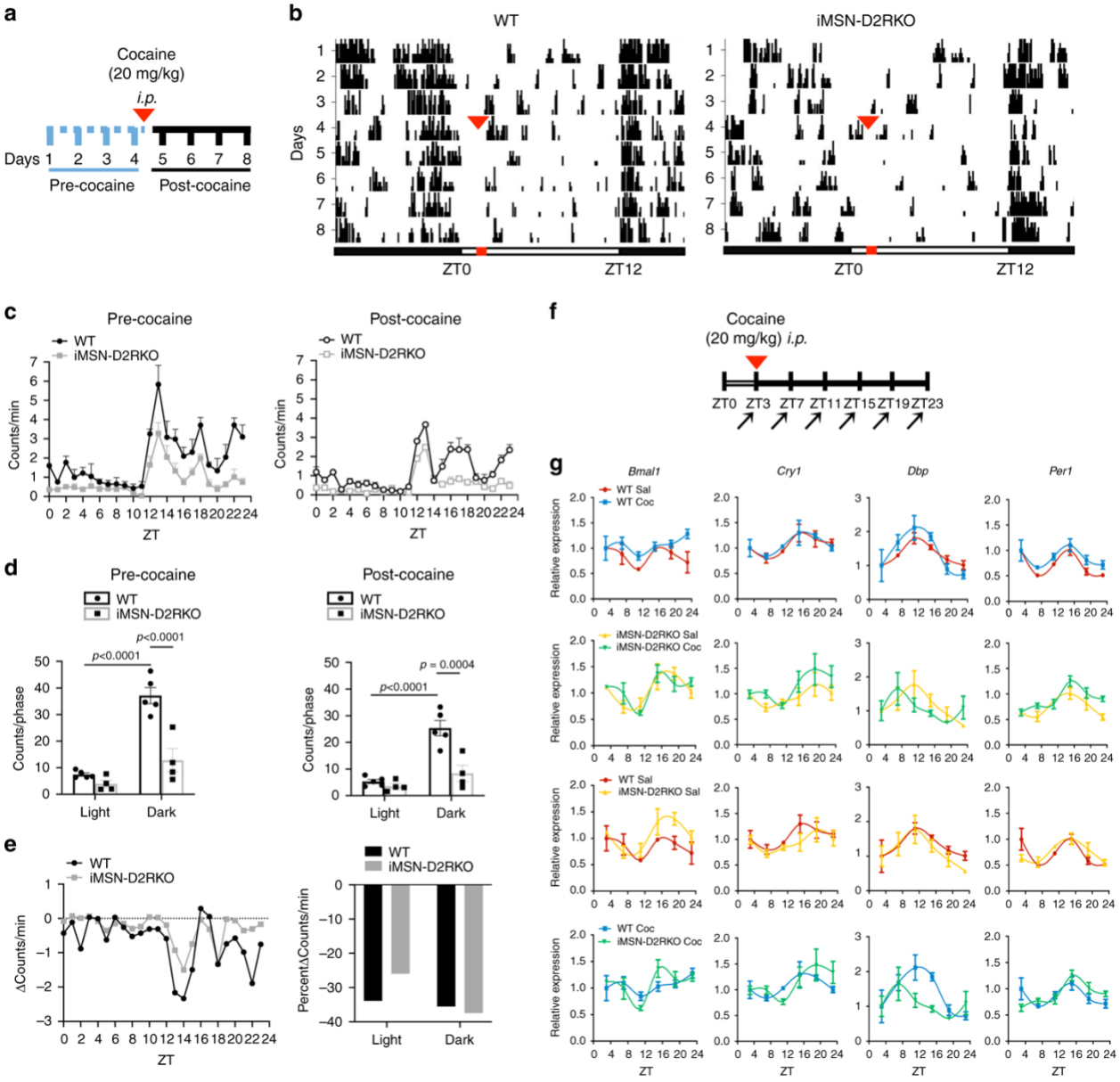

Figure 1 Effects of Acute Cocaine on Circadian Clock Genes

a, Schematic of the experimental design in b. **b**, Actograms of 24 h locomotor activity in 12h-Light/12h-Dark cycles in WT (n=5) and iMSN-D2RKO mice (n=4) during the 4 days preceding and following cocaine administration. Cocaine (20 mg kg^{-1}, i.p.) was given once at ZT3 on day 4 (red arrowheads in 1a and 1b). **c**, Locomotor activity analyses from b in WT (circles) and iMSN-D2RKO (squares) mice. Graphical representation of the number of beam breaks/min/circadian time (ZT) during the days preceding (Pre-Cocaine; left) or following cocaine injection (Post-Cocaine; right). **d**, Total beam breaks per phase in WT (circles) (n=5) and iMSN-D2RKO (squares) (n=4); inactive phase (Light), active phase (Dark), Pre-cocaine (two-way ANOVA, Genotype: $F_{(1, 14)} = 27.31$, $p=0.0001$; Time: $F_{(1, 14)} = 52.41$, $p<0.0001$; Interaction: $F_{(1, 14)} = 15.20$, $p=0.0016$) and Post-cocaine (two-way ANOVA, Genotype: $F_{(1, 14)} = 18.15$, $p=0.0008$; Time: $F_{(1, 14)} = 31.86$, $p<0.0001$; Interaction: $F_{(1, 14)} = 12.01$, $p=0.0038$). Tukey's multiple comparison test p-values as indicated. **e**, Left: The mean change in counts/min at each time point in pre-cocaine vs post-cocaine time in WT (circles) and iMSN-D2RKO (squares). Right: same as e) *left,* but represented as percent change during the light (ZT0-11) and dark (ZT12-23) phases. **f**, Schematic of the circadian experimental design in g. Mice were injected with cocaine (20 mg kg^{-1}, i.p) at ZT3 and NAcc samples were collected every 4 hours following cocaine injection at ZT 3, 7, 11, 15, 19 and 23 (arrows). **g**, Expression of core clock and clock-controlled genes: *Bmal1, Cry1, Dbp*, and *Per1* in WT saline (Sal; red circles) or cocaine (Coc; blue squares) and iMSN-D2RKO (Sal; yellow upward triangles) or (Coc; green downward triangles) analyzed by quantitative real-time PCR (n=3/genotype). (*three-way ANOVA;* For statistics see Supplementary Table 1). Data are presented as mean values ± SEM.

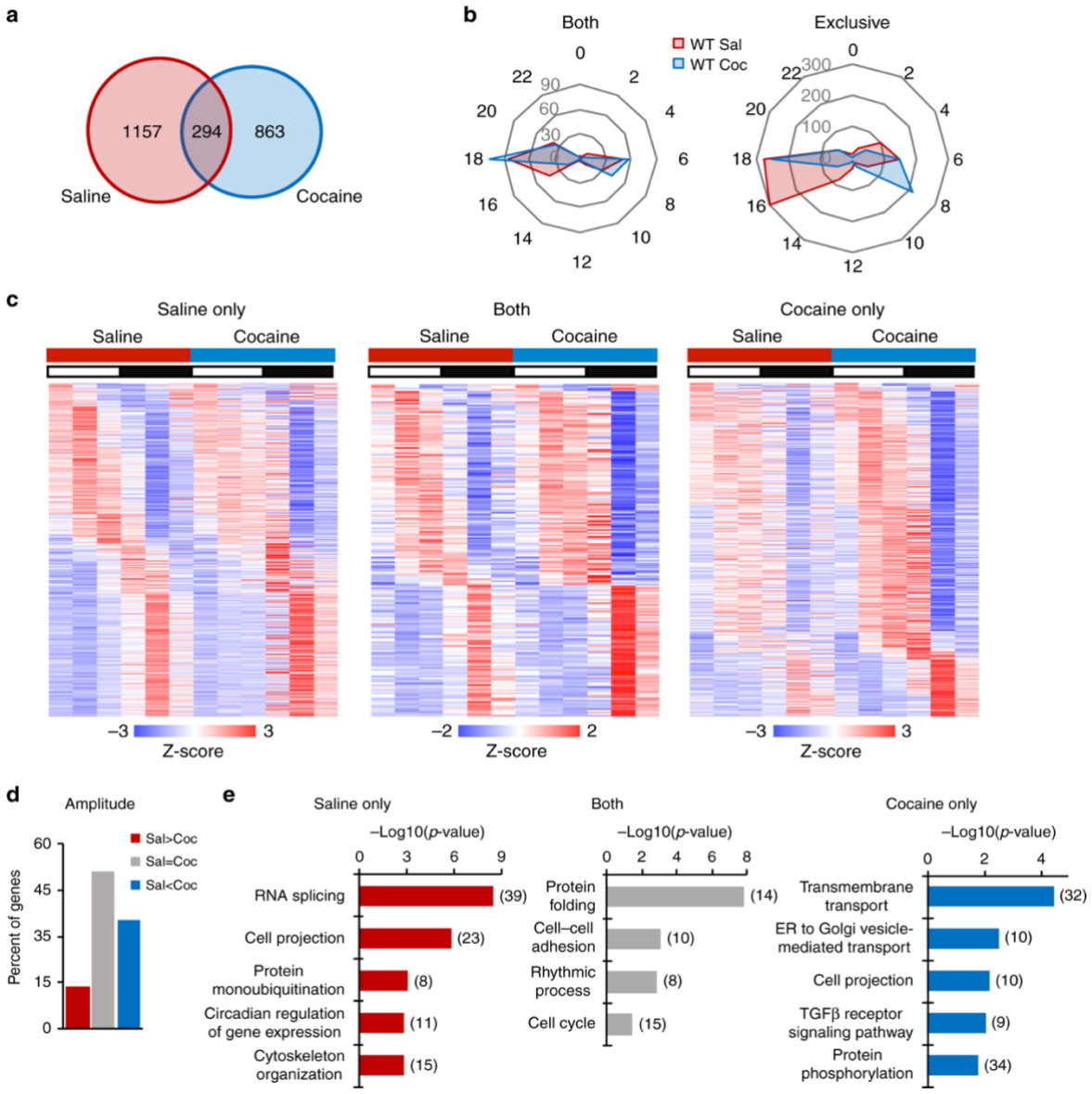

Figure 2 Cocaine Rewires the Striatal Circadian Transcriptome in WT mice

a, Venn diagram representing the striatal rhythmic genes in saline and cocaine treated WT mice (n = 3, JTK_Cycle, cutoff p<0.01). **b**, Radar plots representing the phase analysis of genes whose expression is circadian in both saline (Sal) and cocaine (Coc) treated mice (left) and genes exclusively circadian in saline or cocaine conditions (right). **c**, Heat maps representing genes significantly circadian (n=3, JTK_cycle, cutoff p<0.01) in saline- (left), in cocaine-treated mice (right) and commonly circadian in saline and cocaine treated mice (middle). White and black bars indicate the light (ZT3, 7, 11) and dark (ZT15, 19, 23) timepoints respectively. **d**, Amplitude analysis of striatal transcripts rhythmic in both saline (Sal) and cocaine (Coc) injected mice. The percentage of genes with amplitude higher, lower or equal to saline condition is reported. **e**, DAVID Gene Ontology Biological Process analysis of circadian genes oscillating in saline only (left), both (middle) and cocaine only (right). Bar charts represent the -Log10(p-value) of each enriched term. The number of genes identified in each pathway is shown in parenthesis.

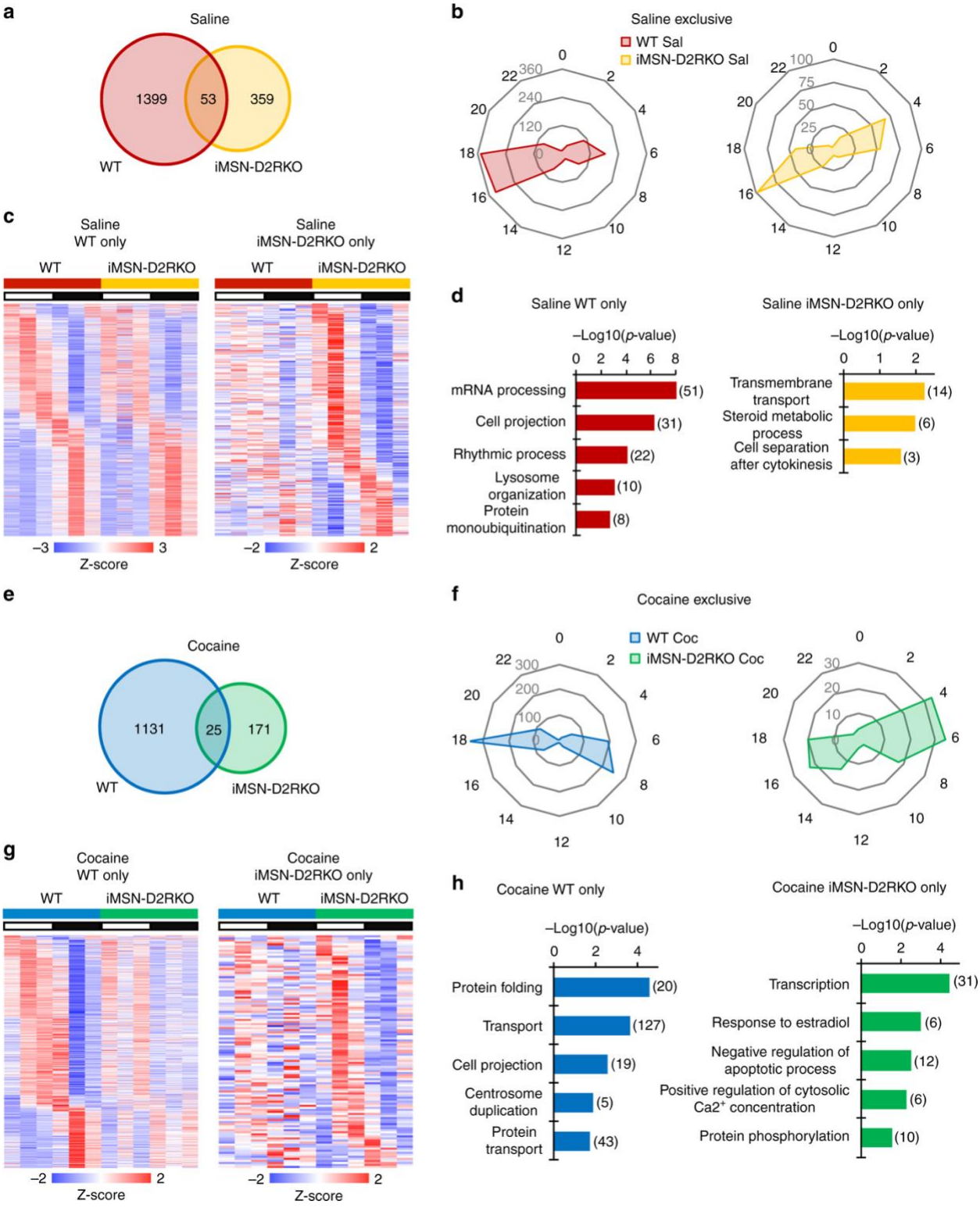
a
Saline
1399
53
359
WT
iMSN-D2RKO
b
Saline exclusive
WT Sal
iMSN-D2RKO Sal
c
Saline
WT only
Saline
iMSN-D2RKO only
WT
iMSN-D2RKO
Z-score
d
Saline WT only
–Log10(p-value)
mRNA processing (51)
Cell projection (31)
Rhythmic process (22)
Lysosome organization (10)
Protein monoubiquitination (8)
Saline iMSN-D2RKO only
Transmembrane transport (14)
Steroid metabolic process (6)
Cell separation after cytokinesis (3)
e
Cocaine
1131
25
171
WT
iMSN-D2RKO
f
Cocaine exclusive
WT Coc
iMSN-D2RKO Coc
g
Cocaine
WT only
Cocaine
iMSN-D2RKO only
h
Cocaine WT only
Protein folding (20)
Transport (127)
Cell projection (19)
Centrosome duplication (5)
Protein transport (43)
Cocaine iMSN-D2RKO only
Transcription (31)
Response to estradiol (6)
Negative regulation of apoptotic process (12)
Positive regulation of cytosolic Ca2+ concentration (6)
Protein phosphorylation (10)

Figure 3 D2R ablation from iMSN reorganizes the striatal circadian transcriptome
a, Venn diagram of striatal oscillating genes in saline treated WT and iMSN-D2RKO mice (n = 3, JTK_Cycle, cutoff p<0.01). **b**, Radar plots displaying the phase analysis of genes whose expression is exclusively circadian in WT mice (left) or in iMSN-D2RKO saline-treated (Sal) mice (right). **c**, Heat maps of genes significantly circadian (n=3, JTK_Cycle, cutoff p<0.01) only in WT (left) or in iMSN-D2RKO (right) saline-treated mice. White and black bars indicate the light (ZT3, 7, 11) and dark (ZT15, 19, 23) timepoints respectively. **d**, DAVID Gene Ontology Biological Process analysis of circadian genes oscillating in saline WT only (left) and in saline iMSN-D2RKO only (right). Bar charts represent the -Log10(p-value) of each enriched term. The number of genes identified in each pathway is shown in parenthesis. **e**, Venn diagram of striatal oscillating genes in cocaine treated WT and iMSN-D2RKO mice (n = 3, JTK_Cycle, cutoff p<0.01). **f**, Radar plots displaying the phase analysis of genes whose expression is exclusively circadian in WT (left) or in iMSN-D2RKO cocaine-treated (Coc) mice (right). **g**, Heat maps of genes significantly circadian (n=3, JTK_Cycle, cutoff p<0.01) only in WT (left) or in iMSN-D2RKO (right) cocaine-treated mice. White and black bars indicate the light (ZT3, 7, 11) and dark (ZT15, 19, 23) timepoints respectively. **h**, DAVID Gene Ontology Biological Process analysis of circadian genes oscillating in cocaine WT only or in cocaine iMSN-D2RKO only. Bar charts represent the -Log10(p-value) of each enriched term. The number of genes identified in each pathway is shown in parenthesis.

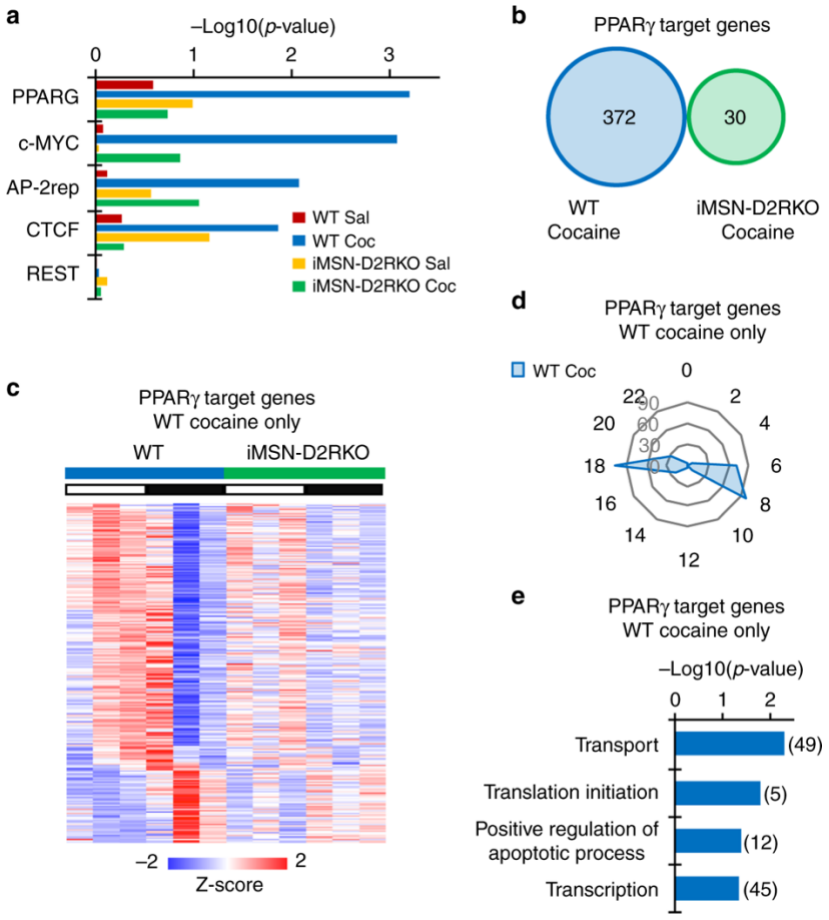

Figure 4 Cocaine-driven *de novo* oscillation of PPARγ target genes
a, Comparison of transcription factor binding site (TFBS) analysis between WT saline (Sal), WT cocaine (Coc), iMSN-D2RKO saline, and iMSN-D2RKO cocaine. The charts report the -Log10(p-value). **b**, Venn diagram representing the rhythmic PPARγ target transcripts after cocaine treatment in WT and iIMSN-D2RKO mice (n = 3, JTK_Cycle, cutoff p<0.01). **c**, Heat map displaying PPARγ target genes oscillating only in WT cocaine-treated mice compared to iMSN-D2RKO cocaine-treated mice (n=3, JTK_Cycle, cutoff p<0.01). White and black bars indicate the light (ZT3, 7, 11) and dark (ZT15, 19, 23) timepoints respectively. **d**, Radar plots displaying the phase analysis of PPARγ target genes whose expression is exclusively circadian in WT cocaine-treated (Coc) mice. **e**, DAVID Gene Ontology Biological Process analysis of oscillatory PPARγ target genes in cocaine-treated WT mice (n=3, JTK_Cycle, cutoff p<0.01). Bar charts represent the -Log10(p-value) of each enriched term. The number of genes identified in each pathway is shown in parenthesis.

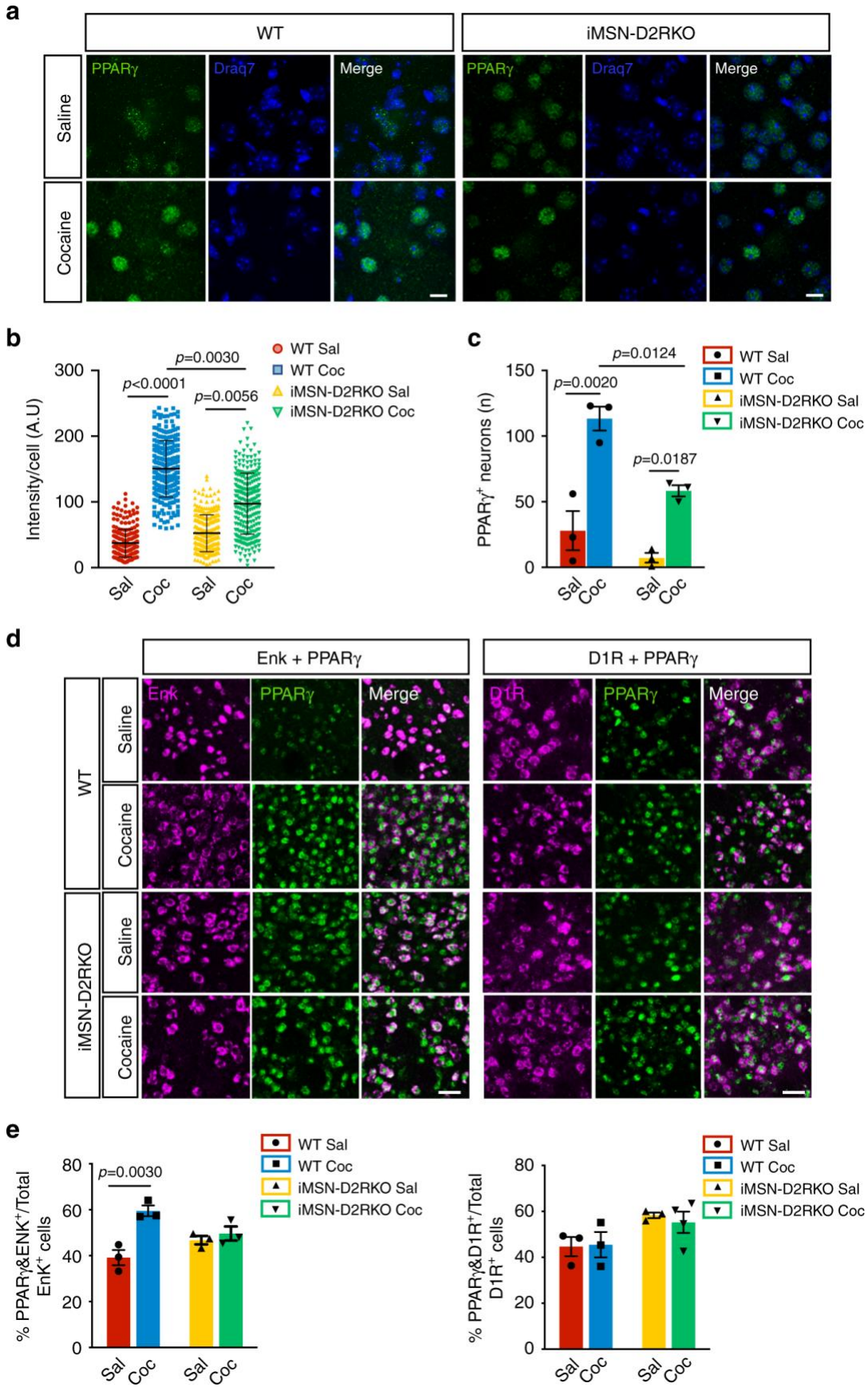
a
WT
iMSN-D2RKO
PPARγ
Draq7
Merge
Saline
Cocaine
b
Intensity/cell (A.U)
p<0.0001
p=0.0030
p=0.0056
WT Sal
WT Coc
iMSN-D2RKO Sal
iMSN-D2RKO Coc
Sal
Coc
c
PPARγ+ neurons (n)
p=0.0020
p=0.0124
p=0.0187
d
Enk + PPARγ
D1R + PPARγ
Enk
D1R
e
% PPARγ&ENK+/Total Enk+ cells
% PPARγ&D1R+/Total D1R+ cells
p=0.0030

Figure 5 Cocaine-induced nuclear PPARγ is impaired in iMSN-D2RKO mice

a, Immunolabeling of PPARγ and nuclei on striatal sections of saline and cocaine treated WT and iMSN-D2RKO mice. Scale bar: 25 µm. **b**, Quantification of the fluorescent intensity of PPARγ immunolabeling in WT and iMSN-D2RKO mice treated with saline (Sal; WT: red circles; iMSN-D2RKO: yellow upward triangles) or cocaine (Coc; WT: blue squares; iMSN-D2RKO: green downward triangles). Data were analyzed by two-way ANOVA using the mean ± SD of intensity/cell for each biological replicate (n=4/group) (Genotype: $F_{(1, 12)} = 8.458$, p=0.0131; Treatment: $F_{(1, 12)} = 91.23$, p<0.0001; Interaction: $F_{(1, 12)} = 12.81$, p=0.0038), Tukey's multiple comparison test. **c**, Quantification of PPARγ positive neurons with the indicated treatment (n=3/group). Significance was calculated using two-way ANOVA (Genotype: $F_{(1, 8)} = 16.87$, p=0.0034; Treatment: $F_{(1, 8)} = 54.77$, p<0.0001; Interaction: $F_{(1, 8)} = 3.474$, p=0.0993) Tukey's multiple comparison test. **d**, Double *in-situ*/immunofluorescence for *Enkephalin* (Enk) or *D1R* mRNA and PPARγ protein in cocaine treated WT and iMSN-D2RKO mice. Scale bar: 50 µm. **e**, Percentage of PPARγ- and Enk- or D1R-positive cells in cocaine and saline treated WT and iMSN-D2RKO mice (Enk: n=3/group; D1R: n=3 WT Sal, n=3 WT Coc, n=3 iMSN-D2RKO Sal, n=4 iMSN-D2RKO Coc). Two-way ANOVA (Enk: Genotype: $F_{(1, 8)} = 0.1782$, p=0.6841; Treatment: $F_{(1, 8)} = 18.69$, p=0.0025; Interaction: $F_{(1, 8)} = 10.53$, p=0.0118; D1R: Genotype: $F_{(1, 9)} = 7.117$, p=0.0257; Treatment: $F_{(1, 9)} = 0.06215$, p=0.8087; Interaction: $F_{(1, 9)} = 0.1943$, p=0.6697). Tukey's multiple comparison test. Data in c and e are presented as mean values ± SEM.

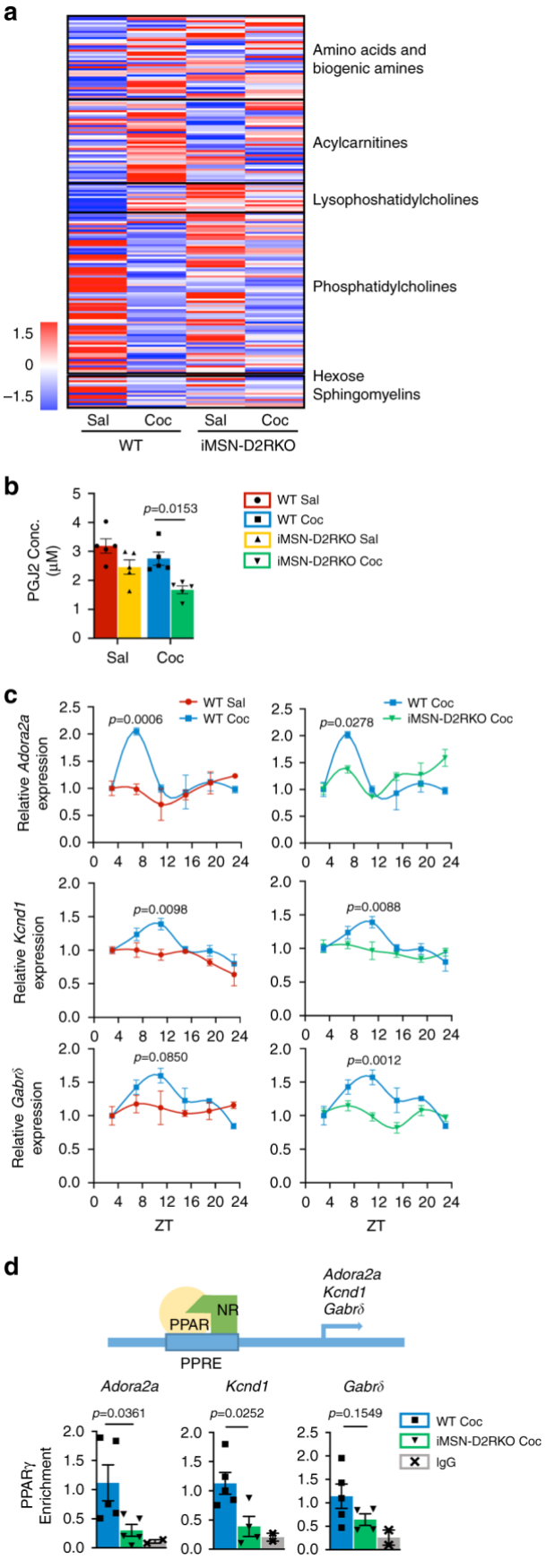
a
Amino acids and biogenic amines
Acylcarnitines
Lysophoshatidylcholines
Phosphatidylcholines
Hexose
Sphingomyelins
1.5
0
−1.5
Sal
Coc
Sal
Coc
WT
iMSN-D2RKO
b
PGJ2 Conc. (μM)
p=0.0153
WT Sal
WT Coc
iMSN-D2RKO Sal
iMSN-D2RKO Coc
Sal
Coc
c
Relative Adora2a expression
Relative Kcnd1 expression
Relative Gabrδ expression
p=0.0006
p=0.0278
p=0.0098
p=0.0088
p=0.0850
p=0.0012
WT Sal
WT Coc
WT Coc
iMSN-D2RKO Coc
ZT
ZT
d
Adora2a
Kcnd1
Gabrδ
PPAR
NR
PPRE
Adora2a
Kcnd1
Gabrδ
p=0.0361
p=0.0252
p=0.1549
PPARγ Enrichment
WT Coc
iMSN-D2RKO Coc
IgG

Figure 6 PPARγ signaling is altered in iMSN-D2RKO mice

a, Heatmap of the 180 metabolites analyzed in WT and iMSN-D2RKO mice, either saline or cocaine-treated (n=5/group). Metabolites were measured at ZT7 after saline or cocaine was injected at ZT3. Classes of metabolites measured are indicated on the right. **b**, Prostaglandin PGJ2-type (15-deoxy-$\Delta^{12,14}$-PGJ2) concentration assessed by enzyme-linked immunosorbent assay (ELISA) at ZT7 in WT and iMSN-D2RKO mice treated with saline (Sal: WT, red circles; iMSN-D2RKO, yellow upward triangles) or cocaine (Coc: WT, blue squares; iMSN-D2RKO, green downward triangles) (n=5/group/genotype). Two-way ANOVA (Genotype: $F_{(1,\ 16)} = 0.1696$, p=0.0008; Treatment: $F_{(1,\ 16)} = 7.719$, p=0.0134; Interaction: $F_{(1,\ 16)} = 0.6034$, p=0.4486). Tukey's multiple comparison test p-values as indicated. **c**, Circadian expression of selected PPARγ target genes *Adora2a*, *Kcnd1*, *Gabrδ* as determined by quantitative real time PCR (n=3/group). WT Sal (red circles), WT Coc (blue squares), iMSN-D2RKO Coc (green downward triangles). Two-way ANOVA *Adora2a* WT Sal vs WT Coc: Treatment: $F_{(1,\ 24)} = 4.372$, p=0.0473; Time: $F_{(5,\ 24)} = 4.253$, p=0.0065; Interaction: $F_{(5,\ 24)} = 3.983$, p=0.0090; *Adora2a* WT Coc vs iMSN-D2RKO Coc: Genotype: $F_{(1,\ 24)} = 0.4260$, p=0.5201; Time: $F_{(5,\ 24)} = 7.429$, p=0.0002; Interaction: $F_{(5,\ 24)} = 4.363$, p=0.0058; *Kcnd1* WT Sal vs WT Coc: Treatment: $F_{(1,\ 24)} = 10.98$, p=0.0029; Time: $F_{(5,\ 24)} = 6.118$, p=0.0009; Interaction: $F_{(5,\ 24)} = 1.640$, p=0.1878; *Kcnd1* WT Coc vs iMSN-D2RKO Coc: Genotype: $F_{(1,\ 24)} = 5.302$, p=0.0303; Time: $F_{(5,\ 24)} = 4.360$, p=0.0058; Interaction: $F_{(5,\ 24)} = 2.743$, p=0.0426; *Gabrδ* WT Sal vs WT Coc: Treatment: $F_{(1,\ 24)} = 2.940$, p=0.0993; Time: $F_{(5,\ 24)} = 2.690$, p=0.0456; Interaction: $F_{(5,\ 24)} = 2.124$, p=0.0972; *Gabrδ* WT Coc vs iMSN-D2RKO Coc: Genotype: $F_{(1,\ 24)} = 15.59$, p=0.0006; Time: $F_{(5,\ 24)} = 5.308$, p=0.0020; Interaction: $F_{(5,\ 24)} = 3.961$, p=0.0092. Bonferroni's multiple comparison test p-values as indicated. **d**, Chromatin recruitment of PPARγ at PPAR response element (PPRE) binding site contained in *Adora2a* (p=0.0361; WT Coc (blue squares) n=5, iMSN-D2RKO Coc (green downward triangles) n=5, IgG (grey X's) n=2), *Kcnd1* (p=0.0252; WT Coc n=5, n=4 iMSN-D2RKO Coc, IgG n=2) and *Gabrδ* promoters (p=0.1549; WT Coc n=5, iMSN-D2RKO Coc n=4, IgG n=2. unpaired Student's t-test. Data are presented as mean values ± SEM.

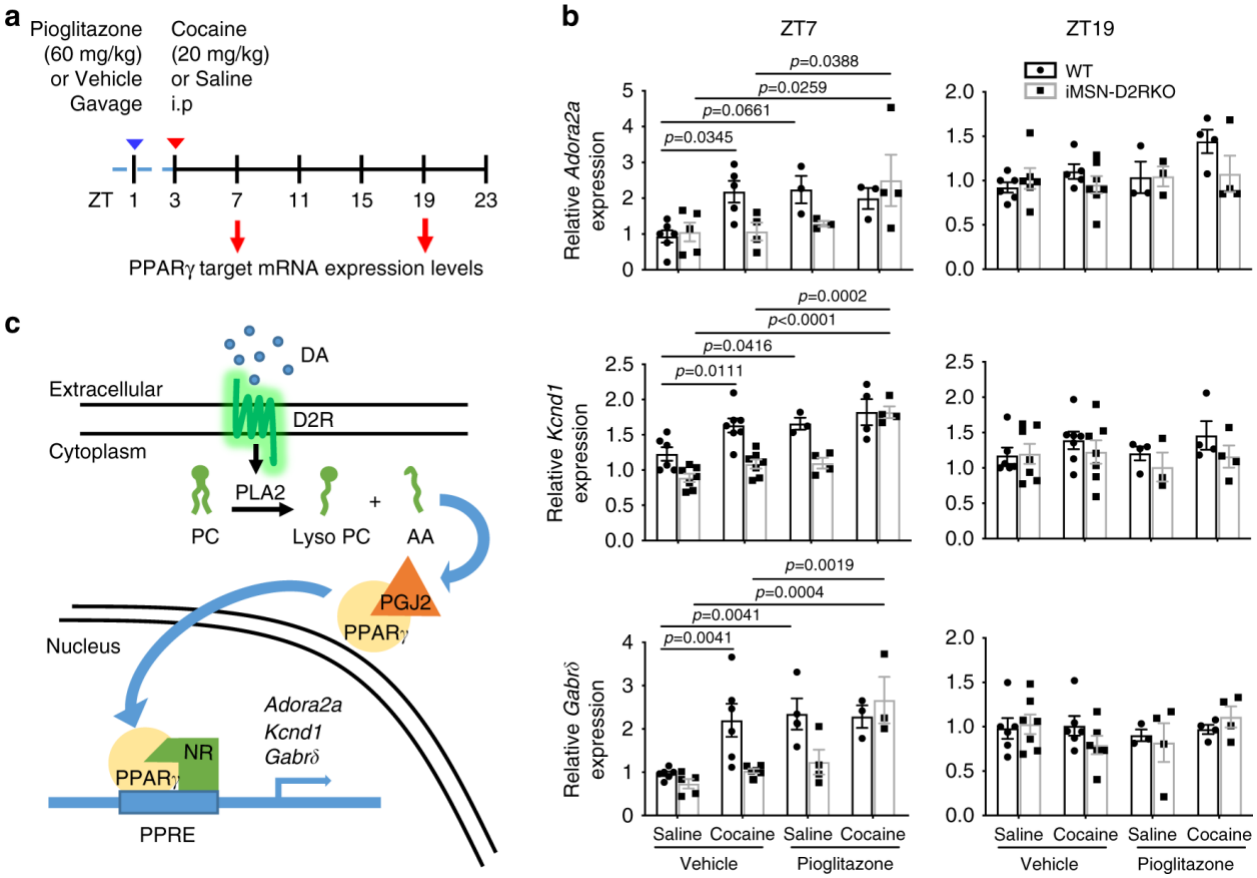

Figure 7 Pharmacological activation of PPARγ restores PPARγ signaling in iMSN-D2RKO mice

a, Schematic representation of the experimental design, arrowheads indicate the time and treatment of Pioglitazone (blue) and Cocaine treatments (red). **b**, Expression of selected PPARγ target genes *Adora2a, Kcnd1*, and *Gabrδ* as determined by quantitative real time PCR at ZT7 and ZT19 in presence or absence of Pioglitazone (60 mg kg^{-1}) prior to saline or cocaine (20 mg kg^{-1}) (*Adora2a* ZT7: Genotype: $F_{(1, 25)} = 2.003$, p=0.1693; Treatment: $F_{(3, 25)} = 4.682$, p=0.0099; Interaction: $F_{(3, 25)} = 2.479$, p=0.0845 (Vehicle and Saline: WT n=6, iMSN-D2RKO n=5; Vehicle and Cocaine: WT n=5, iMSN-D2RKO n=4; Pioglitazone and Saline: WT n=3, iMSN-D2RKO n=3; Pioglitazone and Cocaine: WT n=3, iMSN-D2RKO n=4); *Kcnd1* ZT7: Genotype: $F_{(1, 34)} = 26.20$, p<0.0001; Treatment: $F_{(3, 34)} = 20.05$, p<0.0001; Interaction: $F_{(3, 34)} = 3.130$, p=0.0383 (Vehicle and Saline: WT n=6, iMSN-D2RKO n=7, Vehicle and Cocaine WT n=7, iMSN-D2RKO n=7; Pioglitazone and Saline: WT n=3, iMSN-D2RKO n=4, Pioglitazone and Cocaine WT n=4, iMSN-D2RKO n=4); *Gabrδ* ZT7 Genotype: $F_{(1, 29)} = 7.445$, p=0.0107; Treatment: $F_{(3, 29)} = 11.26$, p<0.0001; Interaction: $F_{(3, 29)} = 3.378$, p=0.0315 (Vehicle and Saline: WT n=6, iMSN-D2RKO n=5, Vehicle and Cocaine: WT n=6, iMSN-D2RKO n=6; Pioglitazone and Saline: WT n=4, iMSN-D2RKO n=4; Pioglitazone and Cocaine: WT n=3, iMSN-D2RKO n=3); *Adora2a* ZT19: Genotype: $F_{(1,30)} = 1.352$, p=0.2540; Treatment: $F_{(3, 30)} = 2.071$, p=0.1250; Interaction: $F_{(3, 30)} = 1.406$, p=0.2603 (Vehicle and Saline: WT n=6, iMSN-D2RKO n=6; Vehicle and Cocaine: WT n=5, iMSN-D2RKO n=7; Pioglitazone and Saline: WT n=3, iMSN-D2RKO n=3; Pioglitazone and Cocaine WT n=4,

iMSN-D2RKO n=4); *Kcnd1* ZT19: Genotype: $F_{(1, 34)} = 1.903$, p=0.1767; Treatment: $F_{(3, 34)} = 0.7013$, p=0.5578; Interaction: $F_{(3, 34)} = 0.3919$, p=0.7596 (Vehicle and Saline: WT n=6, iMSN-D2RKO n=7; Vehicle and Cocaine WT n=7, iMSN-D2RKO n=7; Pioglitazone and Saline: WT n=4, iMSN-D2RKO n=3; Pioglitazone and Cocaine: WT n=4, iMSN-D2RKO n=4); *Gabrδ* ZT19 Genotype: $F_{(1, 32)} = 0.09598$, p=0.7587; Treatment: $F_{(3, 32)} = 0.8134$, p=0.4959; Interaction: $F_{(3, 32)} = 0.8259$, p=0.4893 (Vehicle and Saline: WT n=6, iMSN-D2RKO n=7; Vehicle and Cocaine WT n=6, iMSN-D2RKO n=6; Pioglitazone and Saline WT n=3, iMSN-D2RKO n=4; Pioglitazone and Cocaine: WT n=4, iMSN-D2RKO n=4)). Tukey's multiple comparison test p-values as indicated. Data are presented as mean values ± SEM. **c**, Simplified overview depicting D2R-mediated cocaine effect on circadian transcription of PPARγ target genes through PPARγ activation by prostaglandins (PGJ2). Dopamine (DA) activation of D2R stimulates Phospholipase A2 (PLA2) converting phosphatidylcholine (PC) to lysophosphatidylcholine (Lyso PC) and arachidonic acid (AA); AA is later converted into Prostaglandin (PGJ2). PGJ2 induces PPARγ nuclear translocation and transcriptional activation.

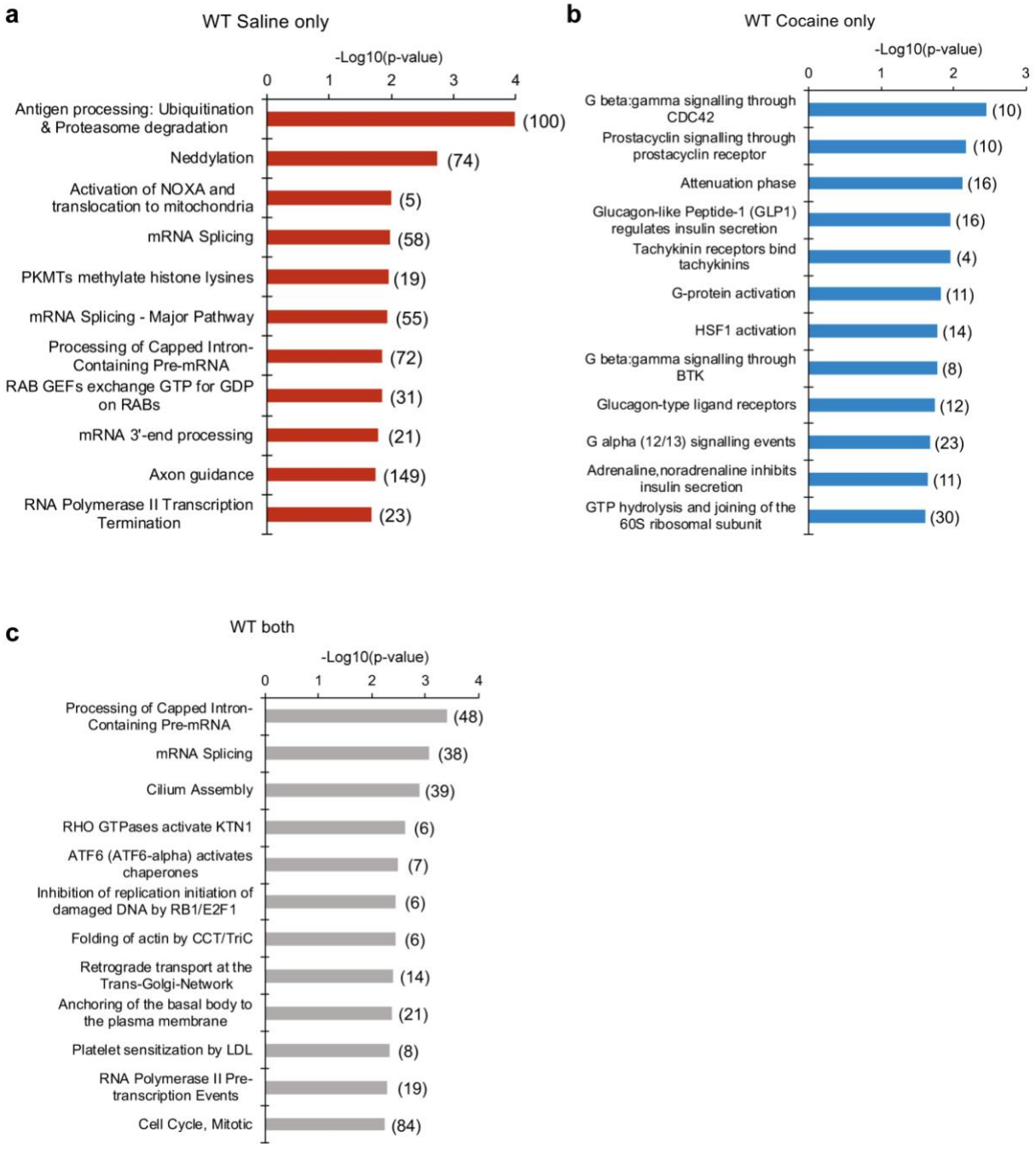

Supplementary Figure 1. Pathway analyses in WT and iMSN-D2RKO mice
a-c, Reactome Pathway analysis of circadian genes oscillating in saline only (a), cocaine only (b), and both (c). Bar charts represent the -Log10(p-value) of each enriched term. The number of genes identified in each pathway is shown in parenthesis.

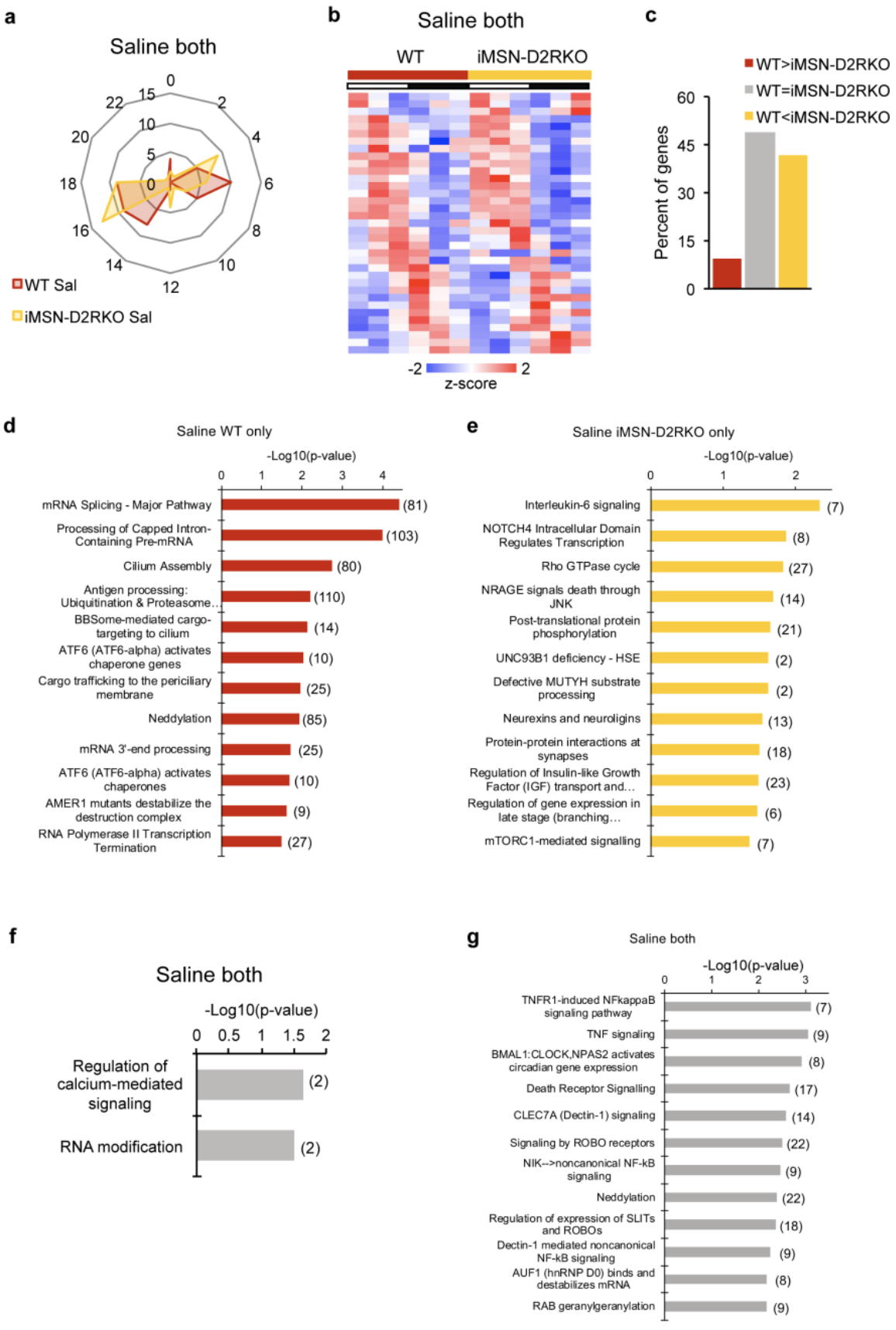
a
Saline both
WT Sal
iMSN-D2RKO Sal
b
Saline both
WT
iMSN-D2RKO
-2
2
z-score
c
WT>iMSN-D2RKO
WT=iMSN-D2RKO
WT<iMSN-D2RKO
Percent of genes
d
Saline WT only
-Log10(p-value)
mRNA Splicing - Major Pathway (81)
Processing of Capped Intron-Containing Pre-mRNA (103)
Cilium Assembly (80)
Antigen processing: Ubiquitination & Proteasome... (110)
BBSome-mediated cargo-targeting to cilium (14)
ATF6 (ATF6-alpha) activates chaperone genes (10)
Cargo trafficking to the periciliary membrane (25)
Neddylation (85)
mRNA 3'-end processing (25)
ATF6 (ATF6-alpha) activates chaperones (10)
AMER1 mutants destabilize the destruction complex (9)
RNA Polymerase II Transcription Termination (27)
e
Saline iMSN-D2RKO only
-Log10(p-value)
Interleukin-6 signaling (7)
NOTCH4 Intracellular Domain Regulates Transcription (8)
Rho GTPase cycle (27)
NRAGE signals death through JNK (14)
Post-translational protein phosphorylation (21)
UNC93B1 deficiency - HSE (2)
Defective MUTYH substrate processing (2)
Neurexins and neuroligins (13)
Protein-protein interactions at synapses (18)
Regulation of Insulin-like Growth Factor (IGF) transport and... (23)
Regulation of gene expression in late stage (branching... (6)
mTORC1-mediated signalling (7)
f
Saline both
-Log10(p-value)
Regulation of calcium-mediated signaling (2)
RNA modification (2)
g
Saline both
-Log10(p-value)
TNFR1-induced NFkappaB signaling pathway (7)
TNF signaling (9)
BMAL1:CLOCK,NPAS2 activates circadian gene expression (8)
Death Receptor Signalling (17)
CLEC7A (Dectin-1) signaling (14)
Signaling by ROBO receptors (22)
NIK-->noncanonical NF-kB signaling (9)
Neddylation (22)
Regulation of expression of SLITs and ROBOs (18)
Dectin-1 mediated noncanonical NF-kB signaling (9)
AUF1 (hnRNP D0) binds and destabilizes mRNA (8)
RAB geranylgeranylation (9)

Supplementary Figure 2 Phase and pathway analyses in WT and iMSN-D2RKO saline-treated mice

a, Radar plots representing the phase analysis of genes whose expression is circadian in both WT and iMSN-D2RKO saline-treated (Sal) mice. **b,** Heat maps representing genes significantly circadian (n=3, JTK_cycle, cutoff $p<0.01$) in both WT and iMSND2RKO saline-treated mice. White and black bars indicate the light (ZT3, 7, 11) and dark (ZT15, 19, 23) timepoints respectively. **c,** Amplitude analysis of NAcc transcripts rhythmic in "both" WT and iMSN-D2RKO saline-treated mice. The percentage of genes with amplitude higher, lower or equal to WT is reported. d and e, Reactome Pathway analysis of circadian genes oscillating in WT only **(d)** and iMSN-D2RKO only **(e)** saline treated mice. Bar charts represent the -Log10(p-value) of each enriched term. The number of genes identified in each pathway is shown in parenthesis. **f,** DAVID Gene Ontology Biological Process analysis of circadian genes oscillating in both WT and iMSN-D2RKO saline-treated mice. Bar charts represent the -Log10(p-value) of each enriched term. **g,** Reactome Pathway analysis of circadian genes oscillating in both WT and iMSN-D2RKO saline-treated mice. Bar charts represent the -Log10(p-value) of each enriched term. The number of genes identified in each pathway is shown in parenthesis.

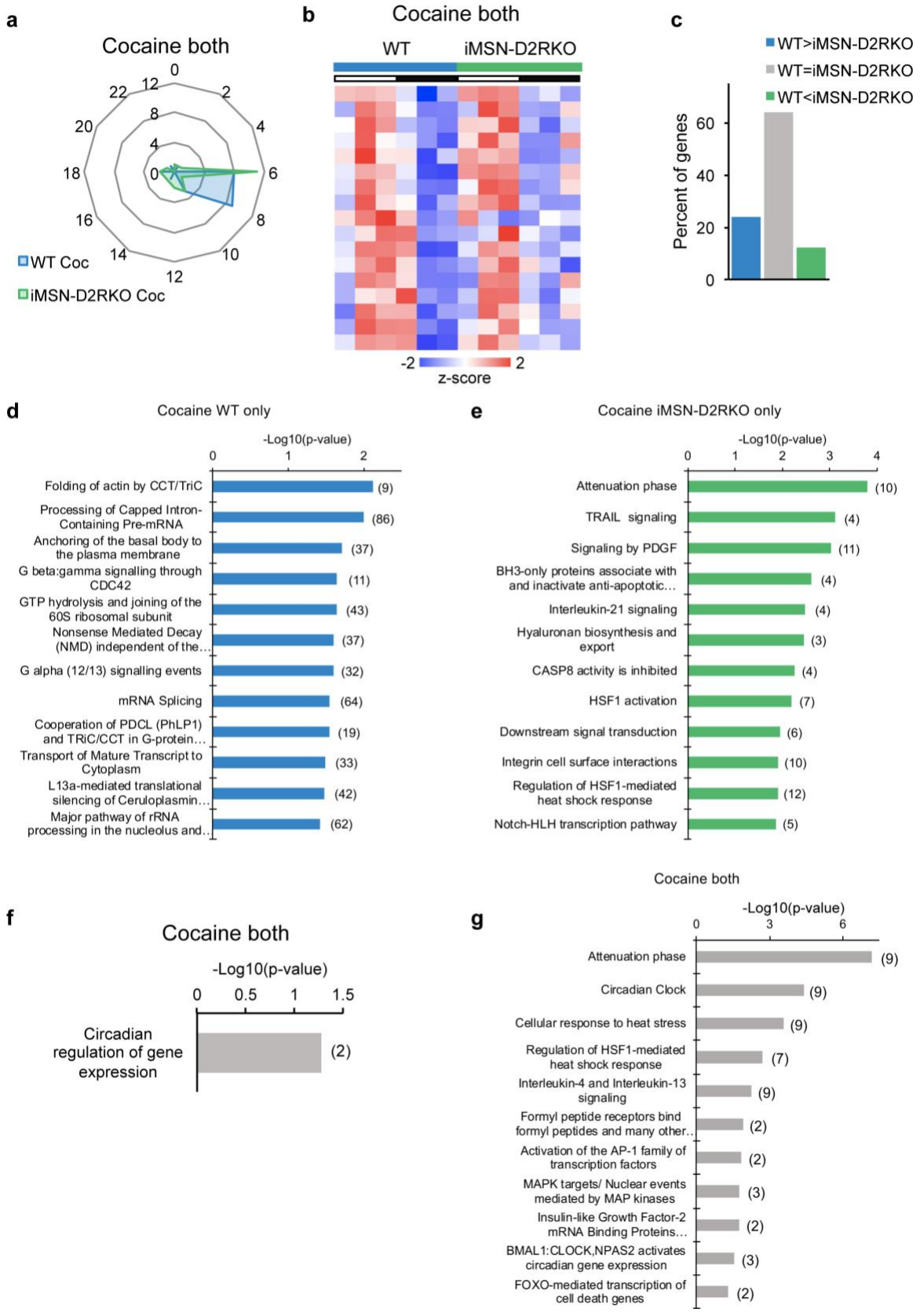
a
Cocaine both
WT Coc
iMSN-D2RKO Coc
b
Cocaine both
WT
iMSN-D2RKO
-2
2
z-score
c
WT>iMSN-D2RKO
WT=iMSN-D2RKO
WT<iMSN-D2RKO
Percent of genes
d
Cocaine WT only
-Log10(p-value)
Folding of actin by CCT/TriC (9)
Processing of Capped Intron-Containing Pre-mRNA (86)
Anchoring of the basal body to the plasma membrane (37)
G beta:gamma signalling through CDC42 (11)
GTP hydrolysis and joining of the 60S ribosomal subunit (43)
Nonsense Mediated Decay (NMD) independent of the… (37)
G alpha (12/13) signalling events (32)
mRNA Splicing (64)
Cooperation of PDCL (PhLP1) and TRiC/CCT in G-protein… (19)
Transport of Mature Transcript to Cytoplasm (33)
L13a-mediated translational silencing of Ceruloplasmin… (42)
Major pathway of rRNA processing in the nucleolus and… (62)
e
Cocaine iMSN-D2RKO only
-Log10(p-value)
Attenuation phase (10)
TRAIL signaling (4)
Signaling by PDGF (11)
BH3-only proteins associate with and inactivate anti-apoptotic… (4)
Interleukin-21 signaling (4)
Hyaluronan biosynthesis and export (3)
CASP8 activity is inhibited (4)
HSF1 activation (7)
Downstream signal transduction (6)
Integrin cell surface interactions (10)
Regulation of HSF1-mediated heat shock response (12)
Notch-HLH transcription pathway (5)
f
Cocaine both
-Log10(p-value)
Circadian regulation of gene expression (2)
g
Cocaine both
-Log10(p-value)
Attenuation phase (9)
Circadian Clock (9)
Cellular response to heat stress (9)
Regulation of HSF1-mediated heat shock response (7)
Interleukin-4 and Interleukin-13 signaling (9)
Formyl peptide receptors bind formyl peptides and many other… (2)
Activation of the AP-1 family of transcription factors (2)
MAPK targets/ Nuclear events mediated by MAP kinases (3)
Insulin-like Growth Factor-2 mRNA Binding Proteins… (2)
BMAL1:CLOCK,NPAS2 activates circadian gene expression (3)
FOXO-mediated transcription of cell death genes (2)

Supplementary Figure 3 Phase and pathway analyses in WT and iMSN-D2RKO cocaine-treated mice

a, Radar plots representing the phase analysis of genes whose expression is circadian in both WT and iMSN-D2RKO cocaine-treated (Coc) mice. **b,** Heat maps representing genes significantly circadian (n=3, JTK_cycle, cutoff $p<0.01$) in both WT and iMSND2RKO cocaine-treated mice. White and black bars indicate the light (ZT3, 7, 11) and dark (ZT15, 19, 23) timepoints respectively. **c,** Amplitude analysis of striatal transcripts rhythmic in "both" WT and iMSN-D2RKO cocaine-treated mice. The percentage of genes with amplitude higher, lower or equal to WT is reported. d and e, Reactome Pathway analysis of circadian genes oscillating in WT only **(d)** and iMSN-D2RKO only **(e)** cocaine-treated mice. Bar charts represent the -Log10(p-value) of each enriched term. The number of genes identified in each pathway is shown in parenthesis. **f,** DAVID Gene Ontology Biological Process analysis of circadian genes oscillating in both WT and iMSN-D2RKO cocaine-treated mice. Bar charts represent the -Log10(p-value) of each enriched term. **g,** Reactome Pathway analysis of circadian genes oscillating in both WT and iMSN-D2RKO cocaine-treated mice. Bar charts represent the -Log10(pvalue) of each enriched term. The number of genes identified in each pathway is shown in parenthesis.

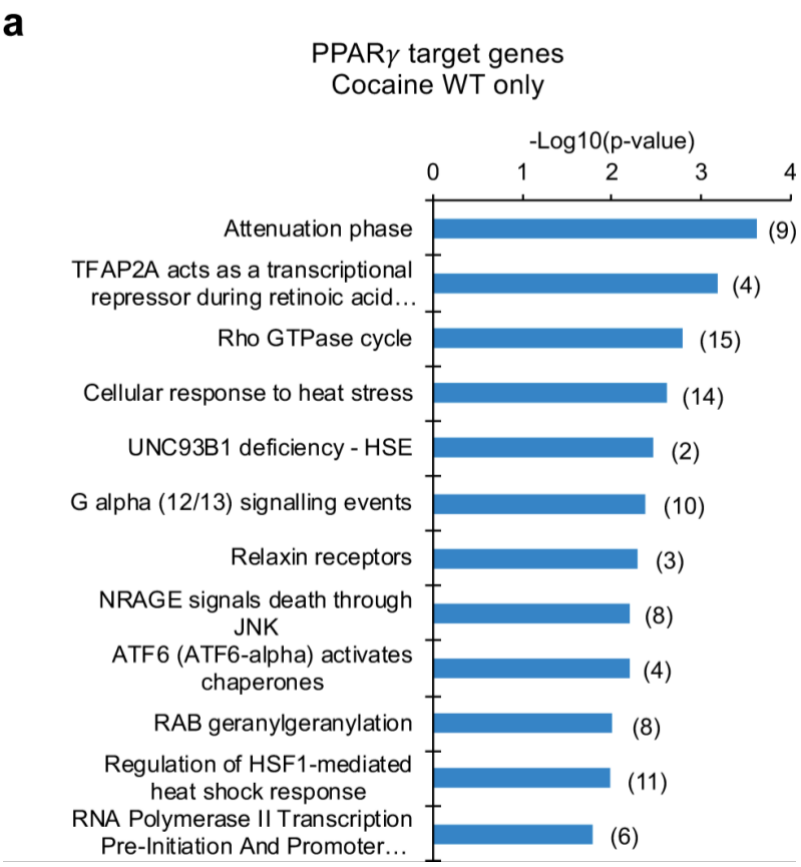

Supplementary Figure 4 Pathway analysis of PPAR target genes in WT cocaine treated Mice

a, Reactome pathway analysis of oscillatory PPARγ target genes in cocaine-treated WT mice (n=3, JTK_Cycle, cutoff $p < 0.01$). Bar charts represent the -Log10(p-value) of each enriched term. The number of genes identified in each pathway is shown in parenthesis.

Supplementary Table 1 Statistics for Figure 1g

Bmal1	**SS**	**DF**	**MS**	**F (DFn, DFd)**	**P value**
Time	1.811	5	0.3622	F (5, 48) = 6.805	P<0.0001
Treatment	0.1942	1	0.1942	F (1, 48) = 3.649	P=0.0621
Genotype	0.2022	1	0.2022	F (1, 48) = 3.798	P=0.0572
Time x Treatment	0.4559	5	0.09119	F (5, 48) = 1.713	P=0.1497
Time x Genotype	0.2632	5	0.05264	F (5, 48) = 0.9889	P=0.4345
Treatment x Genotype	0.1025	1	0.1025	F (1, 48) = 1.926	P=0.1716
Time x Treatment x Genotype	0.1459	5	0.02917	F (5, 48) = 0.5481	P=0.7389
Cry1	SS	DF	MS	F (DFn, DFd)	P value
Time	1.743	5	0.3487	F (5, 48) = 5.429	P=0.0005
Treatment	0.006013	1	0.006013	F (1, 48) = 0.09362	P=0.7609
Genotype	0.1796	1	0.1796	F (1, 48) = 2.796	P=0.1010
Time x Treatment	0.3174	5	0.06349	F (5, 48) = 0.9885	P=0.4346
Time x Genotype	0.08598	5	0.0172	F (5, 48) = 0.2678	P=0.9285
Treatment x Genotype	0.1282	1	0.1282	F (1, 48) = 1.996	P=0.1641
Time x Treatment x Genotype	0.17	5	0.034	F (5, 48) = 0.5294	P=0.7529
Per1	SS	DF	MS	F (DFn, DFd)	P value
Time	0.9461	5	0.1892	F (5, 48) = 6.215	P=0.0002
Treatment	0.005365	1	0.005365	F (1, 48) = 0.1762	P=0.6765
Genotype	0.3202	1	0.3202	F (1, 48) = 10.52	P=0.0022
Time x Treatment	0.685	5	0.137	F (5, 48) = 4.500	P=0.0019
Time x Genotype	0.1803	5	0.03607	F (5, 48) = 1.185	P=0.3307
Treatment x Genotype	0.0006089	1	0.0006089	F (1, 48) = 0.02000	P=0.8881
Time x Treatment x Genotype	0.08812	5	0.01762	F (5, 48) = 0.5789	P=0.7159
Dbp	SS	DF	MS	F (DFn, DFd)	P value
Time	7.595	5	1.519	F (5, 48) = 6.853	P<0.0001
Treatment	0.7277	1	0.7277	F (1, 48) = 3.283	P=0.0762
Genotype	0.002965	1	0.002965	F (1, 48) = 0.01338	P=0.9084
Time x Treatment	0.9625	5	0.1925	F (5, 48) = 0.8685	P=0.5092
Time x Genotype	0.364	5	0.07281	F (5, 48) = 0.3285	P=0.8933
Treatment x Genotype	0.0834	1	0.0834	F (1, 48) = 0.3763	P=0.5425
Time x Treatment x Genotype	1.899	5	0.3799	F (5, 48) = 1.714	P=0.1495

Chapter 4: Dopamine D2 receptor signaling in the brain modulates circadian liver metabolomic profiles

ABSTRACT

The circadian clock is tightly intertwined with metabolism and relies heavily on multifaceted interactions between organ systems to maintain proper timing. Genetic and/or environmental causes can disrupt communication between organs and alter rhythmic activities. Substance use leads to altered dopamine signaling followed by reprogramming of circadian gene expression and metabolism in the reward system. However, whether altered dopamine signaling in the brain affects circadian metabolism in peripheral organs has not been fully explored. We show that dopamine D2 receptors (D2R) in striatal medium spiny neurons (MSNs) play a key role in regulating diurnal liver metabolic activities. In addition, drugs that increase dopamine levels, such as cocaine, disrupt circadian metabolic profiles in the liver which is exacerbated by loss of D2R signaling in MSNs. These results uncover a strict communication between neurons/brain areas and liver metabolism, as well as the association between substance use and systemic deficits.

SIGNIFICANCE STATEMENT

In this study, we analyzed the liver metabolome of mice deficient in the expression of the dopamine D2 receptor (D2R) in striatal medium spiny neurons (iMSN-D2RKO mice) and found profound changes in the liver circadian metabolome as compared to control mice. In addition, we show that activation of dopaminergic circuits by acute cocaine administration in iMSN-D2RKO mice reprograms the circadian liver metabolome in response to cocaine. D2R signaling in medium spiny neurons is key for striatal output and is essential for regulating the first response to the cellular and rewarding effects of cocaine. Thus, our results suggest that changes in dopamine signaling in specific striatal neurons evoke major changes in liver physiology. Dysregulation of liver metabolism could contribute to an altered allostatic state and therefore be involved in continued use of drugs.

INTRODUCTION

Substance use disorders affect millions of people world-wide (Grant et al. 2016). The rewarding properties of substances such as alcohol, nicotine, opioids, and psychostimulants, are linked to their ability to increase dopamine levels in brain areas that control emotions and induce pleasure (Di Chiara and Imperato 1988). Drug intake modifies neuronal plasticity and is at the start of the process of addiction, which leads vulnerable individuals to continually seek and abuse these substances despite the adverse consequences on their lives. Addiction causes long-term molecular and cellular changes in brain circuits involved in signaling reward (Nestler 2013).

The striatum is a key reward region that receives dopaminergic inputs from the ventral tegmental area and substantia nigra. Dorsal and ventral regions of the striatum are critical for the effects of addictive drugs. The dorsal striatum is critical for the motor stimulating effects of drugs, decision making, and habitual behavior (Balleine et al. 2007; Burton et al. 2015; Lipton et al. 2019). On the other hand, the ventral striatum - particularly the nucleus accumbens (NAcc), is involved in reward evaluation and incentive-based learning (Schultz et al. 1992; Alcaro et al. 2007; Daniel and Pollmann 2014). Prominent cell types in the striatum are the inhibitory γ-aminobutyric acid-producing medium spiny neurons (MSNs), which make up 90-95% of the striatal neuronal population (Graveland and DiFiglia 1985). Two output pathways originate from MSNs - the direct pathway formed by MSNs (dMSNs) expressing dopamine D1 receptors (D1R) and the indirect pathway formed by MSNs (iMSNs) expressing dopamine D2 receptors (D2R). Dopamine signaling in dMSNs and iMSNs is critical for the integration of- and response to- rewarding stimuli. Dysregulation of these neurons' activity has been extensively implicated in addiction (Lobo and Nestler 2011).

The development and progression of substance use disorders generates perturbations in circadian rhythms (Hasler et al. 2012; Logan et al. 2014). Disrupted circadian rhythms may result from a combination of substance abuse with genetic and environmental factors (Hasler et al. 2012; Logan et al. 2014), which interfere with metabolism. Transcription factors, CLOCK and BMAL1, regulate the rhythmic expression of mammalian clock-controlled genes (Asher and Sassone-Corsi 2015). Among these genes, *Period* (*Per1-3*), and *Cryptochrome* (*Cry1-2*) subsequently inhibit CLOCK-BMAL1-mediated gene expression (Green et al. 2008), driving a transcriptional-translational circadian feedback loop that operates in a 24-hour cycle.

Importantly, the circadian clock is a network of biological pacemakers, found in virtually all tissues of the body. These pacemakers direct and maintain proper rhythmic homeostasis through various endocrine and metabolic pathways (Partch et al. 2014; Bass and Lazar 2016). Circadian clocks are influenced by environmental cues such as food intake, physical exercise, and social activities that show tissue-specific effects (Welsh et al. 2010; Albrecht 2012). Indeed, the same clock genes display tissue-specific profiles dictated by the transcriptional machinery unique to each tissue and condition; thus, generating large networks of oscillating clocks.

Inter-organ communication is critical for maintaining organismal synchrony and systemic homeostasis as demonstrated by the plastic response of metabolites among various organs upon an environmental stressor (Mohawk et al. 2012). We investigated the inter-organ communication between the striatum and the liver by analyzing wild type (WT) mice and their littermates carrying a cell-specific deletion of D2R in iMSNs (iMSN-D2RKO). We further deepened our studies by analyzing this inter-organ communication in response to a widely abused drug, cocaine, as an external stressor. This way, we assessed whether cocaine-induced dopamine elevation in the striatum might affect liver homeostasis and the circadian fluctuation of metabolites. Interestingly,

in addition to metabolic changes found in untreated mice between genotypes, cocaine administration in iMSN-D2RKO mice leads to reprogramming of circadian gene expression in the NAcc (Eckel-Mahan et al. 2013). While an acute cocaine challenge induces variation in the profiles of rhythmic metabolites in the liver of WT mice, in iMSN-D2RKO mice, loss of D2R in the striatum alters this rhythmic profile. We determined the time-dependent distribution of metabolites in the liver after acute cocaine treatment. Furthermore, we observed dynamic diurnal changes in the number and class of rhythmic metabolites in saline-treated mice. Strikingly, the liver of mice administered cocaine showed a dampened response to the time-of-day variances. In combination with loss of D2R in iMSNs, cocaine increased the total number of oscillating metabolites as compared to WT mice. These results indicate that environmental and genetic changes in brain areas central for the rewarding effects of cocaine affect liver metabolic responses. Thus, we reveal a tight inter-organ interaction in response to cocaine, which strongly modifies the basal physiology and circadian rhythms not only in the brain (Brami-Cherrier et al. 2020), but also in the liver. These results highlight an unexpected level of communication between striatal neurons and liver metabolism, which might also contribute to development of substance use disorders.

RESULTS

Diurnal metabolic behavioral phenotypes of iMSN-D2RKO mice

In the striatum, dopamine receptor signaling is critical for the control of physiological responses including eating (Volkow et al. 2011) and motor behavior (Salamone 1992) which greatly influence metabolism. Thus, we analyzed the impact of typical or altered dopamine D2R signaling in the striatum on physiological parameters through comparisons between WT mice and littermates with the specific deletion of D2R in iMSNs (iMSN-D2RKO).

Since food intake and motor activity influence body weight (Foster-Schubert et al. 2012), we recorded the weights of mice of both genotypes from birth to adulthood. Interestingly, we observed no differences in body weight during the first 5 weeks after birth; thereafter, iMSN-D2RKO mice had reduced weight in comparison to WT controls (Two-Way ANOVA Mixed-effects analysis; Time $F_{(16,436)}=548.7$ $p<0.0001$, Genotype $F_{(1,41)}=78.08$ $p<0.0001$, Interaction $F_{(16,436)}=2.24$ $p=0.0040$) (Fig 1A). Thus, we examined diurnal activity and energy expenditure along with eating and drinking behaviors in calorimetic cages which could explain this difference between adult iMSN-D2RKO and WT mice. In agreement with previous data (Kharkwal et al. 2016b), we found that in actimetric cages, iMSN-D2RKO mice show significantly lower beam break counts as compared to WT littermates during their active phase (dark phase, $p=0.0099$), but not during their inactive phase (light phase, $p=0.9922$) (Fig. 1B). Moreover, energy expenditure of iMSN-D2RKO mice was markedly reduced in both dark ($p=0.0001$) and light phases ($p=0.0125$) (Fig. 1C), as compared to WT littermates. Relatedly, iMSN-D2RKO mice showed decreased chow consumption (Fig. 1D) as compared to their WT littermates during the dark phase

(p=0.0019), but not the light phase (p=0.5951); the same trend was observed for water intake (Dark, p=0.0345; Light, p=0.4292) (Fig. 1E). Interestingly, despite decreased chow consumption and lower weight, adult iMSN-D2RKO mice had significantly higher gonadal fat content as compared to their WT counterparts (p=0.0001) (Fig. 1F).

Profiling of the circadian metabolome in iMSN-D2RKO mouse liver

The liver plays a central role in metabolic processes. Both genetic and environmental challenges are capable of reprogramming the liver metabolome (Eckel-Mahan et al. 2012, 2013; Adamovich et al. 2014; Masri et al. 2014; Aviram et al. 2016; Krishnaiah et al. 2017; Dyar et al. 2018) along the circadian cycle. Thus, we analyzed hepatic metabolites during the circadian cycle in iMSN-D2RKO and WT siblings. For this, we harvested liver tissue from mice of both genotypes every four hours spanning a full circadian cycle for a total of six time points (ZT 3, 7, 11, 15, 19, 23). Gene expression of core clock genes confirmed the rhythmicity of the samples used for metabolite analyses (Fig. S1). The hepatic metabolome was quantified by mass spectrometry. Circadian rhythmicity was analyzed using JTK_CYCLE(33), a non-parametric test, to determine the number of significantly oscillating ($p<0.05$; with a period of ~24h) circadian metabolites for each genotype (Fig. 2A). We found nearly 20% of the 180 metabolites analyzed were significantly oscillating ($p<0.05$) in both genotypes (34 and 32 metabolites in the WT and iMSN-D2RKO mice, respectively). This finding is in general agreement with the percentage of rhythmic metabolites identified in previous studies (Eckel-Mahan et al. 2012, 2013; Adamovich et al. 2014; Masri et al. 2014; Aviram et al. 2016; Krishnaiah et al. 2017; Dyar et al. 2018). Importantly, ~80% of the oscillating metabolites were lipids including acylcarnitines, phosphatidylcholines,

sphingomyelins, and lysophosphatidylcholines. The remaining oscillating metabolites belonged to the amino acids and biogenic amines groups (Fig. 2B). Specifically, ~32% of the rhythmic metabolites in the WT and 46% in the iMSN-D2RKO livers were amino acid-derived metabolites. Phase analyses revealed ZT8 and ZT14-18 as the main timepoints at which circadian metabolites peak in abundance (Fig. 2C). Likewise, the amplitudes of the oscillating metabolites are nearly consistent in both WT and iMSN-D2RKO mice (Fig. S2A). These data show that rhythmic metabolites in WT and iMSN-D2RKO livers display similar circadian patterns. However, in addition to a subset of metabolites that oscillate in both genotypes, and despite the similarities in circadian parameters, comparisons of individual metabolites oscillating in each genotype identified unique metabolites exclusively oscillating either in WT or in iMSN-D2RKO livers (Fig. 2D and 2E). Surprisingly, in iMSN-D2RKO mice, ~44% of liver metabolites lost rhythmicity when compared to WT controls. In addition, ~40% of metabolites show *de novo* oscillations in iMSN-D2RKO livers not observed in the WT. Among the metabolites analyzed, acylcarnitines show the greatest loss of rhythmicity in iMSN-D2RKO livers (Fig. 2F and 2G). We analyzed the circadian gene expression profile of the metabolic enzyme carnitine palmitoyltransferase 1A (*Cpt1a*) which catalyzes the transfer of an acyl-group onto carnitines in the production of acylcarnitines, which showed a significantly elevated expression in iMSN-D2RKO mouse liver at ZT11 and ZT15 by qPCR (Fig. S2B). It is tempting to speculate that this increased expression is likely to contribute to the loss of rhythmicity of the five acylcarnitines in the iMSN-D2RKO livers (Fig. S2C). Conversely, a three-fold increase was found for newly oscillating metabolites in the iMSN-D2RKO livers, which consisted of some amino acids, including methionine and leucine. Metabolites consistently rhythmic in both genotypes included amino acids, biogenic amines, acylcarnitines and phosphatidylcholines. These analyses demonstrate a previously ignored

influence of striatal neurons on the liver, as distinct metabolites show altered circadian profiles in the liver of iMSN-D2RKO mice as compared to WT.

Loss of D2R in iMSNs alters the rhythmic liver metabolome of cocaine treated mice

The impact of absent D2R signaling in iMSNs on circadian liver metabolites under basal conditions (saline) prompted us to analyze the effect of a dopaminergic challenge on liver metabolism in WT and mutant mice. We used cocaine which is known to increase dopamine levels in the striatum and disrupt the circadian cycle (Brami-Cherrier et al. 2020). For this, we compared the liver metabolome in saline- and cocaine- treated (administered at ZT3) WT and iMSN-D2RKO mice. Strikingly, ~73% of the metabolites oscillating in saline treated WT mice lose their rhythmicity after cocaine administration. Only ~26% of the previously oscillating metabolites in saline conditions retain their rhythmicity after acute cocaine (Fig. 3A and 3B). The amplitude of circadian oscillations in both saline and cocaine treated WT mice followed similar patterns, indicating that the robustness of the oscillations is unchanged by cocaine (Fig. S3A). Intriguingly, in WT livers, cocaine administration led to four times less oscillating acylcarnitines (Fig. 3C). 25% of circadian metabolites in iMSN-D2RKO livers lost rhythmicity after cocaine
as compared to saline treated control mouse tissue (Fig. 3D). Conversely, 75% of oscillating metabolites in saline treated iMSN-D2RKO mice are unaffected by cocaine administration. Nevertheless, a staggering number of *de novo* oscillating metabolites were induced in iMSN-D2RKO livers after cocaine treatment as compared to livers from saline treated mice (Fig. 3D and 3E). Treatments (Sal or Coc) did not affect the amplitude of the oscillations in iMSN-D2RKO liver metabolites (Fig. S3B). Interestingly, the number of rhythmic acylcarnitines and

phosphatidylcholines identified in the cocaine treated iMSN-D2RKO mice increased well above that of saline treated mice (Fig. 3F). Thus, loss of D2R signaling in the striatal iMSNs critically affects hepatic metabolism not only under basal conditions, but also in response to a cocaine challenge.

Cocaine disrupts circadian gene expression and metabolic profiles in the striatum involving D2R-mediated regulation of iMSNs(Lynch et al. 2008; Brami-Cherrier et al. 2020). Thus, we analyzed and compared the full circadian metabolic profiles of livers from iMSN-D2RKO and WT mice given a single injection of cocaine at ZT3 (Fig. 3G-I). No major changes were observed in the amplitude of oscillating metabolites common between cocaine treated iMSN-D2RKO and WT mice (Fig. S3C). Moreover, 16% of detected metabolites were oscillating in WT mice treated with cocaine, whereas up to ~41% were oscillating in iMSN-D2RKO mice (Fig. 3G). Additionally, the phase of the identified circadian metabolites did not coincide between cocaine treated WT and iMSN-D2RKO mice. In WT mice, the peak in rhythmicity during the light phase was observed around ZT8, whereas in iMSN-D2RKO mice it shifted between ZT2-ZT6. This difference in peak between the WT and iMSN-D2RKO cocaine treated groups is not dependent on the injection itself, as all groups received an injection of saline or cocaine at the same time point. On the contrary, the dark phase metabolite peak at about ZT16 remained consistent in both genotypes (Fig. 3H). Notably, in WT cocaine-treated mice, acylcarnitines comprised only ~7% of oscillating metabolites in the liver, but made up ~30% of circadian metabolites in iMSN-D2RKO mice (Fig. 3I). Our data point to a striatal D2R-mediated control of circadian liver metabolites and shows that dopamine signaling in the brain contributes to the regulation of liver physiology.

Effects of cocaine on the diurnal liver metabolome

Environmental cues including light, food intake, and exercise help maintain circadian synchrony of central and peripheral tissues (Tahara et al. 2017). Disturbances to these cues can result in systemic clock desynchrony and have detrimental effects on the organismal homeostasis(Patke et al. 2020). To determine time-of-day dependent differences in metabolite levels in the liver, we compared the metabolomic profiles of cocaine treated WT and iMSN-D2RKO mice during the light and dark phases at ZT11 and ZT23, the last time points in each phase, respectively (Fig. 4A). The majority of the metabolomic changes observed in the WT saline-treated mouse liver between ZT11 and 23 are found in phosphatidylcholines, acylcarnitines and, to a lesser extent, biogenic amines ($p<0.05$, ANOVA Benjamini-Hochberg corrected). Only after cocaine treatment did time-of-day dependent metabolites in the WT liver include sphingomyelins and lysophosphatidylcholines ($p<0.05$, ANOVA Benjamini-Hochberg corrected) (Fig. 4A). iMSN-D2RKO mice treated with cocaine show a striking decrease in the number of phosphatidylcholines that change with time in the liver ($p<0.05$, ANOVA Benjamini-Hochberg corrected), an indication that a combination of cocaine and a loss of D2R greatly perturb phospholipid metabolism. Principal component analysis was performed to assess the correlation between and within the four experimental conditions: WT saline, WT cocaine, iMSN-D2RKO saline and iMSN-D2RKO cocaine at each time point (Fig. S4). When both time points are combined, no obvious correlation can be determined among the four datasets, suggesting the genotype x treatment interaction is influenced by time. Indeed, when separated by time point, clusters for each group are apparent, although less so at ZT23 (Fig. S4). Further, we compared the upregulation of the metabolites at ZT11 and ZT23 (Fig. 4B). In the liver of saline treated mice, we

found over 50% of the metabolites that change between time points exhibited higher levels during the dark phase (ZT23) ($p<0.05$, ANOVA Benjamini-Hochberg corrected). Indeed, in the saline condition, a time-dependent upregulation of phosphatidylcholines was observed at ZT23 in the WT and iMSN-D2RKO livers (Fig. 4C). Surprisingly, cocaine reversed this trend and induced higher metabolite levels at ZT11 than at ZT23 in the liver of WT mice ($p<0.05$, ANOVA Benjamini-Hochberg corrected) (Fig. 4B). Cocaine upregulated lysophosphatidylcholines, sphingomyelins, and phosphatidylcholines in the WT mice at ZT11 ($p<0.05$, ANOVA Benjamini-Hochberg corrected). Conversely, at ZT11, livers of cocaine-treated iMSN-D2RKO mice show an upregulation primarily of amino acids and biogenic amines ($p<0.05$, ANOVA Benjamini-Hochberg corrected). Taken together, our findings demonstrate that disrupted D2R signaling in iMSNs and an acute cocaine challenge alters temporal liver metabolism.

DISCUSSION

Drugs of abuse hijack brain circuits that belong to the reward system. Indeed, all abused drugs elevate dopamine levels in the brain and most notably in the mesolimbic dopamine system, thereby generating pleasure and reward. The mesolimbic circuitry consists of dopaminergic projections arising from the midbrain and projecting to the striatum. The dorsal striatum has involvement in decision making including initiation and action selection, controls habitual behavior, and mediates valiance and magnitude (Balleine et al. 2007; Burton et al. 2015; Lipton et al. 2019). Relatedly, the ventral striatum, in particular the NAcc, is most appreciated for its involvement in reward processing and evaluation as well as incentive-based learning (Schultz et al. 1992; Alcaro et al. 2007; Daniel and Pollmann 2014). The connections and mechanisms linking

different neurons to the generation of reward is a topic of great importance and interest (Ikemoto and Panksepp 1999; Knutson et al. 2001). The major constituents of the striatum, the MSNs, serve as this brain structure's exclusive output neurons (Girault 2012). Human studies have shown that people with addiction have decreased D2R binding availability in the striatum regardless of the class of drug being used (Volkow et al. 1997). Thus, our iMSN-D2RKO mouse appears to be a good candidate to model this human condition as this model has a deletion of D2R throughout the dorsal and ventral regions of striatum. Despite the presence of cocaine, loss of D2R results in a reduced movement and locomotor behavior (Fig. 1B) (Kharkwal et al. 2016b). The absence of D2R alone alters a number of metabolic parameters including body weight, food intake, energy expenditure, and fat tissue accumulation (Fig. 1C-E). As expected, these metabolic parameters changed in a time-of-day dependent manner due to the intimate link between metabolism and the circadian clock. Thus, to further investigate the contributions of D2R on metabolism, we performed metabolomic analysis on the livers of WT and iMSN-D2RKO littermates throughout a full circadian cycle for a greater time point resolution.

The cell-specific loss of D2R did not change the overall circadian parameters of the metabolites in the liver (Fig. 2). Yet, quite surprisingly, we demonstrate the changes induced in the absence of D2R are found in the distribution of the number of oscillating metabolites of each class. Notably, acylcarnitines show the greatest change to the number of oscillating metabolites that lose rhythmicity in the iMSN-D2RKO mouse liver and instead display constitutively higher levels throughout the day. Of these, we have identified hydroxybutyrylcarnitine as a metabolite significantly rhythmic in the WT but not in the iMSN-D2RKO. Previous studies demonstrate a strong association between acylcarnitines and insulin resistance in people suffering from type 2 diabetes (Soeters et al. 2012; Schooneman et al. 2013).

The peripheral metabolic impact of the loss of striatal D2R signaling could be clearly seen in the presence of cocaine. Indeed, this dopaminergic challenge resulted in almost 3-fold more oscillating metabolites in cocaine treated iMSN-D2RKO mice as compared to WT controls (Fig. 3A). A large number of these metabolites could be the result of an increase in metabolites oscillating between ZT2-6 in iMSN-D2RKO mice that is not present in WT mice (Fig. 3B). Importantly, we found that acylcarnitines and phosphatidylcholines were metabolite classes in the liver highly altered by cocaine administration in iMSN-D2RKO. It can be argued that some of the observed changes can be ascribed to the genetic manipulation of the D2R gene or to the CRE line used to obtain iMSN-D2RKO mice. While we cannot completely exclude this possibility, we are confident that this is not the case. In support of our findings, changes of these metabolites were also found by NMR in the blood of crack-cocaine addicts (Costa et al. 2019).

The liver uses excess glucose from food and converts it into fatty acids which are stored as visceral fat in order to promote long term energy storage. We find that the iMSN-D2RKO animals have a higher fat to body weight ratio than WT littermates (Fig. 1F). Lipidomic analyses of cocaine treated mice discovered an increase in lipid metabolism resulted in a protective effect against hepatotoxicity (Aviram et al. 2016). The changes we observed in the lipid metabolites may be attributed to an additive accumulation of liver insults induced by cocaine and indirectly by the loss of D2R. Communication between the suprachiasmatic nucleus and the striatum have been recently identified (Verwey et al. 2016; Miyazaki et al. 2021). The neurochemistry of these connections may be affected in the absence of D2R in iMSNs which could then result in a dysregulation of peripheral organs including the liver. Recent work has shown that the nuclear receptor, PPARγ, plays a role in inducing changes to the molecular clock in the striatum in an iMSN-D2R-dependent

manner (Brami-Cherrier et al. 2020). We might speculate that through striatal D2R signaling, cocaine might induce a proinflammatory response that affects liver function.

A high fat dietary challenge proved to have substantial effects on circadian metabolite coordination between tissues (Dyar et al. 2018). Metabolic inter-tissue communication is highly dynamic and easily influenced by external factors introduced to the body. Our findings support this notion as cocaine, a dopaminergic challenge, has a striatal-dependent impact on the liver, with a more striking effect in the absence of D2R in iMSNs (Fig. 4). Here, using light and dark phase timepoints (ZT11 and ZT23, respectively), we identified liver metabolites changing in a time-dependent manner. Intriguingly, cocaine induced altered levels of sphingomyelins in the liver. Sphingomyelins, typically associated with neuronal axons, when detected in the liver can serve as biomarkers for hepatotoxicity and liver damage (Apostolopoulou et al. 2018; Simon et al. 2020). Future studies will be aimed at examining the specific metabolites identified in greater detail to unravel the mechanisms underlying the regulation of liver rhythmicity by striatal D2R signaling. Our results lead us to conclude that challenging the dopaminergic reward system by cocaine use and altered striatal D2R signaling can contribute to the progression of metabolic diseases.

In this study, we took an unconventional angle to study the effects of the dopaminergic pathways and the consequences of drugs of abuse on the periphery. We describe that the circadian metabolic state of the liver in iMSN-D2RKO mice is more prone to induce *de novo* rhythmic acylcarnitines after a cocaine challenge. Importantly, our findings also show that the desynchrony between the liver and striatum, in the absence of D2R in a neuron type specific manner, influences liver homeostasis; only to be heightened by cocaine. These findings link metabolites to drug use-mediated alterations in the brain affecting peripheral tissues. Based on our data, it is tempting to propose a tight association between drug use and the increased susceptibility to metabolic diseases

(Drake et al. 1990; Warner et al. 1998; Henry 2000; Virmani et al. 2007; Li and Zhao 2021; Della Fazia and Servillo) via altered modulation of acylcarnitines and sphingomyelins in the liver. Future studies should seek to identify other key players of the inter-tissue communication in an aim to prevent drug use-induced metabolic disorders.

METHODS

Animals

3-month-old male, iMSN-D2RKO mice were generated by mating $D2R^{flox/flox}$ mice (WT) with $D2R^{flox/flox/D1R\text{-}CRE+/-}$ mice (iMSN-D2RKO) with a genetic background of 98.44% C57BL6 × 1.56% 129 SV(Anzalone et al. 2012). The ability of D1R CRE to eliminate D2R in iMSNs stems from the common expression of D1R and D2R in embryonic MSN precursors (Aizman et al. 2000). D2R ablation in iMSNs was previously confirmed by recording D2R-specific binding using 3H-labeled ligand on striatal extracts, as well as *in situ* hybridization experiments using riboprobes targeting GAT1 as an MSN marker and exon 2 of D2R (Anzalone et al. 2012). Mice were maintained on a standard 12 h light/ 12 h dark cycle; food and water were available *ad libitum* in ~25 °C; humidity was 40–60%. Animals' care and use was in accordance with guidelines of the Institutional Animal Care and Use Committee at the University of California, Irvine. Genotype identification was performed by Southern blot and PCR analyses of DNA extracted from tails biopsies.

Motor activity and food intake

Motor activity was measured using actimetric boxes with a photo beam system and recorded with Lab watcher software. WT and iMSN-D2RKO mice were single housed during testing. Beam breaks (counts)/minute were averaged every 12 h during the light cycle 6:30 am-6:30 pm, and during the dark cycle 6:30 pm-6:30 am or every hour. Chow intake was measured every day for 5 consecutive days at 6 pm. Food intake was calculated as the grams of food consumed in 24 h over the body weight of the mouse.

Cocaine treatment

Before cocaine treatments, mice were handled for at least 3 days for 5 min. On the day of treatment, mice were administered either cocaine or saline. Cocaine (Sigma, Cat. #C5776) was dissolved in saline (NaCl 0.9%) and injected intraperitoneally (i.p.) at the dose of 20 mg kg^{-1}.

Metabolomics analyses

Metabolite levels were measured from WT and iMSN-D2RKO mouse liver tissue harvested at ZT3, 7, 11, 15, 19, 23 after an intraperitoneal injection of saline or cocaine at a dose of 20 mg kg−1 at ZT3, 5 replicates were used/timepoint/treatment. Metabolomic analyses were performed by Biocrates (Innsbruck, Austria) focusing on metabolites critical for neuronal structure, function and signaling (Adibhatla and Hatcher 2007; Piomelli et al. 2007) using the AbsoluteIDQ p180 platform. Briefly, to extract metabolites from liver tissue, the samples were first suspended in an 85% ethanol/ 15% 10 mM phosphate buffer (pH 7.4), using 3 µL extraction buffer per mg wet weight. The samples were then sonicated, vortexed and homogenized using a Precellys-24

instrument (Bertin Technologies, Montigny le Bretonneux, France). After homogenization, an aliquot of each supernatant was centrifuged and used for metabolomics measurements.

The measurements were run according to the AbsoluteIDQ® p180 kit manufacturer's instructions. The experimental metabolomics measurement technique is described in detail by patents EP1897014B1 (https://patents.google.com/patent/EP1897014B1) and EP1875401B1 (https://patents.google.com/patent/EP1875401B1). In short, Biocrates' commercially available kit plates were used for the quantification of amino acids, acylcarnitines, sphingomyelins, phosphatidylcholines, hexoses, and biogenic amines. The fully automated assay was based on phenyl isothiocyanate (PITC) derivatization in the presence of internal standards, followed by Flow injection analysis-tandem mass spectrometry (FIA-MS/MS) for acylcarnitines, lipids, and hexose and Liquid chromatography-tandem mass spectrometry (LC-MS/MS) for amino acids and biogenic amines using an AB SCIEX 4000 QTrap® mass spectrometer (AB SCIEX, Darmstadt, Germany) with electrospray ionization. Data were quantified using Sciex Analyst® and imported into the biocrates MetIDQ™ software for further analysis.

Statistics and bioinformatics analyses

Statistical and bioinformatics analyses were performed based on pairwise comparisons, where the effect of cocaine treatment was analyzed while controlling the genotype or the difference between genotypes (WT or iMSN-D2RKO) were compared while controlling the treatment. Dixon's test was performed to reduce outlier effects, filtering out up to 1 outlier replicate from each condition. Heat maps for the metabolite profiles were generated using the RStudio software. Row z-scores are displayed and were calculated using the 'heatmap.2' function of the gplots package. GraphPad Prism 9.2.0 (La Jolla California, USA) was used to perform statistical analyses

and generate principal component analysis plots. Two-Way Analysis of Variance (ANOVA) or Two-Way ANOVA Mixed-effects model followed by Tukey's multiple comparison post hoc test was used as appropriate; $p < 0.05$ was considered statistically significant. Values are presented as mean±SEM. ANOVA Benjamini-Hochberg corrected statistical analysis was performed to calculate the time-dependent effects.

Figure Legends

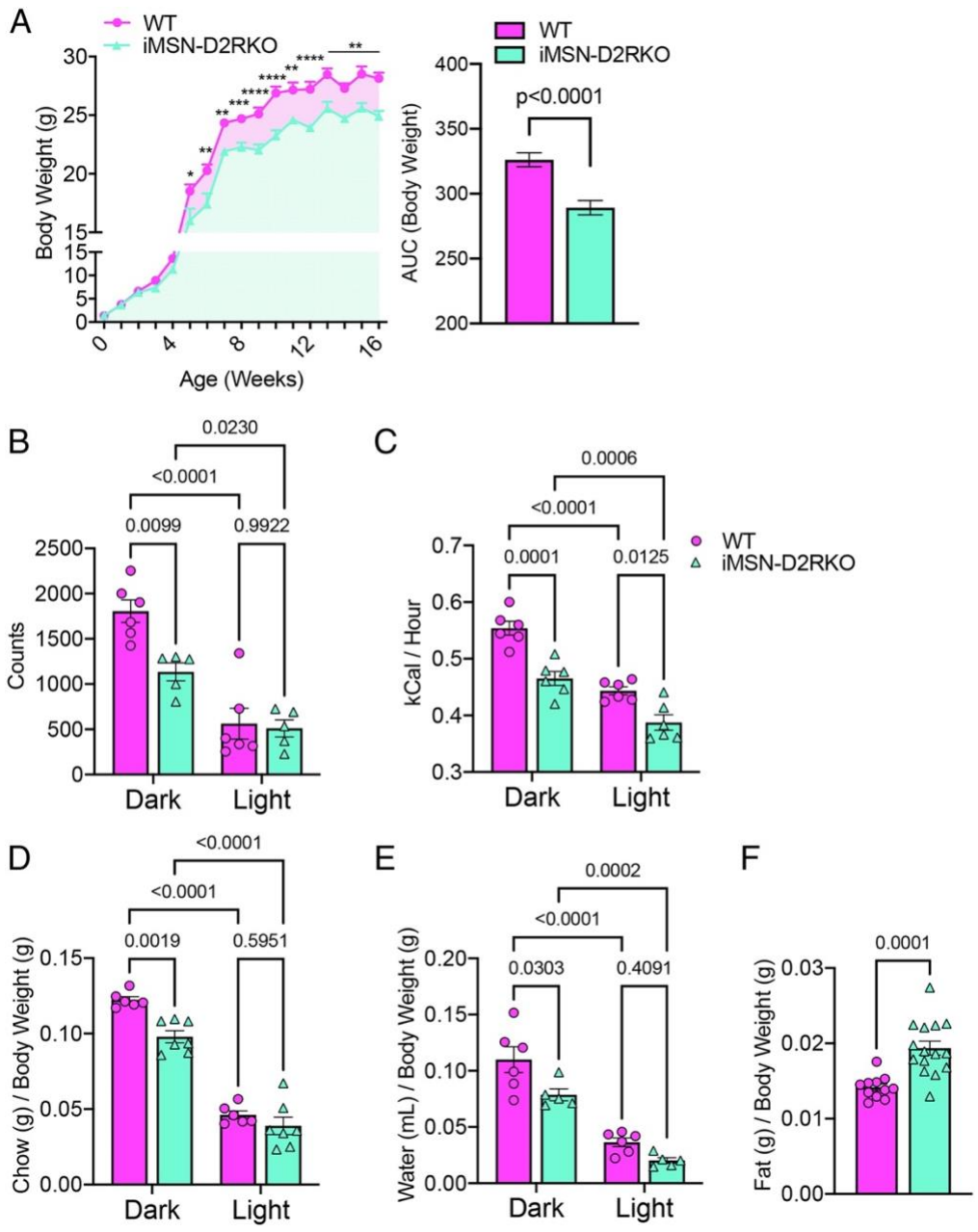

Fig. 1 Diurnal metabolic behavioral phenotypes of iMSN-D2RKO mice. A. *Left:* Body weights of WT (pink circles) and iMSN-D2RKO (blue triangles) mice were recorded once a week from birth to 16-weeks in age. Two-Way ANOVA Mixed-effects analysis; Time $F_{(16,436)}$=548.7 p<0.0001, Genotype $F_{(1,41)}$=78.08 p<0.0001, Interaction $F_{(16,436)}$=2.24 p=0.0040. Bonferroni post-hoc test: *p<0.05, **p<0.01, ***p<0.001, ****p<0.0001. *Right:* Area under the curve (AUC) from the body weight curve (*left)*. Unpaired student's t-test p<0.0001. **B.** Diurnal activity of iMSN-D2RKO and WT mice presented as beam break counts in an actimetric cage during the light and dark phases. Two-Way ANOVA; Phase $F_{(1,18)}$=50.22 p<0.0001, Genotype $F_{(1,18)}$=7.540 p=0.0133, Interaction $F_{(1,18)}$=5.533 p=0.0302 **C.** Energy expenditure while in the metabolic cages was recorded in iMSN-D2RKO and WT. Two-Way ANOVA; Phase $F_{(1,22)}$=271.3 p<0.0001, Genotype $F_{(1,22)}$=14.99 p=0.0008, Interaction $F_{(1,22)}$=4.352 p=0.0488. **D.** Bar graph showing the chow consumption (Phase $F_{(1,18)}$=84.35 p<0.0001, Genotype $F_{(1,18)}$=10.88 p=0.0040, Interaction $F_{(1,20)}$=1.995 p=0.1731) and **E.** Water intake of iMSN-D2RKO and WT mice in the metabolic cages as a portion of their body weight. Two-Way ANOVA; Phase $F_{(1,18)}$=84.35 p<0.0001, Genotype $F_{(1,18)}$=10.88 p=0.0040, Interaction $F_{(1,20)}$=1.995 p=0.1731 **f.** Gonadal fat of iMSN-D2RKO mice and their WT controls was dissected and weighed after metabolic testing. Student's t-test p=0.0001. All WT and iMSN-D2RKO mice were males, $n \geq 5$ as indicated by individual data points in each graph.

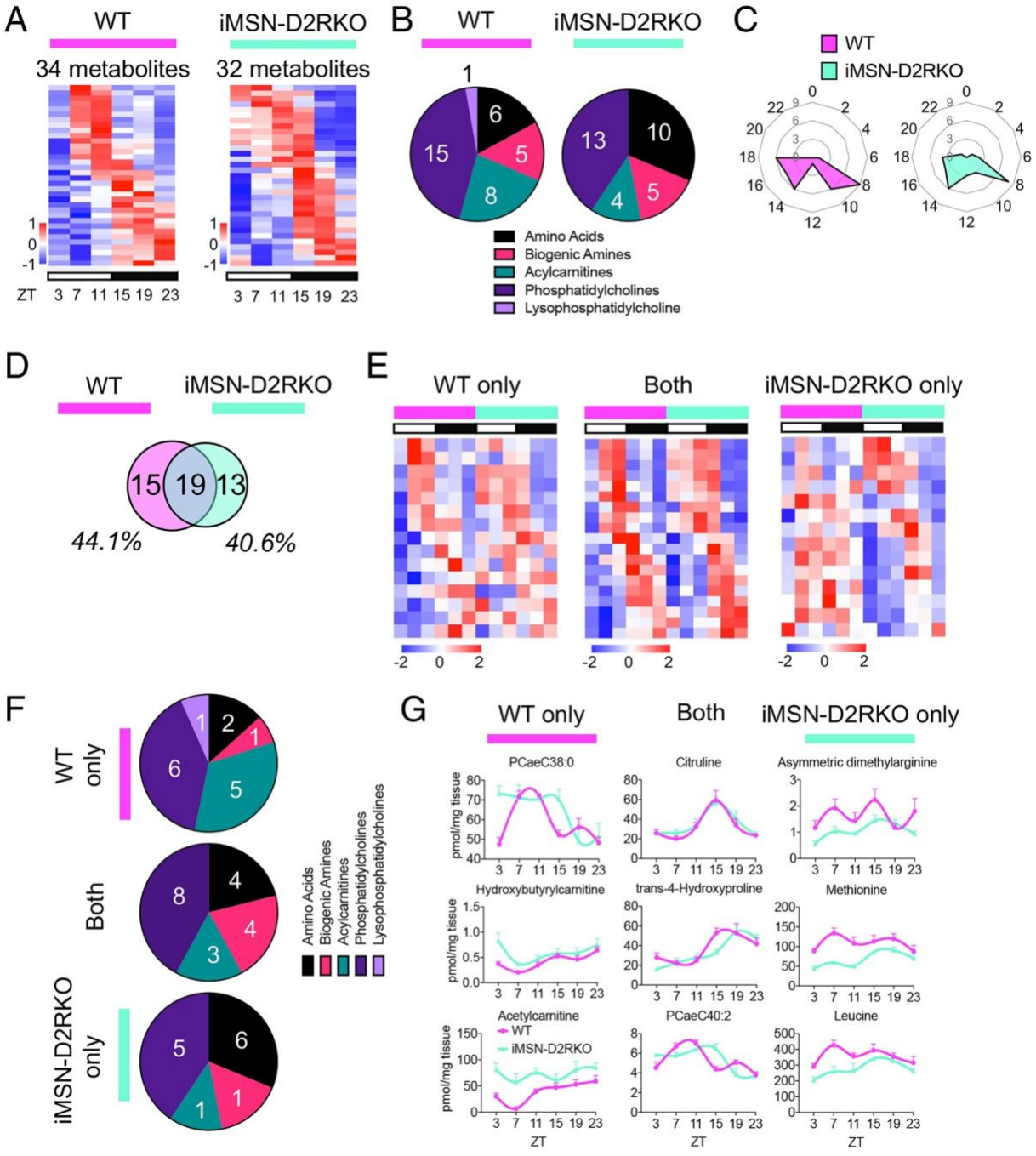
A
WT
iMSN-D2RKO
34 metabolites
32 metabolites
ZT 3 7 11 15 19 23
B
WT
iMSN-D2RKO
Amino Acids
Biogenic Amines
Acylcarnitines
Phosphatidylcholines
Lysophosphatidylcholine
C
WT
iMSN-D2RKO
D
WT
iMSN-D2RKO
44.1%
40.6%
E
WT only
Both
iMSN-D2RKO only
F
WT only
Both
iMSN-D2RKO only
G
WT only
Both
iMSN-D2RKO only
PCaeC38:0
Citruline
Asymmetric dimethylarginine
Hydroxybutyrylcarnitine
trans-4-Hydroxyproline
Methionine
Acetylcarnitine
PCaeC40:2
Leucine
pmol/mg tissue
ZT

Fig. 2 Profiling of the circadian metabolome in iMSN-D2RKO mouse liver. A. Heat maps of circadian metabolites in WT (left, pink) or iMSN-D2RKO mouse liver (right, blue). White and black bars indicate the light (ZT3, 7, 11) and dark (ZT15, 19, 23) timepoints respectively. **B.** Pie charts representing the percentage of metabolites of each class displaying rhythmic oscillations in WT (left, pink) or iMSN-D2RKO mouse liver (right, blue). **C.** Radar plots displaying the phase analysis of metabolites cycling in WT (left, pink) or iMSN-D2RKO mouse liver (right, blue). **D.** Venn diagram representing the hepatic rhythmic metabolites in WT (pink) and iMSN-D2RKO (blue) mice. **E.** Heat maps of circadian metabolites exclusively in WT (pink) or iMSN-D2RKO mouse liver (blue), and commonly circadian in both (middle). White and black bars indicate the light (ZT3, 7, 11) and dark (ZT15, 19, 23) timepoints respectively. **F.** Pie charts representing the percentage of metabolites of each class displaying rhythmic oscillations exclusively in WT (pink) or iMSN-D2RKO mouse liver (blue), and circadian in both genotypes (middle). **G.** Representative circadian profiles of metabolites oscillating in WT (pink) or iMSN-D2RKO mouse liver (blue), and circadian in both genotypes (middle). n=5, JTK_CYCLE, cutoff $p < 0.05$. All tissues used for analyses were collected from male mice.

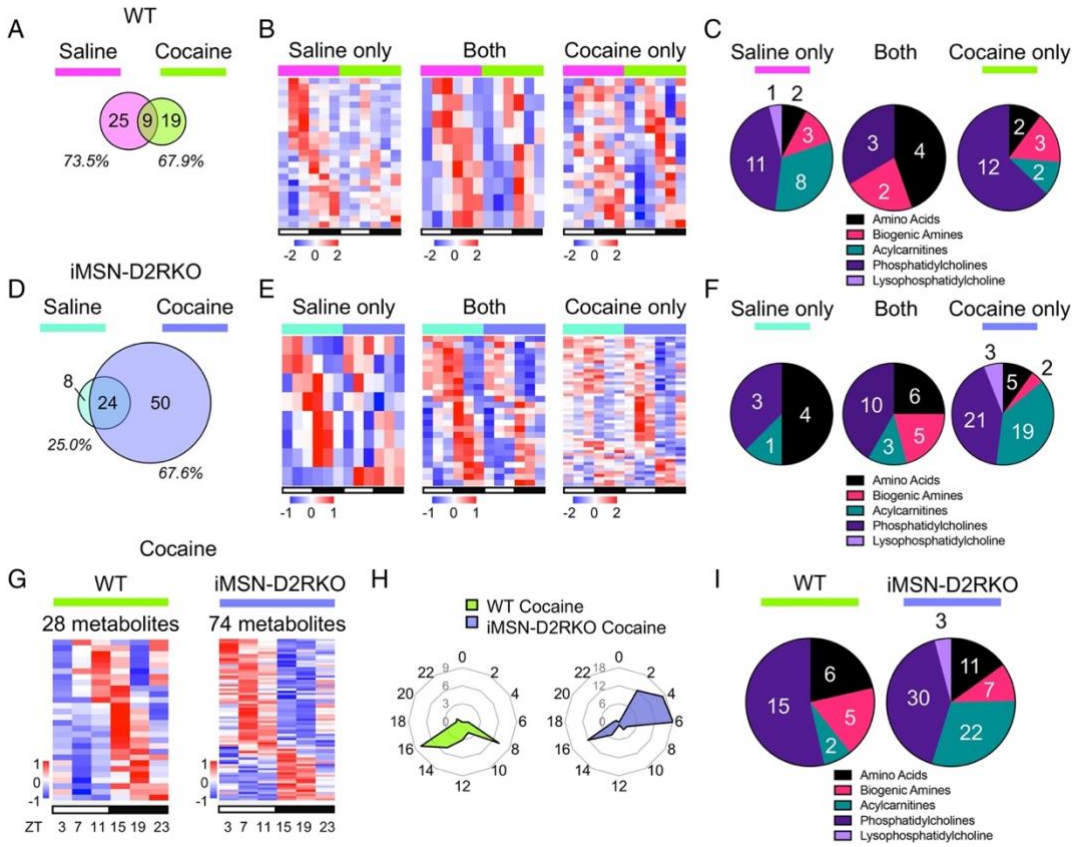

Fig. 3 Cocaine-induced disruption of liver circadian metabolites. A. Venn diagram representing the hepatic rhythmic metabolites in Saline (pink) and Cocaine (green) treated WT mouse liver. **B.** Heat maps of circadian metabolites exclusively in Saline (pink) or Cocaine (green) treated WT mouse liver, and circadian in both (middle). White and black bars indicate the light (ZT3, 7, 11) and dark (ZT15, 19, 23) timepoints respectively. **C.** Pie charts representing the percentage of metabolites of each class displaying rhythmic oscillations exclusively in Saline (pink) or Cocaine (green) treated WT mouse liver, and circadian in both (middle). **D.** Venn diagram representing the hepatic rhythmic metabolites in Saline (blue) and Cocaine (purple) treated iMSN-D2RKO mouse liver. **E.** Heat maps of circadian metabolites exclusively in Saline (blue) or Cocaine (purple) treated iMSN-D2RKO mouse liver, and circadian in both (middle). White and black bars indicate the light (ZT3, 7, 11) and dark (ZT15, 19, 23) timepoints respectively. **F.** Pie charts representing the percentage of metabolites of each class displaying rhythmic oscillations exclusively in Saline (blue) or Cocaine (purple) treated iMSN-D2RKO mouse liver, and circadian in both (middle). **G.** Heat maps of circadian metabolites in livers of Cocaine treated WT (green) or iMSN-D2RKO mice (purple). White and black bars indicate the light (ZT3, 7, 11) and dark (ZT15, 19, 23) timepoints respectively. **H.** Radar plots displaying the phase analysis of metabolites cycling in livers of Cocaine treated WT (green) or iMSN-D2RKO mice (purple). **I.** Pie charts representing the percentage of metabolites of each class displaying rhythmic oscillations in livers of Cocaine treated WT (green) or iMSN-D2RKO mice (purple). n=5, JTK_CYCLE, cutoff p< 0.05. All tissues used for analyses were collected from male mice.

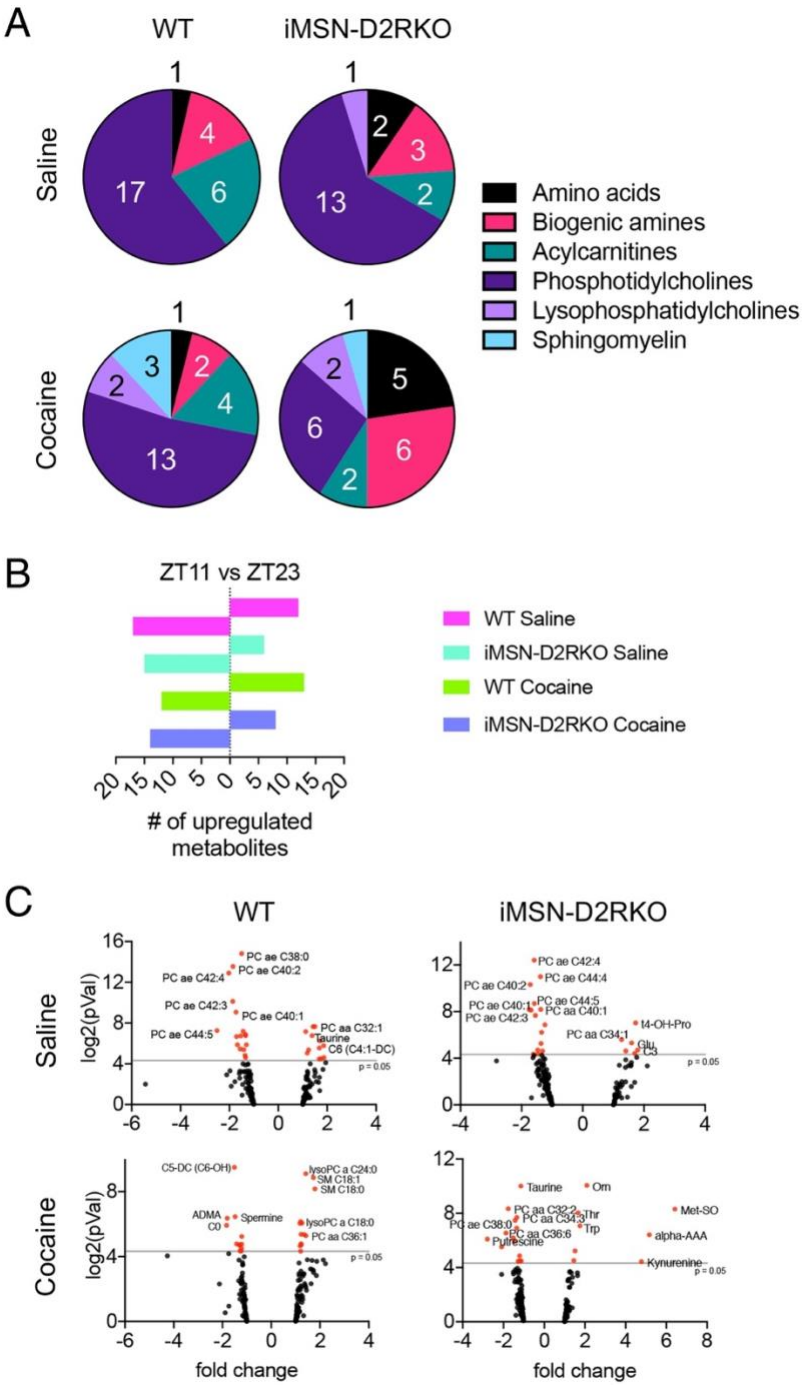

Fig. 4 Differential effects of cocaine on the liver metabolome. A. Pie charts representing the percentage of liver metabolites of each class displaying differential levels at ZT11 versus ZT23 in Saline or Cocaine treated WT or iMSN-D2RKO mice as indicated. **B.** Number of metabolites upregulated at either ZT11 or ZT23 in Saline or Cocaine treated mice as indicated. **C.** Volcano plots of metabolites at ZT11 and ZT23 in livers from WT or iMSN-D2RKO mice treated with Saline or Cocaine. Metabolites with significant changes between timepoints were identified when $p < 0.05$ (red dots). n=5, ANOVA Benjamini-Hochberg corrected, cutoff $p< 0.05$.

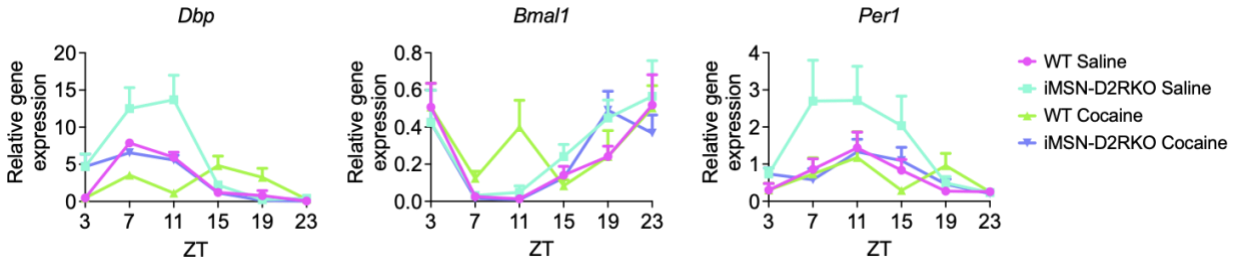

Fig. S1 Rhythmicity of core clock genes. qPCR analysis of *Dbp*, *Arntl* (Bmal1), and *Per1* in the liver samples used for metabolomics.

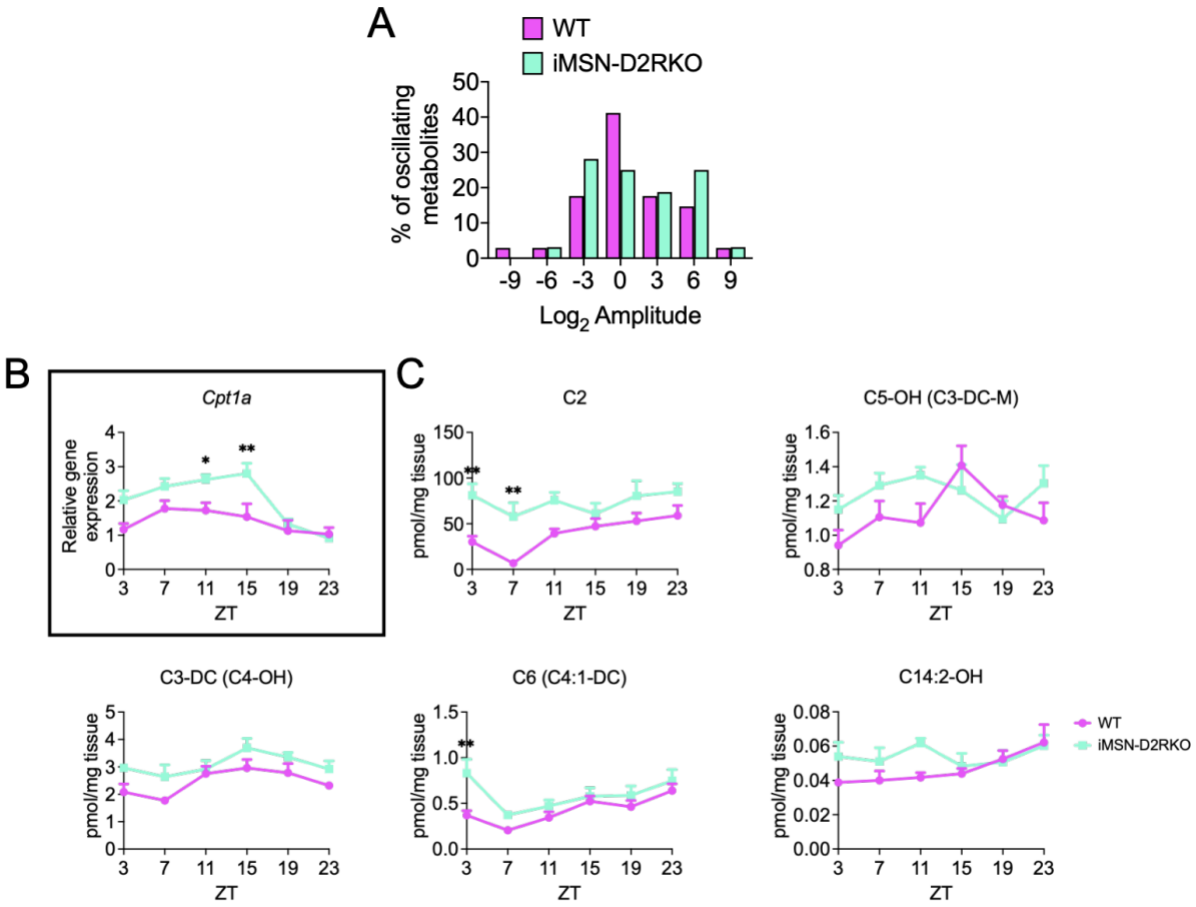

Fig. S2 Analysis of rhythmic metabolites in WT and iMSN-D2RKO mouse liver. A. Analysis of the distribution of amplitude size as a percentage of hepatic oscillating metabolites in WT (pink) or iMSN-D2RKO (blue) mice. **B.** qPCR analysis of *Cpt1a* gene expression in WT or iMSN-D2RKO mouse livers along the circadian timepoints. **C.** Concentrations of the five acylcarnitines which significantly lost rhythmicity in the iMSN-D2RKO mice compared to the WT mice. *p < 0.05, **p < 0.01. 2-way ANOVA followed by Tukey's multiple comparisons test.

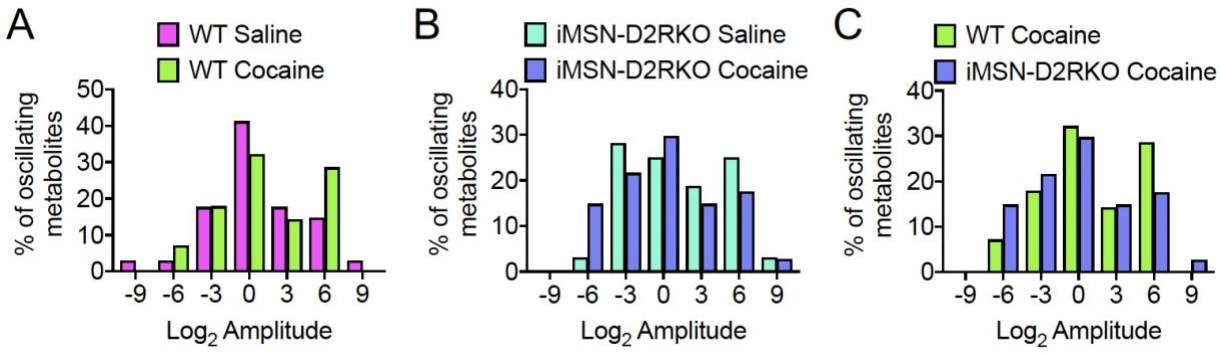

Fig. S3 Cocaine fails to alter metabolite amplitudes. A. Analysis of the distribution of amplitude size as a percentage of hepatic oscillating metabolites in WT treated with Saline (pink) or Cocaine (green). **B.** Analysis of the distribution of amplitude size as a percentage of hepatic oscillating metabolites in iMSN-D2RKO treated with Saline (blue) or Cocaine (purple). **C.** Analysis of the distribution of amplitude size as a percentage of hepatic oscillating metabolites in WT (green) or iMSN-D2RKO (purple) mice after Cocaine treatment.

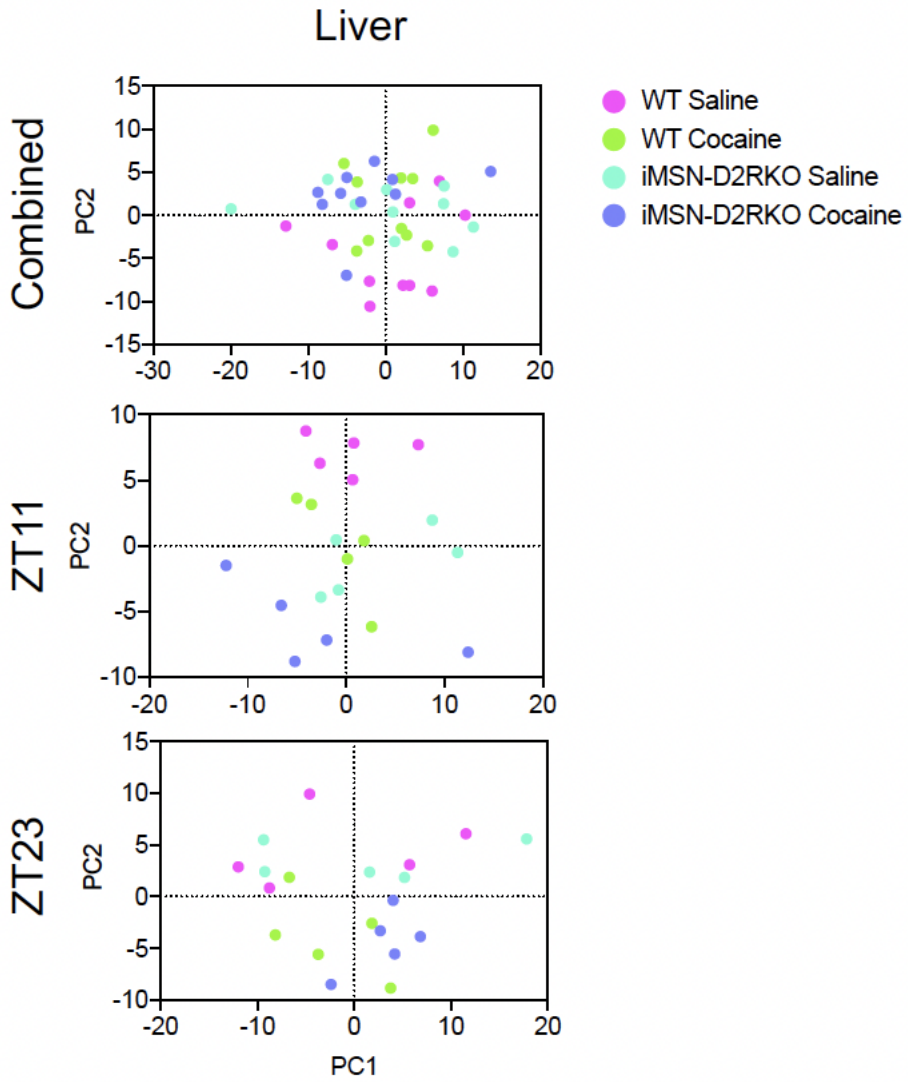

Fig. S4 Principal component analysis of metabolomic data from liver. Principal components for the combined ZT11 and ZT23 (top) datasets of each condition, WT Saline, WT Cocaine, iMSN-D2RKO Saline and iMSN-D2RKO Cocaine treated were analyzed in the liver. PCA plots for the ZT11 datasets (center) and ZT23 datasets (bottom) of each condition, WT Saline, WT Cocaine, iMSN-D2RKO Saline and iMSN-D2RKO Cocaine treated were analyzed in the liver.

Chapter 5: Dopaminergic Control of Striatal Cholinergic Interneurons Underlies Cocaine Induced Psychostimulation

Abstract

Cocaine drastically elevates dopamine (DA) levels in the striatum, a brain region that is critical for the psychomotor and rewarding properties of the drug. DA signaling regulates intrastriatal circuits connecting medium spiny neurons (MSNs) with afferents fibers and interneurons. While cocaine-mediated increase of DA signaling on MSNs is well documented, its effect on cholinergic interneurons (ChIs) has been more difficult to assess. Using combined pharmacological, chemogenetic and cell-specific ablation approaches, we reveal that D2R-dependent inhibition of acetylcholine (ACh) signaling is fundamental for the cocaine-induced changes in behavior and the striatal genomic response. We show that the D2R-dependent control of striatal ChIs enables the motor, sensitized and reinforcing properties of cocaine. This study highlights the importance of the DA- and D2R-mediated inhibitory control of ChIs activity in the normal functioning of striatal networks.

Introduction

Cocaine elevates dopamine (DA) levels in the brain by blocking the DA transporter (Cone 1995; Hyman et al. 2006). This leads to increased DA signaling in areas receiving dopaminergic afferents, including the striatum. The striatum is subdivided in functional districts, with the dorsal area involved in the control of movement and action selection (Graybiel et al. 1994; Surmeier et al. 2009; Marche et al. 2017) and the ventral area mostly implicated in reward processing (Carelli 2002; Day et al. 2007). The medium spiny neurons (MSNs) are the major constituent of the striatum representing 90-95% of the neuronal population; while a minor population is constituted by interneurons (5-10%) (Graveland and DiFiglia 1985; Oorschot 2013). MSNs are GABAergic neurons that project either directly (dMSNs) or indirectly (iMSNs) to output structures of the basal ganglia (Nelson and Kreitzer 2014). The expression of stimulatory DA D1 receptors (D1R) defines dMSNs, while iMSNs are characterized by the expression of inhibitory DA D2 receptors (D2R). Thus, the elevation of DA levels which follows cocaine intake activates dMSNs and inhibits iMSNs (Lobo and Nestler 2011).

Striatal cholinergic interneurons (ChIs) represent 1-2% of the striatal cell population; DA signaling is simultaneously inhibitory through D2R (Pisani et al. 2000; Oldenburg and Ding 2011; Kharkwal et al. 2016a) and excitatory through D5R (Centonze et al. 2003; Berlanga et al. 2005) on ChIs activity and ACh release. At the same time, ACh inhibits dMSNs through activation of muscarinic type 4 receptors (M4R) (Jeon et al. 2010; Threlfell et al. 2010; Mamaligas and Ford 2016) and excites iMSNs through muscarinic type 1 receptors (M1R) (Shen et al. 2007; Moehle et al. 2017). Thus, due to the reciprocal functional control of MSNs and ChIs, altering the striatal DA/ACh balance (Aosaki et al. 2010) has major consequences on MSNs, which are the sole output of the striatum.

At the level of intracellular signaling, the cocaine-dependent increase of DA activates cAMP and ERK pathways in dMSNs which leads to increased expression of immediate early genes, like *c-fos* and other signaling molecules (Valjent et al. 2000; Hyman and Malenka 2001; Philibin et al. 2011). These effects are mediated by activation of D1R, since they are absent upon administration of D1R antagonists or in D1R-knockout mice (Young et al. 1991; Xu et al. 1994). Nevertheless, the dMSNs-mediated motor response to cocaine and induction of *c-fos* in these same neurons requires intact D2R signaling in iMSNs (Lemos et al. 2016; Kharkwal et al. 2016b). It has been proposed that this effect depends on increased GABAergic signaling within striatal circuits in the absence of D2R in iMSNs (Centonze et al., 2004; Kharkwal et al., 2016b; Lemos et al., 2016).

Due to their low abundance, the influence of ChIs on the overall regulation of striatal circuitries has been difficult to assess. Furthermore, D2R-mediated modulation of ChIs in the context of cocaine response is not yet fully explored in vivo. In this study, we sought to address this gap in knowledge by analyzing the response to cocaine of ChI-D2RKO mice lacking inhibitory D2R signaling in ChIs. These mice are characterized by normal motor behavior in basal conditions (Kharkwal et al., 2016a). Here, we explored the motor, sensitizing and reinforcing properties of cocaine in ChI-D2RKO mice in comparison to wild-type (WT) littermates.

Notably, we found that the acute and sensitized motor response to cocaine was severely lowered in ChI-D2RKO mice. The behavioral phenotype was paralleled by loss of induction of c-fos and other striatal genes typically elevated by cocaine (Thiriet et al. 2000; McClung and Nestler 2003; Hope et al. 2006; Gao et al. 2017). These effects are assigned to increased ACh signaling in ChI-D2RKO mice, as shown by the reversal of the behavioral and cellular phenotype in these mice by chemogenetic silencing of ChIs or by blocking muscarinic M4R signaling. Importantly, we

found that not only the motor response is affected in ChI-D2RKO mice but also the reinforcing properties of cocaine were reduced.

Collectively, our study underlines the importance of the dopaminergic control on cholinergic tone in striatal responses to cocaine and might pave the way for future therapeutic strategies to treat addiction. We propose that D2R signaling exerts a major control over ChIs and ACh release which is required for the normal functioning of striatal circuits.

Results

Absence of D2R signaling in ChIs leads to reduced cocaine response

We previously generated ChI-D2RKO mice carrying the selective ablation of D2R in ChIs and showed that under basal conditions motor activity is intact in these mice (*p=0.1247*) (Fig. S1A) (Kharkwal et al. 2016a). In this study, we analyzed the motor and reinforcing properties of cocaine in ChI-D2RKO mice. We hypothesized that cocaine-induced DA elevation would generate a stronger response of ChIs in the absence of D2R in ChI-D2RKO mice as compared to WT siblings. Indeed, stimulation of D1-like receptors on ChIs in the absence of the inhibitory D2R signaling might lead to increased ACh signaling in the striatum.

A cocaine dose-response curve generated made to compare the motor response of male ChI-D2RKO mice to their WT littermates. Cocaine (5, 10, 15 and 20 mg/kg) or saline were injected intraperitoneally (ip) and motor activity recorded for 1 hour in a novel home cage (NHC). Interestingly, while WT mice dose-dependently respond to cocaine with an increase of their horizontal locomotion, the response of ChI-D2RKO mice was significantly attenuated (*p=0.0003*) (Fig. 1A). Indeed, while WT mice show a significant motor response to cocaine starting at 10 mg/kg compared to saline treated mice of the same genotype (*p=0.0016*), ChI-D2RKO mice

displayed a significant response to the drug only at 20 mg/kg (*p<0.0001*), the highest dose tested, which was nonetheless ~ 40% lower than that of equally treated WT mice (*p<0.0001*).

The cocaine driven increase of DA and glutamate signaling in dMSNs is reflected by the induction of the immediate early gene c-Fos in the dorsomedial (DMS) and the ventral striatum (Torres and Rivier 1993; Jenab et al. 2003) and of post-translational modifications involving the phosphorylation of the ribosomal protein S6 on the serine residues 235/236 (p-rpS6$^{S235/236}$) (Puighermanal et al. 2017). By difference to c-fos induction, p-rpS6$^{S235/236}$ requires only DA- D1R-mediated activation of the cAMP pathway in dMSNs (Biever et al. 2015). Therefore, analyzing levels of c-fos and rpS6$^{S235/236}$ phosphorylation served as monitors of dopaminergic and cortical inputs to dMSNs. Thus, striatal brain sections from WT and ChI-D2RKO mice were analyzed 1 hour after saline or cocaine by immunofluorescence (IF) using antibodies directed against c-Fos and p-rpS6$^{S235/236}$. Strikingly, we observed a significantly reduced number of c-Fos positive cells in the DMS of ChI-D2RKO mice as compared to equally treated WT controls (*p=0.0004)* (Fig. 1B). The same decrease was observed in the ChI-D2RKO ventral striatum (*p<0.0001*) (Fig. S1B). In parallel, a lower number of p-rpS6$^{S235/236}$ positive cells were observed in the DMS (*p=0.0004*) (Fig. 1C) as well as the ventral striatum (*p=0.0118*) of ChI-D2RKO mice in comparison to WT (Fig. S1C). The reduced induction of c-Fos affected dMSNs, as shown by double fluorescent in situ hybridization (FISH) on striatal tissue sections, hybridized with a *c-fos* specific riboprobe along with either a *D1R*-specific probe as marker of dMSNs or an *enkephalin (Enk)* probe to label iMSNs. Quantifications of FISH analyses showed that in cocaine treated WT striata, *c-fos* induction was observed in 61% of *D1R*-positive dMSNs (Fig. 1D) and only 9% in *Enk*-positive iMSNs (Fig. 1E). In contrast, *c-fos* positive neurons were estimated at 9% in *D1R*-positive dMSNs and 4% of *Enk*-positive iMSNs in cocaine treated ChI-D2RKO mice. These results show that D2R

expression in ChIs is required for the well-known behavioral and cellular effects of cocaine in dMSNs.

Altered transcriptomic profile in the striatum of ChI-D2RKO mice

Loss of c-Fos induction in response to cocaine in ChI-D2RKO striata prompted us to perform an unbiased analysis to identify genes differentially expressed in the DMS between WT and ChI-D2RKO using RNA-sequencing (RNA-seq). Male WT and ChI-D2RKO mice (n=4/group) were administered a single injection of saline or cocaine (20 mg/kg; ip) and sacrificed 1 hour later. RNAs from the DMS were then prepared and processed for RNA-seq.

Saline treated WT and ChI-D2RKO striata had a total of 871 differentially expressed transcripts, 365 were down-regulated and 506 were up-regulated in WT mice as compared to ChI-D2RKO mice (Fig. S2A). After cocaine, differential expression analyses revealed a total of 969 differentially expressed transcripts between the two genotypes ($p<0.05$) (Fig. S2B). This is comprised of 595 transcripts up-regulated and 374 down-regulated by cocaine; only 59 genes were found to be in common in these two analyses (Fig. S2C). Among all differentially expressed transcripts identified in cocaine treated mice, we extracted 60 highly significant genes (padj < 0.05) which represent the bona-fide signature of cocaine-induced genomic response (Fig. 2A) (Hope et al. 1992; Fosnaugh et al. 1995; McClung and Nestler 2003; Chandra and Lobo 2017; Gonzales et al. 2019).

Consistent with our previous IF analyses, *c-fos* was found among the most significant differentially expressed genes ($p=7.91*10^{-22}$) (Fig. 2A and B). In addition to *c-fos*, other members of the AP-1 transcription factor complex: *Fosb*, *Fosl2*, and *Junb* (Curran and Franza 1988; Su et al. 2017) and of the nuclear receptor subfamily 4 group A such as *Nr4a1* and *Nr4a3* (Volakakis et al. 2010), together with early growth response transcription factors *Egr1*, *Egr2*, *Egr3* and *Egr4*

(Duclot and Kabbaj 2017, p. 3; Gao et al. 2017), were induced in the WT, but not in the ChI-D2RKO DMS (Fig. 2A and B).

Gene ontology analyses performed using the Database for Annotation, Visualization and Integrated Discovery (DAVID) indicated that differentially expressed genes with significant fold changes found in cocaine treated mice (Fig. 2B; in red), were heavily involved in the regulation of transcription. Functional annotation categories such as "Positive regulation of transcription", "Transcription from RNA pol II promoter", and "Transcription factor binding" were highly significant (Fig. 2C).

We performed an enrichment analysis using ChEA3 (Keenan et al. 2019), to identify transcription factors which putatively regulate the 969 differentially expressed genes in cocaine treated mice (Fig. S2B). Of the top 25 transcription factors enriched for targeting our gene set, 10 of them were found among our most significant differentially expressed genes (Fig. 2A and D). Importantly, each of the 10 transcription factors identified were increased in WT, but not ChI-D2RKO mice (Fig 2A and D). Thus, loss of induction of genes previously identified as genomic signatures of cocaine's effects indicates that the inhibitory dopaminergic control exerted by D2R on ACh signaling enables the acute induction of gene expression.

Elevated ChI activity mediates deficits in ChI-D2RKO mice response to cocaine

We hypothesized that the lowered response to cocaine of ChI-D2RKO mice originates from increased ACh signaling in the striatum generated by absence of the modulatory D2R in ChIs. To validate our hypothesis, we treated male WT mice with the acetylcholinesterase inhibitor, donepezil, which blocks ACh degradation (Karvat and Kimchi 2014). We administered saline or donepezil (1 mg/kg; ip) 15 minutes before cocaine and evaluated motor activity for the following hour. In line with our hypothesis, donepezil administration prior to cocaine severely abates the

motor response of WT mice as compared to cocaine only treated animals ($p<0.0001$) (Fig. 3A).

Next we sought to directly show that increased ACh signaling in the DMS is responsible for the reduced response to cocaine of ChI-D2RKO. We used a chemogenetic approach to specifically silence ChI activity in ChI-D2RKO mice using the designer receptor exclusively activated by designer drugs (DREADD), hM4Di, upon administration of clozapine-N-oxide (CNO) or JHU37160 (J60). For this purpose, we performed stereotaxic injections of the adeno-associated viral vector carrying hM4Di (Roth 2016), whose expression is Cre-recombinase-dependent, into the DMS of ChI-D2RKO mice. Two weeks after surgery, we analyzed and confirmed the specific expression of hM4Di in ChIs by IF using antibodies directed against the mCherry tag of hM4Di along with choline acetyltransferase (ChAT), a ChI marker (Fig. S3A). We confirmed that CNO (3 mg/kg; ip) and J60 (0.1 mg/kg; ip) (Bonaventura et al. 2018) did not affect locomotion in the absence of cocaine in hM4Di expressing ChI-D2RKO mice (hM4Di ChI-D2RKO) throughout 7 days of exposure ($p=0.7071$) (Fig. S3B).

hM4Di ChI-D2RKO mice were treated with CNO (3 mg/kg; ip) 30 minutes prior to cocaine (15 mg/kg; ip) and motor activity recorded for the following hour. Strikingly, hM4Di ChI-D2RKO showed a response to cocaine, upon CNO administration, that was significantly increased from that of ChI-D2RKO mice not expressing hM4Di ($p<0.0002$) or to saline treated hM4Di ChI-D2RKO mice ($p=0.0002$). Importantly, hM4Di ChI-D2RKO mice response to cocaine did not differ from that of WT mice ($p>0.99$) (Fig. 3B).

Cocaine sensitization in mice with a deletion of D2R in ChIs

Repeated intake of cocaine causes maladaptive changes of the mesolimbic dopamine system that lead to an enhanced motor response to the drug (Kalivas and Stewart 1991; Boudreau and Wolf 2005; Robinson and Berridge 2008). Thus, we focused on determining if the behavioral

deficits of ChI-D2RKO mice observed after acute administration would also affect cocaine sensitization. To test this, male mice that were habituated to a home cage for two days were then administered cocaine (15 mg/kg; ip) daily for 5 days and had their motor activity recorded for 1 hour. Chronic cocaine administration induced a linear increase of the motor activity in all mice tested (Fig. 3C). Interestingly, ChI-D2RKO mice also showed a significant increase of the motor response between day 1 and 5 ($p=0.0204$); however, their response was significantly lower than that of cocaine treated WT mice ($p=0.0001$) (Fig. 3C and D). We then assessed whether silencing ChIs using the DREADD system in the DMS might restore cocaine sensitization to WT levels. In line with previous results, hM4Di ChI-D2RKO mice treated with CNO (3 mg/kg; ip) prior to cocaine, during the five days of repeated administration, increased motor activity as compared to ChI-D2RKO mice not expressing hM4Di ($p<0.0001$) (Fig. 3C). Importantly, the response of hM4Di ChI-D2RKO mice treated with cocaine and CNO did not differ from that of WT mice treated with cocaine. Similar results were obtained using J60 (0.1 mg/kg, ip) ($p<0.0001$) (Fig. S3C), thereby excluding possible interference of CNO with DA receptors.

To further verify the long-term effect of sensitization in mice of both genotypes, we left mice untreated for 7 days and then challenged them with a lower dose of cocaine (10 mg/kg; ip). Interestingly, while WT mice showed a sensitized response after the withdrawal period, ChI-D2RKO mice did not. The response to the cocaine challenge of ChI-D2RKO mice did not differ from the one observed on the first day of cocaine treatment ($p>0.99$) (Fig. 3D). Consistent with elevated ACh levels as being responsible for the impaired sensitization of ChI-D2RKO mice, hM4Di ChI-D2RKO mice treated with CNO showed cocaine sensitization that did not differ from that of WT mice ($p>0.99$) (Fig. 3C). Interestingly, both induction of c-Fos expression (Fig. 3E) and of rpS6$^{S235/236}$ phosphorylation (Fig. 3F) 1 hour after the challenge injection were increased in

hM4Di ChI-D2RKO mice given CNO and cocaine (c-Fos: $p=0.0057$ and p-rpS6$^{S235/236}$: $p=0.0006$) as compared to ChI-D2RKO mice not expressing hM4Di. Similar results were obtained using J60 and cocaine in hM4Di ChI-D2RKO mice ($p=0.0310$) (Fig. S3D).

Antagonism of muscarinic receptors enables cocaine response in ChI-D2RKO mice

ACh in the striatum activates muscarinic and nicotinic receptors (Lim et al. 2014). MSNs are major targets of ACh signaling dependent on activation of muscarinic M4R and M1R. To elucidate the mechanism underlying the weakened response of ChI-D2RKO mice to cocaine, we sought to determine whether muscarinic signaling was involved. Accordingly, we tested the effect of the non-selective muscarinic antagonist, scopolamine, prior to cocaine administration on motor activity. To perform these experiments, we controlled that ChI-D2RKO mice can respond to scopolamine as WT mice with an increase in their forward locomotion by performing a dose-response experiment using 0.5 and 1.0 mg/kg of scopolamine. At 0.5 mg/kg scopolamine, mice of both genotypes showed a trend toward an increase of motor activity which did not reach statistical significance ($p>0.99$), while at the dose of 1 mg/kg both WT and ChI-D2RKO mice showed a significant increase of motor activity ($p<0.0001$) of similar intensity as compared to saline treated mice of both genotypes (Fig. S4). The sub-threshold dose of 0.5 mg/kg was then chosen to perform experiments with cocaine (Fig. 4A). For each genotype, male mice were divided into four groups: saline, scopolamine (0.5 mg/kg; ip), cocaine (20 mg/kg; ip) or the combination of both. Scopolamine was administered 15 minutes prior to saline or cocaine and forward locomotion recorded for 1 hour after the last injection. Strikingly, the combination of scopolamine and cocaine specifically increased the motor response to cocaine of ChI-D2RKO mice as compared to cocaine only treated mice of the same genotype ($p<0.0001$) (Fig. 4A); this increase resulted in the absence of differences in forward locomotion between ChI-D2RKO and WT mice ($p>0.99$).

Importantly, blocking muscarinic signaling also translated into the cellular rescue of c-Fos induction and of rpS6 phosphorylation, as assessed by IF quantifications of the number of neurons positive for c-Fos ($p=0.0128$) (Fig. 4B and D) and for p-rpS6$^{S235/236}$ ($p<0.0001$) (Fig. 4C and E) in the DMS of ChI-D2RKO and WT mice analyzed 1 hour after cocaine administration. Together, these results indicate that the elevated muscarinic signaling is responsible for the reduced motor and cellular responses to cocaine in ChI-D2RKO mice.

The inhibitory control of D2R on ChIs prevents M4R over-activation

Next, we analyzed whether the behavioral and cellular phenotype of ChI-D2RKO mice might depend on increased ACh stimulation of M4R and/or of M1R. Indeed, while M4R activation could directly inhibit dMSNs, M1R activation of iMSNs might indirectly lead to dMSNs inhibition through iMSNs GABAergic collaterals (Kharkwal et al., 2016b; Lemos et al., 2016).

Thus, male ChI-D2RKO and WT littermates were administered either M4R- or M1R-selective antagonists 15 min prior to cocaine. Mice of each genotype received either saline, the M4R-selective antagonist, tropicamide (10 mg/kg; ip), or the M1R-selective antagonist, VU0255035 (60 mg/kg; ip) (Sheffler et al. 2009) in the presence or absence of cocaine (20 mg/kg; ip). Forward locomotion was recorded for 1 hour following cocaine administration. Our results show that the selective blockade of M4R prior to cocaine rescues the motor inducing effects of cocaine in the ChI-D2RKO mice to WT levels as compared to the cocaine only group of the same genotype ($p<0.0001$) (Fig. 5A). Mirroring the effect of tropicamide on motor activity, the number of c-Fos ($p=0.0036$) and p-rpS6$^{S235/236}$ ($p<0.0001$) positive neurons was significantly increased in ChI-D2RKO mice when this antagonist was administered prior to cocaine as compared to cocaine only treated mice (Fig. 5B-E). Overall the presence of tropicamide, abolished the observed differences between cocaine treated WT and ChI-D2RKO mice ($p>0.99$).

In contrast with M4R antagonisms, blockade of M1R with VU0255035 had a negative effect as it reduced cocaine response in WT mice as compared to the cocaine only group (*p<0.0003*) while having no effect on the motor activity of cocaine-treated ChI-D2RKO mice with or without VU0255035 (*p<0.2599*) (Fig. 6A). At the intracellular level, M1R antagonism significantly lowered cocaine-mediated c-Fos induction in WT mice (*p=0.0002*) (Fig. 6B and D). However, the only positive effect of VU0255035 pretreatment on ChI-D2RKO was a significant increase of the number of p-rpS6$^{S235/236}$ positive neurons (*p=0.0025*) (Fig 6C and E). This increase might be caused by a direct effect of the M1R antagonist on dMSNs or alternative undefined mechanisms of M1R antagonism in the striatum.

The reinforcing properties of cocaine are affected by loss of dopaminergic inhibition of ChIs

Next, we aimed at studying the effect of loss of the dopaminergic inhibition on ChIs on reward related mechanisms by analyzing the ability to associate an environment with cocaine. For this, we performed the conditioned place preference (CPP) test on male mice of both genotypes. On day 1, a pre-conditioning test was performed, and the time spent by each mouse in the two compartments of the CPP apparatus was evaluated for 20 minutes. A drug-paired compartment was then randomly assigned to mice and conditioning started. Four groups of mice for each genotype were made: saline/saline, saline/cocaine (10 mg/kg; ip), saline/tropicamide (10 mg/kg; ip) and tropicamide/cocaine (10 mg/kg; ip of each drug). Tropicamide was administered 15 minutes prior to cocaine. During conditioning, mice were restricted for 20 minutes to either the drug-associated compartment where they received the drugs on days 2, 4, 6 and 8 or to the other compartment where they received saline on days 3, 5, 7 and 9. On day 10, the preference for the drug-associated compartment was tested by leaving the mouse free to choose between

compartments for 20 minutes (Fig. 7A). Motor activity did not differ between genotypes neither during the pre-conditioning (*p=0.3463*) (Fig S5A) nor during the test (p=0.0555) (Fig. S5B).

Strikingly, ChI-D2RKO mice did not show a significant CPP to cocaine as compared to WT mice (*p=0.0003*) (Fig. 7B) indicating that the reinforcing properties of cocaine are affected in ChI-D2RKO mice as compared to WT littermates. Importantly, M4R antagonism prior to cocaine administration restored both cocaine-induced locomotion and CPP in ChI-D2RKO mice as compared to the cocaine only group of the same genotype (*p=0.0223*) and to WT levels (*p<0.99*) (Fig. 7B; Fig. S5C and D).

Analyses of *c-fos* induction by FISH in striatal sections from mice sacrificed 1 hour after the test session, showed a blunted response both in the DMS (Fig. S5E) and ventral striatum (Fig. S5F) (DMS: *p=0.0145*; ventral striatum: *p=0.0011*) of ChI-D2RKO mice conditioned with cocaine as compared to WT controls. Analogous with the CPP results, prior tropicamide treatment during the conditioning phase rescued the *c-fos* deficit as compared to the cocaine alone group of ChI-D2RKO mice (DMS: *p=0.0183*; ventral striatum: *p=0.0254)*.

To assess whether the inhibitory D2R-mediated control of ChIs is required for the expression of reward, we analyzed CPP in response to food (cocoa pebbles), as the reinforcer. The same CPP protocol was used with the exception that cocoa pebbles replaced the drug in the compartment on days 2, 4, 6, and 8, and no food was presented in the opposite compartment on days 3, 5, 7, and 9. Surprisingly, while WT mice displayed a strong place preference to the food associated compartment (*p=0.0094*), ChI-D2RKO mice did not (*p>0.99*) (Fig. S6A) despite a normal consumption of cocoa pebbles during the conditioning phase. In agreement with this response, *c-fos* was induced in the DMS and the ventral striatum of WT mice (DMS: *p=0.0006*;

ventral striatum: *p=0.0002*) but not of ChI-D2RKO mice, as evaluated 1 hour after the test session (DMS: *p=0.6197*; ventral striatum: *p>0.99*) (Fig. S6B and C).

Absence of CPP to cocaine and food in ChI-D2RKO mice appears independent from altered memory, as established by the absence of significant differences between male WT and ChI-D2RKO mice in the novel object recognition test (Fig. S7). Indeed, WT and ChI-D2RKO mice are equally able to recognize a novel object (Fig. S7A and B) (*p=0.4178*) with no differences in motor activity in the testing apparatus (Fig. S7C) (*p=0.7129*).

Discussion

All drugs of abuse, including cocaine, increase DA signaling in the mesolimbic pathway, which is involved in the control of motor and reward-related behaviors. The psychomotor effects of cocaine are mostly attributed to DA activation of dMSNs resulting into the stimulation of the basal ganglia direct pathway (Zhang et al. 2002; Bertran-Gonzalez et al. 2008). Nevertheless, the DA-mediated effects of cocaine on dMSNs are regulated by iMSNs through D2Rs (Lemos et al. 2016; Kharkwal et al. 2016b). In addition, striatal interneurons connecting to output MSNs (Mamaligas and Ford 2016; Cai and Ford 2018; Gong and Ford 2019; Francis et al. 2019), as well as corticostriatal, thalamic and mesolimbic afferents to MSNs and interneurons (Pancani et al. 2015; Qi et al. 2016; Kosillo et al. 2016; Cai and Ford 2018) further enhance the level of complexity in unraveling how cocaine induces motor and reinforcing effects. In most of these connections, DA plays a critical role through activation of D2Rs. These receptors are located pre- and postsynaptically in striatal and afferent neurons. Thus, the role discovered for D2R in iMSNs in facilitating cocaine-mediated dMSNs responses (Lemos et al. 2016; Kharkwal et al. 2016b) might be a general feature of D2R signaling in the striatum. D2R activation might serve as a

general modulator of the responses of dMSNs through heterologous control of striatal neurotransmitters and neuromodulators in neurons and afferents.

Our findings show that D2R activation is indeed central for ChIs. We show that the D2R-mediated inhibition of ChIs is required to maintain balanced cholinergic signals, which directly affect dMSNs responses to cocaine. Indeed, loss of the D2R inhibitory control of ChIs results in significantly diminished motor and cellular responses to the drug. We hypothesized that this phenotype is the result of an increased cholinergic tone in striatal circuits due to the unopposed stimulation of D5Rs on ChIs and the consequent increase in ACh release. Our hypothesis is supported by the impaired response to cocaine of WT mice in which ACh degradation is inhibited using donepezil before cocaine administration (Fig. 3A). In line with these findings, pharmacological approaches were able to restore the acute effects of cocaine on motor and cellular responses to cocaine in ChI-D2RKO mice; indeed, scopolamine administered prior to cocaine restored the cocaine mediated motor and cellular effects to WT levels. We defined that the M4R specific antagonist, tropicamide (Fig. 5), but not the M1R specific antagonist, VU0255035 (Fig. 6), was able to give the same effects than scopolamine (Fig. 4). These results point to the important regulation of dMSNs activity by ACh through M4R signaling (Weiner et al. 1990; Klawonn et al. 2018). M4R The observation that tropicamide reverses the phenotype of ChI-D2RKO, excludes a possible interference of M4R autoreceptors blockade in these effects, which should further increase ACh release. In contrast, the presence of M4R on corticostriatal and thalamic fibers might greatly influence both dMSNs and iMSNs activity through modulation of glutamate release (Yohn et al., 2018; Moehle and Conn, 2019). Our results showing the rescue of c-Fos induction by tropicamide suggests that cortical and thalamic fibers might well be affected by the increased ACh tone in ChI-D2RKO mice.

Silencing of ChIs through the expression of hM4Di in these neurons, in the presence of CNO (Fig. 3B), further supports our hypothesis of increased ACh signaling in ChI-D2RKO mice since this manipulation restored cocaine responses of mutant mice to WT levels. These results convincingly establish that the basis of the altered cocaine effects in ChI-D2RKO mice is the increased ACh levels resulting from absence of D2R signaling in ChIs.

The impaired behavioral response of ChI-D2RKO mice to the drug was paralleled by the absence of induction of the immediate early gene c-fos. Induction of c-fos, a transcription factor of the AP1 family, is a hallmark of the cellular effect of drugs of abuse. This striking effect prompted us to perform a genome-wide analysis by RNA-seq comparing WT and ChI-D2RKO DMS transcriptomic profiles in the absence or presence of cocaine. These analyses revealed a reprogramming of gene expression profiles in the mutants as compared to equally treated WT mice, in both conditions. Interestingly, among genes differentially expressed, *c-fos* was found among the most significant, thus validating our IF analyses. In addition to *c-fos*, other members of the AP1 family together with other families of transcription factors were found differentially expressed. The implication of the AP1 family, *Egr*s and other transcription factors in the effects of cocaine underlines the immediate effect of cocaine in reprogramming genomic profiles, even after the first encounter with the drug, which likely leads to subsequent maladaptive changes of synaptic plasticity. In addition, our findings reveal that the D2R-mediated control of ACh signaling is critically linked to cocaine effects.

To explore the impact of altered cholinergic signaling in the more advanced stages of drug use, we utilized two behavioral paradigms: the sensitization and the CPP. Behavioral sensitization is related to changes of the motor effects of the drug while CPP correlates to the reward-related effects (Cunningham et al. 2006; Robinson and Berridge 2008). Notably, ChI-D2RKO mice

behaved differently than their WT littermates in both tests. We observed a partially escalating motor response to cocaine in ChI-D2RKO mice during the repetitive five days of treatment as compared to WT mice. However, after one week of withdrawal, a challenge injection to a lower dose of cocaine did not result in the expected enhanced response to the drug in the ChI-D2RKO as it did in WT mice. These results suggest that the D2R-mediated control of ACh signaling is required for the induction of long-term modifications leading to sensitization. We might speculate that absence or lowered inductions of the different transcription factors identified by RNA-seq could at least in part be responsible for the aberrant response. Similarly, by difference with WT, ChI-D2RKO mice appear insensitive to the reinforcing effects of cocaine as well as of food as measured by CPP. This result is highly relevant since ChIs activity contributes to associative learning (Brown et al. 2012; Zhang et al. 2018). ChIs receive dopaminergic, GABAergic and glutamatergic signals from the VTA that induce the pausing of these neurons (Brown et al. 2012; Kharkwal et al. 2016a; Cai and Ford 2018; Zhang and Cragg 2017). Absence of D2Rs by removing the dopaminergic inhibitory input (Kharkwal et al, 2016) might disrupt the ChI-dependent mechanism required to signal saliency of an event or conversely signals any event as salient, making it hard for the subject to associate the drug to the right compartment. These conclusions are supported by the effect of chemogenetic and pharmacological approaches in restoring sensitization and CPP.

In conclusion, the analysis of D2R cell-specific knockout mice has been instrumental to clarify the role of this receptor in the control of striatal circuits (Anzalone et al. 2012; Kharkwal et al. 2016a, b; Lemos et al. 2016). Importantly, the absence of D2R either in iMSN- or in ChI-D2RKO mice shows that D2R signaling in both neurons is a requirement for the control of dMSNs-

mediated functions and cocaine-mediated effects. Our findings suggest that the identification of molecules downstream of D2R might offer leads for the treatment of cocaine addiction.

Methods

Lead Contact and Materials Availability

Further information and requests for resources and reactions should be directed to and fulfilled by the Lead Contact, Emiliana Borrelli (borrelli@uci.edu). All unique/stable materials and models generated from this study are available from the Lead Contact with a completed Materials Transfer Agreement.

Experimental Model and Subject Details

All protocols were submitted and approved by the University of California, Irvine Institutional Animal Care and Use Committee in accordance with the National Institute of Health guidelines. Mice were group housed and maintained at standard 12h/12h light/dark cycle, at ~25°C, and humidity levels at 45-60%. Animals were group housed and fed *ad libitum* unless otherwise specified. Female ChI-D2RKO and WT littermates mice did not differ in motor behavior compared to male mice in their response to cocaine and therefore all experiments were performed in males. Thus, we exclusively used adult male mice aged 8 to 14 weeks old for all experiments. ChI-D2RKO mice were generated by mating $D2R^{floxflox}$ mice (used as WT controls) with choline acetyltransferase (ChAT)-Cre mice generating $D2R^{floxflox/ChAT\ Cre/+}$ mice, as previously described (Kharkwal et al., 2016a). For all behavioral testing, mice were manipulated at least 2 days prior to experimental start for 5 min/day.

Method Details

Stereotaxic Surgery

3% vaporized isoflurane (Kent Scientific) was used to anesthetize mice before they were placed in the stereotaxic frame (David Kopf Instruments). A nose cone was placed over the mouse and isoflurane concentration was lowered to 1-2%; temperature and breathing were closely monitored throughout the surgery. Adeno-associated viruses carrying designer receptors exclusively activated by designer drugs (DREADD) hM4Di (AAV-hSyn-DIO-hM4D(Gi)-mCherry; AddGene) were injected with in the dorsomedial striatum (DMS) (anterior-posterior, 0.98 mm; medial-lateral, ± 1.2 mm; dorso-ventral, −3 mm, from Bregma) according to the mouse brain atlas. 1.5 μL (6900 Genome Copies/hemisphere) were infused bilaterally over a period of 3 min. Following surgery, mice were monitored daily for at least 14 days prior to experiments.

Drugs

Cocaine HCl (Sigma), Tropicamide HCl (Tocris), Scopolamine HBr Trihydrate (Sigma), Donepezil HCl (Sigma), VU0255035 HCl (UCI), Clozapine-N-Oxide (CNO) (NIH), and JHU37160 dihydrochloride (J60) (HelloBio) were dissolved in sterile saline (0.9% NaCl pH 7.4). All drugs were administered intraperitoneally.

Behavioral Analyses

Acute

Locomotor activity was analyzed and recorded in a novel home cage (NHC) (20 cm × 30 cm x 13 cm transparent plastic box) using a video-tracking system (Viewpoint; Lyon France). Mice were habituated to the NHC for 2 hours prior to administration of saline or cocaine; motor behavior was monitored for the following hour. For experiments requiring the use of scopolamine, tropicamide, VU0255035, or donepezil, mice were habituated in their NHC for 2 hours, then

administered these pharmacological agents or saline. 15 minutes later, mice were then given either saline or cocaine and motor responses recorded for the following hour. Experiments requiring the use of DREADD agonists were performed in the same way with the exception that cocaine or saline was given 30 minutes after CNO.

Sensitization

As in acute experiments, locomotor activity was analyzed and recorded in a NHC using video-tracking. Mice were habituated to their NHC for 30 minutes each day of the experiment; during the first two days of the protocol, all mice received only saline. The following 5 days, mice were given cocaine (15 mg/kg; ip) after 30 minutes of habituation and motor response was recorded for the following hour. After a one-week withdrawal period, mice were challenged with a lower dose of cocaine (10 mg/kg; ip) using the same method. For experiments using the DREADD system, hM4Di ChI-D2RKO mice were injected with clozapine-N-oxide (3 mg/kg; ip) or J60 (0.1 mg/kg; ip) immediately before the 30-minute habituation period.

Cocaine Conditioned Place Preference

The CPP testing apparatus consisted of two compartments (15.5 cm x 16.5 cm x 20.3 cm) divided by a neutral space (15.5 cm x 5 cm x 20.3 cm); each compartment contained visual and tactile cues on the walls and floors. Each genotype was divided into two groups by conditioning mice to receive either saline or cocaine (10 mg/kg; ip) in a specific compartment. On day 1, mice were placed into the apparatus for 20 minutes and left free to explore both sides of the apparatus; time spent in each compartment was recorded and scored. The following day, conditioning started using an unbiased protocol in which the drug-paired compartment was randomly assigned to mice in each group. During conditioning, mice were given either cocaine or saline on alternate days and restricted to the appropriate compartment for 20 minutes. Cocaine was administered on days 2, 4,

6, and 8 with alternating saline injections on days 3, 5, 7, and 9. On day 10, the CPP test was performed by leaving the mice free of choosing between the two compartments for 20 minutes. Tropicamide (10 mg/kg; ip) was administered 15 minutes before saline or cocaine treatments on days 2, 4, 6, and 8.

Food Conditioned Place Preference

Food CPP was performed on mice that were food restricted to lose 10% of their starting body weight. After this, mice selected to be given the food reward were exposed to the reinforcer, Post Cocoa Pebbles cereal, for 2 days until all mice were observed eating the food reward. Then, CPP was performed using the same experimental timeline as the cocaine CPP. Five pieces of cereal were placed inside the food-paired room on days 2, 4, 6, and 8 with mice receiving nothing in the other compartment on days 3, 5, 7, and 9. For cocaine and food experiments, a CPP score was calculated by determining the difference between time spent in the reward associated compartment before and after conditioning.

Novel Object Recognition Test

Mice were habituated to the open-field testing apparatus (30 cm x 30 cm x 19 cm white box) 3 times for 5 minutes with 1 hour in between each habitation session. The following day, mice underwent a training session for 10 minutes during which each object was positioned 6 cm away from diagonal corners of the apparatus. On the testing day, 1 object was replaced with a novel object in a manner that was counter balanced, and mice were place in the apparatus for 10 minutes while being video tracked (See Fig. S7A). Time investigating the object was determined as the time spent in a 4 cm x 4 cm area surrounding the object. The ability to discriminate between the known object and the novel object was calculated as a discrimination index using the formula $(time_{novel} - time_{known}) / (time_{novel} + time_{known})$.

RNA preparation for RNA-sequencing

After behavioral testing, brains were dissected and were rapidly frozen in 2-methylbutane on dry ice. For RNA preparation, bilateral tissue punches were obtained and rapidly homogenized in Trizol (Thermo Fisher) using a 26 ½ gauge needle attached to a 1 mL syringe. RNA isolation was completed following the manufacturer's protocol. RNA was resuspended in H_2O.

Library Preparation for RNA-Sequencing

Library preparation and sequencing were performed at the University of California, Irvine Genomic High-Throughput Facility. Total RNA was monitored for quality control using the Nanodrop absorbance ratios for 260/280nm and 260/230nm and the Agilent Bioanalyzer Nano RNA chip (Table S1). Library construction was performed according to the Illumina TruSeq® Stranded mRNA Sample Preparation Guide. The input quantity for total RNA was 150 ng and mRNA was enriched using oligo dT magnetic beads. The enriched mRNA was chemically fragmented for three minutes. First strand synthesis used random primers and reverse transcriptase to make cDNA. After second strand synthesis the double stranded cDNA was cleaned using AMPure XP beads and the cDNA was end repaired and then the 3' ends were adenylated. Illumina barcoded adapters were ligated on the ends and the adapter ligated fragments were enriched by nine cycles of PCR. The resulting libraries were validated by qPCR and sized by Agilent Bioanalyzer DNA high sensitivity chip. The concentrations for the libraries were normalized and then multiplexed together. The multiplexed libraries were sequenced on four lanes using single end 100 cycles chemistry on the HiSeq 4000. The version of HiSeq control software was HCS 3.4.0.38 with real time analysis software.

Bioinformatics

Read quality was assessed by FastQC (www.bioinformatics.babraham.ac.uk/projects/fastqc/). Sequence alignment was performed using the *mus musculus* GENCODE reference genome (GTF file from release M23 GRCm38.p6) using STAR 2.6.0c software (Dobin et al. 2013) (Table S2). Annotation and count matrices were generated using Genomic Features (Carlson et al. 2019) and Genomic Alignments (Pagès et al. 2019). Differential expression analysis was performed using DESeq2 (Love et al. 2019). Read counts were normalized using the relative log expression method of DESeq2. Normalized read counts were converted into the log-read counts which were then used for identifying differentially expressed genes; in our comparisons saline treated WT mice were used as the control. Unadjusted and adjusted p-values were determined for each gene; $p<0.05$ was considered statistically significant. Volcano plots were generated using the EnhancedVolcano R package (Blighe et al. 2019). Biological processes represented by the differentially expressed genes were determined using the Database for Annotation, Visualization, and Integrated Discovery (DAVID) annotation tool (v. 6.8). Genes with a significance $p<0.05$ and a Log2 Fold-Change greater than 1 and less than -1 were compiled and entered into DAVID; Benjamini test $p<0.05$ was considered significant. Transcription factor enrichment analysis was performed using ChEA3 (Keenan et al. 2019). 969 differentially expressed genes from our differential expression analysis in cocaine treated mice were used. Data shown is from the "Top Rank" library option. The top 25 transcription factors obtained from this analysis were compared against the 60 most significant differentially expressed genes (padj < 0.05).

Immunofluorescence

1-hour after cocaine or saline administration, mice were deeply anesthetized with Euthasol followed by transcardial perfusion with 4% paraformaldehyde in PBS ($Na_2HPO_4$10 mM, KH_2PO_4

1.8 mM, NaCl 137 mM, KCl 2.7 mM). Whole brains were then post-fixed over-night in 4% paraformaldehyde in PBS. 30 μm coronal striatal sections were obtained using a vibratome (Leica) and preserved in a cryoprotectant (30% glycerol and 30% ethylene glycol in PBS) and stored at -20C until use.

Tissue sections were washed three times in PBS, permeabilized for 15 min using 0.5% Triton X-100 in PBS and then rinsed twice in same buffer. Non-specific site were blocked by incubation in PBS with 5% Normal Goat Serum (NGS) for 1 hour at room temperature. Sections were incubated with primary antibodies: rabbit anti-c-fos (1:3000; Abcam), rabbit anti-p-rpS6$^{S235/236}$ (1:1000; Cell Signaling), goat anti-choline acetyltransferase (1:800; Millipore), and mouse anti-mCherry (1:800; Abcam) in PBS 1% NGS overnight at 4°C alone or in combination. The following day, sections were rinsed three times in PBS for 10 min. Sections were then incubated in secondary antibodies (goat anti-rabbit Alexa Fluor 488, donkey anti-goat Alexa Fluor 488, or goat anti-mouse Alexa Fluor 546) which were used at a 1:2000 concentration in PBS 1% NGS. The sections were rinsed twice with PBS before nuclei were stained with Draq 7 (1:1000; Biostatus). Images were taken on an SP5 confocal microscope (Leica). Striatal neurons positive for c-Fos or p-rpS6$^{S235/236}$ were quantified using LAS-X (Leica; version 3.7.0) software. Three 387.5 × 387.5 μm regions of interest in the dorsomedial and ventral striatum from 3-8 mice/treatment/genotype were used in experimenter blinded analyses. Values shown from IF experiments are represented as cell counts per mm^2.

Fluorescent in situ hybridization

Brain sections were obtained and hybridized with fluorescein-labeled *D1R or enkephalin (Enk)* and digoxigenin (DIG)-labeled *c-fos* riboprobes (Roche), as previously described (Anzalone et al. 2012; Kharkwal et al. 2016b), followed by anti–Fluorescein-POD (1:1000, Roche) and anti–

DIG-AP (1:1000, Roche) antibodies. To amplify the signal the TSA PLUS fluorescein System (Perkin Elmer) and HNPP (2-hydroxy-3-naphtoic acid-2'-phenylanilide phosphate) fluorescent Detection Set (Roche) were used. Nuclei were stained with Draq7 1:1000. The percentage of double positive *c-fos* and *D1R or Enk* cells compared to the total *D1R or Enk* positive cells were determined. 3 mice/treatment/genotype were used in experimenter blinded analyses.

Quantification and Statistical Analysis

All values are presented as mean ± SEM. GraphPad Prism 8.3.0 (La Jolla California, USA) was used to perform statistical analyses. One, Two, or Three-way Analysis of Variance (ANOVA) followed by Bonferroni's multiple comparison post-hoc test was used as appropriate; $p < 0.05$ was considered statistically significant.

Data and Code Availablility

The RNA-Sequencing data sets generated during this study are available at ArrayExpress: E-MTAB-8589

Key Resource Table

REAGENT or RESOURCE	SOURCE	IDENTIFIER
Antibodies		
Rabbit anti-c-fos	Abcam	ab190289
Rabbit anti-phospho-S6 Ribosomal Protein (Ser235/236)	Cell Signaling	2211
Goat anti-choline acetyltransferase	Millipore/Sigma	AB144P
Mouse anti-mCherry	Abcam	ab167453
Sheep anti-digoxigenin-AP Fab fragments	Roche	11093274910
Sheep anti-fluorescein-POD Fab fragments	Roche	11426346910
Donkey anti-goat Alexa Fluor 488	Abcam	ab150129
Goat anti-rabbit Alexa Fluor 488	ThermoFisher	A-11034
Goat anti-rabbit Alexa Fluor 546	ThermoFisher	A-11010
Goat anti-mouse Alexa Fluor 546	ThermoFisher	A-11003
Bacterial and Virus Strains		
pAAV-hSyn-DIO-hM4D(Gi)-mCherry	AddGene	44362-AAV2
Critical Commercial Supplies		
DIG RNA Labeling Kit	Roche	11175025910
Fluorescein RNA Labeling Kit	Roche	11685619910
TSA Fluorescein Kit	Perkin Elmer	SAT701001KT
HNPP Fluorescent Detection Set	Roche	11758888001
Chemicals, Peptides, and Recombinant Proteins		
Cocaine HCl	Sigma	C5776
Donepezil HCl	Sigma	D6821
Scopolamine HBr Trihydrate	Sigma	PHR1470
Tropicamide HCl	Tocris	0909
VU0255035 HCl	UCI	N/A
Clozapine-N-Oxide	NIH	027862
JHU37160	HelloBio	HB6261
Deposited Data		
Raw and processed RNA-Seq Data	This Paper	ArrayExpress E-MTAB-8589
Software and Algorithms		
Prism 8.3.0	GraphPad	https://www.graphpad.com/scientific-software/prism/
Viewpoint VideoTack	ViewPoint Behavior Technology	http://www.viewpoint.fr/en/p/software/videotrack
HCS 3.4.0.38	Illumina	https://support.illumina.com/downloads/hiseq-4000-3000-hcs-v3-4-0.html

Leica Application Suite X v 3.7.0	Leica	https://www.leica-microsystems.com/products/microscope-software/p/leica-las-x-ls/
FastQC	Babraham Bioinformatics	https://www.bioinformatics.babraham.ac.uk/projects/fastqc/
STAR 2.6.0c	Dobin et al. 2018	https://github.com/alexdobin/STAR/releases
Genomic Features	Lawrence et al., 2013	https://bioconductor.org/packages/release/bioc/html/GenomicFeatures.html
Genomic Alignments	Lawrence et al., 2013	https://bioconductor.org/packages/release/bioc/html/GenomicAlignments.html
DESeq2	Love et al., 2014	https://bioconductor.org/packages/release/bioc/html/DESeq2.html
EnhancedVolcano	Blighe et al., 2019	https://bioconductor.org/packages/release/bioc/html/EnhancedVolcano.html
DAVID v6.8	The Database for Annotation, Visualization and Integrated Discovery	https://david.ncifcrf.gov/
ChEA3	Keenan et al., 2019	https://amp.pharm.mssm.edu/chea3/

Figure Legends

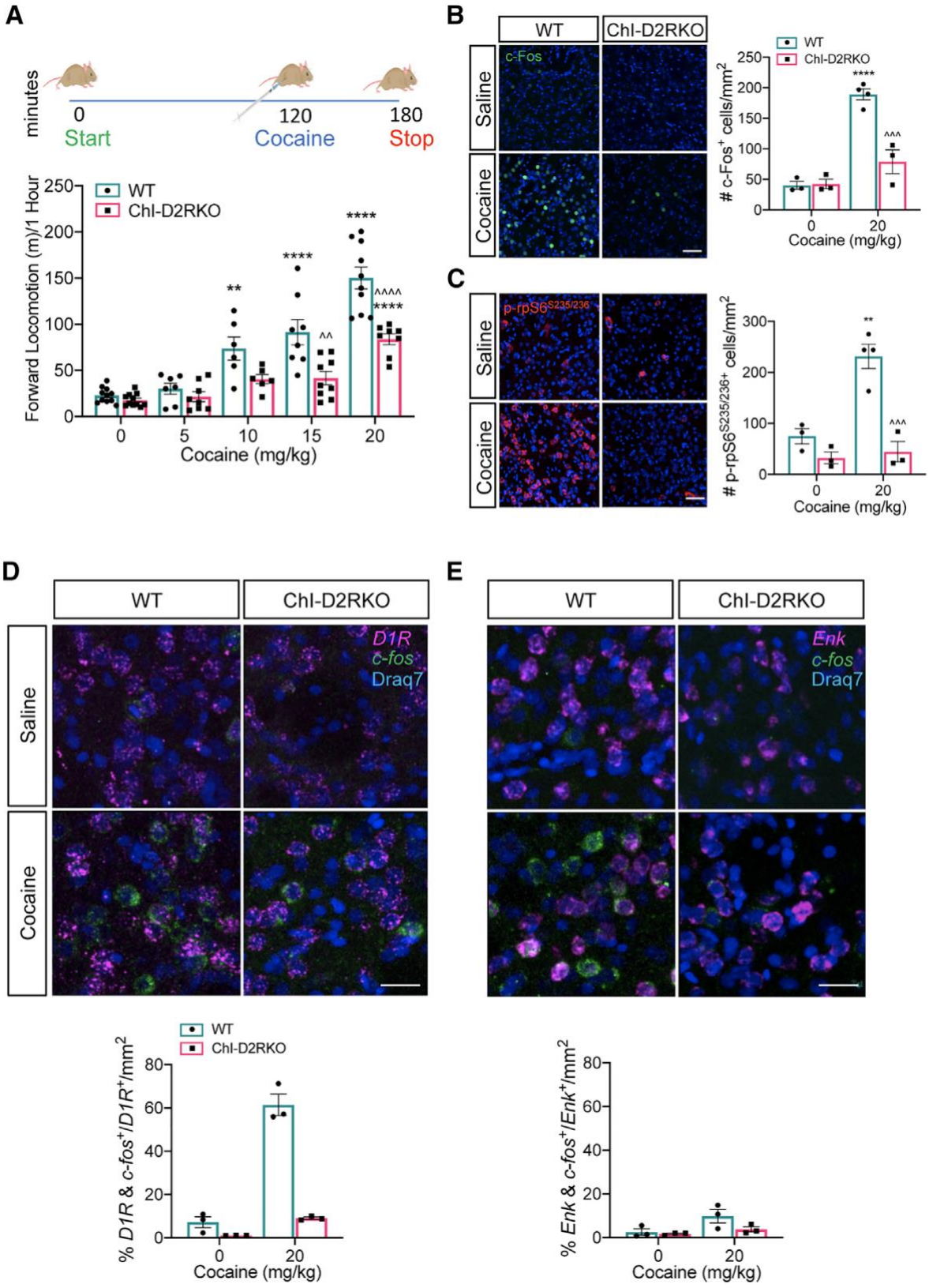

Figure 1. Absence of D2R signaling in ChIs leads to reduced cocaine response.
(A) *Top:* Protocol followed for studying cocaine effects; *Bottom:* Cocaine dose-dependent induction of motor activity in WT and ChI-D2RKO mice (n=6-11/group). *Genotype:* $F_{(1, 4)}$= *41.54, p<0.0001; Treatment:* $F_{(4, 74)}$= *53.19, p<0.0001; Interaction:* $F_{(4, 74)}$= *6.121, p=0.0003*.
(B and C) *Left:* Representative images of IF experiments in cocaine treated WT and ChI-D2RKO mice using c-Fos and p-rpS6$^{S235/236}$ antibodies, respectively; *Right*: quantifications of c-Fos (*Genotype:* $F_{(1, 9)}$ *= 21.92, p=0.0009; Treatment:* $F_{(1, 9)}$ *= 63.97, p<0.0001; Interaction:* $F_{(1, 9)}$ *= 23.85, p=0.0011)* and p-rpS6$^{S235/236}$ positive neurons (*Genotype:* $F_{(1, 9)}$ *= 33.12, p=0.0003; Treatment:* $F_{(1, 9)}$ *= 17.90, p=0.0022; Interaction:* $F_{(1, 9)}$ *= 13.17, p=0.0055* positive neurons) (n=3-4/group).
(D and E) *Top:* Representative images of FISH experiments using *D1R or Enk* riboprobes along with *c-fos* riboprobes and *Bottom*: Percentage of double positive cells over the total number of *D1R or Enk* positive neurons per mm^2.
**p<0.01, **p<0.001 ****p<0.0001 vs saline of same genotype; ^^p<0.01 ^^^^p<0.0001 vs WT with same treatment. Scale bars for B and C are 50 µm; for D and E are 25 µm. In A-E bars represent the mean ± SEM.

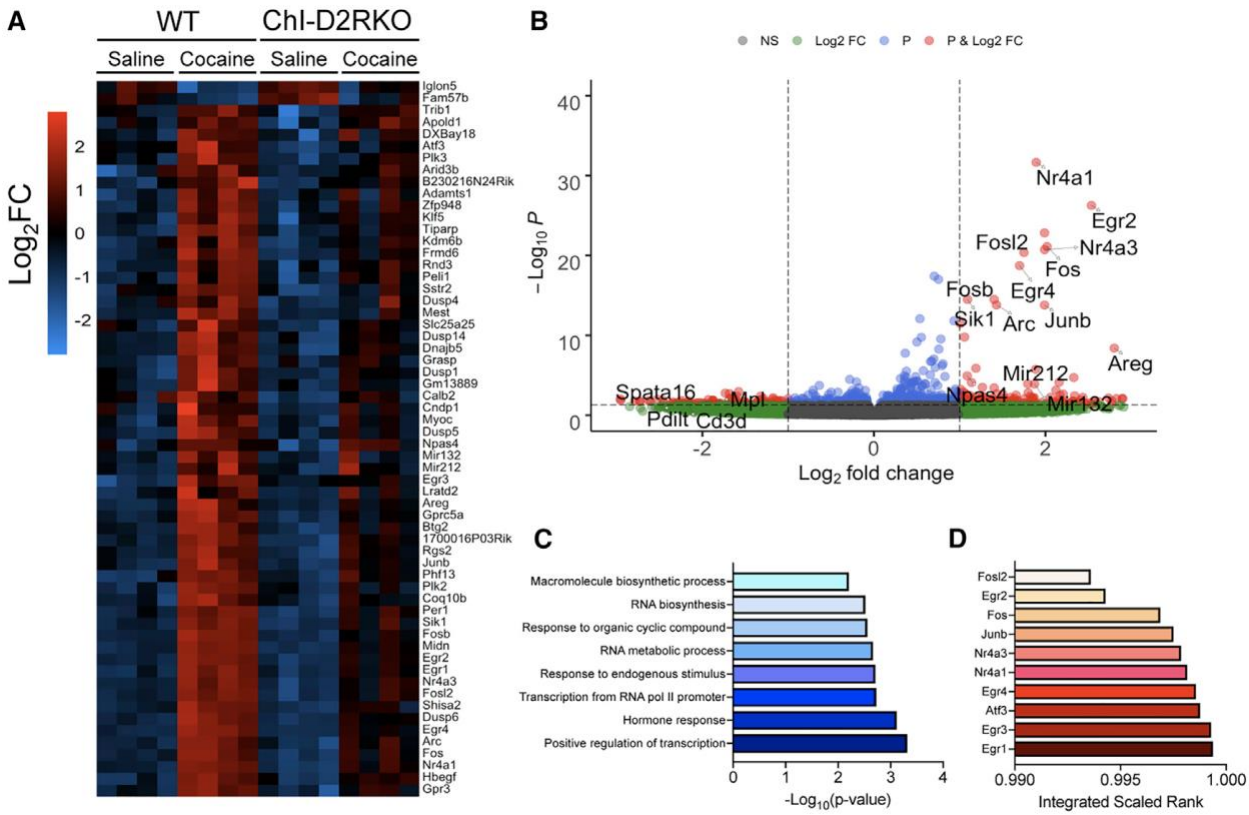

Figure 2. Altered transcriptomic profile in the striatum of ChI-D2RKO mice.
(**A**) Heatmap illustrating the log2-fold change (Log_2FC) of genes differentially expressed (padj <0.05) in cocaine treated (20 mg/kg; ip) WT and ChI-D2RKO mice; up-regulation (red) down-regulation (blue).
(**B**) Volcano plot based on the -log10 p-value ($-Log_{10}P$) vs the Log_2FC of the DMS transcriptome. Cutoffs are shown as dotted lines ($p<0.05$) and $log_2FC \pm 1$.
(**C**) Gene ontology determined by DAVID using genes with $p<0.05$ and log_2FC above 1 and below -1 (shown in red in Fig. 2B).
(**D**) Transcription factor enrichment analysis of the 969 differentially expressed genes (See Fig. S2B) using ChEA3. The top 25 enriched transcription factors were compared with the most significant genes (padj <0.05); the resulting 10 transcription factor's integrated scaled rank is shown.

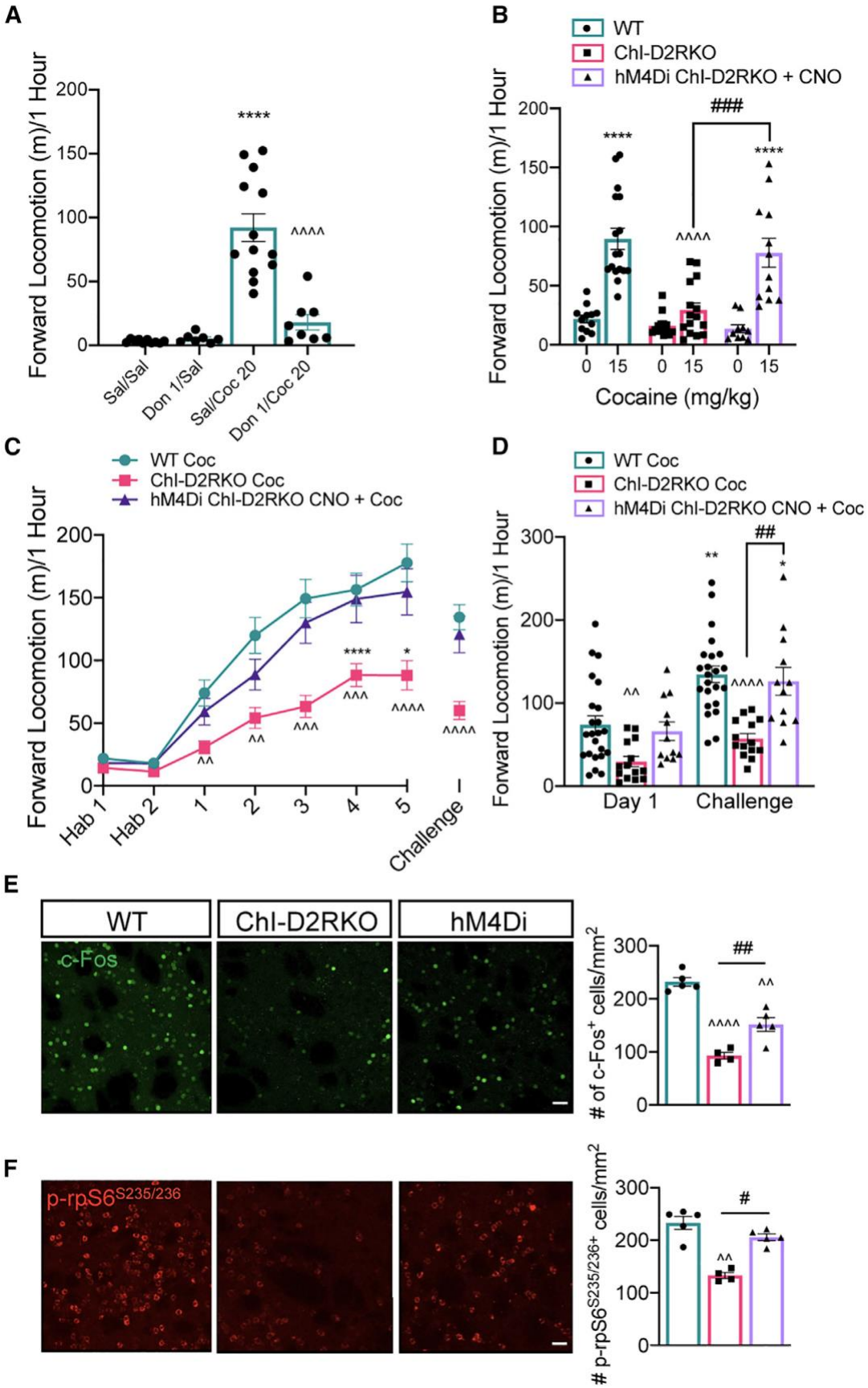
A
Forward Locomotion (m)/1 Hour
Sal/Sal
Don 1/Sal
Sal/Coc 20
Don 1/Coc 20
B
WT
Chl-D2RKO
hM4Di Chl-D2RKO + CNO
Cocaine (mg/kg)
C
WT Coc
Chl-D2RKO Coc
hM4Di Chl-D2RKO CNO + Coc
Hab 1
Hab 2
Challenge
D
Day 1
Challenge
E
WT
Chl-D2RKO
hM4Di
c-Fos
# of c-Fos+ cells/mm2
F
p-rpS6S235/236
p-rpS6S235/236+ cells/mm2

Figure 3. Cocaine sensitization in mice with a deletion of D2R in ChIs.
(**A**) Donepezil lowers the motor response to cocaine in WT mice (n=7-13/group). (*Treatment:* $F_{(3, 34)} = 33.30, p<0.0001$). Bonferroni test: ****p<0.0001 vs Sal/Sal; ^^^^p<0.0001 vs Sal/Coc 20.
(**B**) Silencing of ChIs by in ChI-D2RKO mice restores their acute cocaine response (n=10-14/group). *Genotype:* $F_{(1, 9)} = 33.12, p=0.0003$; *Treatment:* $F_{(1, 9)} = 17.90, p=0.0022$; *Interaction:* $F_{(1, 9)} = 13.17, p=0.0055$. Bonferroni test: ****p<0.0001 vs saline in the same genotype; ^^^^p<0.0001 vs WT Coc; ###p<0.001 vs ChI-D2RKO Coc.
(**C**) Locomotor sensitization to cocaine (n=14-22/group). *Genotype:* $F_{(2, 48)} = 12.57, p<0.0001$; *Day:* $F_{(7, 336)} = 82.06, p<0.0001$; *Interaction:* $F_{(14, 336)} = 3.633, p<0.0001$. Bonferroni test: *p<0.05, ****p<0.0001, vs Day 1 in mice of the same genotype; ^^p<0.01, ^^^p<0.001, ^^^^p<0.0001 vs WT on the same day.
(**D**) Comparison of motor responses on day 1 and the challenge day from C. *Genotype:* $F_{(2, 48)} = 12.57, p<0.0001$; *Day:* $F_{(7, 336)} = 82.06, p<0.0001$; *Interaction:* $F_{(14, 336)} = 3.633, p<0.0001$. Bonferroni test: *p<0.05, **p<0.01, vs Day 1 in mice with the same genotype; ^^p<0.01, ^^^^p<0.0001 vs WT on the same day of the experiment; ##p<0.01 vs ChI-D2RKO on the same day.
(**E and F**) *Left:* Representative images and *Right:* quantification of c-Fos (*Genotype:* $F_{(2, 12)} = 35.28, p<0.0001$) and p-rpS6$^{S235/236}$ (*Genotype:* $F_{(2, 16)} = 9.686; p=0.0018$) IF experiments in the DMS 1 hour after the challenge per mm^2 (n=4/group) . Bonferroni test: ^^p<0.01, ^^^^p<0.0001 vs WT; #p<0.05, ##p<0.01 vs ChI-D2RKO. Values in A-F are mean ± SEM. Scale bars: 50 µm.

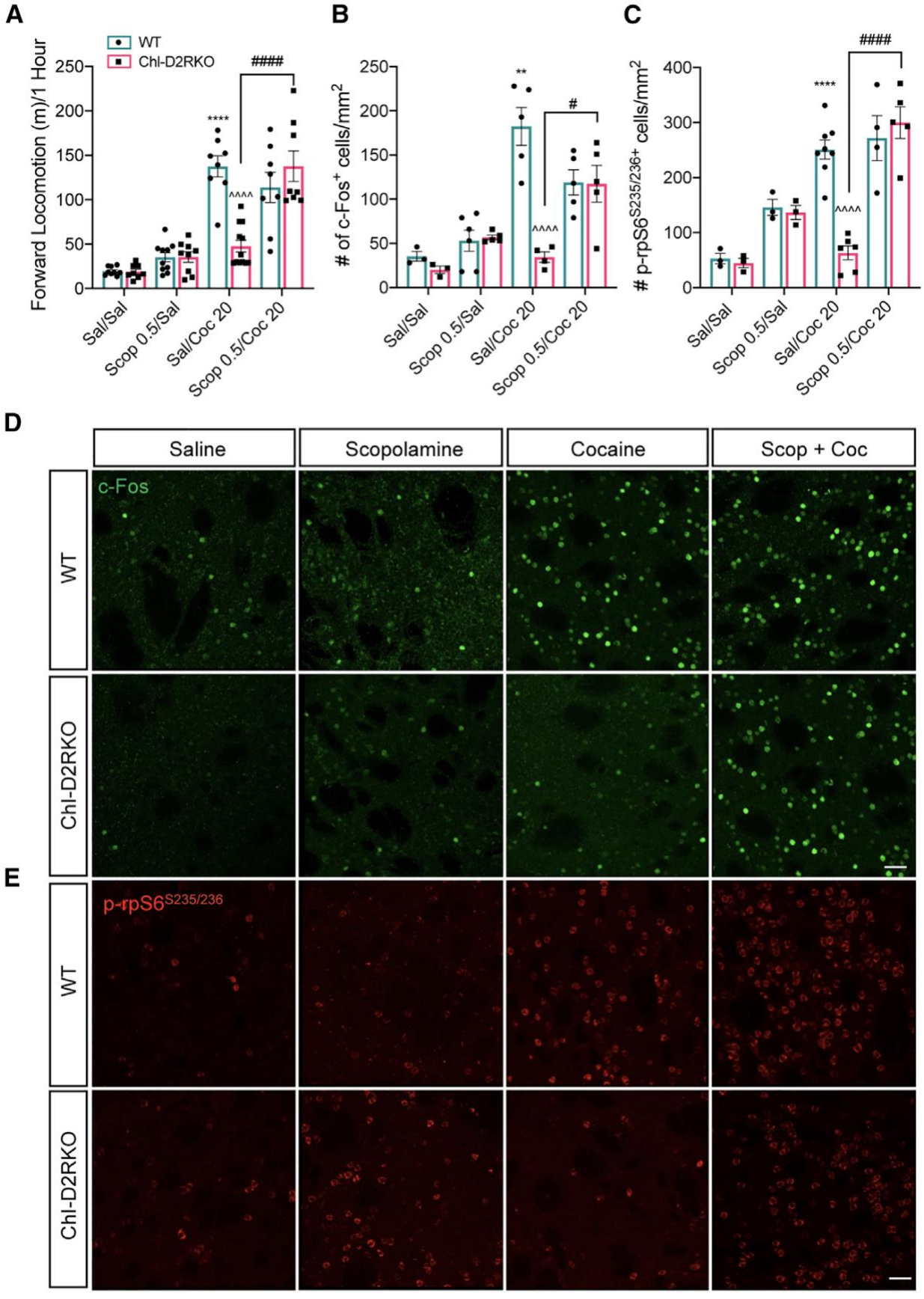
A
B
C
WT
Chl-D2RKO
Forward Locomotion (m)/1 Hour
# of c-Fos+ cells/mm2
p-rpS6S235/236+ cells/mm2
Sal/Sal
Scop 0.5/Sal
Sal/Coc 20
Scop 0.5/Coc 20
****
^^^^
####
**
#
D
Saline
Scopolamine
Cocaine
Scop + Coc
c-Fos
WT
Chl-D2RKO
E
p-rpS6S235/236

Figure 4. Antagonism of muscarinic receptors enables cocaine response in ChI-D2RKO mice.

(**A**) Motor activity in the presence or absence of scopolamine administered 15 minutes prior to cocaine (n=8-12/group). *Genotype:* $F_{(1, 64)} = 5.971$, $p=0.0173$; *Treatment:* $F_{(3, 64)} = 51.346$, $p<0.0001$; *Interaction:* $F_{(3, 64)} = 14.22$, $p<0.0001$.

(**B and C**) Quantification of the number of c-Fos (*Genotype:* $F_{(1, 28)} = 14.19$, $p=0.0008$; *Treatment:* $F_{(3, 28)} = 15.47$, $p<0.0001$; *Interaction* $F_{(3, 28)} = 12.26$, $p<0.0001$) and p-rpS6$^{S235/236}$ (*Genotype:* $F_{(1, 27)} = 11.79$, $p<0.0001$; *Treatment:* $F_{(3, 27)} = 31.41$, $p<0.0001$; *Interaction* $F_{(3, 27)} = 6.640$, $p=0.0158$) positive neurons per mm^2 within the DMS 1 hour after cocaine (n=3-6/group).

For A-C Bonferroni test: *p<0.05, **p<0.01, ****p<0.0001 vs Sal of same genotype; ^^^^p<0.0001 vs WT Coc 20; #p<0.05, ##p<0.01, ###p>0.001, ####p<0.0001 vs treatment within the same genotype. All values are mean ± SEM.

(**D**) Representative images of c-Fos and **E**) of p-rpS6$^{S235/236}$ positive neurons in the DMS of mice treated as in A-C. Scale bars: 50 µm.

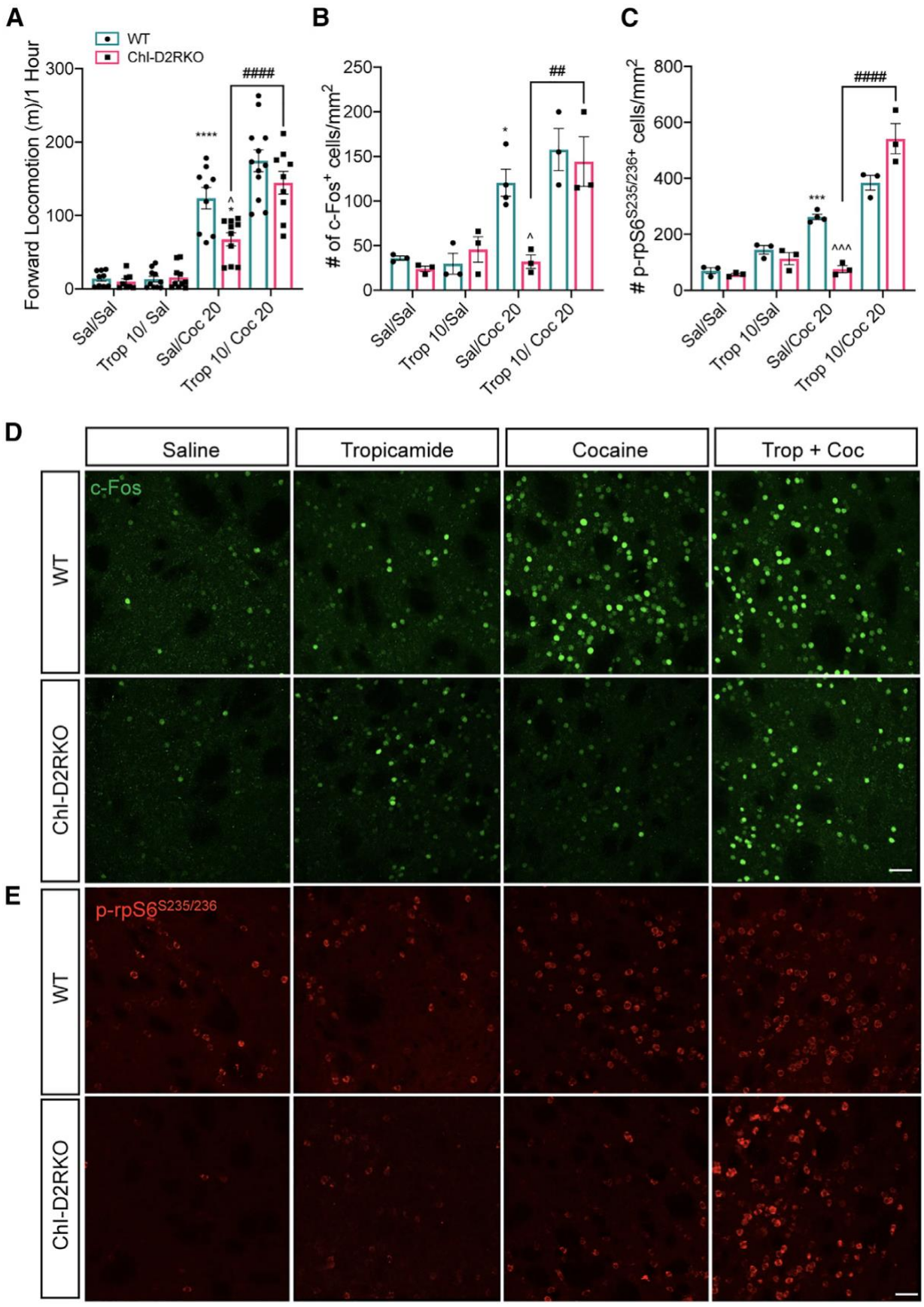
A
WT
Chl-D2RKO
Forward Locomotion (m)/1 Hour
300
200
100
0
****
*
^
####
Sal/Sal
Trop 10/ Sal
Sal/Coc 20
Trop 10/ Coc 20
B
# of c-Fos+ cells/mm2
250
200
150
100
50
0
*
^
##
Sal/Sal
Trop 10/Sal
Sal/Coc 20
Trop 10/ Coc 20
C
p-rpS6S235/236+ cells/mm2
800
600
400
200
0
***
^^^
####
Sal/Sal
Trop 10/Sal
Sal/Coc 20
Trop 10/Coc 20
D
Saline
Tropicamide
Cocaine
Trop + Coc
c-Fos
WT
Chl-D2RKO
E
p-rpS6S235/236
WT
Chl-D2RKO

Figure 5. Antagonism of muscarinic receptors enables cocaine response in ChI-D2RKO mice.

(**A**) Tropicamide given 15 minutes prior cocaine restores the cocaine effects in ChI-D2RKO mice (n=8-11/group). *Genotype: $F_{(1, 69)} = 8.413$, $p<0.0050$; Treatment: $F_{(3, 69)} = 90.63$, $p<0.0001$; Interaction: $F_{(3, 69)} = 3.126$, $p=0.0313$.*

(**B**) Quantification of the number of c-Fos positive neurons *(Genotype: $F_{(1,17)} = 4.744$, $p=0.0438$; Treatment: $F_{(3,17)} = 23.53$, $p<0.0001$; Interaction: $F_{(3,17)} = 4.213$, $p=0.0212$)* and (**C**) of p-rpS6$^{S235/236}$ positive neurons per mm^2 within the DMS 1 hour after cocaine (N=3-6/group) (*Genotype: $F_{(1, 17)} = 1.230$, $p=0.2828$; Treatment: $F_{(3, 17)} = 110.3$, $p<0.0001$; Interaction: $F_{(3, 17)} = 18.60$, $p<0.0001$).*

Bonferroni test: * p<0.05, ***p<0.001, ****p<0.0001 vs saline of same genotype; ^p<0.05, ^^^p<0.001 vs WT Sal/Coc 20; #p<0.05, ##p<0.01, ####p<0.0001 vs ChI-D2RKO Sal/Coc 20. Values shown in A-C are mean ± SEM.

(**D**) Representative images of c-Fos positive neurons and (**E**) of p-rpS6$^{S235/236}$ positive neurons in the DMS of mice treated as in A-C. Scale bars: 50 µm.

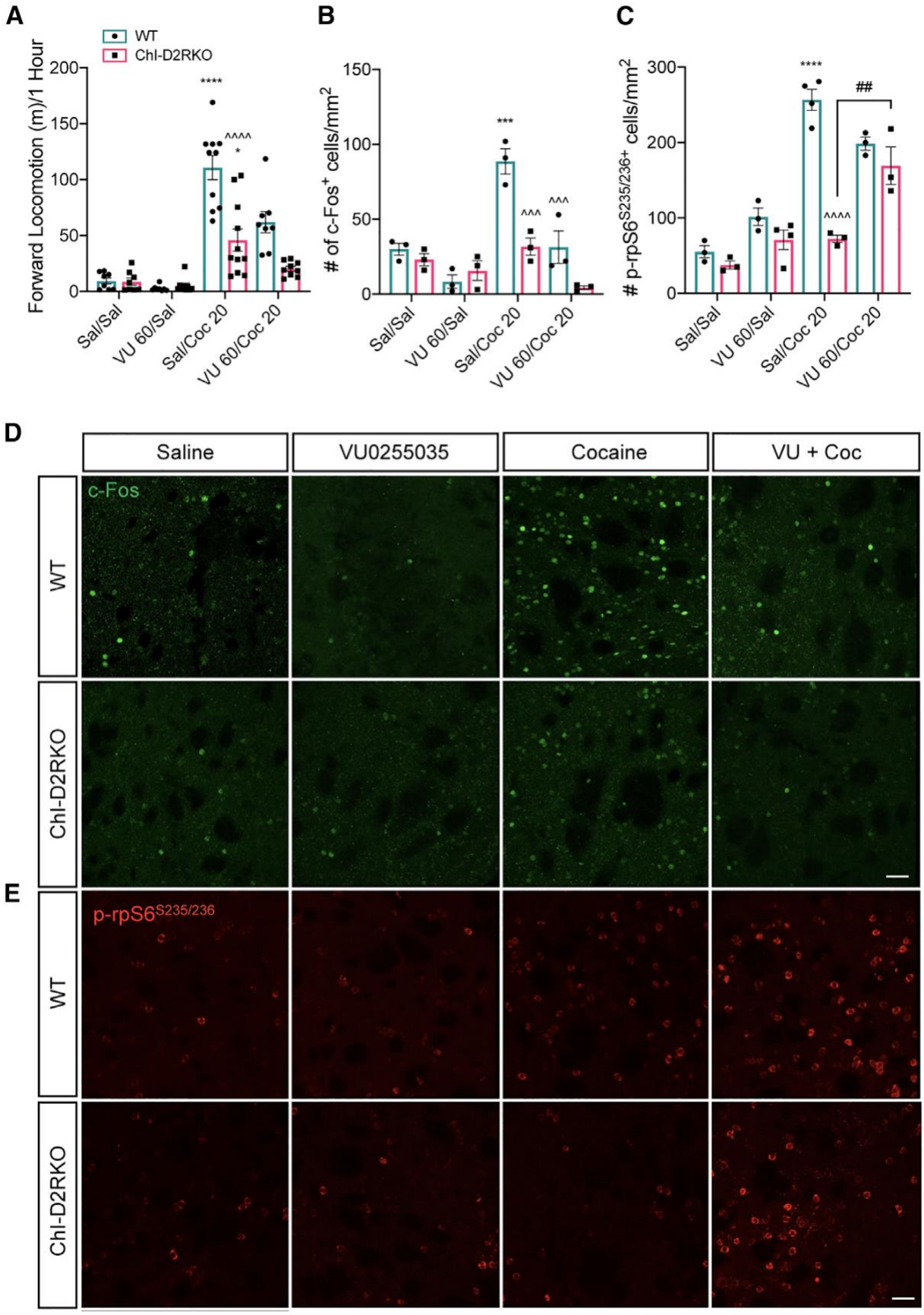
A
WT
Chl-D2RKO
Forward Locomotion (m)/1 Hour
200
150
100
50
0
****
^^^^
*
Sal/Sal
VU 60/Sal
Sal/Coc 20
VU 60/Coc 20
B
# of c-Fos+ cells/mm2
150
100
50
0
***
^^^
^^^
Sal/Sal
VU 60/Sal
Sal/Coc 20
VU 60/Coc 20
C
p-rpS6S235/236+ cells/mm2
300
200
100
0
****
##
^^^^
Sal/Sal
VU 60/Sal
Sal/Coc 20
VU 60/Coc 20
D
Saline
VU0255035
Cocaine
VU + Coc
WT
Chl-D2RKO
c-Fos
E
WT
Chl-D2RKO
p-rpS6S235/236

Figure 6. Antagonism of muscarinic receptors enables cocaine response in ChI-D2RKO mice.

(**A**) The selective M1R antagonist fails to rescue cocaine induced motor activity in ChI-D2RKO mice (n=8-11/group). *Genotype:* $F_{(1, 63)} = 26.35$, $p<0.0001$; *Treatment:* $F_{(3, 63)} = 49.22$, $p<0.0001$; *Interaction:* $F_{(3, 63)} = 10.88$, $p<0.0001$.

(**B**) Quantification of the number of c-Fos positive neurons (*Two-Way ANOVA Genotype:* $F_{(1, 16)} = 21.85$, $p=0.0003$; *Treatment:* $F_{(3, 16)} = 23.16$, $p<0.0001$; *Interaction:* $F_{(3, 16)} = 9.701$, $p=0.0007$) and (**C**) of p-rpS6$^{S235/236}$ positive neurons per mm^2 within the DMS 1 hour after cocaine (n=3-6/group) *(Genotype:* $F_{(1, 18)} = 49.10$, $p<0.0001$; *Treatment:* $F_{(3, 18)} = 46.67$, $p<0.0001$; *Interaction:* $F_{(3, 18)} = 18.86$, $p<0.0001$).

Bonferroni test: ***p<0.001, ****p<0.0001 vs saline of same genotype; ^^^p<0.001, ^^^^p<0.0001 vs WT Sal/Coc 20; #p<0.05, ##p<0.01, ####p<0.0001 vs specified treatment with same genotype. Values shown in A-C are mean ± SEM.

(**D**) Representative images of c-Fos positive neurons and (**E**) of p-rpS6$^{S235/236}$ positive neurons in the DMS of mice treated as in A-C. Scale bar: 50 µm.

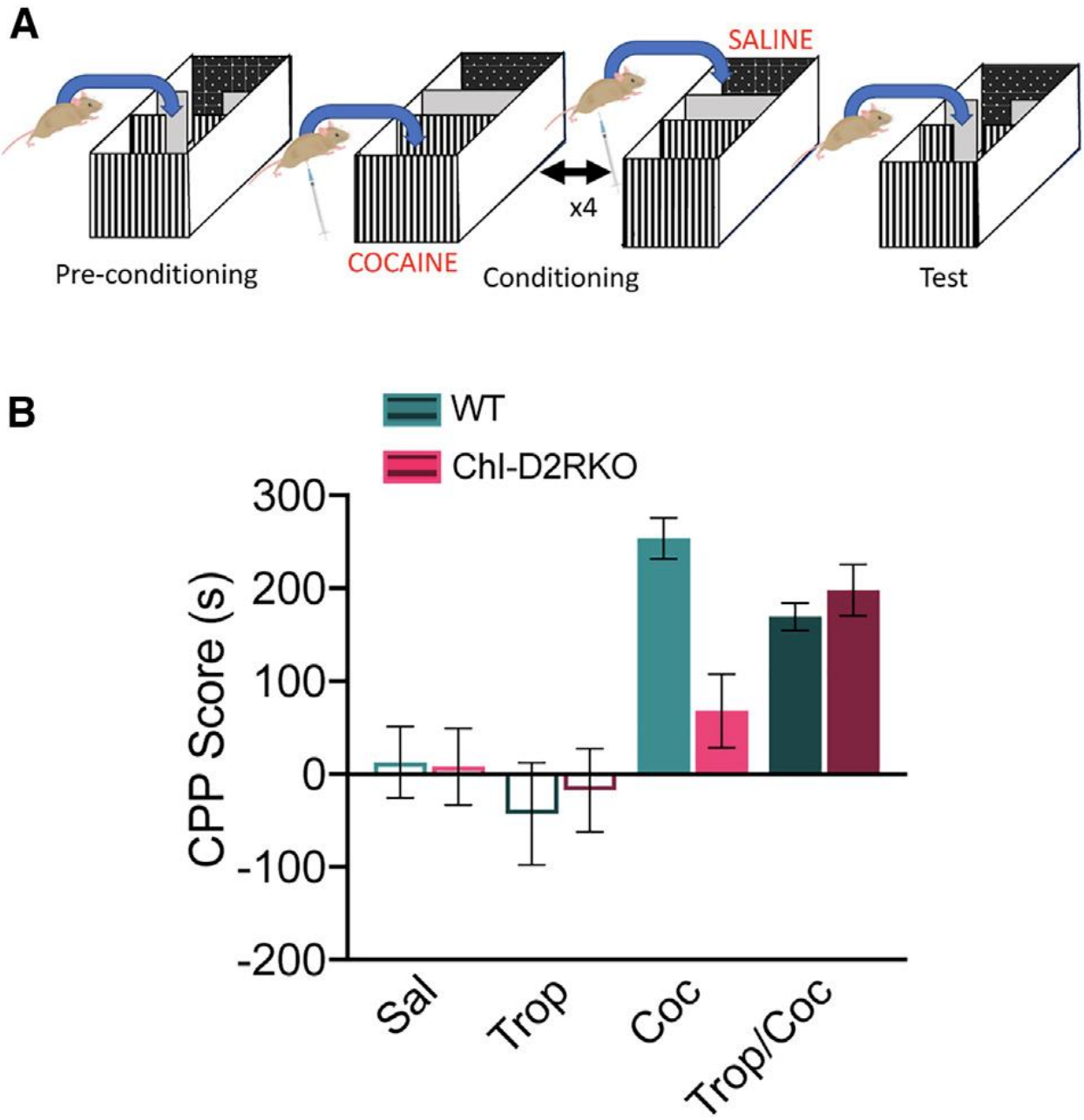

Figure 7. The reinforcing properties of cocaine are affected by loss of dopaminergic inhibition of ChIs

(**A**) Cartoon illustrating the protocol used to perform the CPP test.

(**B**) CPP score after conditioning with either saline (Sal), tropicamide (Trop), cocaine (Coc) or Trop + Coc (Trop/Coc) in WT and ChI-D2RKO mice (n=8-16/group). *Genotype:* $F_{(1, 76)} = 1.989$, $p=0.1226$; *Treatment:* $F_{(3, 76)} = 12.84$, $p<0.0001$; *Interaction* $F_{(3, 76)} = 3.756$, $p=0.0143$.

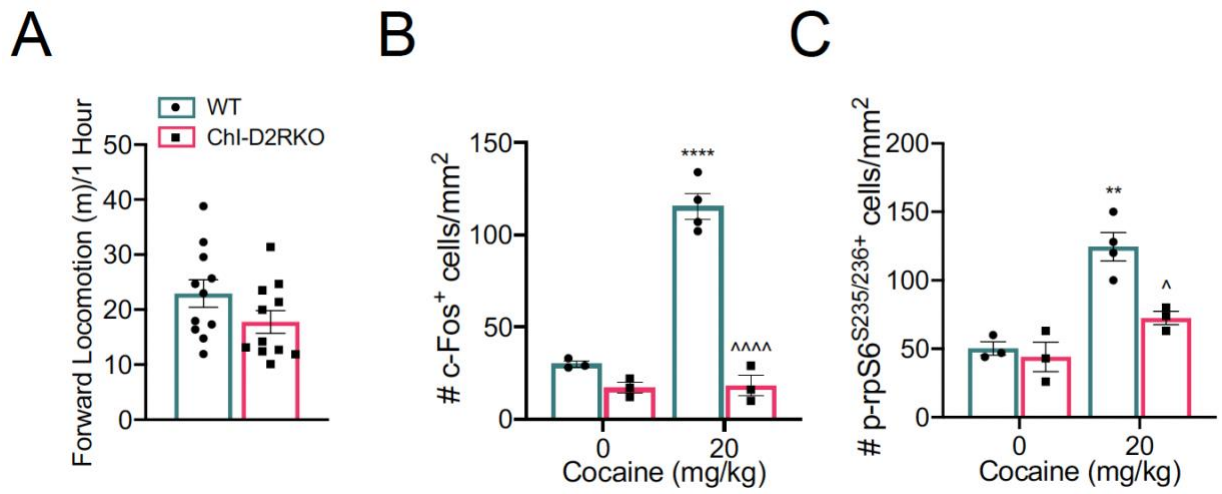

Figure S1: Absence of D2R signaling in ChIs leads to reduced cocaine response. Related to Figure 1.

(A) Motor activity of saline treated WT and ChI-D2RKO mice over 1 hour (n=11/genotype) (*student's t-test, p=0.1247*).

(**B**) Quantifications of c-Fos positive neurons (*Genotype: $F_{(1, 9)} = 101.4$, $p<0.0001$; Treatment: $F_{(1, 9)} = 63.00$, $p<0.0001$; Interaction: $F_{(1, 9)} = 59.19$, $p<0.0001$)* and (**C**) of p-rpS6$^{S235/236}$ positive neurons per mm^2 in the ventral striatum of mice 1 hour after cocaine (20 mg/kg; ip) or saline (n= 3-4/group) (*Genotype: $F_{(1, 9)} = 10.89$, $p=0.0092$; Treatment: $F_{(1, 9)} = 33.44$, $p=0.0003$; Interaction: $F_{(1, 9)} = 6.686$, $p=0.0294$*). Bonferroni test: **p<0.01, ****p<0.0001 vs saline of same genotype; ^p<0.05, ^^^^p<0.0001 vs cocaine treated WT. All values shown are mean ± SEM.

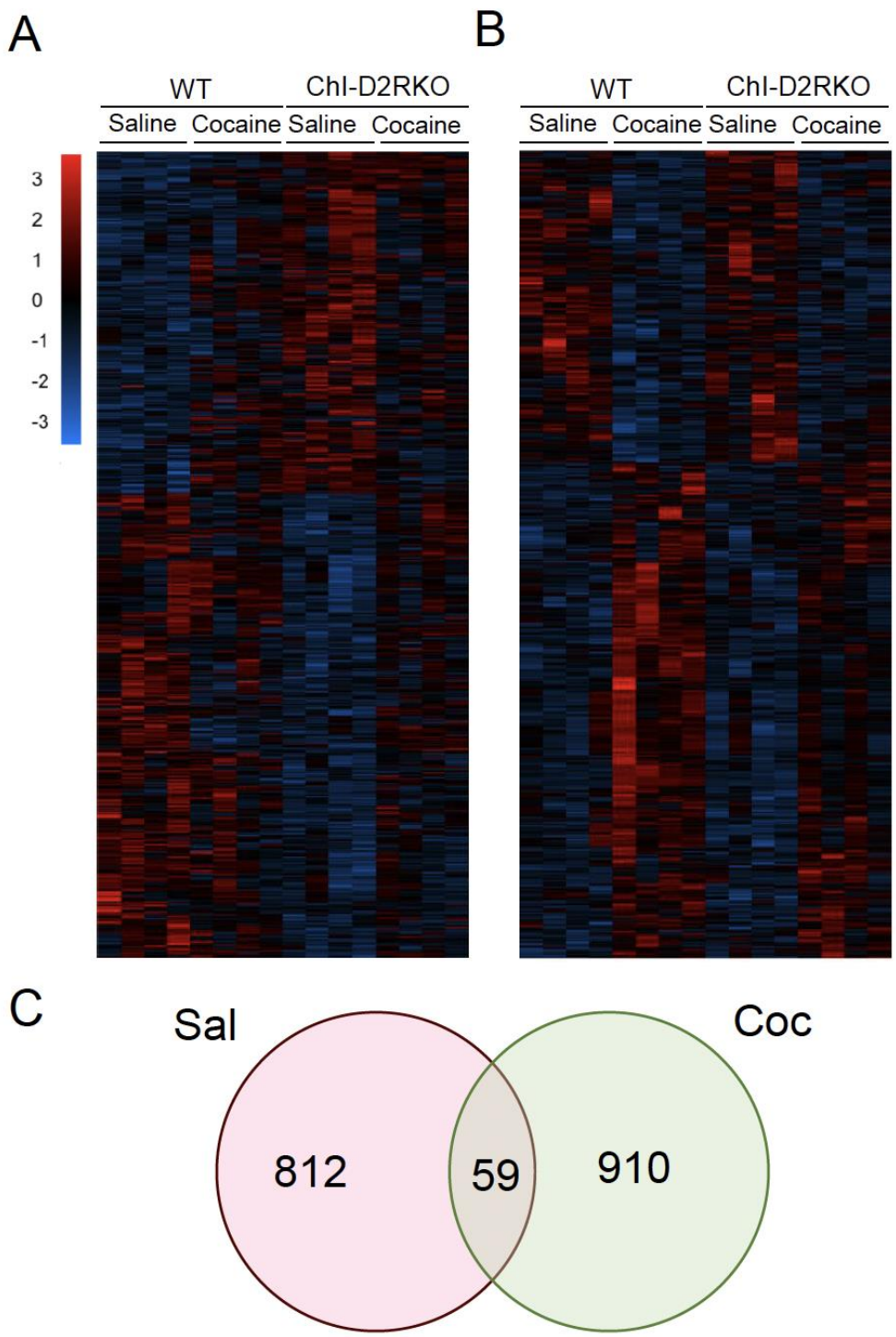

Figure S2: Altered transcriptomic profile in the striatum of ChI-D2RKO mice. Related to Figure 2.

(**A**) Heatmap illustrating the log2-fold change (Log_2FC) in genes identified to be differentially expressed ($p<0.05$) in saline or **(B)** cocaine treated WT and ChI-D2RKO mice. Red represents up-regulation while blue represents down-regulation.
(**C**) Venn diagram showing the overlap between significant genes found in each analysis.

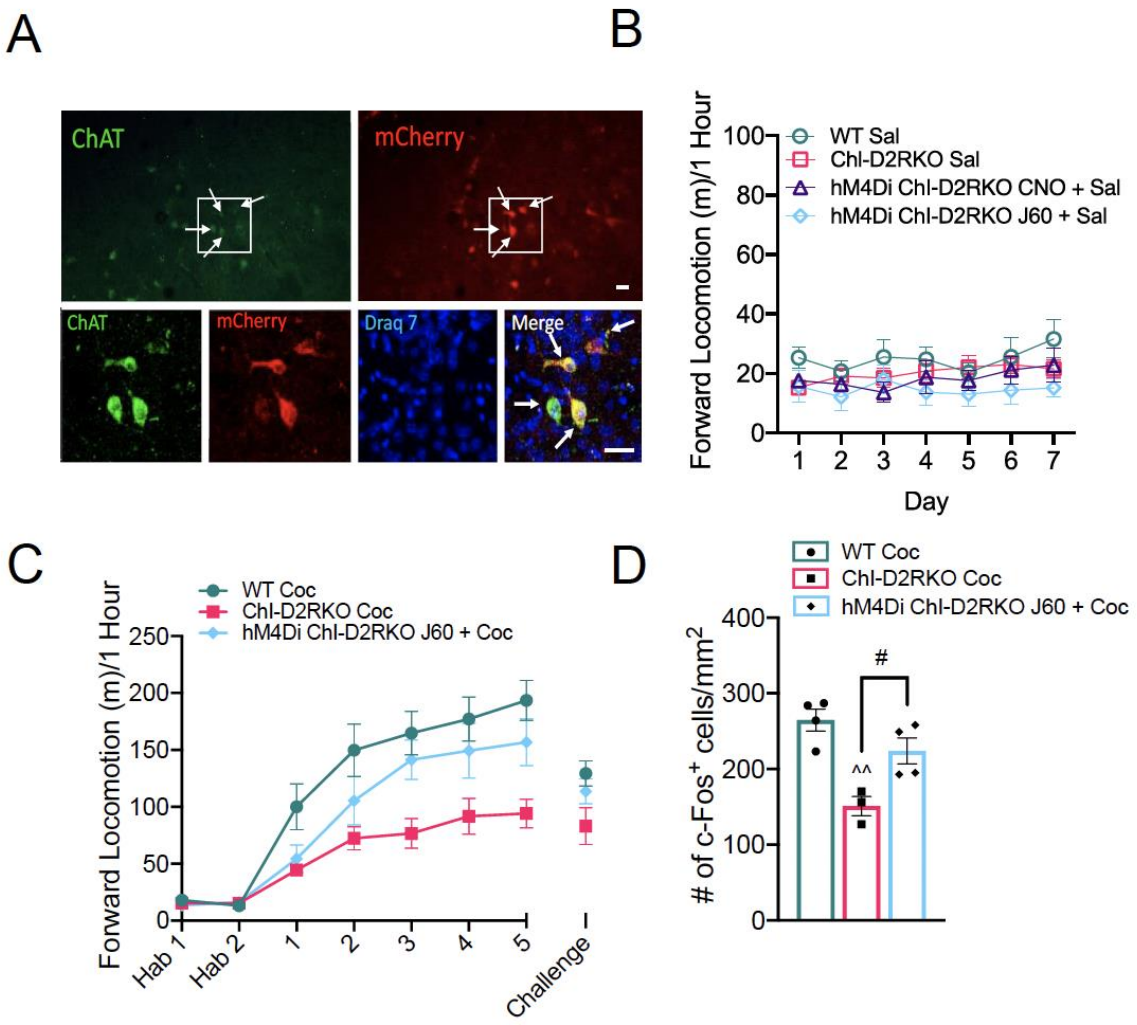

Figure S3: Cocaine sensitization in mice with a deletion of D2R in ChIs. Related to Figure 3.

(**A**) IF testing Selective hM4Di expression in the ChIs of ChI-D2RKO mice using mCherry and choline acetyltransferase (ChAT) antibodies. Arrows indicate double positive cells. Scale bars: 25 µm.
(**B**) CNO (3 mg/kg; ip) and J60 (0.1 mg/kg; ip) treatment do not alter motor activity in hM4Di ChI-D2RKO as compared to saline treated WT and ChI-D2RKO mice (n= 6-12/group). (*Genotype:* $F_{(3, 38)} = 1.444$, $p=0.2453$; *Day:* $F_{(6, 228)} = 1.635$, $p=0.1823$; *Interaction:* $F_{(18, 228)} = 0.7935$, $p=0.7071$).
(**C**) Forward locomotion in response to cocaine (sensitization protocol: 15 mg/kg; ip) during 1 hour in WT, ChI-D2RKO, and hM4Di ChI-D2RKO mice using J60 (0.1 mg/kg; ip) 30 minutes prior to cocaine (n=7-8/group) (*Genotype:* $F_{(2, 20)} = 6.585$, $p=0.0064$; *Day:* $F_{(7, 140)} = 86.45$, $p<0.0001$; *Interaction:* $F_{(14, 140)} = 4.567$, $p<0.0001$).
(**D**) Quantifications of the number of c-Fos positive neurons per mm^2 (n=4/group) in the DMS 1 hour after the challenge injection of cocaine (10 mg/kg; ip) as shown in C. *Genotype:* $F_{(2, 8)} = 12.44$; $p=0.0035$. Bonferroni test: ^^p<0.01 vs WT; #p<0.05 vs ChI-D2RKO. n= 3-4/group. Values shown in B-D are mean ± SEM.

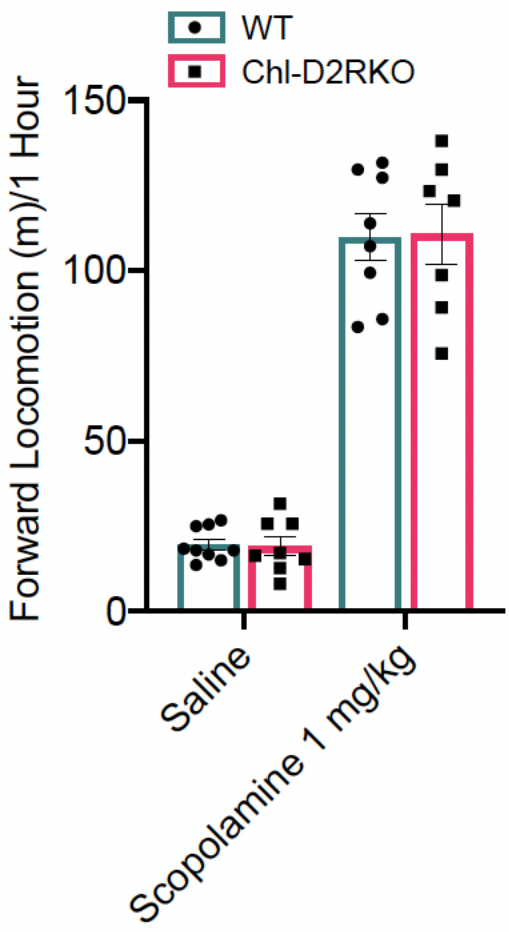

Figure S4: Antagonism of muscarinic receptors enables cocaine response in ChI-D2RKO mice. Related to Figure 4.
1 mg/kg of scopolamine induces motor activity in both ChI-D2RKO and WT mice to the same level (n=7-9/group). *Genotype:* $F_{(1, 28)} = 0.001413$, $p=0.9703$; *Treatment:* $F_{(1, 28)} = 287.2$, $p<0.0001$; *Interaction:* $F_{(1, 28)} = 0.01977$, $p=0.8892$. All values shown are mean ± SEM.

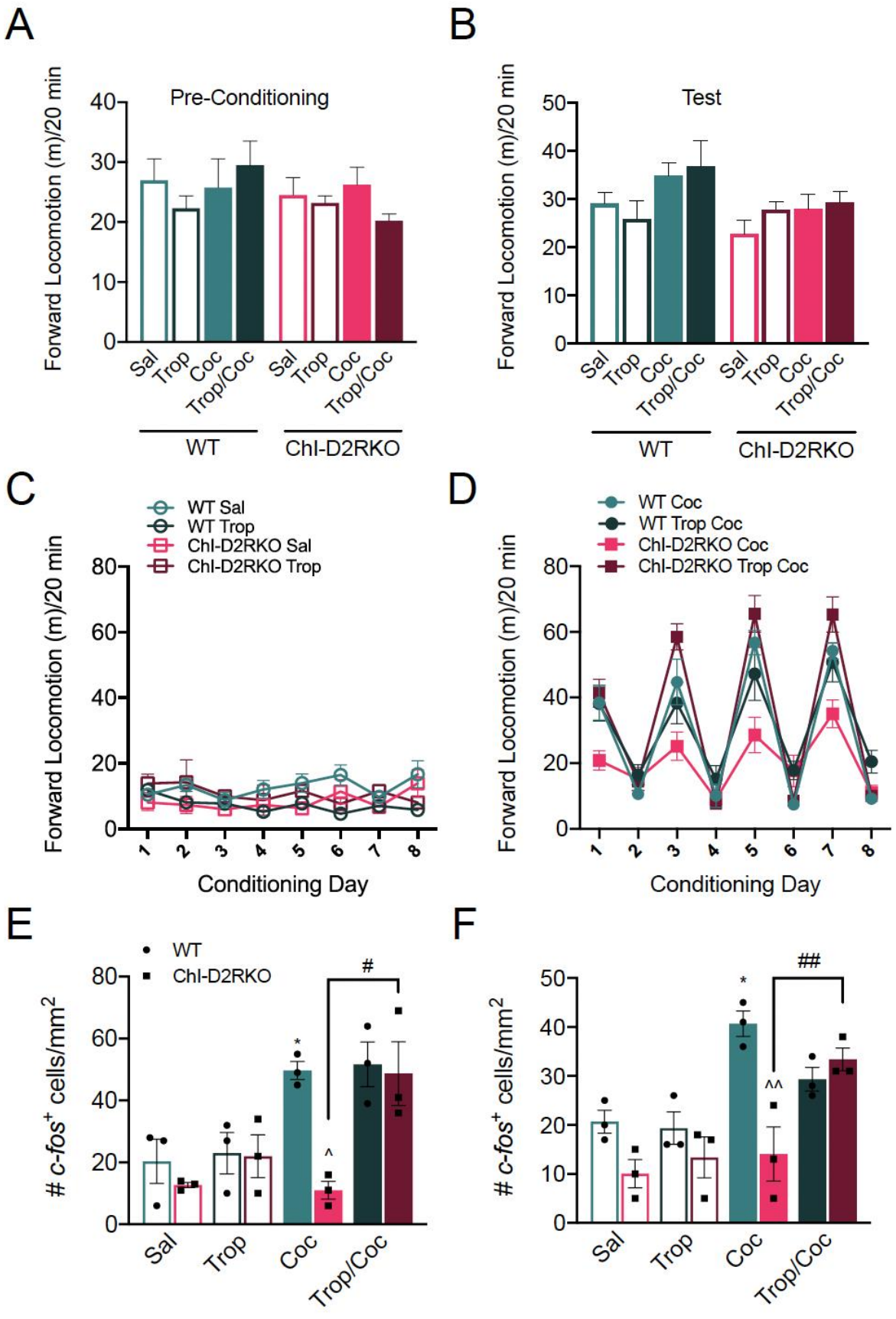
A
Pre-Conditioning
Forward Locomotion (m)/20 min
Sal
Trop
Coc
Trop/Coc
WT
ChI-D2RKO
B
Test
C
WT Sal
WT Trop
ChI-D2RKO Sal
ChI-D2RKO Trop
Conditioning Day
D
WT Coc
WT Trop Coc
ChI-D2RKO Coc
ChI-D2RKO Trop Coc
E
WT
ChI-D2RKO
c-fos+ cells/mm2
F

Figure S5: The reinforcing properties of cocaine are affected by loss of dopaminergic inhibition of ChIs. Related to Figure 7.

(**A**) Forward locomotion did not differ between WT and ChI-D2RKO mice during the pre-conditioning (*Genotype:* $F_{(1, 68)} = 0.8990$, $p=0.3464$; *Treatment:* $F_{(3, 68)} = 0.2518$, $p=0.8598$; *Interaction:* $F_{(3, 68)} = 0.7180$, $p=0.5446$) or the (**B**) test day in the cocaine CPP experiment (*Genotype:* $F_{(1, 68)} = 3.797$, $p=0.0555$; *Treatment:* $F_{(3, 68)} = 2.233$, $p=0.0922$; *Interaction:* $F_{(1, 68)} = 0.6334$, $p=0.5960$).

(C) Forward locomotion in WT and ChI-D2RKO mice during conditioning in the presence or absence of tropicamide (*Genotype:* $F_{(1, 22)} = 0.4011$, $p=0.4011$; *Treatment:* $F_{(1, 22)} = 0.06136$, $p=0.8067$, *Day:* $F_{(4.495, 98.90)} = 1.036$, $p=0.3973$; *Day x Treatment x Genotype:* $F_{(7, 154)} = 0.3786$, $p=0.9138$) and **(D)** during conditioning in cocaine treated mice in the presence or absence of tropicamide; days are as indicated (*Genotype:* $F_{(1, 43)} = 3.296$, $p=0.0764$; *Treatment:* $F_{(1, 43)} = 0.6232$, $p=0.4342$, *Day:* $F_{(7, 301)} = 80.68$, $p<0.0001$; *Day x Treatment x Genotype:* $F_{(7, 301)} = 2.051$, $p=0.0487$). Values shown in B-D are mean ± SEM.

(**E**) Quantification of the number of *c-fos*-positive neurons in the DMS (*Genotype:* $F_{(1, 16)} = 7.208$, $p=0.0008$; *Treatment:* $F_{(3, 16)} = 11.22$, $p=0.0003$; *Interaction:* $F_{(3, 16)} = 7.208$, $p=0.0028$) and the **(D)** ventral striatum (*Genotype:* $F_{(1, 16)} = 7.945$, $p=0.0124$; *Treatment:* $F_{(3, 16)} = 10.79$, $p=0.0004$; *Interaction* $F_{(3, 16)} = 3.891$, $p=0.0290$) per mm^2 observed 1 hour after the completion of the test session (n=3/group). *p<0.05, vs saline of same genotype; ^^p<0.01 ^^^^p<0.0001 vs WT with same treatment. All values shown are mean ± SEM.

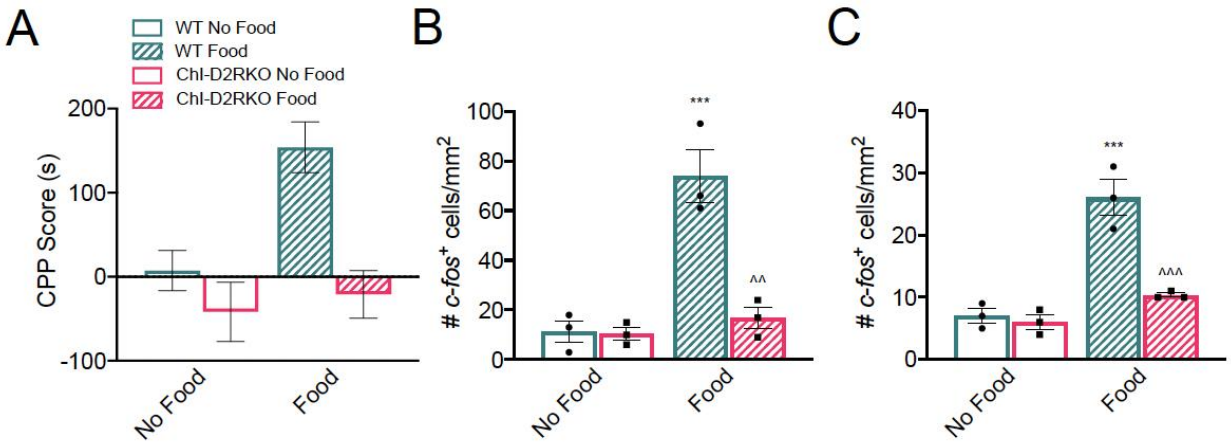

Figure S6: The reinforcing properties of food are affected by loss of dopaminergic inhibition of ChIs. Related to Figure 7.

(A) CPP score calculated for the specified groups (n=7-8/group). *Genotype:* $F_{(1, 27)} = 14.53$, $p=0.0008$; *Treatment:* $F_{(1, 27)} = 8.114$, $p=0.0085$; *Interaction:* $F_{(1, 27)} = 4.596$, $p=0.0416$. (**B**) Quantification of the number of *c-fos*-positive neurons in the DMS (*Genotype:* $F_{(1, 8)} = 21.63$, $p=0.0016$; *Treatment:* $F_{(1, 8)} = 30.26$, $p=0.0006$; *Interaction:* $F_{(1, 8)} = 20.17$, $p=0.0020$) and the **(C)** ventral striatum (*Genotype:* $F_{(1, 8)} = 25.00$, $p=0.0011$; *Treatment:* $F_{(1, 8)} = 49.00$, $p=0.0001$; *Interaction* $F_{(1, 8)} = 19.36$, $p=0.0023$) per mm^2 1 hour after the test session (n=3/group). All values depict mean ± SEM.

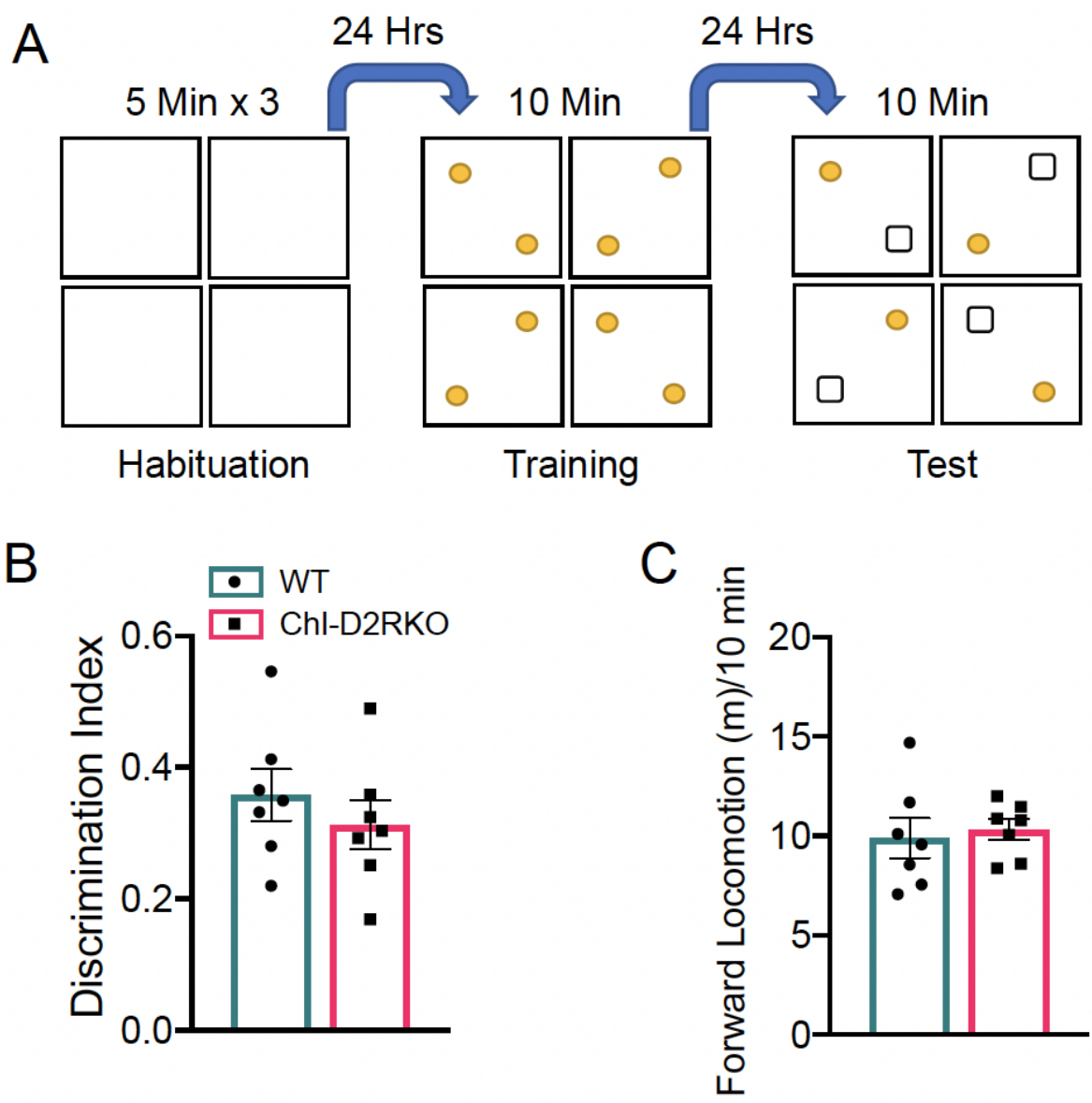

Figure S7: Intact spatial memory in ChI-D2RKO mice. Related to Figure 7.
(A) Cartoon illustrating the protocol used to perform the novel object recognition test.
(B) Discrimination index summarizing the time spent investigating the novel object as compared to the known object during the testing session. *Student's t-test, p=0.4178.*
(C) Forward locomotion during the test session (n=7/group). *Student's t-test, p=0.7129.* Values shown in B and C are mean ± SEM.

Chapter 6: Summary and Conclusions

In Chapter 2, we defined D2R isoform specific roles for cocaine's effects. In basal conditions, each individual isoform is sufficient for the control of motor activity and stereotypies. Using D2R selective compounds however, the individual roles of each isoform can be observed. We found that D2SKO mice are less sensitive to the motor reducing effects of the D2R agonist, quinpirole, compared to WT and D2LKO mice. Relatedly, tyrosine hydroxylase phosphorylation, which is linked to presynaptic D2R activation, is similarly unaffected in D2SKO mice. This suggests a predominant presynaptic function for D2S. In contrast, D2LKO mice do not display catalepsy to the D2R antagonist haloperidol, while WT and D2SKO mice did. Lack of catalepsy in D2LKO mice mirrors that of mice with ablation of D2R in ChIs. This suggests that D2L mediated control of ChIs plays a key role in regulating the effects of D2R selective compounds. However, future studies using mice with specific deletions of D2L in ChIs will need to be used to carve out this hypothesis. Still, D2L has a clear function in the control of GABA release in striatal neurons.

D2LKO mice have an abated psychomotor response to cocaine and lose the induction of c-fos, indicating that loss of D2L in iMSNs also affects dMSN activation. The induction of c-fos is rescued upon intrastriatal administration of the $GABA_a$ receptor antagonist, bicuculine, which is comparable to observations seen in mice lacking both D2R isoforms in iMSNs. Thus, D2L in iMSNs appears to be critical for intrastriatal regulation through the control of collateral projections from iMSNs to dMSNs. It is clear from this study that D2L's heteroreceptor functions are critical for regulating striatal output. However, the generation and study of mice with a genetic deletion of D2L in iMSN's or ChI's will be necessary to elucidate how the expression of D2L in each

neuron type contributes to the overall postsynaptic function of D2R as well as its role in regulating cocaine's effects.

In Chapter 3, we examined how D2R in iMSNs regulates the circadian clock of the nucleus accumbens; we link D2R signaling in iMSNs with PPARγ activation in the regulation of *de novo* oscillatory gene expression. In this study, WT and iMSN-D2RKO mice were given a single injection of cocaine at the beginning of the light phase (ZT3). With this single exposure to cocaine, observed that despite an overall lower motor behavior in iMSN-D2RKO mice compared to WT controls, both genotypes maintained circadian rhythmicity in motor behavior. Relatedly, core clock gene expression remained largely unaffected. Interestingly, transcriptomic analyses using RNA-sequencing in the NAcc indicated an alteration in cycling transcripts. Indeed, cocaine treated mice showed only 2% of rhythmic transcripts overlapped in in the NAcc between WT and iMSN-D2RKO mice. By comparing detected cycling transcripts in each genotype-treatment condition, we determined a list of *de novo* rhythmic genes. Analysis of the promoters of these genes revealed PPARγ as a critical regulator of cocaine regulated gene rhythmicity in WT but not iMSN-D2RKO mice. Using immunofluorescence and in situ hybridization, we were able to visualize an increase in nuclear PPARγ in WT but not iMSN-D2RKO mice and determined that the lack of PPARγ expression was specific to iMSNs.

We then sought to understand how D2R signaling may regulate the cocaine driven activation of PPARγ as well as how this activation effected downstream gene expression. Using ELISA, we found that cocaine increased PGJ2, a natural PPARγ ligand. This finding corresponded with an increase in the expression of PPARγ target genes found in WT but not iMSN-D2RKO mice as well as increased PPARγ enrichment at the promoters of these genes. Pharmacological activation of PPARγ using pioglitazone overrides D2R's control on PPARγ activation, rescuing

gene expression in iMSN-D2RKO mice. In context, PPARγ is known to be an anti-inflammatory molecule through its inhibition of inflammatory cytokines (Martin 2010). Several studies have linked increased inflammation to neurological and psychiatric disorders (Degan et al. 2018; Skaper et al. 2018; Bauer and Teixeira 2019; Kohno et al. 2019). It is tempting to speculate that people with addiction who demonstrate low D2R binding availability in the striatum, much like the iMSN-D2RKO mice studied here, lose the ability to regulate neuroinflammation possibly through interactions between glial and neuroimmuno cells (Lacagnina et al. 2017). This dysregulation in the mesolimbic system could possibly contribute to the transition from single use to addiction.

In Chapter 4, we took an unconventional approach to studying the effects of cocaine and D2R signaling on liver physiology and circadian metabolism. We first observed that, in addition to lower motor activity as previously observed, iMSN-D2RKO mice have reduced metabolic parameters including body weight, calorie expenditure, chow consumption, water intake, and gonadal fat content. This suggested that metabolism could possibly be disrupted in iMSN-D2RKO mice. We looked to the liver, a highly metabolic peripheral organ that is sensitive to perturbation and found that iMSN-D2RKO mice show a difference in the distribution of the number of rhythmic metabolites compared to WT mice. Cocaine administration resulted in almost three-fold more oscillating metabolites in iMSN-D2RKO mice compared to WT controls. It's possible that this results from the increase in metabolites oscillating from ZT2-ZT6 in iMSN-D2RKO mice that is not present in WT mice. Indeed, iMSN-D2RKO mice are more prone to induce *de novo* rhythmic acylcarnitines after a cocaine challenge. Importantly, our findings show that the desynchrony between the liver and striatum, in the absence of D2R in a neuron-type–specific manner, influences liver homeostasis, which is exacerbated by cocaine. These findings link metabolites to drug use–mediated alterations in the brain affecting peripheral tissues. We propose that a tight association

exists between drug use and the increased susceptibility to metabolic diseases via altered modulation of acylcarnitines and sphingomyelins in the liver.

In Chapter 5, we identified a key role for D2R in regulating cholinergic interneuron (ChI) activity which underlies cocaine's psychostimulating and rewarding effects. We discovered that mice lacking D2R in ChIs (ChI-D2RKO) have a reduction in the motor stimulating effects of cocaine as well as dMSN activation markers, c-fos and p-RPS6$^{Ser235/236}$. RNA-sequencing revealed a transcriptomic rewiring of the dorsomedial striatum. Key transcription factors known to be induced after addictive drug intake and are implicated in addiction increase in WT mice, but not in ChI-D2RKO mice. Since D2R is an inhibitory receptor, we hypothesized that the absence of D2R in ChIs leads to increased ChI activity following cocaine intake. In support of this hypothesis, chemogenetic inhibition of ChIs rescues acute and sensitization effects of cocaine. We then found that muscarinic receptor activation was leading to the reduced motor activity and dMSN cellular activation because prior administration with a subthreshold dose of scopolamine, a non-selective muscarinic antagonist, rescues the effects of cocaine in ChI-D2RKO mice. Muscarinic type 1 receptors (M1R) are expressed mainly in iMSNs while Muscarinic type 4 receptors (M4R) are overexpressed in dMSNs. We tested whether this increase in ChI activity and consequent ACh levels directly inhibited dMSNs through M4R activation or if M1R activation in iMSNs inhibits dMSNs through inhibitory collaterals. The M1R antagonist, VU0255035, fails to rescue the ChI-D2RKO phenotypes while the M4R antagonist tropicamide rescues the motor and cellular effects of cocaine. Finally, ChI-D2RKO mice do not exhibit cocaine conditioned place preference. However, with prior administration of tropicamide during the conditioning phase, cocaine CPP is rescued in ChI-D2RKO mice. It is clear that the balance of dopamine and ACh in the striatum (Cachope et al. 2012; Cachope and Cheer 2014) is critical for regulating the effects of cocaine.

M4R overstimulation, as a result of a shift in the balance towards ACh, prevents the cellular, motor, and reinforcing effects of cocaine. Therefore, it is tempting to speculate that ChI mediated control of the striatum plays a much greater role in reward processing than one might expect based on their abundance. A common future of drugs of abuse, in addition to increasing dopamine levels, may be to dysregulate (lower) striatal ACh tone from ChIs as a means of controlling reward processing. This control of cholinergic tone may then affect signal transduction pathways in MSNs that underlies changes in synaptic plasticity and drive continued substance use. If so, compounds allowing for the selective activation of ChIs or those activating downstream ACh receptors (e.g. M4R) may be useful in the treatment of substance use disorders. Future studies assessing this possibility and the molecular mechanisms driving striatal ACh's control on reward will need to be conducted.

References

Abarca C, Albrecht U, Spanagel R (2002) Cocaine sensitization and reward are under the influence of circadian genes and rhythm. Proc Natl Acad Sci U S A 99:9026–9030. https://doi.org/10.1073/pnas.142039099

Adamovich Y, Rousso-Noori L, Zwighaft Z, et al (2014) Circadian clocks and feeding time regulate the oscillations and levels of hepatic triglycerides. Cell Metab 19:319–330. https://doi.org/10.1016/j.cmet.2013.12.016

Adibhatla RM, Hatcher JF (2007) Role of Lipids in Brain Injury and Diseases. Future Lipidol 2:403–422. https://doi.org/10.2217/17460875.2.4.403

Aizman O, Brismar H, Uhlén P, et al (2000) Anatomical and physiological evidence for D 1 and D 2 dopamine receptor colocalization in neostriatal neurons. Nature Neuroscience 3:226–230. https://doi.org/10.1038/72929

Albrecht U (2012) Timing to perfection: the biology of central and peripheral circadian clocks. Neuron 74:246–260. https://doi.org/10.1016/j.neuron.2012.04.006

Alcaro A, Huber R, Panksepp J (2007) Behavioral Functions of the Mesolimbic Dopaminergic System: an Affective Neuroethological Perspective. Brain Res Rev 56:283–321. https://doi.org/10.1016/j.brainresrev.2007.07.014

Anzalone A, Lizardi-Ortiz JE, Ramos M, et al (2012) Dual control of dopamine synthesis and release by presynaptic and postsynaptic dopamine D2 receptors. J Neurosci 32:9023–9034. https://doi.org/10.1523/JNEUROSCI.0918-12.2012

Aosaki T, Miura M, Suzuki T, et al (2010) Acetylcholine–dopamine balance hypothesis in the striatum: An update. Geriatrics & Gerontology International 10:S148–S157. https://doi.org/10.1111/j.1447-0594.2010.00588.x

Apostolopoulou M, Gordillo R, Koliaki C, et al (2018) Specific Hepatic Sphingolipids Relate to Insulin Resistance, Oxidative Stress, and Inflammation in Nonalcoholic Steatohepatitis. Diabetes Care. https://doi.org/10.2337/dc17-1318

Asher G, Sassone-Corsi P (2015) Time for Food: The Intimate Interplay between Nutrition, Metabolism, and the Circadian Clock. Cell 161:84–92. https://doi.org/10.1016/j.cell.2015.03.015

Aviram R, Manella G, Kopelman N, et al (2016) Lipidomics Analyses Reveal Temporal and Spatial Lipid Organization and Uncover Daily Oscillations in Intracellular Organelles. Mol Cell 62:636–648. https://doi.org/10.1016/j.molcel.2016.04.002

Baik JH, Picetti R, Saiardi A, et al (1995) Parkinsonian-like locomotor impairment in mice lacking dopamine D2 receptors. Nature 377:424–428. https://doi.org/10.1038/377424a0

Balleine BW, Delgado MR, Hikosaka O (2007) The Role of the Dorsal Striatum in Reward and Decision-Making. J Neurosci 27:8161–8165. https://doi.org/10.1523/JNEUROSCI.1554-07.2007

Bass J, Lazar MA (2016) Circadian time signatures of fitness and disease. Science 354:994–999. https://doi.org/10.1126/science.aah4965

Bateup HS, Svenningsson P, Kuroiwa M, et al (2008) Cell type-specific regulation of DARPP-32 phosphorylation by psychostimulant and antipsychotic drugs. Nat Neurosci 11:932–939. https://doi.org/10.1038/nn.2153

Bauer ME, Teixeira AL (2019) Inflammation in psychiatric disorders: what comes first? Ann N Y Acad Sci 1437:57–67. https://doi.org/10.1111/nyas.13712

Beaulieu J-M, Espinoza S, Gainetdinov RR (2015) Dopamine receptors – IUPHAR Review 13. Br J Pharmacol 172:1–23. https://doi.org/10.1111/bph.12906

Beaulieu J-M, Tirotta E, Sotnikova TD, et al (2007) Regulation of Akt signaling by D2 and D3 dopamine receptors in vivo. J Neurosci 27:881–885. https://doi.org/10.1523/JNEUROSCI.5074-06.2007

Bello EP, Mateo Y, Gelman DM, et al (2011) Cocaine supersensitivity and enhanced motivation for reward in mice lacking dopamine D2 autoreceptors. Nat Neurosci 14:1033–1038. https://doi.org/10.1038/nn.2862

Berlanga ML, Simpson TK, Alcantara AA (2005) Dopamine D5 receptor localization on cholinergic neurons of the rat forebrain and diencephalon: a potential neuroanatomical substrate involved in mediating dopaminergic influences on acetylcholine release. J Comp Neurol 492:34–49. https://doi.org/10.1002/cne.20684

Bertran-Gonzalez J, Bosch C, Maroteaux M, et al (2008) Opposing patterns of signaling activation in dopamine D1 and D2 receptor-expressing striatal neurons in response to cocaine and haloperidol. J Neurosci 28:5671–5685. https://doi.org/10.1523/JNEUROSCI.1039-08.2008

Beuming T, Kniazeff J, Bergmann ML, et al (2008) The binding sites for cocaine and dopamine in the dopamine transporter overlap. Nat Neurosci 11:780–789. https://doi.org/10.1038/nn.2146

Biever A, Puighermanal E, Nishi A, et al (2015) PKA-dependent phosphorylation of ribosomal protein S6 does not correlate with translation efficiency in striatonigral and striatopallidal medium-sized spiny neurons. J Neurosci 35:4113–4130. https://doi.org/10.1523/JNEUROSCI.3288-14.2015

Blighe K, Rana S, Lewis M (2019) EnhancedVolcano: Publication-ready volcano plots with enhanced colouring and labeling. Version 1.4.0. Bioconductor version: Release (3.10). URL https://bioconductor.org/packages/EnhancedVolcano/

Bonaventura J, Eldridge MA, Hu F, et al (2018) Chemogenetic ligands for translational neurotheranostics. Neuroscience

Boudreau AC, Wolf ME (2005) Behavioral Sensitization to Cocaine Is Associated with Increased AMPA Receptor Surface Expression in the Nucleus Accumbens. J Neurosci 25:9144–9151. https://doi.org/10.1523/JNEUROSCI.2252-05.2005

Brager AJ, Stowie AC, Prosser RA, Glass JD (2013) The mPer2 clock gene modulates cocaine actions in the mouse circadian system. Behav Brain Res 243:255–260. https://doi.org/10.1016/j.bbr.2013.01.014

Brami-Cherrier K, Lewis RG, Cervantes M, et al (2020) Cocaine-mediated circadian reprogramming in the striatum through dopamine D2R and PPARγ activation. Nature Communications 11:4448. https://doi.org/10.1038/s41467-020-18200-6

Brami-Cherrier K, Valjent E, Hervé D, et al (2005) Parsing molecular and behavioral effects of cocaine in mitogen- and stress-activated protein kinase-1-deficient mice. J Neurosci 25:11444–11454. https://doi.org/10.1523/JNEUROSCI.1711-05.2005

Brown MTC, Tan KR, O'Connor EC, et al (2012) Ventral tegmental area GABA projections pause accumbal cholinergic interneurons to enhance associative learning. Nature 492:452–456. https://doi.org/10.1038/nature11657

Brown SA (2016) Circadian Metabolism: From Mechanisms to Metabolomics and Medicine. Trends Endocrinol Metab 27:415–426. https://doi.org/10.1016/j.tem.2016.03.015

Burton AC, Nakamura K, Roesch MR (2015) From ventral-medial to dorsal-lateral striatum: Neural correlates of reward-guided decision-making. Neurobiol Learn Mem 0:51–59. https://doi.org/10.1016/j.nlm.2014.05.003

Cachope R, Cheer JF (2014) Local control of striatal dopamine release. Front Behav Neurosci 8:188. https://doi.org/10.3389/fnbeh.2014.00188

Cachope R, Mateo Y, Mathur BN, et al (2012) Selective activation of cholinergic interneurons enhances accumbal phasic dopamine release: setting the tone for reward processing. Cell Rep 2:33–41. https://doi.org/10.1016/j.celrep.2012.05.011

Cai Y, Ford CP (2018) Dopamine Cells Differentially Regulate Striatal Cholinergic Transmission across Regions through Corelease of Dopamine and Glutamate. Cell Rep 25:3148-3157.e3. https://doi.org/10.1016/j.celrep.2018.11.053

Caine SB, Negus SS, Mello NK, et al (2002) Role of dopamine D2-like receptors in cocaine self-administration: studies with D2 receptor mutant mice and novel D2 receptor antagonists. J Neurosci 22:2977–2988. https://doi.org/20026264

Carelli RM (2002) Nucleus accumbens cell firing during goal-directed behaviors for cocaine vs. "natural" reinforcement. Physiol Behav 76:379–387. https://doi.org/10.1016/s0031-9384(02)00760-6

Carlson M, Pagès H, Aboyoun P, et al (2019) GenomicFeatures: Conveniently import and query gene models. Version 1.38.0. Bioconductor version: Release (3.10). URL https://bioconductor.org/packages/GenomicFeatures/

Castañeda TR, de Prado BM, Prieto D, Mora F (2004) Circadian rhythms of dopamine, glutamate and GABA in the striatum and nucleus accumbens of the awake rat: modulation by light. J Pineal Res 36:177–185. https://doi.org/10.1046/j.1600-079x.2003.00114.x

Castro SW, Strange PG (1993) Differences in the ligand binding properties of the short and long versions of the D2 dopamine receptor. J Neurochem 60:372–375. https://doi.org/10.1111/j.1471-4159.1993.tb05863.x

Cates HM, Lardner CK, Bagot RC, et al (2019) Fosb Induction in Nucleus Accumbens by Cocaine Is Regulated by E2F3a. eNeuro 6:ENEURO.0325-18.2019. https://doi.org/10.1523/ENEURO.0325-18.2019

Centonze D, Grande C, Usiello A, et al (2003) Receptor subtypes involved in the presynaptic and postsynaptic actions of dopamine on striatal interneurons. J Neurosci 23:6245–6254

Centonze D, Gubellini P, Usiello A, et al (2004) Differential contribution of dopamine D2S and D2L receptors in the modulation of glutamate and GABA transmission in the striatum. Neuroscience 129:157–166. https://doi.org/10.1016/j.neuroscience.2004.07.043

Centonze D, Picconi B, Baunez C, et al (2002) Cocaine and amphetamine depress striatal GABAergic synaptic transmission through D2 dopamine receptors. Neuropsychopharmacology 26:164–175. https://doi.org/10.1016/S0893-133X(01)00299-8

Cervantes M, Lewis RG, Della-Fazia MA, et al (2022) Dopamine D2 receptor signaling in the brain modulates circadian liver metabolomic profiles. Proceedings of the National Academy of Sciences 119:e2117113119. https://doi.org/10.1073/pnas.2117113119

Challet E (2019) The circadian regulation of food intake. Nat Rev Endocrinol 15:393–405. https://doi.org/10.1038/s41574-019-0210-x

Chandra R, Lobo MK (2017) Beyond Neuronal Activity Markers: Select Immediate Early Genes in Striatal Neuron Subtypes Functionally Mediate Psychostimulant Addiction. Front Behav Neurosci 11:. https://doi.org/10.3389/fnbeh.2017.00112

Chaturvedi RK, Beal MF (2008) PPAR: a therapeutic target in Parkinson's disease. J Neurochem 106:506–518. https://doi.org/10.1111/j.1471-4159.2008.05388.x

Chung S, Lee EJ, Yun S, et al (2014) Impact of circadian nuclear receptor REV-ERBα on midbrain dopamine production and mood regulation. Cell 157:858–868. https://doi.org/10.1016/j.cell.2014.03.039

Cone EJ (1995) Pharmacokinetics and pharmacodynamics of cocaine. J Anal Toxicol 19:459–478. https://doi.org/10.1093/jat/19.6.459

Costa TBBC, Lacerda ALT, Mas CD, et al (2019) Insights into the Effects of Crack Abuse on the Human Metabolome Using a NMR Approach. J Proteome Res 18:341–348. https://doi.org/10.1021/acs.jproteome.8b00646

Cunningham CL, Gremel CM, Groblewski PA (2006) Drug-induced conditioned place preference and aversion in mice. Nature Protocols 1:1662–1670. https://doi.org/10.1038/nprot.2006.279

Curran T, Franza BR (1988) Fos and jun: The AP-1 connection. Cell 55:395–397. https://doi.org/10.1016/0092-8674(88)90024-4

Czoty PW, Gage HD, Nader MA (2010) Differences in D2 dopamine receptor availability and reaction to novelty in socially housed male monkeys during abstinence from cocaine. Psychopharmacology (Berl) 208:585–592. https://doi.org/10.1007/s00213-009-1756-4

Daily K, Patel VR, Rigor P, et al (2011) MotifMap: integrative genome-wide maps of regulatory motif sites for model species. BMC Bioinformatics 12:495. https://doi.org/10.1186/1471-2105-12-495

Daniel R, Pollmann S (2014) A universal role of the ventral striatum in reward-based learning: Evidence from human studies. Neurobiol Learn Mem 0:90–100. https://doi.org/10.1016/j.nlm.2014.05.002

Day JJ, Roitman MF, Wightman RM, Carelli RM (2007) Associative learning mediates dynamic shifts in dopamine signaling in the nucleus accumbens. Nat Neurosci 10:1020–1028. https://doi.org/10.1038/nn1923

De Mei C, Ramos M, Iitaka C, Borrelli E (2009) Getting specialized: presynaptic and postsynaptic dopamine D2 receptors. Curr Opin Pharmacol 9:53–58. https://doi.org/10.1016/j.coph.2008.12.002

DeBoer P, Abercrombie ED (1996) Physiological release of striatal acetylcholine in vivo: modulation by D1 and D2 dopamine receptor subtypes. J Pharmacol Exp Ther 277:775–783

Degan D, Ornello R, Tiseo C, et al (2018) The Role of Inflammation in Neurological Disorders. Curr Pharm Des 24:1485–1501. https://doi.org/10.2174/1381612824666180327170632

Della Fazia MA, Servillo G Foie gras and liver regeneration: a fat dilemma. Cell Stress 2:162–175. https://doi.org/10.15698/cst2018.07.144

Delle Donne KT, Sesack SR, Pickel VM (1997) Ultrastructural immunocytochemical localization of the dopamine D2 receptor within GABAergic neurons of the rat striatum. Brain Res 746:239–255. https://doi.org/10.1016/s0006-8993(96)01226-7

Di Chiara G, Bassareo V (2007) Reward system and addiction: what dopamine does and doesn't do. Current Opinion in Pharmacology 7:69–76. https://doi.org/10.1016/j.coph.2006.11.003

Di Chiara G, Imperato A (1988) Drugs abused by humans preferentially increase synaptic dopamine concentrations in the mesolimbic system of freely moving rats. Proc Natl Acad Sci U S A 85:5274–5278

Dobbs LK, Kaplan AR, Lemos JC, et al (2016) Dopamine Regulation of Lateral Inhibition between Striatal Neurons Gates the Stimulant Actions of Cocaine. Neuron 90:1100–1113. https://doi.org/10.1016/j.neuron.2016.04.031

Dobin A, Davis CA, Schlesinger F, et al (2013) STAR: ultrafast universal RNA-seq aligner. Bioinformatics 29:15–21. https://doi.org/10.1093/bioinformatics/bts635

Doi M, Yujnovsky I, Hirayama J, et al (2006) Impaired light masking in dopamine D2 receptor-null mice. Nat Neurosci 9:732–734. https://doi.org/10.1038/nn1711

Doyle SE, Grace MS, McIvor W, Menaker M (2002) Circadian rhythms of dopamine in mouse retina: the role of melatonin. Vis Neurosci 19:593–601. https://doi.org/10.1017/s0952523802195058

Drake TR, Henry T, Marx J, Gabow PA (1990) Severe acid-base abnormalities associated with cocaine abuse. The Journal of Emergency Medicine 8:331–334. https://doi.org/10.1016/0736-4679(90)90015-N

Duclot F, Kabbaj M (2017) The Role of Early Growth Response 1 (EGR1) in Brain Plasticity and Neuropsychiatric Disorders. Front Behav Neurosci 11:. https://doi.org/10.3389/fnbeh.2017.00035

Dunlap JC (1999) Molecular Bases for Circadian Clocks. Cell 96:271–290. https://doi.org/10.1016/S0092-8674(00)80566-8

Dyar KA, Lutter D, Artati A, et al (2018) Atlas of Circadian Metabolism Reveals System-wide Coordination and Communication between Clocks. Cell 174:1571-1585.e11. https://doi.org/10.1016/j.cell.2018.08.042

Eckel-Mahan KL, Patel VR, de Mateo S, et al (2013) Reprogramming of the Circadian Clock by Nutritional Challenge. Cell 155:1464–1478. https://doi.org/10.1016/j.cell.2013.11.034

Eckel-Mahan KL, Patel VR, Mohney RP, et al (2012) Coordination of the transcriptome and metabolome by the circadian clock. PNAS 109:5541–5546. https://doi.org/10.1073/pnas.1118726109

Edgar RS, Green EW, Zhao Y, et al (2012) Peroxiredoxins are conserved markers of circadian rhythms. Nature 485:459–464. https://doi.org/10.1038/nature11088

Everitt BJ, Robbins TW (2013) From the ventral to the dorsal striatum: devolving views of their roles in drug addiction. Neurosci Biobehav Rev 37:1946–1954. https://doi.org/10.1016/j.neubiorev.2013.02.010

Fabregat A, Sidiropoulos K, Viteri G, et al (2017) Reactome pathway analysis: a high-performance in-memory approach. BMC Bioinformatics 18:142. https://doi.org/10.1186/s12859-017-1559-2

Ferris MJ, España RA, Locke JL, et al (2014) Dopamine transporters govern diurnal variation in extracellular dopamine tone. PNAS 111:E2751–E2759. https://doi.org/10.1073/pnas.1407935111

Forman BM, Tontonoz P, Chen J, et al (1995) 15-Deoxy-delta 12, 14-prostaglandin J2 is a ligand for the adipocyte determination factor PPAR gamma. Cell 83:803–812. https://doi.org/10.1016/0092-8674(95)90193-0

Fosnaugh JS, Bhat RV, Yamagata K, et al (1995) Activation of arc, a putative "effector" immediate early gene, by cocaine in rat brain. J Neurochem 64:2377–2380. https://doi.org/10.1046/j.1471-4159.1995.64052377.x

Foster-Schubert K, Alfano C, Duggan C, et al (2012) Effect of diet and exercise, alone or combined, on weight and body composition in overweight-to-obese post-menopausal women. Obesity (Silver Spring) 20:1628–1638. https://doi.org/10.1038/oby.2011.76

Francis TC, Yano H, Demarest TG, et al (2019) High-Frequency Activation of Nucleus Accumbens D1-MSNs Drives Excitatory Potentiation on D2-MSNs. Neuron 103:432-444.e3. https://doi.org/10.1016/j.neuron.2019.05.031

Gallardo CM, Darvas M, Oviatt M, et al (2014) Dopamine receptor 1 neurons in the dorsal striatum regulate food anticipatory circadian activity rhythms in mice. eLife 3:e03781. https://doi.org/10.7554/eLife.03781

Gantz SC, Robinson BG, Buck DC, et al (2015) Distinct regulation of dopamine D2S and D2L autoreceptor signaling by calcium. eLife 4:e09358. https://doi.org/10.7554/eLife.09358

Gao P, Limpens JHW, Spijker S, et al (2017) Stable immediate early gene expression patterns in medial prefrontal cortex and striatum after long-term cocaine self-administration. Addict Biol 22:354–368. https://doi.org/10.1111/adb.12330

Girault J-A (2012) Integrating Neurotransmission in Striatal Medium Spiny Neurons. In: Kreutz MR, Sala C (eds) Synaptic Plasticity: Dynamics, Development and Disease. Springer, Vienna, pp 407–429

Gittis AH, Kreitzer AC (2012) Striatal microcircuitry and movement disorders. Trends Neurosci 35:557–564. https://doi.org/10.1016/j.tins.2012.06.008

Gittis AH, Nelson AB, Thwin MT, et al (2010) Distinct Roles of GABAergic Interneurons in the Regulation of Striatal Output Pathways. J Neurosci 30:2223–2234. https://doi.org/10.1523/JNEUROSCI.4870-09.2010

Gong S, Ford CP (2019) Cholinergic Interneurons Provide a Link to Balance Excitation across Striatal Output Neurons. Neuron 103:351–353. https://doi.org/10.1016/j.neuron.2019.07.023

Gonzales BJ, Mukherjee D, Ashwal-Fluss R, et al (2019) Subregion-specific rules govern the distribution of neuronal immediate-early gene induction. PNAS. https://doi.org/10.1073/pnas.1913658116

Grant BF, Saha TD, Ruan WJ, et al (2016) Epidemiology of DSM-5 Drug Use Disorder. JAMA Psychiatry 73:39–47. https://doi.org/10.1001/jamapsychiatry.2015.2132

Graveland GA, DiFiglia M (1985) The frequency and distribution of medium-sized neurons with indented nuclei in the primate and rodent neostriatum. Brain Res 327:307–311. https://doi.org/10.1016/0006-8993(85)91524-0

Graybiel AM, Aosaki T, Flaherty AW, Kimura M (1994) The basal ganglia and adaptive motor control. Science 265:1826–1831. https://doi.org/10.1126/science.8091209

Green CB, Takahashi JS, Bass J (2008) The meter of metabolism. Cell 134:728–742. https://doi.org/10.1016/j.cell.2008.08.022

Grippo RM, Güler AD (2019) Dopamine Signaling in Circadian Photoentrainment: Consequences of Desynchrony. Yale J Biol Med 92:271–281

Hasler BP, Smith LJ, Cousins JC, Bootzin RR (2012) Circadian rhythms, sleep, and substance abuse. Sleep Med Rev 16:67–81. https://doi.org/10.1016/j.smrv.2011.03.004

Henry JA (2000) Metabolic consequences of drug misuse. BJA: British Journal of Anaesthesia 85:136–142. https://doi.org/10.1093/bja/85.1.136

Hikida T, Kimura K, Wada N, et al (2010) Distinct roles of synaptic transmission in direct and indirect striatal pathways to reward and aversive behavior. Neuron 66:896–907. https://doi.org/10.1016/j.neuron.2010.05.011

Hood S, Cassidy P, Cossette M-P, et al (2010) Endogenous Dopamine Regulates the Rhythm of Expression of the Clock Protein PER2 in the Rat Dorsal Striatum via Daily Activation of D2 Dopamine Receptors. J Neurosci 30:14046–14058. https://doi.org/10.1523/JNEUROSCI.2128-10.2010

Hope B, Kosofsky B, Hyman SE, Nestler EJ (1992) Regulation of immediate early gene expression and AP-1 binding in the rat nucleus accumbens by chronic cocaine. Proc Natl Acad Sci USA 89:5764–5768. https://doi.org/10.1073/pnas.89.13.5764

Hope BT, Simmons DE, Mitchell TB, et al (2006) Cocaine-induced locomotor activity and Fos expression in nucleus accumbens are sensitized for 6 months after repeated cocaine administration outside the home cage. Eur J Neurosci 24:867–875. https://doi.org/10.1111/j.1460-9568.2006.04969.x

Huang DW, Sherman BT, Lempicki RA (2009) Systematic and integrative analysis of large gene lists using DAVID bioinformatics resources. Nat Protoc 4:44–57. https://doi.org/10.1038/nprot.2008.211

Hughes ME, Hogenesch JB, Kornacker K (2010) JTK_CYCLE: an efficient nonparametric algorithm for detecting rhythmic components in genome-scale data sets. J Biol Rhythms 25:372–380. https://doi.org/10.1177/0748730410379711

Hyman SE, Malenka RC (2001) Addiction and the brain: the neurobiology of compulsion and its persistence. Nat Rev Neurosci 2:695–703. https://doi.org/10.1038/35094560

Hyman SE, Malenka RC, Nestler EJ (2006) Neural mechanisms of addiction: the role of reward-related learning and memory. Annu Rev Neurosci 29:565–598. https://doi.org/10.1146/annurev.neuro.29.051605.113009

Iaccarino C, Samad TA, Mathis C, et al (2002) Control of lactotrop proliferation by dopamine: essential role of signaling through D2 receptors and ERKs. Proc Natl Acad Sci U S A 99:14530–14535. https://doi.org/10.1073/pnas.222319599

Iijima M, Nikaido T, Akiyama M, et al (2002) Methamphetamine-induced, suprachiasmatic nucleus-independent circadian rhythms of activity and mPer gene expression in the striatum of the mouse. Eur J Neurosci 16:921–929. https://doi.org/10.1046/j.1460-9568.2002.02140.x

Ikemoto S, Panksepp J (1999) The role of nucleus accumbens dopamine in motivated behavior: a unifying interpretation with special reference to reward-seeking. Brain Research Reviews 31:6–41. https://doi.org/10.1016/S0165-0173(99)00023-5

Imbesi M, Yildiz S, Arslan AD, et al (2009) Dopamine receptor-mediated regulation of neuronal "clock" gene expression. Neuroscience 158:537–544. https://doi.org/10.1016/j.neuroscience.2008.10.044

Jenab S, Festa ED, Russo SJ, et al (2003) MK-801 attenuates cocaine induction of c-fos and preprodynorphin mRNA levels in Fischer rats. Brain Res Mol Brain Res 117:237–239. https://doi.org/10.1016/s0169-328x(03)00319-x

Jeon J, Dencker D, Wörtwein G, et al (2010) A Subpopulation of Neuronal M4 Muscarinic Acetylcholine Receptors Plays a Critical Role in Modulating Dopamine-Dependent Behaviors. J Neurosci 30:2396–2405. https://doi.org/10.1523/JNEUROSCI.3843-09.2010

Jiang Q, Heneka M, Landreth GE (2008) The role of peroxisome proliferator-activated receptor-gamma (PPARgamma) in Alzheimer's disease: therapeutic implications. CNS Drugs 22:1–14. https://doi.org/10.2165/00023210-200822010-00001

Kalivas PW, Stewart J (1991) Dopamine transmission in the initiation and expression of drug- and stress-induced sensitization of motor activity. Brain Res Brain Res Rev 16:223–244. https://doi.org/10.1016/0165-0173(91)90007-u

Kanterman RY, Mahan LC, Briley EM, et al (1991) Transfected D2 dopamine receptors mediate the potentiation of arachidonic acid release in Chinese hamster ovary cells. Mol Pharmacol 39:364–369

Karvat G, Kimchi T (2014) Acetylcholine Elevation Relieves Cognitive Rigidity and Social Deficiency in a Mouse Model of Autism. Neuropsychopharmacology 39:831–840. https://doi.org/10.1038/npp.2013.274

Keenan AB, Torre D, Lachmann A, et al (2019) ChEA3: transcription factor enrichment analysis by orthogonal omics integration. Nucleic Acids Res 47:W212–W224. https://doi.org/10.1093/nar/gkz446

Kelz MB, Chen J, Carlezon WA, et al (1999) Expression of the transcription factor deltaFosB in the brain controls sensitivity to cocaine. Nature 401:272–276. https://doi.org/10.1038/45790

Kemp JM, Powell TP (1971) The structure of the caudate nucleus of the cat: light and electron microscopy. Philos Trans R Soc Lond, B, Biol Sci 262:383–401. https://doi.org/10.1098/rstb.1971.0102

Khan MA, Alam Q, Haque A, et al (2019) Current Progress on Peroxisome Proliferator-activated Receptor Gamma Agonist as an Emerging Therapeutic Approach for the Treatment of Alzheimer's Disease: An Update. Curr Neuropharmacol 17:232–246. https://doi.org/10.2174/1570159X16666180828100002

Kharkwal G, Brami-Cherrier K, Lizardi-Ortiz JE, et al (2016a) Parkinsonism Driven by Antipsychotics Originates from Dopaminergic Control of Striatal Cholinergic Interneurons. Neuron 91:67–78. https://doi.org/10.1016/j.neuron.2016.06.014

Kharkwal G, Radl D, Lewis RG, Borrelli E (2016b) Dopamine D2 receptors in striatal output neurons enable the psychomotor effects of cocaine. PNAS 113:11609–11614. https://doi.org/10.1073/pnas.1608362113

Kiyota Y, Kondo T, Maeshiba Y, et al (1997) Studies on the metabolism of the new antidiabetic agent pioglitazone. Identification of metabolites in rats and dogs. Arzneimittelforschung 47:22–28

Klawonn AM, Wilhelms DB, Lindström SH, et al (2018) Muscarinic M4 Receptors on Cholinergic and Dopamine D1 Receptor-Expressing Neurons Have Opposing Functionality for Positive Reinforcement and Influence Impulsivity. Front Mol Neurosci 11:. https://doi.org/10.3389/fnmol.2018.00139

Kliewer SA, Forman BM, Blumberg B, et al (1994) Differential expression and activation of a family of murine peroxisome proliferator-activated receptors. Proc Natl Acad Sci U S A 91:7355–7359. https://doi.org/10.1073/pnas.91.15.7355

Knutson B, Adams CM, Fong GW, Hommer D (2001) Anticipation of Increasing Monetary Reward Selectively Recruits Nucleus Accumbens. J Neurosci 21:RC159–RC159. https://doi.org/10.1523/JNEUROSCI.21-16-j0002.2001

Kohno M, Link J, Dennis LE, et al (2019) Neuroinflammation in addiction: A review of neuroimaging studies and potential immunotherapies. Pharmacol Biochem Behav 179:34–42. https://doi.org/10.1016/j.pbb.2019.01.007

Korpi ER, den Hollander B, Farooq U, et al (2015) Mechanisms of Action and Persistent Neuroplasticity by Drugs of Abuse. Pharmacol Rev 67:872–1004. https://doi.org/10.1124/pr.115.010967

Korshunov KS, Blakemore LJ, Trombley PQ (2017) Dopamine: A Modulator of Circadian Rhythms in the Central Nervous System. Front Cell Neurosci 11:91. https://doi.org/10.3389/fncel.2017.00091

Kosillo P, Zhang Y-F, Threlfell S, Cragg SJ (2016) Cortical Control of Striatal Dopamine Transmission via Striatal Cholinergic Interneurons. Cereb Cortex 26:4160–4169. https://doi.org/10.1093/cercor/bhw252

Krishnaiah SY, Wu G, Altman BJ, et al (2017) Clock Regulation of Metabolites Reveals Coupling between Transcription and Metabolism. Cell Metab 25:961-974.e4. https://doi.org/10.1016/j.cmet.2017.03.019

Kuehl FA, Egan RW (1980) Prostaglandins, arachidonic acid, and inflammation. Science 210:978–984. https://doi.org/10.1126/science.6254151

Lacagnina MJ, Rivera PD, Bilbo SD (2017) Glial and Neuroimmune Mechanisms as Critical Modulators of Drug Use and Abuse. Neuropsychopharmacol 42:156–177. https://doi.org/10.1038/npp.2016.121

Lawrence M, Huber W, Pagès H, et al (2013) Software for Computing and Annotating Genomic Ranges. PLOS Computational Biology 9:e1003118. https://doi.org/10.1371/journal.pcbi.1003118

Lemos JC, Friend DM, Kaplan AR, et al (2016) Enhanced GABA Transmission Drives Bradykinesia Following Loss of Dopamine D2 Receptor Signaling. Neuron 90:824–838. https://doi.org/10.1016/j.neuron.2016.04.040

Lewis RG, Serra M, Radl D, et al (2020) Dopaminergic Control of Striatal Cholinergic Interneurons Underlies Cocaine-Induced Psychostimulation. Cell Reports 31:. https://doi.org/10.1016/j.celrep.2020.107527

Li N, Zhao H (2021) Role of Carnitine in Non-alcoholic Fatty Liver Disease and Other Related Diseases: An Update. Front Med (Lausanne) 8:689042. https://doi.org/10.3389/fmed.2021.689042

Lim SAO, Kang UJ, McGehee DS (2014) Striatal cholinergic interneuron regulation and circuit effects. Front Synaptic Neurosci 6:. https://doi.org/10.3389/fnsyn.2014.00022

Lindgren N, Xu ZQ, Herrera-Marschitz M, et al (2001) Dopamine D(2) receptors regulate tyrosine hydroxylase activity and phosphorylation at Ser40 in rat striatum. Eur J Neurosci 13:773–780. https://doi.org/10.1046/j.0953-816x.2000.01443.x

Lipton DM, Gonzales BJ, Citri A (2019) Dorsal Striatal Circuits for Habits, Compulsions and Addictions. Front Syst Neurosci 13:. https://doi.org/10.3389/fnsys.2019.00028

Lobo MK, Nestler EJ (2011) The striatal balancing act in drug addiction: distinct roles of direct and indirect pathway medium spiny neurons. Front Neuroanat 5:41. https://doi.org/10.3389/fnana.2011.00041

Logan RW, Parekh PK, Kaplan GN, et al (2019) NAD+ cellular redox and SIRT1 regulate the diurnal rhythms of tyrosine hydroxylase and conditioned cocaine reward. Mol Psychiatry 24:1668–1684. https://doi.org/10.1038/s41380-018-0061-1

Logan RW, Williams WP, McClung CA (2014) Circadian rhythms and addiction: Mechanistic insights and future directions. Behav Neurosci 128:387–412. https://doi.org/10.1037/a0036268

Love M, Ahlmann-Eltze C, Anders S, Huber W (2019) DESeq2: Differential gene expression analysis based on the negative binomial distribution. Version 1.26.0. Bioconductor version: Release (3.10). URL https://bioconductor.org/packages/DESeq2/

Lüscher C, Bellone C (2008) Cocaine-evoked synaptic plasticity: a key to addiction? Nat Neurosci 11:737–738. https://doi.org/10.1038/nn0708-737

Lüscher C, Malenka RC (2011) Drug-evoked synaptic plasticity in addiction: from molecular changes to circuit remodeling. Neuron 69:650–663. https://doi.org/10.1016/j.neuron.2011.01.017

Lynch WJ, Girgenti MJ, Breslin FJ, et al (2008) Gene Profiling the Response to Repeated Cocaine Self-administration in Dorsal Striatum: A Focus on Circadian Genes. Brain Res 1213:166–177. https://doi.org/10.1016/j.brainres.2008.02.106

Mamaligas AA, Ford CP (2016) Spontaneous Synaptic Activation of Muscarinic Receptors by Striatal Cholinergic Neuron Firing. Neuron 91:574–586. https://doi.org/10.1016/j.neuron.2016.06.021

Mangelsdorf DJ, Thummel C, Beato M, et al (1995) The nuclear receptor superfamily: the second decade. Cell 83:835–839. https://doi.org/10.1016/0092-8674(95)90199-x

Marche K, Martel A-C, Apicella P (2017) Differences between Dorsal and Ventral Striatum in the Sensitivity of Tonically Active Neurons to Rewarding Events. Front Syst Neurosci 11:. https://doi.org/10.3389/fnsys.2017.00052

Martin H (2010) Role of PPAR-gamma in inflammation. Prospects for therapeutic intervention by food components. Mutat Res 690:57–63. https://doi.org/10.1016/j.mrfmmm.2009.09.009

Masri S, Rigor P, Cervantes M, et al (2014) Partitioning Circadian Transcription by SIRT6 Leads to Segregated Control of Cellular Metabolism. Cell 158:659–672. https://doi.org/10.1016/j.cell.2014.06.050

McClung CA, Nestler EJ (2003) Regulation of gene expression and cocaine reward by CREB and DeltaFosB. Nat Neurosci 6:1208–1215. https://doi.org/10.1038/nn1143

McClung CA, Sidiropoulou K, Vitaterna M, et al (2005) Regulation of Dopaminergic Transmission and Cocaine Reward by the Clock Gene. Proceedings of the National Academy of Sciences of the United States of America 102:9377–9381

Meiser J, Weindl D, Hiller K (2013) Complexity of dopamine metabolism. Cell Communication and Signaling 11:34. https://doi.org/10.1186/1478-811X-11-34

Mendoza J, Challet E (2014) Circadian insights into dopamine mechanisms. Neuroscience 282:230–242. https://doi.org/10.1016/j.neuroscience.2014.07.081

Miller WR, Fox RG, Stutz SJ, et al (2018) PPARγ agonism attenuates cocaine cue reactivity. Addict Biol 23:55–68. https://doi.org/10.1111/adb.12471

Miyazaki S, Tahara Y, Colwell CS, et al (2021) Chronic methamphetamine uncovers a circadian rhythm in multiple-unit neural activity in the dorsal striatum which is independent of the suprachiasmatic nucleus. Neurobiol Sleep Circadian Rhythms 11:100070. https://doi.org/10.1016/j.nbscr.2021.100070

Moehle MS, Pancani T, Byun N, et al (2017) Cholinergic Projections to the Substantia Nigra Pars Reticulata Inhibit Dopamine Modulation of Basal Ganglia through the M4 Muscarinic Receptor. Neuron 96:1358-1372.e4. https://doi.org/10.1016/j.neuron.2017.12.008

Mohawk JA, Green CB, Takahashi JS (2012) Central and peripheral circadian clocks in mammals. Annu Rev Neurosci 35:445–462. https://doi.org/10.1146/annurev-neuro-060909-153128

Montmayeur JP, Bausero P, Amlaiky N, et al (1991) Differential expression of the mouse D2 dopamine receptor isoforms. FEBS Lett 278:239–243. https://doi.org/10.1016/0014-5793(91)80125-m

Murakami M, Tognini P, Liu Y, et al (2016) Gut microbiota directs PPARγ-driven reprogramming of the liver circadian clock by nutritional challenge. EMBO Rep 17:1292–1303. https://doi.org/10.15252/embr.201642463

Nader MA, Morgan D, Gage HD, et al (2006) PET imaging of dopamine D2 receptors during chronic cocaine self-administration in monkeys. Nat Neurosci 9:1050–1056. https://doi.org/10.1038/nn1737

Nelson AB, Kreitzer AC (2014) Reassessing Models of Basal Ganglia Function and Dysfunction. Annual Review of Neuroscience 37:117–135. https://doi.org/10.1146/annurev-neuro-071013-013916

Nestler EJ (2005) The Neurobiology of Cocaine Addiction. Sci Pract Perspect 3:4–10

Nestler EJ (2013) Cellular basis of memory for addiction. Dialogues Clin Neurosci 15:431–443

Neve KA, Seamans JK, Trantham-Davidson H (2004) Dopamine receptor signaling. J Recept Signal Transduct Res 24:165–205. https://doi.org/10.1081/rrs-200029981

Nosjean O, Boutin JA (2002) Natural ligands of PPARgamma: are prostaglandin J(2) derivatives really playing the part? Cell Signal 14:573–583. https://doi.org/10.1016/s0898-6568(01)00281-9

Oldenburg IA, Ding JB (2011) Cholinergic modulation of synaptic integration and dendritic excitability in the striatum. Curr Opin Neurobiol 21:425–432. https://doi.org/10.1016/j.conb.2011.04.004

Oorschot DE (2013) The percentage of interneurons in the dorsal striatum of the rat, cat, monkey and human: A critique of the evidence. Basal Ganglia 3:19–24. https://doi.org/10.1016/j.baga.2012.11.001

Ozburn AR, Kern J, Parekh PK, et al (2017) NPAS2 Regulation of Anxiety-Like Behavior and GABAA Receptors. Front Mol Neurosci 10:360. https://doi.org/10.3389/fnmol.2017.00360

Pagès H, Obenchain V, Morgan M (2019) GenomicAlignments: Representation and manipulation of short genomic alignments. Version 1.22.1. Bioconductor version: Release (3.10). URL https://bioconductor.org/packages/GenomicAlignments/

Pancani T, Foster DJ, Moehle MS, et al (2015) Allosteric activation of M4 muscarinic receptors improve behavioral and physiological alterations in early symptomatic YAC128 mice. Proc Natl Acad Sci U S A 112:14078–14083. https://doi.org/10.1073/pnas.1512812112

Panda S (2016) Circadian physiology of metabolism. Science 354:1008–1015. https://doi.org/10.1126/science.aah4967

Parekh PK, Logan RW, Ketchesin KD, et al (2019) Cell-Type-Specific Regulation of Nucleus Accumbens Synaptic Plasticity and Cocaine Reward Sensitivity by the Circadian Protein, NPAS2. J Neurosci 39:4657–4667. https://doi.org/10.1523/JNEUROSCI.2233-18.2019

Partch CL, Green CB, Takahashi JS (2014) Molecular architecture of the mammalian circadian clock. Trends Cell Biol 24:90–99. https://doi.org/10.1016/j.tcb.2013.07.002

Patel VR, Eckel-Mahan K, Sassone-Corsi P, Baldi P (2012) CircadiOmics: integrating circadian genomics, transcriptomics, proteomics and metabolomics. Nat Methods 9:772–773. https://doi.org/10.1038/nmeth.2111

Patke A, Young MW, Axelrod S (2020) Molecular mechanisms and physiological importance of circadian rhythms. Nat Rev Mol Cell Biol 21:67–84. https://doi.org/10.1038/s41580-019-0179-2

Paulson PE, Robinson TE (1996) Regional Differences in the Effects of Amphetamine Withdrawal on Dopamine Dynamics in the Striatum. Neuropsychopharmacology 14:325–337. https://doi.org/10.1016/0893-133X(95)00141-Y

Philibin SD, Hernandez A, Self DW, Bibb JA (2011) Striatal Signal Transduction and Drug Addiction. Front Neuroanat 5:. https://doi.org/10.3389/fnana.2011.00060

Piomelli D, Astarita G, Rapaka R (2007) A neuroscientist's guide to lipidomics. Nat Rev Neurosci 8:743–754. https://doi.org/10.1038/nrn2233

Piomelli D, Pilon C, Giros B, et al (1991) Dopamine activation of the arachidonic acid cascade as a basis for D1/D2 receptor synergism. Nature 353:164–167. https://doi.org/10.1038/353164a0

Pisani A, Bonsi P, Centonze D, et al (2000) Activation of D2-like dopamine receptors reduces synaptic inputs to striatal cholinergic interneurons. J Neurosci 20:RC69

Puighermanal E, Biever A, Pascoli V, et al (2017) Ribosomal Protein S6 Phosphorylation Is Involved in Novelty-Induced Locomotion, Synaptic Plasticity and mRNA Translation. Front Mol Neurosci 10:. https://doi.org/10.3389/fnmol.2017.00419

Puighermanal E, Castell L, Esteve-Codina A, et al (2020) Functional and molecular heterogeneity of D2R neurons along dorsal ventral axis in the striatum. Nat Commun 11:1957. https://doi.org/10.1038/s41467-020-15716-9

Qi J, Zhang S, Wang H-L, et al (2016) VTA glutamatergic inputs to nucleus accumbens drive aversion by acting on GABAergic interneurons. Nature Neuroscience 19:725–733. https://doi.org/10.1038/nn.4281

Radl D, Chiacchiaretta M, Lewis RG, et al (2018) Differential regulation of striatal motor behavior and related cellular responses by dopamine D2L and D2S isoforms. PNAS 115:198–203. https://doi.org/10.1073/pnas.1717194115

Radl D, De Mei C, Chen E, et al (2013) Each individual isoform of the dopamine D2 receptor protects from lactotroph hyperplasia. Mol Endocrinol 27:953–965. https://doi.org/10.1210/me.2013-1008

Ribas-Latre A, Eckel-Mahan K (2016) Interdependence of nutrient metabolism and the circadian clock system: Importance for metabolic health. Mol Metab 5:133–152. https://doi.org/10.1016/j.molmet.2015.12.006

Rice ME, Patel JC, Cragg SJ (2011) Dopamine release in the basal ganglia. Neuroscience 198:112–137. https://doi.org/10.1016/j.neuroscience.2011.08.066

Rivkees SA, Lachowicz JE (1997) Functional D1 and D5 dopamine receptors are expressed in the suprachiasmatic, supraoptic, and paraventricular nuclei of primates. Synapse 26:1–10. https://doi.org/10.1002/(SICI)1098-2396(199705)26:1<1::AID-SYN1>3.0.CO;2-D

Robinson TE, Berridge KC (2008) The incentive sensitization theory of addiction: some current issues. Philos Trans R Soc Lond B Biol Sci 363:3137–3146. https://doi.org/10.1098/rstb.2008.0093

Roth BL (2016) DREADDs for Neuroscientists. Neuron 89:683–694. https://doi.org/10.1016/j.neuron.2016.01.040

Rouge-Pont F, Usiello A, Benoit-Marand M, et al (2002) Changes in extracellular dopamine induced by morphine and cocaine: crucial control by D2 receptors. J Neurosci 22:3293–3301. https://doi.org/20026322

Salamone JD (1992) Complex motor and sensorimotor functions of striatal and accumbens dopamine: involvement in instrumental behavior processes. Psychopharmacology 107:160–174. https://doi.org/10.1007/BF02245133

Samikkannu T, Rao KVK, Ding H, et al (2014) Immunopathogenesis of HIV infection in cocaine users: role of arachidonic acid. PLoS One 9:e106348. https://doi.org/10.1371/journal.pone.0106348

Scheer FAJL, Morris CJ, Shea SA (2013) The internal circadian clock increases hunger and appetite in the evening independent of food intake and other behaviors. Obesity 21:421–423. https://doi.org/10.1002/oby.20351

Scheiermann C, Kunisaki Y, Frenette PS (2013) Circadian control of the immune system. Nat Rev Immunol 13:190–198. https://doi.org/10.1038/nri3386

Schinelli S, Paolillo M, Corona GL (1994) Opposing actions of D1- and D2-dopamine receptors on arachidonic acid release and cyclic AMP production in striatal neurons. J Neurochem 62:944–949. https://doi.org/10.1046/j.1471-4159.1994.62030944.x

Schmitz Y, Schmauss C, Sulzer D (2002) Altered dopamine release and uptake kinetics in mice lacking D2 receptors. J Neurosci 22:8002–8009

Schooneman MG, Vaz FM, Houten SM, Soeters MR (2013) Acylcarnitines: reflecting or inflicting insulin resistance? Diabetes 62:1–8. https://doi.org/10.2337/db12-0466

Schultz W, Apicella P, Scarnati E, Ljungberg T (1992) Neuronal activity in monkey ventral striatum related to the expectation of reward. J Neurosci 12:4595–4610. https://doi.org/10.1523/JNEUROSCI.12-12-04595.1992

Sheffler DJ, Williams R, Bridges TM, et al (2009) A novel selective muscarinic acetylcholine receptor subtype 1 antagonist reduces seizures without impairing hippocampus-dependent learning. Mol Pharmacol 76:356–368. https://doi.org/10.1124/mol.109.056531

Shen W, Tian X, Day M, et al (2007) Cholinergic modulation of Kir2 channels selectively elevates dendritic excitability in striatopallidal neurons. Nat Neurosci 10:1458–1466. https://doi.org/10.1038/nn1972

Sidiropoulos K, Viteri G, Sevilla C, et al (2017) Reactome enhanced pathway visualization. Bioinformatics 33:3461–3467. https://doi.org/10.1093/bioinformatics/btx441

Simon J, Ouro A, Ala-Ibanibo L, et al (2020) Sphingolipids in Non-Alcoholic Fatty Liver Disease and Hepatocellular Carcinoma: Ceramide Turnover. International Journal of Molecular Sciences 21:40. https://doi.org/10.3390/ijms21010040

Skaper SD, Facci L, Zusso M, Giusti P (2018) An Inflammation-Centric View of Neurological Disease: Beyond the Neuron. Front Cell Neurosci 12:72. https://doi.org/10.3389/fncel.2018.00072

Smith AD, Olson RJ, Justice JB (1992) Quantitative microdialysis of dopamine in the striatum: effect of circadian variation. Journal of Neuroscience Methods 44:33–41. https://doi.org/10.1016/0165-0270(92)90111-P

Soccio RE, Chen ER, Rajapurkar SR, et al (2015) Genetic Variation Determines PPARγ Function and Anti-diabetic Drug Response In Vivo. Cell 162:33–44. https://doi.org/10.1016/j.cell.2015.06.025

Soeters MR, Soeters PB, Schooneman MG, et al (2012) Adaptive reciprocity of lipid and glucose metabolism in human short-term starvation. American Journal of Physiology-Endocrinology and Metabolism 303:E1397–E1407. https://doi.org/10.1152/ajpendo.00397.2012

Su Y, Shin J, Zhong C, et al (2017) Neuronal activity modifies the chromatin accessibility landscape in the adult brain. Nat Neurosci 20:476–483. https://doi.org/10.1038/nn.4494

Surmeier DJ, Plotkin J, Shen W (2009) Dopamine and synaptic plasticity in dorsal striatal circuits controlling action selection. Curr Opin Neurobiol 19:621–628. https://doi.org/10.1016/j.conb.2009.10.003

Swanson CR, Joers V, Bondarenko V, et al (2011) The PPAR-γ agonist pioglitazone modulates inflammation and induces neuroprotection in parkinsonian monkeys. J Neuroinflammation 8:91. https://doi.org/10.1186/1742-2094-8-91

Swendsen J, Moal ML (2011) Individual vulnerability to addiction. Annals of the New York Academy of Sciences 1216:73–85. https://doi.org/10.1111/j.1749-6632.2010.05894.x

Tahara Y, Aoyama S, Shibata S (2017) The mammalian circadian clock and its entrainment by stress and exercise. J Physiol Sci 67:1–10. https://doi.org/10.1007/s12576-016-0450-7

Taverna S, Ilijic E, Surmeier DJ (2008) Recurrent Collateral Connections of Striatal Medium Spiny Neurons Are Disrupted in Models of Parkinson's Disease. J Neurosci 28:5504–5512. https://doi.org/10.1523/JNEUROSCI.5493-07.2008

Thiriet N, Aunis D, Zwiller J (2000) C-fos and egr-1 immediate-early gene induction by cocaine and cocaethylene in rat brain: a comparative study. Ann N Y Acad Sci 914:46–57. https://doi.org/10.1111/j.1749-6632.2000.tb05182.x

Threlfell S, Clements MA, Khodai T, et al (2010) Striatal muscarinic receptors promote activity dependence of dopamine transmission via distinct receptor subtypes on cholinergic interneurons in ventral versus dorsal striatum. J Neurosci 30:3398–3408. https://doi.org/10.1523/JNEUROSCI.5620-09.2010

Tirotta E, Fontaine V, Picetti R, et al (2008) Signaling by dopamine regulates D2 receptors trafficking at the membrane. Cell Cycle 7:2241–2248. https://doi.org/10.4161/cc.7.14.6307

Torres G, Rivier C (1993) Cocaine-induced expression of striatal c-fos in the rat is inhibited by NMDA receptor antagonists. Brain Res Bull 30:173–176. https://doi.org/10.1016/0361-9230(93)90055-g

Trapnell C, Hendrickson DG, Sauvageau M, et al (2013) Differential analysis of gene regulation at transcript resolution with RNA-seq. Nat Biotechnol 31:46–53. https://doi.org/10.1038/nbt.2450

Usiello A, Baik JH, Rougé-Pont F, et al (2000) Distinct functions of the two isoforms of dopamine D2 receptors. Nature 408:199–203. https://doi.org/10.1038/35041572

Valjent E, Corvol J-C, Pagès C, et al (2000) Involvement of the Extracellular Signal-Regulated Kinase Cascade for Cocaine-Rewarding Properties. J Neurosci 20:8701–8709. https://doi.org/10.1523/JNEUROSCI.20-23-08701.2000

Vallone D, Picetti R, Borrelli E (2000) Structure and function of dopamine receptors. Neurosci Biobehav Rev 24:125–132. https://doi.org/10.1016/s0149-7634(99)00063-9

Verwey M, Dhir S, Amir S (2016) Circadian influences on dopamine circuits of the brain: regulation of striatal rhythms of clock gene expression and implications for

psychopathology and disease. F1000Res 5:F1000 Faculty Rev-2062. https://doi.org/10.12688/f1000research.9180.1

Virmani A, Binienda ZK, Ali SF, Gaetani F (2007) Metabolic Syndrome in Drug Abuse. Annals of the New York Academy of Sciences 1122:50–68. https://doi.org/10.1196/annals.1403.004

Viswanathan N, Davis FC (1997) Single prenatal injections of melatonin or the D1-dopamine receptor agonist SKF 38393 to pregnant hamsters sets the offsprings' circadian rhythms to phases 180° apart. J Comp Physiol A 180:339–346. https://doi.org/10.1007/s003590050053

Volakakis N, Kadkhodaei B, Joodmardi E, et al (2010) NR4A orphan nuclear receptors as mediators of CREB-dependent neuroprotection. PNAS 107:12317–12322. https://doi.org/10.1073/pnas.1007088107

Volkow ND, Wang G-J, Baler RD (2011) Reward, dopamine and the control of food intake: implications for obesity. Trends Cogn Sci 15:37–46. https://doi.org/10.1016/j.tics.2010.11.001

Volkow ND, Wang G-J, Fowler JS, et al (1997) Decreased striatal dopaminergic responsiveness in detoxified cocaine-dependent subjects. Nature 386:830–833. https://doi.org/10.1038/386830a0

Walker DM, Cates HM, Loh Y-HE, et al (2018) Cocaine Self-administration Alters Transcriptome-wide Responses in the Brain's Reward Circuitry. Biological Psychiatry 84:867–880. https://doi.org/10.1016/j.biopsych.2018.04.009

Wang Y, Xu R, Sasaoka T, et al (2000) Dopamine D2 long receptor-deficient mice display alterations in striatum-dependent functions. J Neurosci 20:8305–8314

Warner EA, Greene GS, Buchsbaum MS, et al (1998) Diabetic Ketoacidosis Associated With Cocaine Use. Archives of Internal Medicine 158:1799–1802. https://doi.org/10.1001/archinte.158.16.1799

Weaver DR, Reppert SM (1995) Definition of the developmental transition from dopaminergic to photic regulation of c-fos gene expression in the rat suprachiasmatic nucleus. Molecular Brain Research 33:136–148. https://doi.org/10.1016/0169-328X(95)00117-B

Weiner DM, Levey AI, Brann MR (1990) Expression of muscarinic acetylcholine and dopamine receptor mRNAs in rat basal ganglia. Proc Natl Acad Sci U S A 87:7050–7054

Welsh DK, Takahashi JS, Kay SA (2010) Suprachiasmatic nucleus: cell autonomy and network properties. Annu Rev Physiol 72:551–577. https://doi.org/10.1146/annurev-physiol-021909-135919

Welter M, Vallone D, Samad TA, et al (2007) Absence of dopamine D2 receptors unmasks an inhibitory control over the brain circuitries activated by cocaine. Proc Natl Acad Sci U S A 104:6840–6845. https://doi.org/10.1073/pnas.0610790104

Xu M, Moratalla R, Gold LH, et al (1994) Dopamine D1 receptor mutant mice are deficient in striatal expression of dynorphin and in dopamine-mediated behavioral responses. Cell 79:729–742. https://doi.org/10.1016/0092-8674(94)90557-6

Yager LM, Garcia AF, Wunsch AM, Ferguson SM (2015) The ins and outs of the striatum: Role in drug addiction. Neuroscience 301:529–541. https://doi.org/10.1016/j.neuroscience.2015.06.033

Yohn SE, Foster DJ, Covey DP, et al (2018) Activation of the mGlu1 metabotropic glutamate receptor has antipsychotic-like effects and is required for efficacy of M4 muscarinic receptor allosteric modulators. Mol Psychiatry. https://doi.org/10.1038/s41380-018-0206-2

Young ST, Porrino LJ, Iadarola MJ (1991) Cocaine induces striatal c-fos-immunoreactive proteins via dopaminergic D1 receptors. Proc Natl Acad Sci USA 88:1291–1295. https://doi.org/10.1073/pnas.88.4.1291

Zhang D, Zhang L, Lou DW, et al (2002) The dopamine D1 receptor is a critical mediator for cocaine-induced gene expression. J Neurochem 82:1453–1464. https://doi.org/10.1046/j.1471-4159.2002.01089.x

Zhang J, Zhang L, Jiao H, et al (2006) c-Fos facilitates the acquisition and extinction of cocaine-induced persistent changes. J Neurosci 26:13287–13296. https://doi.org/10.1523/JNEUROSCI.3795-06.2006

Zhang Y-F, Cragg SJ (2017) Pauses in Striatal Cholinergic Interneurons: What is Revealed by Their Common Themes and Variations? Front Syst Neurosci 11:. https://doi.org/10.3389/fnsys.2017.00080

Zhang Y-F, Reynolds JNJ, Cragg SJ (2018) Pauses in Cholinergic Interneuron Activity Are Driven by Excitatory Input and Delayed Rectification, with Dopamine Modulation. Neuron 98:918-925.e3. https://doi.org/10.1016/j.neuron.2018.04.027